UNIVERSITÉ DU QUÉBEC

THÈSE PRÉSENTÉE À

L'UNIVERSITÉ DU QUÉBEC À CHICOUTIMI

POUR L'OBTENTION DU

DOCTORAT EN RESSOURCES MINÉRALES

par

Damien Gaboury

M. Sc.

ORIGINE VOLCANOGÈNE DES VEINES AURIFÈRES RICHES EN SULFURES DE LA MINE GÉANT DORMANT, ABITIBI, QUÉBEC

Juillet 1999

Bibliothèque
Paul-Émile-Boulet

UQAC
Université du Québec
à Chicoutimi

Mise en garde/Advice

Afin de rendre accessible au plus grand nombre le résultat des travaux de recherche menés par ses étudiants gradués et dans l'esprit des règles qui régissent le dépôt et la diffusion des mémoires et thèses produits dans cette Institution, **l'Université du Québec à Chicoutimi (UQAC)** est fière de rendre accessible une version complète et gratuite de cette œuvre.

Motivated by a desire to make the results of its graduate students' research accessible to all, and in accordance with the rules governing the acceptation and diffusion of dissertations and theses in this Institution, the **Université du Québec à Chicoutimi (UQAC)** is proud to make a complete version of this work available at no cost to the reader.

L'auteur conserve néanmoins la propriété du droit d'auteur qui protège ce mémoire ou cette thèse. Ni le mémoire ou la thèse ni des extraits substantiels de ceux-ci ne peuvent être imprimés ou autrement reproduits sans son autorisation.

The author retains ownership of the copyright of this dissertation or thesis. Neither the dissertation or thesis, nor substantial extracts from it, may be printed or otherwise reproduced without the author's permission.

RÉSUMÉ

Les veines de quartz aurifères riches en sulfures de la mine Géant Dormant sont encaissées dans les roches du premier cycle volcanique (2730-2720 Ma) de la Zone Volcanique Nord de la ceinture archéenne de l'Abitibi. La minéralisation aurifère est centrée sur un complexe felsique recoupant une séquence volcano-sédimentaire, composée de filons-couches mafiques interlités avec des sédiments et des laves mafique et felsique. Un dôme dacitique et des essaims de dykes de FP et de QFP composent le complexe felsique. Deux générations de dykes recoupent la minéralisation: (1) mafiques tholéiitiques et (2) shoshonitiques. Les roches felsiques sont calco-alcalines ($Zr/Y \approx 12$; $[La/Yb]_N=11,6$) et cogénétiques; celles mafiques sont tholéiitiques ($Zr/Y \approx 2,5$; $[La/Yb]_N$ of 0,6-1,9) et sont également cogénétiques entre elles. Les dykes de QFP, datés à 2722 ± 2 Ma (U-Pb sur zircons), sont consistants avec l'âge du premier cycle volcanique. L'empilement volcanique a été construit de manière séquentielle en milieu sous-marin profond (> 3 150 m) à partir de deux sources magmatiques: une source felsique proximale et une mafique distale.

Les couches s'orientent E-O et sont fortement inclinées vers le S, formant une séquence homoclinale normale localisée sur le flanc N d'un pli régional et d'axe E-O subhorizontal. Une schistosité régionale E-O et subverticale, contenant une linéation d'étirement subverticale, se superpose sur toutes les roches. L'intensité de la déformation est faible et hétérogène. Tous les types de roches, incluant les veines aurifères, sont métamorphisés au faciès des schistes verts.

Trois événements successifs de minéralisation aurifère ont été identifiés: (1) une minéralisation volcanogène précoce, manifestée par l'altération (chlorite, séricite, quartz) et la sulfurisation (filonnets et disséminations de pyrrhotite et chalcopyrite) des roches du paléo-fond océanique; (2) une minéralisation autométasomatique correspondant à la chloritisation et à la pyritisation interne du dôme dacitique; et (3) une minéralisation filonienne incluant les veines aurifères et la minéralisation interne des dykes de QFP. Les veines se composent de 5 à 80% (~25%) de sulfures (pyrite, pyrrhotite, chalcopyrite, sphalérite et arsenopyrite). Le quartz et des traces de chlorite, de séricite, de tourmaline ainsi que de calcite et d'actinote métamorphiques composent la gangue. L'altération des épontes est nulle à faible (chlorite-séricite). Le système de veines se compose de 4 familles de veines interconnectées, dont la géométrie devient plus complexe vers la paléo-surface. Les facteurs de contrôle correspondent à des perméabilités primaires que sont: les unités lithologiques spécifiques, les contacts lithostratigraphiques, les failles synvolcaniques, et les joints préexistants. Les dykes de QFP, caractérisés par une intense séricitisation et une

pyritisation, constituent les conduits hydrothermaux pour la formation des veines. Les relations de recoupement, structurales et géométriques indiquent que les veines se sont formées lorsque les couches étaient en position initiale subhorizontale, après l'injection des QFP mais avant la fin du magmatisme mafique tholéiitique, et que la déformation ductile régionale est superposée sur les veines.

Le contenu de concentrés de sulfures en éléments des terres rares (ÉTR) et traces a été déterminé par INAA. Les spectres des ÉTR sont spécifiques pour chaque événement, alors que la teneur en éléments traces définit une tendance évolutive. La pyrrhotite précoce se caractérise par des spectres en ÉTR faiblement fractionnés avec des anomalies négatives en Ce et par des concentrations fortes en Ni et Co et faibles en Au et Ag. Cette signature est cohérente avec le lessivage des éléments à partir de minéraux ferro-magnésiens des basaltes de l'empilement volcanique sous-jacent et avec le mélange entre les fluides hydrothermaux et l'eau de mer oxydante au site de minéralisation. Les sulfures des veines sont caractérisés par des contenus faibles en Ni et Co mais élevés en Au et Ag, ainsi que par un fractionnement prononcé en ÉTR légères et une anomalie positive en Eu. La signature en ÉTR se compare à celle typique des systèmes volcanogènes matures et actifs, dominés par le lessivage des éléments dans les plagioclases des basaltes. Ces données démontrent le lien génétique entre les événements de minéralisation et s'intègrent au sein d'un modèle volcanogène qui a progressivement gagné en maturité.

La valeur moyenne $\delta^{18}O$ du quartz de la minéralisation de fond océanique est de 11,9 ± 0,6‰ et les fluides ont une valeur $\delta^{18}O$ de 3,2‰ calculée à 250°C. Les compositions isotopiques moyennes de l'oxygène pour le quartz et la chlorite des veines aurifères sont respectivement de 12,5 ± 0,3‰ et 5,9 ± 1,1‰. Une température de formation de veines de ~275°C est déterminée en utilisant les valeurs $\delta^{18}O$ du quartz et de la chlorite; cohérente avec celle de 269 ± 10°C, calculée à partir de la composition des chlorites. À 275°C, la valeur $\delta^{18}O$ calculée des fluides à l'origine des veines est de 4,7‰. Les valeurs $\delta^{34}S$ des sulfures pour les trois événements de minéralisation sont comprises entre 0,6 et 2,8‰; comparables avec les valeurs magmatiques. Les géothermomètres isotopiques du souffre indiquent une température de ~350°C pour la précipitation des sulfures dans les veines. Les données isotopiques supportent le lien génétique entre les trois événements de minéralisation et sont compatibles avec un système volcanogène évolutif. La nature évoluée des fluides ($\delta^{18}O$ = 4,7‰) est attribuée à l'apport de fluides magmatiques au système hydrothermal convectif dominé par l'eau de mer modifiée.

Les veines résultent de l'épisode final d'un système volcanogène comportant quatre stades évolutifs. Le Stade 1 implique l'altération et la minéralisation des roches du paléo-fond océanique. Au Stade 2, l'injection des filons-couches mafiques (~1 km) entraîne le colmatage du système hydrothermal. Le Stade 3 correspond à l'introduction du dôme et à la reprise de l'activité hydrothermale. Le Stade 4 implique l'injection des dykes de QFP qui, subséquemment, ont servi de conduits hydrothermaux. Les veines résultent du remplissage de fractures développées à proximité des QFP. La formation des veines est conséquente à la construction séquentielle de l'édifice volcanique à partir des deux sources. L'injection des filons-couches a perturbé l'activité hydrothermale associée au centre felsique. La reprise du magmatisme felsique a généré des fractures pour la formation des veines, qui a été favorisée par la pressurisation lithostatique des fluides au sein d'un milieu imperméable. L'enrichissement en or, du Stade 1 au Stade 4, résulte de l'évolution intrinsèque du système, étant probablement relié à l'ébullition des fluides lors de la formation des veines.

Ces résultats ont une importance particulière pour l'exploration aurifère. À l'échelle du gisement, deux méthodes ont été développées pour faciliter la corrélation spatiale de veines interceptées en forages. Pour l'exploration régionale, cette étude démontre le potentiel aurifère des systèmes volcanogènes. Elle implique également que les minéralisations aurifères filoniennes ne sont pas restreintes chronologiquement à la phase d'accrétion tectonique, et spatialement aux zones majeures de déformation. Enfin, les complexes de filons-couches mafiques, où le magmatique felsique est synchrone, peuvent être considérés comme fertiles pour la formation des veines aurifères volcanogènes.

ABSTRACT

The Géant Dormant sulfide-rich vein-type gold deposit is located within the first volcanic cycle (2730-2720 Ma) of the Northern Volcanic Zone of the Archean Abitibi Subprovince. Gold mineralization is centered about a felsic complex which intrudes a volcano-sedimentary succession composed mainly of mafic sills with lesser interbedded pelagic sediments and mafic pillowed and felsic lavas. The felsic complex comprises a dacitic subvolcanic dome and a swarm of polyphase early felsic FP and late QFP dikes. The post-mineralization dikes comprise: early mafic tholeiitic and late shoshonitic hornblende-rich dikes. All felsic rocks are calc-alkalic and cogenetic ($Zr/Y \approx 12$; $[La/Yb]_N = 11.6$) whereas all mafic rocks, including early post-mineralization dikes, are tholeiitic and cogenetic ($Zr/Y \approx 2.5$; $[La/Yb]_N$ of 0.6-1.9). Zircons from a QFP dike yield U-Pb age of 2722 ± 2 Ma, consistent with the younger ages for the first volcanic cycle. Strata was built from two different volcanic sources: a proximal felsic and a distal mafic one in a deep submarine setting (> 3150 m).

The volcanic strata strike predominantly E-W and dip steeply to the south, forming a single and normal homoclinal stratigraphic succession lying on the northern limb of an east-trending regional syncline with a subhorizontal axis. The weakly penetrative subvertical E-W trending regional schistosity, which contain a steeply plunging mineral stretching lineation, overprints all rock types locally, but the internal deformation within the tilted sequence is weak and heterogeneous. All rock types, including gold-bearing veins, have been metamorphosed to greenschist facies.

Three successive mineralizing events are recognized: (1) a seafloor-related gold poor event, characterized by sericite, chlorite, and quartz alteration with disseminations and stringers of auriferous pyrrhotite and chalcopyrite affecting rocks of paleo-seafloor origin, (2) an autometasomatic event affecting only the dacitic dome, expressed by chloritization and dissemination of auriferous pyrite, and (3) quartz-sulfide vein-style gold mineralization and associated altered and mineralized QFP dikes. Vein mineralization, which is the only economic ore, is composed of 5 to 80% (mean of 25%) of sulfides (pyrite, pyrrhotite, chalcopyrite, sphalerite and arsenopyrite). Quartz is the dominant gangue mineral, with lesser amounts of chlorite, sericite, tourmaline and metamorphic calcite and actinolite. Selvage alteration is weakly developed (chlorite-sericite) to absent. The orebody comprises four main sets of interconnected veins and displays an increasing complexity toward the proposed paleosurface. Vein controls correspond to primary permeable features such as: stratigraphic contacts, specific lithological units, synvolcanic faults, and preexisting joints.

QFP dikes, characterized by strong internal sericitization and disseminated auriferous pyrite, constitute fluid conduits for vein formation. Crosscutting, structural and geometric relationships indicate that: (1) veins formed in original subhorizontal strata, closely after QFP dike injection, but before the end of mafic tholeiitic magmatism, and that; (2) the regional ductile deformation (strata folding, schistosity and metamorphism) overprints the gold-bearing veins.

Rare earth elements (REE) and selected trace elements of sulfide separates were analyzed by INAA. Chondrite-normalized REE patterns are specific for each mineralizing event whereas trace element content defines a consistent evolutive trend. Early seafloor-related pyrrhotite has a weakly fractionated REE pattern with Ce depletion, high Ni and Co and low Au and Ag contents. This signature is consistent with the leaching of trace elements in ferro-magnesian minerals from underling basaltic rocks and mixing with oxidizing seawater during seafloor precipitation. Sulfides in the veins are characterized by low Ni and Co, high Au and Ag contents and strong fractionation of LREE with Eu positive anomalies, comparable with REE patterns of active and mature volcanogenic hydrothermal systems dominated by leaching of trace elements in plagioclase. These data support the genetic link between the various mineralizing events and can be best integrated as the result of the progressive maturation of an unique volcanogenic hydrothermal system.

Quartz $\delta^{18}O$ values of seafloor-related mineralization average 11.9 ± 0.6‰, whereas hydrothermal fluids had a $\delta^{18}O$ value of 3.2‰ calculated at 250°C. The oxygen isotope composition of quartz and chlorite from veins average 12.5 ± 0.3‰ and 5.9 ± 1.1‰ respectively. Assuming an oxygen isotope equilibrium between quartz and chlorite, the veins formed at a temperature of ~275°C, which is consistent with the calculated temperature of 269 ± 10°C for chlorite formation. The mineralizing fluids had a $\delta^{18}O$ value of 4.7‰ at 275°C. The $\delta^{34}S$ values of sulfides from the three gold events range from 0.6 to 2.8‰ and are close to magmatic values. Sulfur isotope geothermometry indicates a temperature of ~350°C for sulfide precipitation in the gold-bearing veins. The isotope data support the genetic link between the three mineralizing events and are compatible with an unique evolving volcanogenic hydrothermal system. The evolved nature of mineralizing fluids ($\delta^{18}O$ = 4.7‰) is attributed to magmatic fluids supply to the seawater dominated convective hydrothermal system.

The gold-bearing vein network was formed during the last stage of a four-stage volcanogenic hydrothermal system. At Stage 1, diffuse seafloor-related hydrothermal fluids

altered and mineralized lavas and Fe-rich sediments. Stage 2 involves the sealing of the hydrothermal system by injection of a 1 km thick stack of impermeable mafic sills. During Stage 3, the mineralizing system was reactivated by the emplacement of the dacitic dome. Stage 4 involves injection of QFP dikes along active synvolcanic faults. These dikes served as conduits for the ascension of mineralizing fluids through the volcanic pile. Gold, and related quartz and sulfides, precipitated in open fractures developed mainly in mafic rocks near QFP dikes. Vein formation is a consequence of the specific two-source volcanic pile. The voluminous mafic sills disturbed the evolution of a volcanogenic hydrothermal system related to the felsic center. Renewed felsic activity generated fractures for vein formation, enhanced by pressurization of mineralizing fluids at near lithostatic pressure within the impermeable host sequence. Gold enrichment from Stage 1 to Stage 4 is consistent with the proposed evolution and likely related to boiling of the mineralizing fluids during vein formation.

These results have significant implications for gold exploration. At mine-scale, two practical methods were developed to facilitate correlation of vein intersections from diamond-drill cores. At a larger scale, this study emphasizes the gold potential of volcanogenic hydrothermal systems and demonstrates that the vein-type gold mineralization is not only restricted temporally to the late accretion stage of Archean supracrustal belts and spatially to major crustal faults. Finally, mafic sill-sediment complexes, coeval with subvolcanic felsic magmatic activity, appear to be prospective environments for volcanogenic-related vein-style gold mineralization.

REMERCIEMENTS

Ce projet de recherche résulte d'une entente tripartite entre Cambior (Mine Géant Dormant), le Ministère des Ressources naturelles du Québec et l'UQAC. Ces organismes ont contribué financièrement à la réalisation de ce projet. Le CRSNG et le FCAR ont également financé le projet par l'émission de bourses d'étude à l'auteur. Je remercie sincèrement mon directeur de thèse, le Dr Réal Daigneault, ainsi que les membres de mon comité, les Drs Wulf Mueller, Jayanta Guha et Jean-François Couture. Je remercie également les Drs Alan Galley (CGC) et Alain Rouleau qui ont agi respectivement à titre de lecteur externe et de président pour l'évaluation de la thèse. Des remerciements sont également adressés à l'équipe de la mine Géant Dormant, en particulier à MM. Claude Gobeil et Elzéar Belzile; à l'équipe du Service Géologique du nord-ouest, en particulier à M. Pierre Pilote pour la réalisation de la datation U-Pb, et au corps professoral et technique de l'UQAC. Le Dr Edward-H. Chown a contribué à rehausser le niveau de l'anglais de plusieurs des manuscrits. Un merci tout spécial est adressé au Dr Ghislain Tourigny qui a directement contribué à la mise en marche du projet. Le Dr Georges Beaudoin a également investi beaucoup de son temps pour la partie isotopique. Les lecteurs critiques des différents journaux scientifiques, anonymes pour la plupart, ont le mérite d'avoir contribué à la qualité de cette thèse. Enfin, je désire exprimer mes plus profonds remerciements à ma compagne de vie, Nathalie Harvey. Sa compréhension, sa patience et ses encouragements ont été exemplaires.

TABLE DES MATIÈRES

CHAPITRE 2

An Archean volcanic-related gold-sulfide-quartz vein orebody: the Géant Dormant mine, Abitibi Subprovince, Quebec, Canada

CHAPITRE 3

Evolution from seafloor-related to sulfide-rich quartz vein-type gold mineralization during deep submarine volcanic construction: The Géant Dormant gold mine, Archean Abitibi Belt, Canada

CHAPITRE 4

Constraints on the evolution of a hydrothermal system from REE and trace-elements of sulfides: Example from the Géant Dormant gold mine, Archean Abitibi Belt, Canada

CHAPITRE 5

Volcanogenic-related origin of sulfide-rich quartz veins: evidence from O and S isotopes at the Géant Dormant gold mine, Abitibi belt, Canada

CHAPITRE 6

Practical methods for correlating diamond-drill core intersections: Applications to complex vein-type orebodies

CHAPITRE 7

DISCUSSION

CHAPITRE 8

Sommaire et conclusions

ANNEXE

ANNEXE 1

The "self-equilibrating" mechanism: a model for flat vein formation in a transitional crustal depth (2-5 km), example from the Géant Dormant gold mine, Canada.

LISTE DES TABLEAUX PAR CHAPITRE ET ANNEXE

CHAPITRE 2

CHAPITRE 3

CHAPITRE 4

CHAPITRE 5

CHAPITRE 7

ANNEXE 1

ANNEXE 2

ANNEXE 3

ANNEXE 4

ANNEXE 5

LISTE DES FIGURES PAR CHAPITRE ET ANNEXE

CHAPITRE 1

CHAPITRE 2

CHAPITRE 3

CHAPITRE 4

CHAPITRE 5

CHAPITRE 6

CHAPITRE 7

ANNEXE 1

CHAPITRE 1

Introduction

PROBLÉMATIQUE

Minéralisations aurifères filoniennes archéennes

Les minéralisations aurifères archéennes de type veine représentent une importante source mondiale d'or (4 700 tonnes métriques d'or, incluant la production et les réserves provenant de la Sous-province de l'Abitibi: Spooner et Barrie, 1993). Elles se retrouvent principalement dans les ceintures de roches supracrustales déformées et métamorphisées aux faciès des schistes verts et des amphibolites. Quoique certaines caractéristiques de la minéralisation soient variables à l'échelle régionale, plusieurs particularités spatiales, temporelles, chimiques et minéralogiques sont communes à l'ensemble des gisements (Colvine et al., 1988; Colvine, 1989; Groves et al., 1989; Hodgson, 1989, 1991; Robert, 1990, 1991). Sur cette base, certains auteurs ont proposé que les minéralisations aurifères de type veine constituent un groupe cohérent de gisements qui résultent d'un processus génétique commun et unifié (Kerrich, 1989, 1993; Kerrich et Wyman, 1990a). Cette interprétation est basée sur l'uniformité des caractéristiques suivantes: (1) la distribution des dépôts le long des failles crustales; (2) le contrôle structural de la minéralisation; (3) la faible teneur en métaux de base des veines aurifères; (4) le rapport Ag/Au faible (0.1-1); (5) l'introduction tardive de la minéralisation par rapport à l'évolution des ceintures de roches vertes; et (6) la composition riche en CO_2 des fluides minéralisateurs. D'autre part, la variabilité locale de certaines caractéristiques est expliquée par la diversité des unités lithologiques encaissantes et par une variation relative de la profondeur de formation. Ce dernier argument constitue d'ailleurs la base du modèle de "continuum" (Groves, 1993) qui intègre génétiquement les minéralisations aurifères encaissées dans des roches métamorphisées variant des faciès granulites aux schistes verts inférieurs. Ce type de minéralisation est maintenant considéré comme un phénomène intrinsèque aux épisodes

d'accrétion tectonique, tant archéenne, protérozoïque que mésozoïque (p. ex. Hodgson et Hamilton, 1988; Barley et al., 1989; Kerrich et Wyman, 1990a; Kerrich, 1993).

Plusieurs modèles métallogéniques furent publiés sur la base d'uniformité. L'origine la plus acceptée repose sur l'advection épisodique de fluides (Sibson et al., 1988; Cox et al., 1990; Sibson, 1990) d'origine métamorphique (Groves et Phillips, 1987; Kerrich, 1990; Kerrich et Feng, 1992; Kerrich et Cassidy, 1994) le long de failles crustales importantes et de leurs subsidiaires (Robert et Brown, 1986a; Eisenlohr et al., 1989) lors de la terminaison de la période d'accrétion tectonique (Barley et al., 1989; Hodgson et Hamilton, 1989; Kerrich et Wyman 1990a, 1990b; Kerrich et Feng, 1992). Ce type génétique est connu sous plusieurs appellations dont: mésothermal, tectonométamorphique, métamorphogénique et orogénique. Il sera ici désigné comme minéralisation orogénique, en accord avec la nomenclature de Groves et al. (1998). Le terme filonien est utilisé ici d'une manière descriptive sans référence à un type génétique particulier.

Minéralisations aurifères de la Sous-province de l'Abitibi

La Sous-province de l'Abitibi est la plus grande ceinture de roches vertes archéennes au monde (Card, 1990), l'une des mieux documentée et l'une des plus productive en terme de métaux de base et précieux (Card et al., 1989; Simard et al., 1990). Elle est subdivisée en deux parties sur la base des successions volcano-sédimentaires, des suites plutoniques et des âges U-Pb (Chown et al., 1992; Mueller et al., 1996). La Zone Volcanique Nord est interprétée comme une unité géotectonique cohérente édifiée initialement à partir d'un arc volcanique diffus, qui a évolué localement vers un arc mature (Chown et al., 1992). Pour la Zone Volcanique Sud, l'assemblage complexe de terrains lithotectoniques est interprété comme le résultat de l'accrétion tectonique de différents

systèmes d'îles en arc et de bassins arrière-arcs (p. ex. Hodgson et Hamilton, 1989; Mueller et Donaldson, 1992) ou de plateaux océaniques (Desrochers et al., 1993).

En Abitibi, les gisements orogéniques représentent le type génétique le plus abondant (Robert, 1990). Toutefois, plusieurs autres types de minéralisations aurifères ont été reconnus (Guha et al., 1988; Robert et Poulsen, 1997; Robert et al., 1997). Ils ont été distingués principalement sur la base (1) de leur chronologie relative de formation par rapport aux divers événements caractérisant l'évolution de la ceinture de l'Abitibi; (2) de leur profondeur crustale de formation; et (3) de leur caractéristique chimique. Les divers gisements aurifères reconnus appartiennent essentiellement à deux groupes (Robert et Poulsen, 1997). Le premier regroupe les gisements formés à une profondeur crustale relativement faible, durant la période de la construction des édifices volcano-plutoniques. Ce groupe est référé ici comme étant d'origine volcanique. Les deuxième groupe inclut les gisements formés à une plus grande profondeur crustale, durant la période plus tardive de l'évolution tectonique qui a affecté les édifices volcano-plutoniques. Les gisements orogéniques composent essentiellement ce groupe. Cette subdivision utilisant les termes volcaniques et orogéniques est imparfaite du point de vue de la nomenclature, étant donné que des événements de volcanisme et de magmatisme sont associés à la période orogénique (p. ex. Chown et al., 1992). Toutefois, elle est valable dans la mesure où ces périodes sont bien délimitées chronologiquement. Pour la Zone Volcanique Nord, par exemple, la période volcanique s'étend de 2730 à 2720 Ma et celle orogénique de 2708 à 2685 Ma (Chown et al., 1992).

Les gisements d'origine volcanique, de par leur formation précoce par rapport à l'évolution de la ceinture, sont communément recoupés par des dykes manifestant la continuité de la construction volcanique. Ils sont également imprégnés par les éléments de la déformation ductile et du métamorphisme régional. La profondeur crustale de formation

de la minéralisation s'étend de la surface à quelques centaines de mètre à l'intérieur de l'empilement volcanique. Les amas lenticulaires sulfurés constituent la morphologie dominante de la minéralisation. L'abondance de sulfures de métaux de base (Cu-Zn) caractérise la minéralogie de ces systèmes hydrothermaux. Cette caractéristique traduit la participation de l'eau de mer comme principal fluide et la grande capacité de transport des complexes chlorurés (Wood, 1987). La mine Horne (Barrett et al., 1991) et les gisements du camp minier de Bousquet (Tourigny et al., 1989 et 1993; Hannington et al., 1997) constituent les cas types de minéralisations aurifères d'origine volcanique.

Les gisements orogéniques se sont formés à différents stades durant le raccourcissement horizontal, s'étendant ainsi de syn- à tardi-tectoniques (p. ex. Couture et al., 1994). Conséquemment, ils montrent différentes relations par rapport à l'empreinte des éléments caractérisant la déformation progressive, le métamorphisme régional et le magmatisme syn-tectonique. Leur profondeur de formation est également variable, mais communément comprise entre 5 et 15 km. La morphologie de la minéralisation est dominée par des veines et des veinules de quartz et dans certains cas, par des disséminations de sulfures. La minéralisation montre une association spatiale avec les grandes zones de failles et le magmatisme associé à ces zones. Ces systèmes hydrothermaux sont communément pauvres en métaux de base et sulfures et riches en carbonates, une caractéristique reliée à la faible salinité et à la forte teneur en CO_2 du fluide minéralisateur, qui est principalement d'origine métamorphique (Wood, 1987). Les exemples classiques du type filonien sont Sigma (Robert et Brown, 1986a; 1986b) et Kiena (Morasse et al., 1995) comme étant respectivement tardi- et syn-tectonique. Le gisement de Beattie (Poulsen, 1995) est un exemple de minéralisation disséminée, formés probablement de manière tardi-tectonique.

Minéralisations aurifères dans les terrains phanérozoïques

Dans les terrains volcaniques phanérozoïques, les minéralisations aurifères filoniennes se subdivisent en deux grands types: celles associées aux régimes d'accrétion tectonique et celles reliées à des régimes en extension (Groves et al., 1998). Le premier type est analogue aux minéralisations archéennes orogéniques (p. ex. Gaboury et al., 1996) et se retrouve dans les copeaux tectoniques de roches volcano-sédimentaires obductés. Le deuxième type est connu sous l'appellation épithermale (p. ex. White et al., 1995). Ce type de minéralisation est génétiquement associé au volcanisme et au magmatisme dans les environnements d'arcs volcaniques subaériens. Le type épithermal filonien est aussi désigné par les attributs *low-sulfidation* (Bonham, 1986) et adulaire-séricite (Heald et al., 1987). La minéralisation se présente sous la forme de veines de quartz-calcédoine-carbonates et ± adulaire qui renferment des proportions variables de sulfures de métaux de base. Les veines sont généralement plus riches en argent qu'en or, caractérisées par des rapports Ag/Au variant de 25 à 1. Les failles normales à coulissantes et les fractures syn-volcaniques contrôlent la formation et la distribution des veines. Plusieurs attitudes de veines composent communément le système filonien. La profondeur de formation des veines est superficielle, comprise en 0 et 2 km.

Comparaison entre les terrains phanérozoïques et archéens

Malgré la diversité et la fertilité en minéralisations aurifères, et l'interprétation des paléo-environnements en tant que segments d'arcs volcaniques, les terrains archéens en général et la ceinture de l'Abitibi en particulier se distinguent des terrains phanérozoïques par la rareté, sinon l'absence de minéralisation filonienne aurifère analogue au type épithermal. Certes, certains gisements abitibiens ont été qualifiés d'épithermaux comme la mine Cu-Zn-Ag-Au de Selbaie (Larsen et Hutchinson, 1993) et les gisements pyriteux du

camp minier de Bousquet (Stone, 1990; Hannington et al., 1997). Cependant, ces exemples ne constituent pas des gisements aurifères de type filonien. Le gisement de Selbaie, qui est pauvre en or, dérive d'un système volcanogène développé en milieu subaérien (Larsen et Hutchinson, 1993). Les gisements de Bousquet, avec leur altération alumineuse (Marquis et al., 1990) et leur minéralisation essentiellement sous la forme de lentilles pyriteuses, représentent probablement des minéralisations analogues au type épithermal *high-sulfidation*, telles que suggérées par Silitoe et al. (1996) et Hannington et al. (1997).

Facteurs limitants les exemples archéens filoniens épithermaux

Deux arguments sont communément avancés pour expliquer la rareté ou l'absence de minéralisation épithermale dans les terrains archéens (Kerrich et Wyman, 1990b). Premièrement, les environnements volcaniques essentiellement sous-marins ne sont pas favorables aux minéralisations épithermales. Deuxièmement, la possibilité de préservation de ces gisements superficiels est pratiquement nulle dans les environnements volcaniques pré-phanérozoïques. Toutefois, ces deux arguments doivent être considérés à tout le moins comme limitants, mais non comme déterminants pour leur formation et leur préservation. En ce sens, des minéralisations sous-marines analogues à celles épithermales ont été récemment documentées (Hannington et al., 1997). Parallèlement, des gîtes épithermaux protérozoïques ont été décrits (Dubé et al., 1998), démontrant ainsi que certains facteurs comme le basculement et l'enfouissement rapides favorisent leur préservation. Enfin, la présence des gisements de Selbaie et de Bousquet, témoigne directement de leur possibilité de préservation.

Si les possibilités de formation et de préservation existent, il faut se demander pourquoi les exemples de minéralisation aurifère filonienne épithermale, précoces par rapport à la période orogénique (pré-orogénique), sont considérés comme absents ou si

rares dans les terrains archéens. La réponse à cette question relève probablement plus du facteur humain que de critères géologiques. En termes chronologiques, le phénomène épithermal est relativement nouveau dans l'histoire de l'exploration en Abitibi. Son apparition coïncide avec la migration des compagnies minières vers les terrains volcaniques cénozoïques de la ceinture de feu et à l'exposition des géologues d'ici à ce type de minéralisation. D'un point de vue génétique, la minéralisation de type veine est en quelque sorte victime de sa popularité comme cible d'exploration. Comme les deux grands épisodes abitibiens de minéralisation sont bien typés au niveau du style, les veines, par opposition aux amas sulfurés, ont été et sont encore aujourd'hui largement considérées comme l'expression d'une formation orogénique. D'autre part, la difficulté de documenter sans équivoque l'origine pré-orogénique d'un gisement aurifère filonien, particulièrement quand celui-ci est encaissé au sein d'un couloir de déformation, constitue une lourde tache. S'ajoute enfin la réticence face aux changements conceptuels de la communauté géologique. Ces deux derniers points sont mis en évidence par le récent article de Penczak et Mason (1997) et par la controverse qu'il a suscité (Tarnocai et al., 1998; Penczak, 1998) concernant l'origine épithermale archéenne de la minéralisation aurifère de type *low-sulfidation* à la mine Campbell.

Importance des minéralisations filoniennes pré-orogéniques

Dans la mesure où les arguments précédents supportent l'existence de minéralisation filonienne pré-orogénique, la question fondamentale demeure: pourquoi est-il important de reconnaître ce type de minéralisation? Le lien génétique entre les minéralisations aurifères et le tectonisme est reconnu depuis longtemps (Newhouse, 1942; McKinstry, 1948). Conséquemment, l'exploration aurifère fut et est encore aujourd'hui essentiellement concentrée le long des corridors de faille majeure. L'identification d'une

minéralisation filonienne pré-orogénique trouve ici sa pertinence dans les nouvelles stratégies d'explorations qu'elle pourrait engendrer. N'étant probablement pas génétiquement relié aux zones de faille majeure (orogénique) dont la trace en surface est bien documentée, ce type de minéralisation devrait ouvrir d'immenses secteurs, considérés comme étant infertiles pour les minéralisations aurifères. La découverte d'un tel type, ou plus précisément son identification, justifiera une documentation détaillée dans le but de proposer un modèle génétique et d'élaborer des critères d'exploration.

Caractéristiques éventuelles d'une minéralisation filonienne pré-orogénique

Par comparaison avec les environnements d'arc, d'éventuelles minéralisations pré-orogéniques sous la forme de veines, préservées dans les ceintures volcano-sédimentaires archéennes déformées et métamorphisées, pourraient présenter certaines des caractéristiques suivantes. (1) Plusieurs attitudes de veines incompatibles structuralement avec les caractéristiques de la déformation régionale. (2) Des facteurs de contrôle sur l'emplacement de la minéralisation de nature primaire, comme des contacts lithologiques et des failles syn-volcaniques. (3) Des évidences de minéralisation et d'altération hydrothermale affectées par la déformation régionale et le métamorphisme. (4) Des métaux de base associés à la minéralisation aurifère. (5) Un rapport Ag / Au relativement élevé (>1). (6) Un cortège métallique caractéristique des systèmes minéralisateurs aurifères syn-volcaniques (Ag, As, Sb, Hg). (7) Des altérations hydrothermales distinctives, comme par exemple une altération alumineuse. (8) Une signature isotopique des veines et une composition des inclusions fluides indiquant une contribution possible de fluides provenant de sources océanique, magmatique et météorique. (9) Un environnement géologique particulier (complexe intrusif, caldeira, centre volcanique) dont les caractéristiques primaires ont influencé l'emplacement de la minéralisation. (10) Le recoupement des

veines par des dykes syn-volcaniques. Toutefois, selon l'intensité de la déformation et du métamorphisme, certaines de ces caractéristiques, sinon l'ensemble, pourrait être complètement oblitérées.

Critères de sélection du gisement à l'étude

La mine Géant Dormant apparaissait comme un endroit tout désigné pour tester l'hypothèse des minéralisations filoniennes pré-orogéniques. Premièrement, la minéralisation filonienne possède des caractéristiques contrastantes par rapport aux minéralisations orogéniques, s'apparentant plutôt à celles épithermales, comme: (1) une géométrie complexe du système de veines aurifères, difficilement conciliable avec les caractéristiques de la déformation ductile régionale; (2) une composition des veines de quartz riche en sulfures et pauvre en carbonates; (3) une composition métallique des veines riche en métaux de base (Cu-Zn); (4) un rapport Ag/Au > 1. Deuxièmement, la localisation de ce gisement dans une zone de jonction triple de la déformation régionale (Daigneault et Archambault, 1990) laissait supposer une faible intensité de la déformation régionale, favorable à la documentation d'éventuelles relations de recoupement et géométriques primaires (relations pré-orogéniques). Enfin, la mine Géant Dormant est spatialement isolée par rapport aux autres camps miniers aurifères. Elle est aussi isolée par rapport aux trois grandes zones de failles E-W de Cadillac-Lader Lake, de Porcupine-Destor et de Casa-Berardi, auxquelles sont principalement associées les minéralisations filoniennes orogéniques (Fig. 1).

OBJECTIFS

L'objectif principal du projet de recherche est d'établir l'origine de la minéralisation aurifère filonienne à la mine Géant Dormant et conséquemment de proposer un modèle

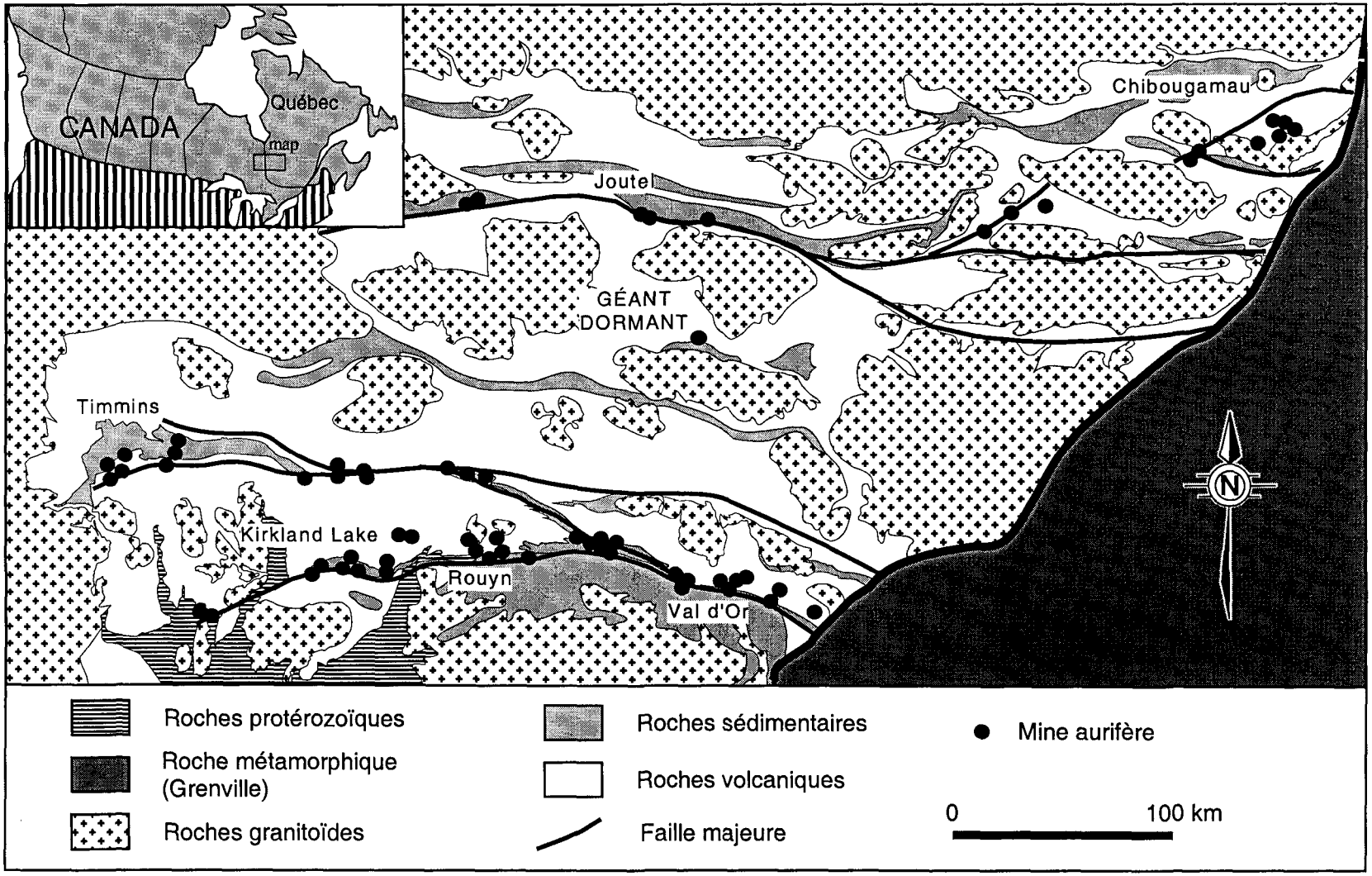

Figure 1. Localisation de la mine Géant Dormant dans son cadre géologique régional. Notez la distribution des gisements aurifères le long des failles majeures et l'isolement du Géant Dormant par rapport à ces mêmes zones de failles et par rapport aux camps miniers aurifères (Kirkland Lake, Timmin, Rouyn, Val d'Or, Chibougamau et Joutel). Figure modifiée de Robert (1990) et Chown et al. (1992). Seules les failles majeures reconnues comme étant aurifères sont représentées sur cette figure.

métallogénique et des guides pour l'exploration. Considérant les caractéristiques de la minéralisation, deux hypothèses étaient plausibles et déterminantes pour l'orientation des travaux: soit que les veines puissent être d'origine orogénique, soit qu'elles puissent être précoces et non reliées génétiquement à la déformation ductile régionale. Dans l'affirmative de la première hypothèse, il s'agit de déterminer les causes expliquant les caractéristiques divergeantes de la minéralisation et conséquemment de préciser un modèle métallogénique existant. Dans le deuxième cas, il s'agit de documenter la minéralisation et son cadre géologique dans le but ultime de formuler un modèle génétique et d'en évaluer l'importance pour l'exploration. Indépendamment des deux hypothèses de base, les quatre objectifs secondaires suivants se devaient d'être considérés. (1) Caractériser la minéralisation aurifère et établir les facteurs qui contrôlent sa mise en place. (2) Caractériser la nature de l'altération hydrothermale et déterminer sa distribution spatiale. (3) Caractériser l'environnement hôte de la minéralisation. (4) Placer les événements de minéralisation dans un cadre évolutif qui intègre les différents événements de magmatisme, de déformation et de métamorphisme.

MÉTHODOLOGIE

L'approche méthodologique préconisée repose essentiellement sur l'établissement des relations géométriques, spatiales et chronologiques entre les unités lithologiques hôtes, la minéralisation, l'altération hydrothermale, la déformation régionale et le métamorphisme. Des travaux de cartographie détaillée, une compilation des données géologiques existantes et un échantillonnage représentatif et systématique ont été effectués dans un premier temps. Ces travaux de base ont permis de déterminer que la mise en place des veines précède l'événement de déformation ductile régionale. Conséquemment les travaux suivants ont porté principalement sur la documentation de ce type particulier de

minéralisation pré-orogénique et sur l'intégration des données au sein d'un modèle métallogénique. Des travaux détaillés de caractérisation en laboratoire ont été réalisés, incluant: (1) des examens pétrographiques; (2) des analyses lithogéochimiques; (3) des analyses par activation neutronique des éléments traces dans les sulfures; (4) des analyses isotopiques du souffre et de l'oxygène; (5) des analyses de minéraux à la microsonde; et (6) une datation U-Pb sur zircon. Ces travaux avaient pour but dans un premier temps de documenter en détail le dépôt aurifère et de préciser les relations établies sur la base de critères empiriques. Dans un deuxième temps, ces données analytiques ont servi de base comparative avec d'autres types de gisements. Enfin, elles ont été utilisées pour valider, d'une manière indépendante, le modèle métallogénique établi initialement à partir de relations de terrain.

La période de cueillette de données dans la mine totalise 14 mois répartis sur quatre étés consécutifs, soit de 1993 à 1996 inclusivement. Durant cette période, la majorité des chantiers a été visitée et cartographiée. Une cartographie complète du niveau 190 au 1:100 a été réalisée pour placer la minéralisation aurifère dans son contexte géologique. Ce travail a été complétée par des cartographies ponctuelles aux échelles 1: 10 et 1: 100 dans des secteurs spécifiques exposant des relations clés et ce sur tous les niveaux de la mine. Plus de 700 échantillons et 600 photographies ont été recueillis pour traitement.

Pour l'aspect pétrographique, 150 lames minces et 66 plaquettes de roches minéralisées ont été étudiées. Les lames minces ont permis de caractériser la minéralogie primaire des roches et celle des différentes altérations hydrothermales. Parallèlement, la composition minéralogique et la paragénèse des différents styles de minéralisation ont été déterminées à partir des plaquettes et des lames minces. Les relations chronologiques relatives entre l'empreinte de la déformation ductile, le métamorphisme et la minéralisation ont aussi été déterminées.

Environ 160 échantillons ont été analysés par le Centre de Recherches Minérales (CRM) pour les éléments majeurs et certains éléments traces (Sn, Ga, Nb, Rb, Sr, Ta, Th, Y, Zr). Une cinquantaine de ces échantillons, jugés représentatifs, a été analysée pour les éléments des terres rares (ETR) et certains éléments incompatibles (Ce, Cs, Eu, Gd, Hf, Ho, La, Lu, Nd, Sm, Sc, Ta, Tb, Th, Tm, U, Yb). Ces données géochimiques ont permis de caractériser la signature primaire des roches en utilisant des diagrammes de caractérisation basés sur la concentration des éléments immobiles durant l'altération hydrothermale comme ceux de Winchester et Floyd (1977), de Pearce (1983) et de Barrett et MacLean (1994). D'autre part, ces données ont été utilisées pour caractériser les changements géochimiques reliés aux différentes altérations hydrothermales en utilisant le calcul de bilan de masse (p. ex. Barrett et MacLean, 1994).

Une vingtaine d'analyses sur des concentrés monominéraliques de sulfures (pyrite, pyrrhotite, chalcopyrite et sphalérite) ont été faites dans le but de caractériser la composition en éléments traces et, sur une base comparative, de déduire certains processus métallogéniques. Ces analyses ont été effectuées au Laboratoire d'activation neutronique de l'Université du Québec à Chicoutimi. Les éléments suivants ont été analysés: Au, Ag, As, Co, Cr, Ni, Sb, Se et W ainsi que certains éléments des terres-rares (La, Ce, Sm, Eu, Tb, Yb et Lu).

Les analyses isotopiques ont été réalisées essentiellement sur des concentrés de minéraux spécifiques sélectionnés à la main sous le binoculaire pour s'assurer de leur pureté. Ainsi, 35 analyses isotopiques de l'oxygène ont été réalisées sur le quartz et la chlorite. De même, quelques analyses de roches totales ont été effectuées. Les analyses de l'oxygène ont été réalisées au Laboratoire d'isotope stable de l'Université Laval, en partenariat avec le Dr Georges Beaudoin. Ces analyses avaient pour but de déterminer la composition isotopique initiale du fluide minéralisateur et de déterminer sa température en

utilisant des paires chlorite-quartz. Une trentaine d'analyses isotopiques du souffre ont aussi été réalisées sur des concentrés monominéralliques de sulfures (pyrite, pyrrhotite, chalcopyrite et sphalérite) au G.G. Hatch Stable Isotope Laboratory de l'Université d'Ottawa. Ces données ont permis de déterminer la composition isotopique initiale du fluide et de calculer la température de formation des sulfures.

Les analyses à la microsonde ont été effectuées à l'Université du Québec à Chicoutimi. La composition quantitative de la chlorite et de la calcite dans les veines, ainsi que la composition semi-quantitative des sulfures ont été déterminées à partir de lames minces polies. L'analyse systématique des chlorites dans les veines a permis de déterminer leur température de cristallisation en utilisant un géothermomètre basé sur la composition chimique (Kranidiotis et MacLean, 1987). L'analyse des phases sulfurées fut réalisée principalement pour fins d'identification.

L'âge U-Pb des zircons provenant d'un échantillon de dyke de QFP a été déterminé au Laboratoire isotopique du Royal Ontario Museum de Toronto. Cette date a été produite dans le cadre du programme annuel de datation du Ministère des ressources naturelle du Québec.

PRÉSENTATION DES RÉSULTATS

La thèse est de type cumul d'articles publiés, en impression ou en évaluation au moment du dépôt final du présent document. Elle est constituée de 6 articles qui sont autant de chapitres distincts et autonomes, présentant un ou des aspects particuliers du travail de recherche. Les différents articles et leur chronologie de réalisation reflètent l'aspect évolutif des travaux de recherche. Spécifiquement, le premier article (chapitre 2) démontre que la minéralisation filonienne précède la déformation ductile régionale. Suite à cette conclusion, les travaux de recherche ont été orientés sur l'aspect génétique de la

minéralisation. Le deuxième article (chapitre 3) présente un modèle métallogénique évolutif, où il est démontré que la minéralisation filonienne résulte de l'évolution particulière d'un système hydrothermal volcanogène. Les deux articles suivants avaient pour but de tester d'une manière indépendante le modèle métallogénique établi précédemment sur la base principale d'observations de terrain. Spécifiquement, le troisième article (chapitre 4) présente les résultats d'une étude des éléments traces contenus dans les sulfures des différents stades hydrothermaux. Le quatrième article (chapitre 5) traite des résultats d'une étude isotopique du souffre et de l'oxygène sur les différents sulfures et minéraux de gangue associés aux différents stades d'hydrothermalisme. Le cinquième article, présenté au chapitre 6, est de nature plus technique et traite d'un aspect particulier relié à l'exploration par forages des systèmes filoniens complexes. Le sixième article, inséré en annexe, présente un mécanisme pour la formation des veines auriferes. Le modèle présenté est une version plus élaborée de celui proposé initialement dans le chapitre de discusson (voir ci-dessous). Il se retrouve en annexe car il n'a pas été examiné intégralement par les membres du jury d'évaluation de la thèse. Toutefois, puisque le modèle qui y est presenté est plus detaillé et plus raffiné, le lecteur est prié de s'y référer.

Les arguments développés dans les chapitres 2 à 5 sont résumés et restructurés au sein d'une discussion générale (chapitre 7) dans le but de démontrer d'une manière concise et cohérente les différents points appuyant le modèle métallogénique proposé. De plus, un mécanisme de formation des veines ainsi que les causes possibles de l'enrichissement en or sont discutés. Enfin, une synthèse des résultats et les grandes conclusions sont présentées au chapitre 8. Le contenu spécifique des différents articles et le journal scientifique dans lesquels ils ont été publiés ou soumis sont présentés ci-dessous.

Le chapitre 2 traite des résultats de l'analyse structurale. Le cadre structural de la minéralisation est documenté ainsi que les relations chronologiques entre l'empreinte de la

déformation ductile et la minéralisation filonienne. Sur la base de relations de recoupement et du manque de compatibilité structurale, il est démontré que la minéralisation filonienne est précoce par rapport à la déformation ductile régionale. Cet article a été publié en 1996 dans le journal *Exploration and Mining Geology* sous le titre: *An Archean volcanic-related gold-sulfide-quartz vein orebody: the Géant Dormant mine, Abitibi Subprovince, Quebec, Canada*. Une version française de cet article est également disponible dans le document ET-98-04: Études géologiques dans la région d'Amos, publié par le Ministère des Ressources naturelles du Québec.

Le chapitre 3 présente un modèle métallogénique évolutif basé sur le parallélisme entre l'histoire de l'édification volcanique et de l'hydrothermalisme. Les caractéristiques volcaniques et géochimiques des roches, les relations de recoupement, la géométrie de l'assemblage lithologique ainsi que la datation U-Pb sont utilisées pour documenter la construction séquentielle de l'empilement volcano-sédimentaire hôte. Les trois différents stades d'hydrothermalisme sont caractérisés sur la base de leur distribution spatiale, de leur paragénèse, de la nature et de la signature géochimique (calcul de bilan de masse) des altérations hydrothermales qui leurs sont associés. Cet article a été publié dans la revue *Economic Geology*, sous le titre: *Evolution from seafloor-related to sulfide-rich quartz vein-type gold mineralization during deep submarine volcanic construction: The Géant Dormant gold mine, Archean Abitibi belt, Canada*. Une version française plus détaillée de cet article est également disponible dans le document ET-98-04: Études géologiques dans la région d'Amos, publié par le Ministère des Ressources naturelles du Québec.

Le chapitre 4 est consacré aux résultats de l'étude du contenu en éléments traces des sulfures. Les différents sulfures composant les trois stades hydrothermaux ont été analysés par activation neutronique (INAA). Les résultats démontrent que les trois stades d'hydrothermalisme reconnus dérivent d'un même système hydrothermal. Il est aussi

démontré que le contenu en éléments traces, qui montre une évolution cohérente dans le temps en fonction des stades, s'accorde avec la maturation progressive d'un système hydrothermal de type volcanogène. Cet article a été soumis pour publication à la revue *The Canadian Mineralogist* sous le titre: *Constraints on the evolution of a hydrothermal system from REE and trace-elements of sulfides: Example from the Géant Dormant gold mine, Archean Abitibi Belt, Canada.*

Le chapitre 5 présente les résultats d'une étude isotopique du souffre et de l'oxygène ainsi que les résultats thermométrique de la chlorite. Cette étude avait pour but de (1) caractériser certains paramètres physico-chimiques comme la température de formation des veines et la signature isotopique des fluides minéralisateurs; (2) de tester le lien génétique entre les trois stades d'hydrothermalisme; (3) de comparer les signatures isotopiques avec les autres systèmes hydrothermaux archéens bien documentés; et (4) de déterminer l'affiliation génétique des veines aurifères. Les résultats isotopiques démontrent que les trois stades d'hydrothermalisme dérivent d'un même système hydrothermal et que celui-ci possède des caractéristiques typiques des systèmes volcanogènes. Cet article est en impression au journal *Mineralium Deposita* sous le titre: *Volcanogenic-related origin of sulfide-rich quartz veins: evidence from O and S isotopes at the Géant Dormant gold mine, Abitibi belt, Canada.*

Le chapitre 6 traite du problème relié à la corrélation de veines minéralisées interceptées en forages. Deux méthodes pratiques de corrélation, utilisant un logiciel de projection stéréographique, sont présentées. La première méthode peut être utilisée pour déterminer si deux ou plusieurs intersections de veines sont corrélatives. La seconde méthode permet de prédire l'attitude des veines principales à partir de plusieurs forages en utilisant une projection sphérique de densité. Cet article a été publié en 1997 dans la revue

CIM bulletin, sous le titre: *Practical methods for correlating diamond-drill core intersections: Applications to complex vein-type orebodies.*

Enfin, le manuscrit en annexe propose un modèle de formation des veines, qui est essentiellement basé sur les caractéristiques géométriques, minéralogiques et texturales des veines et de leur éponte. Selon ce modèle, les veines résultent d'un différentiel de pression, qui se développe lorsque les fluides montent vers la surface, le long de conduits à écoulement restreint, que sont les dykes de QFP. Cet article a été soumis pour publication au journal: *Ore Geology Reviews*, sous le titre: *The self-equilibrating mechanism: a model for flat vein formation in a transitional crustal depth (2-5 km), example from the Géant Dormant gold mine, Canada.*

CADRE DE L'ÉTUDE

Ce projet de doctorat résulte d'une entente tripartite entre les compagnies minières Cambior et Aurizon, propriétaires de la mine Géant Dormant, du Ministère des Ressources naturelles du Québec et de l'Université du Québec à Chicoutimi. Cette entente assura le financement et le soutien technique nécessaire à la réalisation de ce projet de recherche.

Références

Barley, M.E., Eisenlohr, B.N., Groves, D.I., Perring, C.S. et Vearncombe, J.R. 1989. Late Archean convergent margin tectonics and gold mineralization: A new look at the Norseman-Wiluna Belt, Western Australia. Geology, 17: 826-829.

Barrett, T.J., Cattalani, S. et MacLean, W.H. 1991. Massive sulfide deposits of the Noranda area, Quebec. I. The Horne Mine. Journal Canadien des Sciences de la Terre, 28: 465-488.

Barrett, T.J. et MacLean, W.H. 1994. Chemostratigraphy and hydrothermal alteration in exploration for VHMS deposits in greenstones and younger volcanic rocks. Dans: Alteration and alteration processes associated with ore-forming systems. Édité par: D.R. Lentz. Association Géologique du Canada, Short Course Handbook 11, p. 433-467.

Bonham, H.F. Jr. 1986. Models for volcanic-hosted epithermal precious metal deposits; a review. International Volcanological Congress, New Zealand, Proceedings of Symposium 5, p. 13-17.

Card, K.D. 1990. A review of the Superior Province of the Canadian Shield, a product of Archean accretion. Precambrian Research, 48: 99-156.

Card, K.D., Poulsen, K.H. et Robert, F. 1989. The Archean Superior Province of the Canadian Shield and its lode gold deposits. Dans: The Geology of Gold Deposit: The Perspective in 1988. Édité par R.R. Keays, W.R.H. Ramsay et D.I. Groves. Economic Geology, Monograph 6, p. 11-28.

Chown, E. H., Daigneault, R., Mueller, W. et Mortensen, J. K. 1992, Tectonic evolution of the Northern Volcanic Zone, Abitibi belt, Quebec. Journal Canadien des Sciences de la Terre, 29: 2211-2225.

Colvine, A.C. 1989. An empirical model for the formation of Archean gold deposits: products of final cratonization of the Superior province, Canada. Dans: The Geology of

Gold Deposits: The Perspective in 1988. Édité par R.R. Keays, W.R.H. Ramsay et D.I. Groves. Economic Geology, Monograph 6, p. 37-53.

Colvine, A.C., Fyon, K.B., Heather, K.B., Marmont, S., Smith, P.M. et Troop, D.G. 1988. Archean lode gold deposit in Ontario. Ontario Geological Survey, Miscellaneous Paper 139, 136 p.

Couture, J-F., Pilote, P., Machado, N. et Desrochers, J-P. 1994. Timing of gold mineralization in the Val d'Or district, southern Abitibi belt: Evidence for two distinct mineralizing events. Economic Geology, 89: 1542-1551.

Cox, S.F., Etheridge, M.A. et Wall, V. J. 1990. Fluid pressure regimes and fluid dynamics during deformation of low-grade metamorphic terranes: implication for the genesis of the mesothermal gold deposits. Dans: Greenstone Gold and Crustal Evolution. Édité par F. Robert, P.A. Sheahan et S.B. Green. Association Géologique du Canada, p. 46-53.

Daigneault, R. et Archambault, G. 1990. Les grands couloirs de déformation de la sous-provinces de l'Abitibi. Dans: La ceinture polymétallique du Nord-Ouest québécois: synthèse de 60 ans d'exploration minière. Édité par M. Rive, P. Verpaelst, Y. Gagnon, J. M. Lulin, G. Riverin et A. Simard. CIM, Volume Spécial 43, p. 43-64.

Desrochers, J-P, Hubert, C. Ludden, J.N. ET Pilote, P. 1993. Accretion of Archean oceanic plateau fragments in the Abitibi greenstone belt, Canada. Geology, 21: 451-454.

Dubé, B., Dunning, G. et Lauzière, K. 1998. Geology of the Hope Brook Mine, Newfoundland, Canada: A preserved late Proterozoic high-sulfidation epithermal gold deposit and its implications for exploration. Economic Geology, 93: 405-436.

Eisenlohr, B.N., Groves, D.I. et Partington, G.A. 1989. Crustal-scale shear zones and their significance to Archaean gold mineralization in Western Australia. Mineralium Deposita, 24: 1-8.

Gaboury, D., Dubé, B., Laflèche, M.R. et Lauzière, K. 1996. Geology of the Hammer Down mesothermal gold deposit, Newfoundland Appalachians, Canada. Journal Canadien des Sciences de la Terre, 33: 335-350.

Groves, D.I. 1993. The crustal continuum model for Late-Archaean lode-gold deposits of the Yilgarn block, Western Australia. Mineralium Deposita, 28: 266-374.

Groves, D.I. et Phillips, G.N. 1987. The genesis and tectonic control on Archean gold deposits of the Western Australian Shield - a metamorphic replacement model. Ore Geology Reviews, 2: 287-322.

Groves, D.I., Barley, M.E. et Ho, S.E. 1989. Nature, genesis and tectonic setting of the mesothermal gold mineralization in the Yilgarn block, Western Australia. Dans: The Geology of Gold Deposit: The Perspective in 1988. Édité par R.R. Keays, W.R.H. Ramsay et D.I. Groves. Economic Geology, Monograph 6, p. 71-85.

Groves, D.I., Goldfarb, R.J., Gebre-Mariam, M., Hagemann, S.G. et Robert, F. 1998. Orogenic gold deposits: A proposed classification in the context of their crustal distribution and relationship to other gold deposit types. Ore Geology Reviews 13: 7-27.

Guha, J., Dubé, B., Pilote, P., Chown, E.H., Archambault, G. et Bouchard, G. 1988. Gold mineralization patterns in relation to the lithologic and tectonic evolution of the Chibougamau mining district, Quebec, Canada, Mineralium Deposita 23: 293-298.

Hannington, M.D., Poulsen, K.H., Thompson, J.F.H. et Sillitoe, R.H. 1997. Volcanogenic gold and epithermal-style mineralization in the VMS environment. Dans: Volcanogenic-associated massive sulfide deposits: Processes and examples in modern and ancient settings. Édité par: C.T. Barrie et M.D. Hannington. Association Géologique du Canada, Short Course Handbook 13, p. 183-214.

Heald, P., Hayba, D.O. et Foley, N.K. 1987. Comparative anatomy of volcanic-hosted epithermal deposits: acid-sulfate and adularia-sericite types. Economic Geology, 82: 1-26.

Hodgson, C.J. 1989. The structure of the shear-related, vein-type gold deposit: a review. Ore Geology Reviews, 4: 231-273.

Hodgson, C.J. 1991. An overview of the geological characteristics of gold deposits in the Abitibi Subprovince. Dans: Gold and Base Metal Mineralization in the Abitibi Subprovince, Canada, with emphasis on the Quebec segment. Édité par S.E. Ho, F. Robert et D.I. Groves. Université de Western Australia, publication 24, p. 63-94.

Hodgson, C.J. et Hamilton, J.V. 1988. Gold Mineralization in the Abitibi Greenstone Belt: End-Stage Result of Archean Collisional Tectonics ? Dans: The Geology of Gold Deposit: The Perspective in 1988. Édité par R.R. Keays, W.R.H. Ramsay et D.I. Groves. Economic Geology, Monograph 6, p. 86-100.

Kerrich, R. 1989. Geodynamic setting and hydraulic regimes: Shear zone hosted mesothermal gold deposits. Dans: Mineralization and shear zones. Édité par J.T. Bursnall. Association Géologique du Canada, Short Course Notes 6, p. 89-128.

Kerrich, R. 1990. Mesothermal gold deposits: a critique of genetic hypotheses. Dans: Greenstone Gold and Crustal Evolution. Édité par F. Robert, P.A. Sheahan et S.B. Green. Association Géologique du Canada, p. 13-31.

Kerrich, R. 1993. Perspective on genetic models for lode gold deposits. Mineralium deposita, 28: 362-365.

Kerrich, R. et Wyman, D. 1990a. Geodynamic setting of mesothermal gold deposits: An association with accretionary tectonic regimes. Geology, 18: 882-885.

Kerrich, R. et Wyman, D., 1990b, Late evolution of greenstone belts and gold deposits. Dans: Greenstone gold and crustal evolution. Édité par F. Robert, P.A. Sheahan and S.B. Green. Nuna Conference, Val d'Or. Association Géologique du Canada, p. 91-94.

Kerrich, R. et Feng, R. 1992. Archean geodynamics and the Abitibi-Pontiac collision: implication for advection of fluids at transpressive collisional boundaries and the origin of giant quartz vein systems. Earth Science Reviews 32: 33-60.

Kerrich, R. et Cassidy, K.F. 1994. Temporal relationships of lode gold mineralization to accretion, magmatism, metamorphism and deformation - Archean to present: A review. Ore Geology Reviews, 9: 263-310.

Kranidiotis, P, MacLean, W.H. 1987. Systematics of chlorite alteration at the Phelps Dodge massive sulfide deposit, Matagami, Quebec. Economic Geology, 82: 1898-1911.

Larsen, J.E. et Hutchinson, R.W. 1993. The Selbaie Zn-Cu-Ag deposits, Quebec, Canada: An example of evolution from subaqueous to subaerial volcanism and mineralization in an Archean caldera environment. Economic Geology, 88: 1460-1482.

Marquis, P., Brown, A.C., Hubert, C. et Rigg, D.M. 1990. Progressive alteration associated with auriferous massive sulfide bodies at the Dumagami mine, Abitibi greenstone belt, Québec. Economic Geology, 85: 746-764.

McKinstry, H.E. 1948. Mining Geology. Prentice-Hall inc., New York.

Morasse, S., Wasteneys, H. A., Cormier, M., Helmstaedt, H. et Mason, R. 1995. A pre-2686 Ma intrusion-related gold deposit at the Kiena mine, Val d'Or, Québec, Southern Abitibi Subprovince. Ecomonic Geology, 90: 1310-1321.

Mueller, W. et Donaldson, J. A. 1992. Development of sedimentary basins in the Archean Abitibi Belt, Canada: an overview. Journal Canadien des Sciences de la Terre, 29: 2249-2265.

Mueller, W. U., Daigneault, R., Mortensen, J. K. et Chown, E. H. 1996. Archean terrane docking : upper crust collision tectonics, Abitibi greenstone belt, Quebec, Canada. Tectonophysics, 265: 127-150.

Newhouse, W.H. 1942. Structural features associated with ore deposits described in this volume. Dans: Ore deposit as related to structural features. Édité par W.H. Newhouse. Princeton University Press, Princeton, N.J., p. 9-53.

Pearce, J. A. 1983. Role of the subcontinental lithosphere in magma genesis at active continental margins. Dans: Continental basalts and mantle xenoliths. Édité par: C. J. Hawkesworth et M. J. Norry. Shiva, Cheshire, United Kingdom, p. 230-249.

Penczak, R.S. 1998. Metamorphosed Archean epithermal Au-As-Sb-Zn-(Hg) vein mineralisation at the Campbell Mine, Northwestern Ontario – A reply. Economic Geology, 93: 685-688.

Penczak, R.S et Mason, R. 1997. Metamorphosed Archean epithermal Au-As-Sb-Zn-(Hg) vein mineralisation at the Campbell Mine, Northwestern Ontario. Economic Geology, 92: 696-719.

Poulsen, K.H. 1995. Gîtes d'or disséminé de remplacement. Dans: Géologie des types de gîtes minéraux du Canada. Édité par: O.R. Eckstrand, W.D. Sinclair et R.I. Thorpe. Commission Géologique du Canada, Géologie du Canada no 8, p. 423-434.

Robert, F. 1990. An overview of gold deposits in the Eastern Abitibi Subprovince. Dans: La ceinture polymétallique du Nord-Ouest Québécois: Synthèse de 60 ans d'exploration minière. Édité par: M. Rive, P. Verpaelst, Y. Gagnon, J. M. Lulin, G. Riverin et A. Simard. L'institut canadien des mines et de la métallurgie, Volume Spécial 43, p. 93-105.

Robert, F. 1991. Structural Setting and Control of Gold-Quartz Veins of the Val d'Or area, southeastern Abitibi Subprovince. Dans: Gold and Base Metal Mineralization in the

Abitibi Subprovince, Canada, with emphasis on the Quebec segment. Édité par S.E. Ho, F. Robert et D.I. Groves. Université de Western Australia, publication 24, p. 167-209.

Robert, F. et Brown, A. C. 1986a. Archean gold-bearing quartz veins at the Sigma Mine, Abitibi greenstone belt, Québec: Part I. Geologic relations and formation of the vein system. Economic Geology, 81: 578-592.

Robert, F. et Brown, A. C. 1986b. Archean gold-bearing quartz veins formation at the Sigma Mine, Abitibi greenstone belt, Québec: Part II. Vein paragenesis and hydrothermal alteration: Economic Geology, 81: 593-616.

Robert, F. et Poulsen, K.H. 1997. World-class Archaean gold deposits of Canada: An overview. Australian Journal of Earth Sciences, 44: 329-352.

Robert, F., Poulsen, K.H. et Dubé, B. 1997. Gold deposits and their geological classification. Dans: Proceedings of Exploration 97: Fourth Decennial International Conference on Mineral Exploration. Édité par A.G. Gubins, p. 209-220.

Sibson, R.H. 1990. Fault structure and mechanics in relation to greenstone gold deposits. Dans: Greenstone Gold and Crustal Evolution. Édité par F. Robert, P.A. Sheahan et S.B. Green. Association Géologique du Canada, p. 54-60.

Sibson, R. H., Robert, F. et Poulsen, K. H. 1988. High-angle reverses faults, fluid-pressure cycling and mesothermal gold-quartz deposits. Geology, 16: 551-555.

Sillitoe, R.H., Hannington, M.D. et Thompson, J.F.H. 1996. High sulfidation deposits in the volcanogenic massive sulfide environment. Economic Geology, 91: 204-212.

Simard, A. Gobeil, A., Verpaelst, P., Rive, M., Lacroix, S. et Racicot, D. 1990. Relationship between mineral deposits and geologic domains of the Abitibi volcano-plutonic belt of Northwestern Quebec. Dans: La ceinture polymétallique du Nord-Ouest Québécois: Synthèse de 60 ans d'exploration minière. Édité par: M. Rive, P. Verpaelst,

Y. Gagnon, J. M. Lulin, G. Riverin et A. Simard. L'institut canadien des mines et de la métallurgie, Volume spécial 43, p. 1-16.

Spooner, E.T.C. et Barrie, C.T. 1993. A Special issue devoted to Abitibi ore deposits in a modern context, preface. Economic Geology, 88: 1307-1322.

Stone, W.E. 1990. Archean volcanism and sedimentation at the Bousquet gold district, Abitibi greenstone belt, Quebec : implications for stratigraphy and gold concentration. Geological society of America Bulletin, 102: 147-158.

Tarnocai, C.A., Hattori, K. et Stubens, T.C. 1998. Metamorphosed Archean epithermal Au-As-Sb-Zn-(Hg) vein mineralisation at the Campbell Mine, Northwestern Ontario – A reply. Economic Geology, 93: 683-685.

Tourigny, G., Brown, A.C., Hubert, C. et Crépaux, R. 1989. Synvolcanic and syntectonic gold mineralization at the Bousquet mine, Abitibi greenstone belt. Economic Geology, 84: 1875-1890.

Tourigny, G., Doucet, D. et Bourget, A. 1993. Geology of the Bousquet 2 mine: An example of a deformed, gold-bearing polymetallic sulfide deposit. Economic Geology, 88: 1578-1597.

White, N.C., Leake, M. J., McCaughey, S.N. et Parris, B.W. 1995. Epithermal gold deposits of the southwest Pacific. Journal of Geochemical Exploration, 54: 87-136.

Winchester, J. A. et Floyd, P. A. 1977. Geochemical discrimination of different magma series and their differentiation products using immobile elements. Chemical Geology, 20: 325-343.

Wood, S.A. 1987. Application of a multiphase ore mineral solubility experiment to the separation of base metal and gold mineralization in Archean greenstone terrains. Economic Geology, 82: 1044-1048.

CHAPITRE 2

An Archean volcanic-related gold-sulfide-quartz vein orebody: the Géant Dormant mine, Abitibi Subprovince, Quebec, Canada

Ce chapitre représente la version intégrale d'un article publié en 1996 dans le Journal *Exploration and Mining Geology*, Volume 5, page 197-213, par Gaboury, Daigneault, Tourigny et Gobeil.

Abstract

The Géant Dormant gold deposit is located within the Northern Volcanic Zone of the Archean Abitibi Subprovince. Gold-bearing lenses are hosted by an E-W trending, steeply south-dipping and south-facing homoclinal volcano-sedimentary succession and an intrusive felsic complex (dacitic intrusion and swarms of FP and QFP dikes). All these rock units and gold-bearing lenses are cut by hornblende-rich mafic dikes. The bulk ductile deformation is weak, heterogeneous and dominated by a subvertical elongation. It is characterized by a planar fabric containing a steeply plunging mineral stretching lineation that affects all rock types. Gold mineralization occurs in four cogenetic styles that are rich in base-metal sulfides: (1) narrow quartz veins, which are economically most important, (2) stratabound ore within sedimentary horizons, (3) quartz veining within QFP dikes, and (4) quartz veinlet arrays. Ore controls correspond to primary permeable features such as: (1) stratigraphic contacts, (2) specific lithological units, (3) synvolcanic faults and (4) preexisting joints. The geometry of the orebody displays an increasing complexity toward the south, i.e., toward the paleosurface.

A pre-deformational origin for the gold mineralization is indicated by (1) the lack of structural compatibility between features of the orebody and ductile deformation, (2) the systematic overprinting of the gold mineralization by structural elements, and (3) the systematic crosscutting of gold mineralization by foliated hornblende-rich mafic dikes. A volcanic-related origin for the gold mineralization is supported by (1) the primary nature of the ore controls, (2) the selectively altered and mineralized QFP dikes, and (3) the increase in geometrical complexity of the orebody toward the paleosurface. The interpreted volcanic-related origin contrasts with typical shear-related models of Archean gold mineralization, and opens up the potential for locating comparable gold-quartz vein deposits in strain-free parts of Archean greenstone belts, which have been generally considered as infertile gold areas.

Résumé

La mine Géant Dormant est un dépôt aurifère filonien situé dans la Zone Volcanique Nord de la Sous-province de l'Abitibi. La minéralisation est encaissée dans une séquence homoclinale normale, composée de strates volcano-sédimentaires recoupées par un complexe felsique (intrusion dacitique, essaim de dykes felsiques de FP et de QFP). Les couches s'orientent E-W et sont fortement inclinées vers le sud. Des dykes mafiques à hornblende recoupent toutes les unités lithologiques, ainsi que les lentilles aurifères. La déformation régionale à caractère ductile est faible et hétérogène. Elle affecte toutes les unités lithologiques. Elle est dominée par une élongation subverticale qui se manifeste principalement par une schistosité contenant des linéations d'étirement également subverticales. Quatre styles de minéralisations cogénétiques et riches en sulfures sont reconnus: (1) les veines de quartz, (2) un style stratoïde, (3) des stockwerks de veinules développés au sein des dykes felsiques de QFP et (4) des familles de veinules SE-NW. Les facteurs de contrôle sur la minéralisation correspondent à des perméabilités primaires, telles que: (1) les unités lithologiques spécifiques, (2) les contacts stratigraphiques, (3) les failles synvolcaniques, et (4) les joints préexistants. À l'échelle du dépôt, la géométrie du corps minéralisé devient plus complexe vers le sud, soit vers la paléosurface.

Une minéralisation pré-déformation est indiquée par: (1) l'absence de compatibilité structurale entre le corps minéralisé et la déformation ductile, (2) la superposition systématique de la déformation sur la minéralisation, et (3) le recoupement systématique de la minéralisation par les dykes à hornblende schistosés. Une origine reliée au volcanisme est proposée sur la base de: (1) la nature primaire des facteurs de contrôle, (2) l'altération et la minéralisation sélectives des dykes de QFP, et (3) l'augmentation de la complexité du corps minéralisé vers la paléosurface. Cette origine contraste par rapport aux minéralisations aurifères filoniennes synorogéniques. L'exemple du Géant Dormant démontre le potentiel aurifère des secteurs faiblement déformés au sein des ceintures de roches vertes archéennes.

INTRODUCTION

Archean greenstone belts are renowned for their shear-related quartz vein gold deposits. Recent work (e.g., Colvine, 1989; Groves et al., 1989; Kerrich and Wyman, 1990a) has emphasized recurring characteristics among the gold deposits, including (1) distribution along transcrustal faults, (2) structurally controlled ore, (3) low base metal and high Au/Ag contents, (4) late- to syn-orogenic timing, and (5) CO_2-rich mineralizing fluids. Based on these features, it has been proposed that the shear-related gold deposits constitute a single, coherent group that results from a singular and common genetic process related to accretionary tectonism (Kerrich and Wyman, 1990a; Kerrich and Cassidy, 1994).

In the Abitibi belt, gold also occurs in various other types of deposits (descriptive and genetic basis), including: (1) pyritic gold (e.g., Tourigny et al., 1989; 1993; Marquis et al., 1990; Robert, 1990a), (2) stratabound, sub-seafloor related (Chartrand, 1989), (3) epithermal Cu-Zn-Pb-Ag-Au (Larson and Hutchinson, 1993), (4) porphyry Cu-Mo-Au (Pilote et al., 1994; 1995; Sinclair et al., 1994; Kirkham et al., 1995), (5) intrusion-related (Magnan et al., 1995; Morasse et al., 1995), and (6) volcanogenic massive sulfide deposits (e.g., Chartrand and Cattalani, 1990). Clearly, in the Abitibi belt, gold has been concentrated by a variety of processes related to volcanism, magmatism, metamorphism and deformation, and shows relations with host rocks which range from synvolcanic to late-orogenic.

However, relative to recent volcanic terrains, Archean analogs of volcanic-related gold-bearing quartz vein mineralization within the Abitibi and other belts are considered scarce (e.g., Kerrich and Wyman, 1990b). Consequently, quartz vein gold occurrences in Archean terrains are generally regarded as shear-related gold mineralization. Therefore, gold exploration is still focused towards highly deformed areas adjacent to crustal faults.

The Géant Dormant (Sleeping Giant) mine is a gold-bearing quartz vein deposit located within the central part of the Archean Abitibi Subprovince, and away from known auriferous crustal-scale faults. This deposit shows many similarities to Archean shear-related gold deposits with regard to the host rocks, the metamorphic facies and the ore styles. However, the geometry of the orebody and the metal and mineral characteristics of the gold mineralization are different. A metallogenic and structural study of the mineralized lenses and surrounding rocks was undertaken in order to characterize the geological setting. Data were collected by detailed mapping and sampling of the mined and active stopes, drifts and crosscuts within the mine on levels 55, 100, 145, 190, 235, 295, 355 and 415. The aim of this paper is to describe the geological and structural setting and the characteristics of the gold ore in order to establish the relative timing of the mineralization with respect to the ductile deformation. Special emphasis is given to orebody geometry and ore control in order to ascertain the origin of the gold mineralization, which in turn has implications for exploration.

LOCATION AND HISTORY

The Géant Dormant deposit is in northwestern Québec, midway between Matagami to the north and Amos to the south (Fig. 1). The first gold occurrence in the area was discovered in 1976 by Mattagami Lake (Noranda Ltd). In May 1988, commercial underground exploitation of the deposit started, but operations were suspended in May 1991 as the mineable reserves were exhausted. During this period 494 000 tonnes of ore were mined by Aurizon Mines, yielding 96 611 oz of gold (3 005 kg) and 120 590 oz of silver (3750 kg) (*The Mining Magazine*, February 1995). In July of 1993, commercial production at the mine was resumed following an ore definition program. Cambior Inc. is the present operator of the mine under a joint venture with Aurizon Mines. At the time of

writing, production had attained 337 000 tonnes at 11.0 g/t Au, with reserves in all categories evaluated at 626 000 tonnes at 10.5 g/t Au.

REGIONAL GEOLOGICAL SETTING

The Géant Dormant deposit is hosted within the first volcanic cycle of the Northern Volcanic Zone of the Archean Abitibi Subprovince (Chown et al., 1992). The cycle corresponds to an extensive subaqueous basalt plain with scattered felsic volcanic edifices, interstratified with or overlain by volcaniclastic assemblages. The 1 to 3 km thick basaltic assemblage (Chown et al., 1992) is dominantly composed of tholeiitic massive, pillowed and breccia volcanic rocks (Picard and Piboule, 1986), with minor chert, iron formation and volcaniclastic rocks (Mueller and Donaldson, 1992; Pilote, 1989). U-Pb dating of felsic centres in the middle to the upper part of the first volcanic cycle indicate a time interval of 2730-2720 Ma (Mortensen, 1993). The Northern Volcanic Zone is interpreted as a coherent assemblage, initially formed from a diffuse and immature arc (Chown et al., 1992).

The Northern Volcanic Zone was affected by a N-S shortening event from 2708 to 2685 Ma; this comprised a succession of several tectonic pulses of continuous deformation (Chown et al., 1992). The main deformational features are (1) E-W trending, subvertical, regional folds with an axial planar fabric, (2) major E-W trending, 1 to 4 km wide reverse deformation zones of regional extent, and (3) dextral, 1 to 5 km wide, NW-SE trending deformation zones.

At a district-scale, three voluminous synvolcanic and polyphase (diorite-tonalite-leucotonalite) plutons (Chown et al., 1992) are responsible for the disturbed regional structural trend (Fig. 1). The mine is located close to the centre of a triple junction zone of the structural trend (Daigneault and Archambault, 1990). Other important features of the

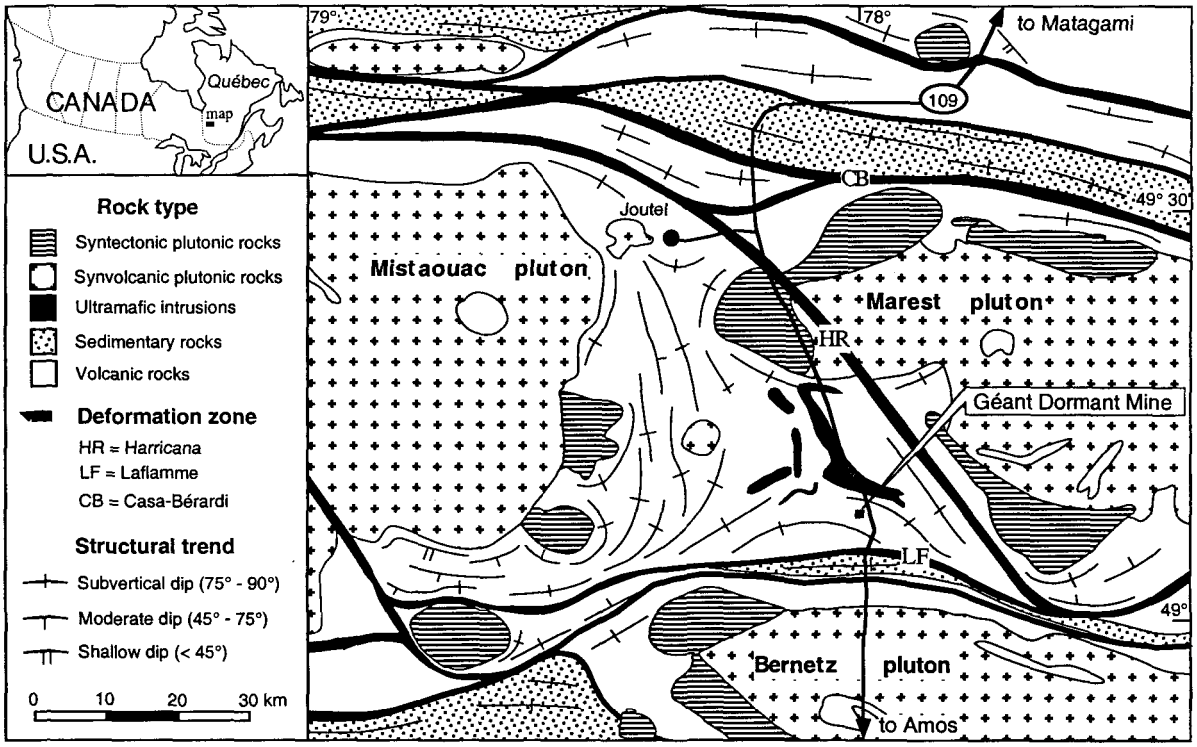

Figure 1. Simplified geological map of the mine district showing the location of the Géant Dormant gold deposit close to the central part of a triple junction of structural trends. Map modified from Hocq (1990) and Chown et al. (1992).

area include the E-W trending Laflamme fault and the NW-SE trending Harricana fault (Fig. 1).

GEOLOGY OF THE MINE

The mine sequence is represented by a volcano-sedimentary succession which is intruded by a felsic complex and transected by late hornblende-rich dikes. Strata strike predominantly E-W and dip steeply to the south, forming a single homoclinal stratigraphic succession (Figs. 2a, 2b). All the rock types have been metamorphosed to greenschist facies, but the prefix "meta" is omitted below to simplify the rock nomenclatures.

Volcano-sedimentary succession

The volcano-sedimentary succession comprises, from north to south, a basaltic flow unit which is overlain by sedimentary rocks with a swarm of intercalated mafic sills. The basaltic flow, the lowest stratigraphic unit exposed within the mine (Fig. 2), exhibits a southward succession of massive, pillowed and pillow breccia which, together with well-preserved pillow configurations, indicate younging to the south. Sedimentary horizons, enclosed between two mafic sills, range in thickness from a few cm to 10 m, with an average of 2 m. Sedimentary rocks consist of fine-grained volcaniclastite, chert and oxide-sulfide facies iron formation. Local flame textures and graded bedding indicate southward younging of the sedimentary succession as well. Mafic sills, 1 to 100 m in thickness, are an ubiquitous feature in the mine environment. They are aphanitic to medium-grained and locally plagioclase-phyric. South of the dacitic body (see below), four main mafic sills of great lateral and vertical continuity are well delineated, whereas the mafic sill swarm is more heterogeneous in the northern part (Figs. 2a, 2c). The mafic rocks have a tholeiitic

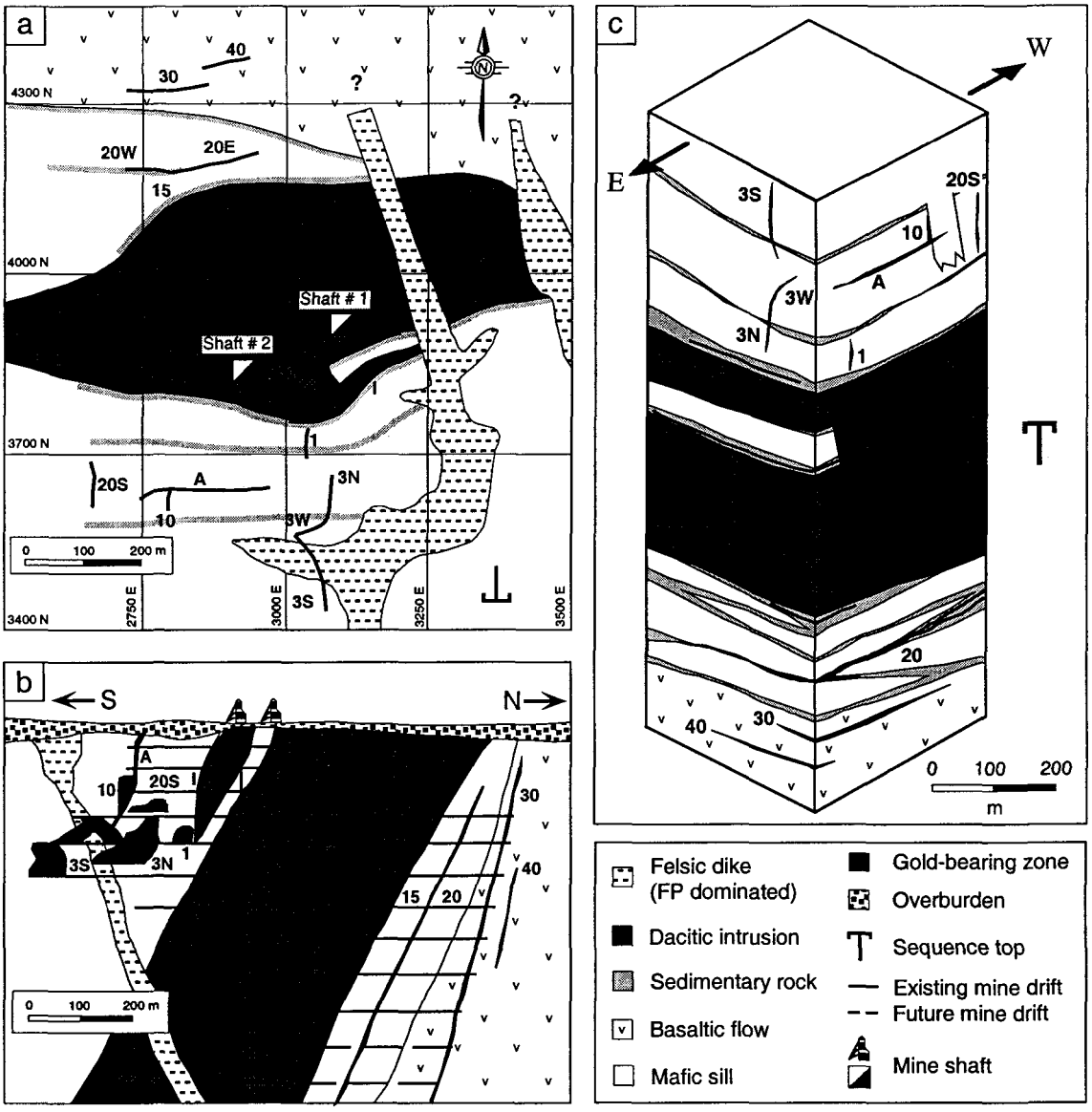

Figure 2. Characteristics of the mine sequence. (a) Simplified geological plan of the Géant Dormant mine area. (b) Idealized vertical N-S cross section. (c) Schematic stratigraphic block. Various gold-bearing zones are labelled: A, 10, 40, etc. Figures a and b modified form maps of Cambior Inc.

geochemical signature (Gaboury, et al., 1998) which is typical of the first volcanic cycle (Picard and Piboule, 1986).

Felsic intrusive complex

The central dacitic body (Fig. 2) and a swarm of felsic porphyry dikes constitute the felsic intrusive complex. The dacite is aphanitic and homogeneous, and forms a 400 m-wide lenticular body injected subconformably into the mafic sill swarm (Fig. 2). Felsic porphyry dikes crosscut both the volcano-sedimentary succession and the dacitic intrusion. Dikes are divided into two main groups on the basis of phenocryst contents: the plagioclase-phyric dikes (FP) and the quartz and plagioclase-phyric dikes (QFP). The QFP dikes systematically crosscut the FP dikes and form tabular injections, whereas the latter are more irregular. The QFP dikes are oriented mainly SE-NW and dip steeply to the NE. Individual dikes are mostly less that 4 m wide; wider dikes are generally composite intrusions of FP and QFP. The dacite and felsic dikes have calc-alkaline geochemical signatures (Gaboury, et al., 1998) which are comparable with those of synvolcanic felsic rocks of group FII (Lesher et al., 1986) and group II (Barrie et al., 1993) from the Abitibi Subprovince.

Late hornblende-rich dikes

Fine- to coarse-grained mafic dikes, containing 40 to 60% euhedral hornblende phenocrysts, are ubiquitous throughout the mine. These dikes (< 5 m wide) crosscut all the previous rock types including the gold-bearing lenses. They display variable attitudes (Fig. 3a), well-developed chilled margins and step-shaped contacts. The shoshonitic geochemical signature of these dikes (Gaboury, et al., 1998) is similar to that of Archean

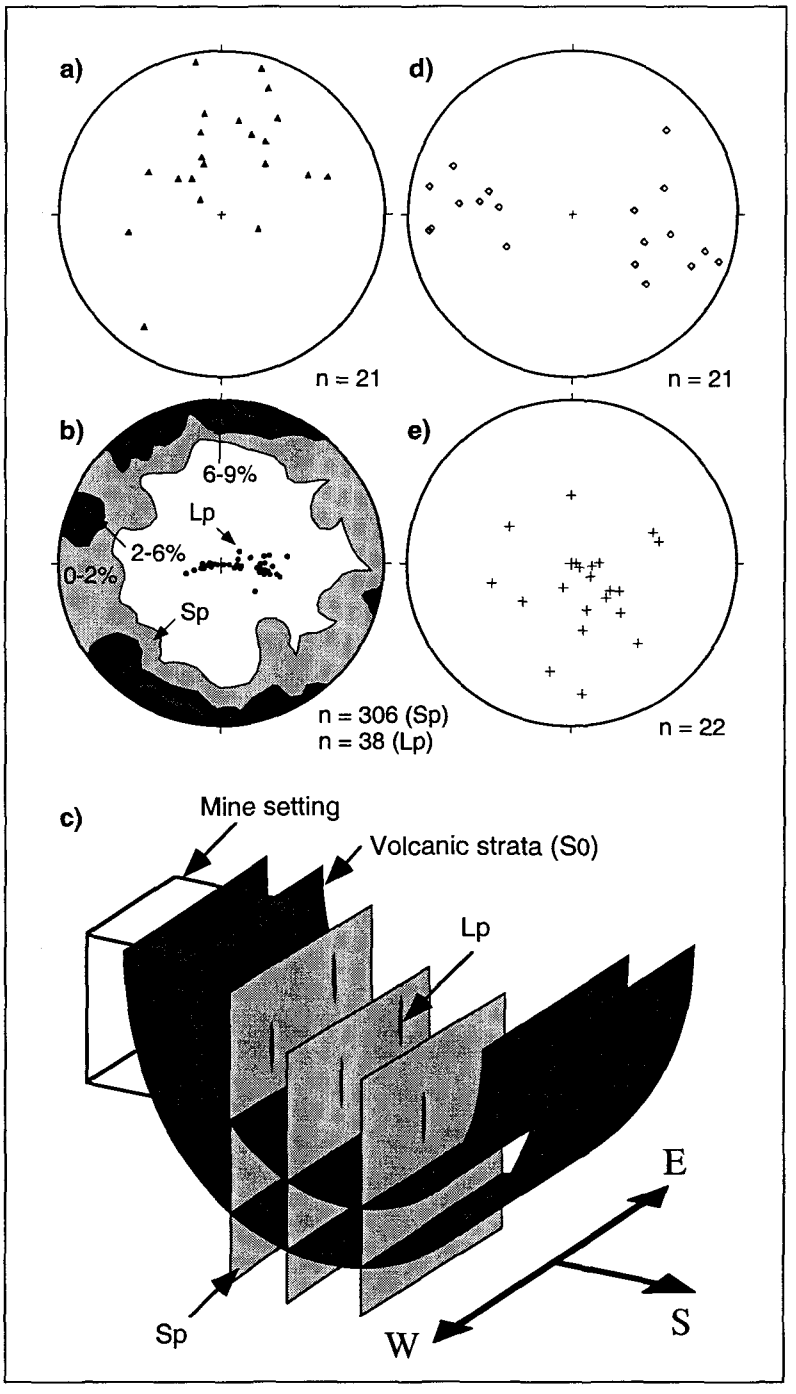

Figure 3. Structural features of the deposit. (a) Equal area projections (lower hemisphere) of Sp planar fabric and Lp stretching lineation. (b) Schematic structural setting of the deposit.

lamprophyres (Wyman and Kerrich, 1993) and late shoshonitic volcanic rocks of the Chibougamau area (Dostal and Mueller, 1992).

STRUCTURAL GEOLOGY

Deformation affecting the host rocks is expressed by (1) the subvertical attitude of the volcanic strata, (2) the development of ductile planar and linear elements, (3) local mesoscopic folds, and (4) subhorizontal extensional calcite veinlets. These features are related to the regional deformation event. Subsequent deformation includes local shear zones and late brittle faults.

Planar and linear elements

A planar fabric, referred to as Sp (for principal surface), affects all rock types, including the hornblende-rich dikes. The Sp fabric is commonly well-developed within the sedimentary horizons, where it is defined by the alignment of phyllosilicates (chlorite and sericite). In other rock types, its intensity is commonly weak. The mafic sills, which host many gold-bearing veins, display generally well-preserved gabbroic textures and lack a planar fabric, implying that the primary features are well-preserved. The Sp fabric strikes predominantly E-W with a subvertical dip (Fig. 3b). Variations of the Sp orientation are common as illustrated by the density contour (0-2%) along the equatorial plane of the stereoplot (Fig. 3b). This distribution does not represent a combination of different fabrics, since no crosscutting relationship was observed either underground or in thin section. Furthermore, the consistency of the geometric relationships throughout the mine is incompatible with polyphase deformation. Instead, progressive changes in orientation are observed and are related to competency contrasts induced by felsic dikes, and, in some cases, by gold-bearing lenses. Therefore, the internal deformation within the tilted

sequence is weak and heterogeneous, i.e., mainly concentrated within the sedimentary horizons and in some places along lithological contacts.

A weak to moderately developed stretching lineation (Lp), defined by mineral elongation, is associated with the Sp planar fabric. Stretching lineation distribution shows a dominant vertical plunge (Fig. 3b) despite variations of the Sp direction. Subhorizontal and planar extensional veinlets (< 1 cm) of calcite, developed within the more strained rocks, are structurally compatible with the stretching lineations. All the characteristics of the planar and linear elements imply that the ductile deformation was dominated by a vertical elongation.

Folds

In vertical cross sections, the subvertical Sp planar fabric and the steeply south-dipping sedimentary bedding (So) define a 10-30° angular relationship. This indicates that the host sequence is on the northern limb of a regional syncline, considering the southward-younging direction of the sequence (Fig. 3c). Subhorizontal E-W intersection lineations between the So and Sp surfaces indicate an E-W trending, shallow plunging fold axis (Fig. 3d). The amplitude of the fold is unknown. Mesoscopic folds are also developed locally within the sedimentary horizons. They exhibit irregular geometry from open to tight closure, with variable fold axis attitudes (Fig. 3e). As these folds occur in both foliated and unfoliated sedimentary horizons, they are best explained as slump structures, locally accentuated by ductile deformation.

Shear zones and late faults

Some NW-SE striking brittle-ductile shear zones (< 2 m thick) with a moderate to steep dip to the NE, crosscut all the rock types, the gold-bearing lenses and the structural

elements related to the regional folding. The sense of movement is dominantly reverse as established by S-C relationships (Berthé et al., 1979), as well as by cm-scale offsets of local markers. Late brittle faults, with apparent cm- to m-scale offset, were also mapped. These shears and faults are sparsely distributed and have only a minor influence on the geometry of the orebody.

GOLD MINERALIZATION

Ore styles

Styles of gold mineralization described below include: (1) gold-bearing veins (economically most important), (2) stratabound ore, (3) SE-NW veinlet arrays, and (4) veining within the QFP dikes. The last two styles are uneconomic, but they are significant in establishing the controls and timing of the gold mineralization.

Gold-bearing veins

Gold-sulfide-quartz veins are generally massive and range from a few cm to 2 m thick (average of 50 cm for the mined veins). The veins are rich in gold with assays commonly > 100 g/t Au (Unpubl. data, Cambior Inc). The vein contacts range from sharp, planar and free of surrounding planar fabric (Fig. 4a), to undulose and schistose. Branching of main veins is a common phenomenon (Fig. 5a) but does not show consistent attitudes. Veins terminate laterally through pinching out or arborescent multi-branching veinlets (Fig. 5b).

Stratabound ore

Stratabound ore corresponds to gold-bearing segments of sedimentary horizons, where mineralization exhibits three main different modes of occurrence: (1)

Figure 4. Photographs showing ore-related features. (a) Typical quartz-sulfide gold-bearing vein hosted within mafic sill, with sharp contacts, high sulfide content and quartz crystals oriented perpendicular to the margin walls. Rock slab from zone 3W, level 235. (b) Concordant, parallel layers of massive sulfides within sedimentary horizon. Zone 20W, level 355. (c) Veining (dark material) and intense sericitic alteration within QFP felsic dike. (d) Dismembered quartz-sulfide-gold-bearing vein (dark material) hosted within foliated QFP dike, yielding apparent shear-related vein relationships. Zone 3S, level 235.

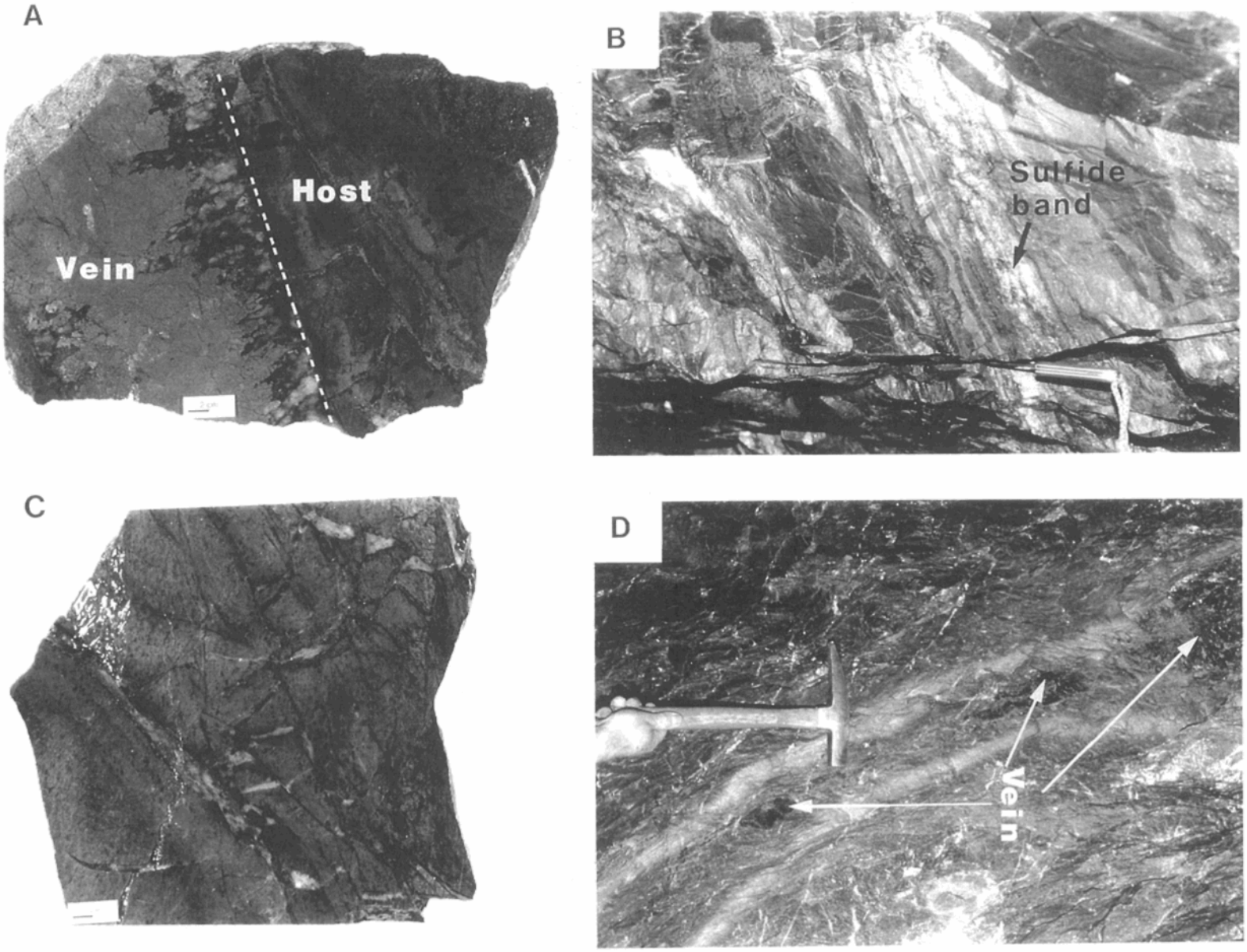
A
Host
Vein
B
Sulfide
band
C
D
Vein

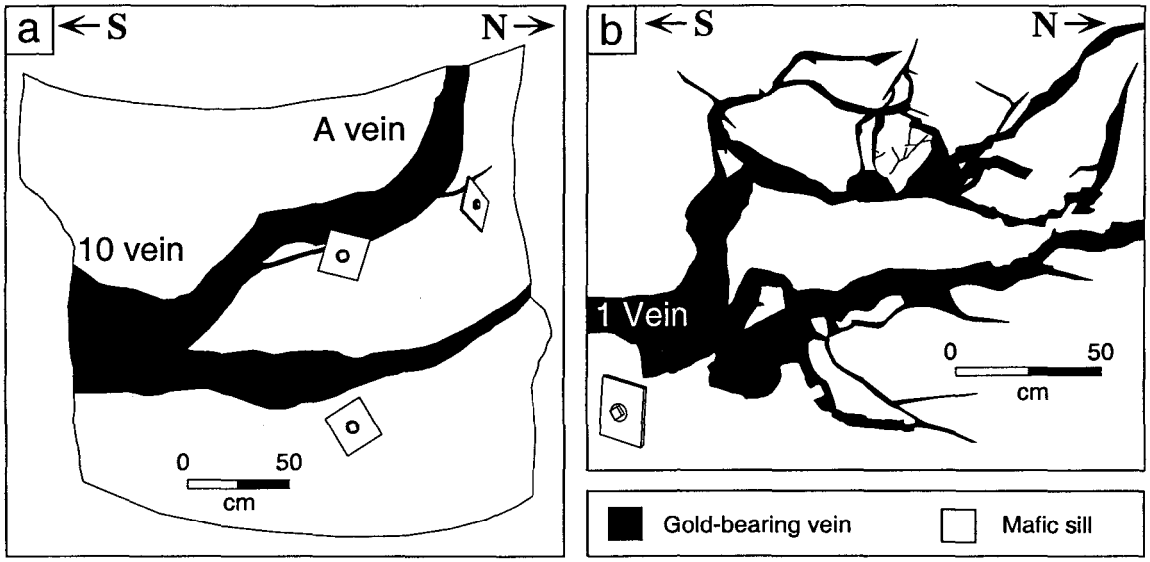

Figure 5. Sketches of vein geometry from photographs. (a) Branching of veins defining the junction between the E-W-striking, steeply south-dipping A vein and the N-S-striking, shallowly east-dipping 10 vein. Vertical view of the pillar separating the A and the 10 stopes, level 145. (b) Lateral vein termination showing arborescent multi-branching veinlets. Vertical view of the northern termination of the N-S-striking, shallowly east-dipping 1 vein, level 235.

subconcordant, mm- to cm-wide quartz-sulfide veinlets (the most common form), (2) concordant, parallel layers of massive sulfides, and (3) disseminated sulfides, mainly pyrrhotite, pyrite and marcasite, with minor chalcopyrite and sphalerite. The sulfide layers are a few mm thick and are mainly composed of pyrrhotite and pyrite, with lesser chalcopyrite and sphalerite (Fig. 4b). In thin section, remnant magnetite grains and pseudomorphs suggest that the sulfide layers, and in part the disseminated sulfides, formed by hydrothermal replacement of magnetite iron-formation. Mineralization occurrences are related both to the compositional (e.g., magnetite and silica contents) and rheological characteristics (e.g., bedding attribute and competency contrast between individual beds) of the sedimentary horizons, and the relative proportions of which are variable. Some sulfide layers were mapped as the lateral termination of subconcordant quartz-sulfide veinlets (Fig. 6). High grade gold mineralization (>100 g/t Au) is restricted to the narrow quartz-sulfide veinlets and sulfide layers.

SE-NW veinlet arrays

Arrays of gold-bearing veinlets occur in close spatial association with the gold-bearing veins hosted by mafic sills. These 1 to 4 cm-wide quartz-sulfide veinlets strike consistently SE-NW and dip steeply to the NE, parallel to the QFP dikes (Fig. 6). Individual veinlets are planar and exhibit a regular distribution, with spacings of 1 to 2 m. The SE-NW veinlets generally have a consistent width, but some are boudinaged in vertical section. The grade of the veinlets ranges from 1 to 10 g/t Au.

Veining within the QFP dikes

This style of mineralization occurs solely within the QFP felsic dike group, where it forms multiple, mm-wide quartz and sulfide veinlets and disseminated auriferous pyrite.

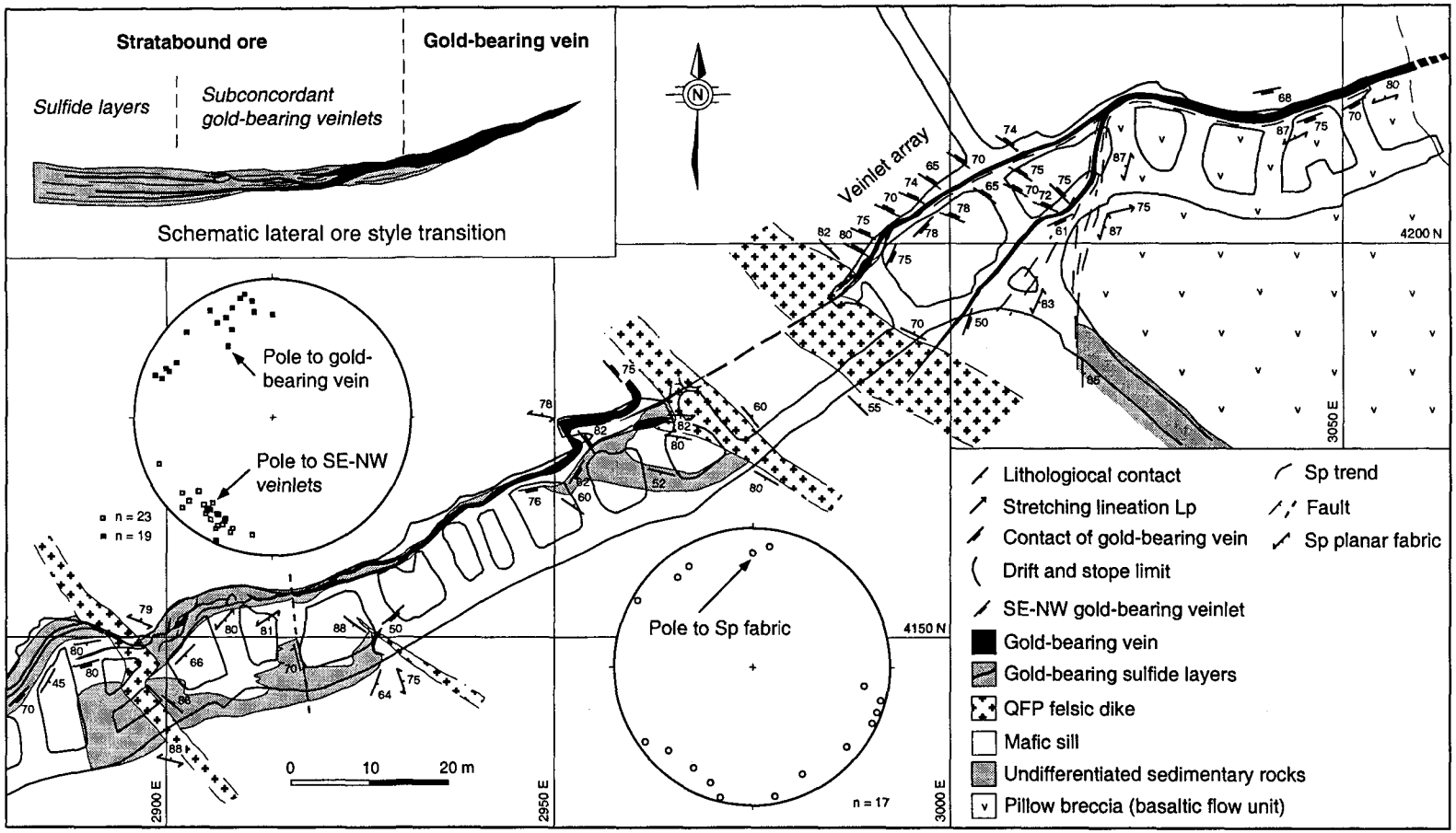

Figure 6. Detailed geological map of the entire 20E-20W zone at level 355, showing the lateral variation of the ore styles, structural elements, gold-bearing SE-NW veinlet array, and equal area projections of structural data (lower hemisphere). Inset shows schematic progressive ore style transition from east to west, and change of mineralization occurrences from quartz-sulfide veinlets to sulfide layers within the stratabound ore at the western end of the zone.

Crosscutting relationships indicate episodic veining injections within the dikes (Fig. 4c). Mineralization within the QFP dikes is a mine-scale phenomenon, but it is best developed in close spatial association with the gold-bearing veins. Systematic assays have revealed erratic gold grades ranging from nil to hundreds of g/t Au.

Vein and veinlet material

Veins and veinlets forming the different styles of gold mineralization share the same mineralogy, and there is no evidence for deposit-scale mineralogical zoning. Gangue minerals are dominated by gray quartz with minor amounts (< 2%) of calcite, chlorite and sericite. In some parts of the gold-bearing veins, milky quartz is abundant and forms subparallel bands ranging in thickness from 1 to 5 cm. These bands are superimposed on the massive gray quartz and are interpreted as evidence of multi-stage vein infilling. The amount of sulfide ranges from 5% (disseminated) to 80% (massive), with an average of 25%. The sulfide assemblage is composed mainly of pyrite and pyrrhotite, with lesser amounts of chalcopyrite and sphalerite and traces of galena and arsenopyrite. In addition to the base metals Cu, $Zn_{,}$, Pb, veins contain lesser amounts of As, Ag, Au and Hg, with an Au/Ag ratio ~ 0.5 (Table 1). Gold, as observed in polished thin section, occurs mainly as μm-scale inclusions in sulfides (pyrite, chalcopyrite, sphalerite and pyrrhotite) and in smaller amounts as fine fracture fillings in pyrite.

Textures of the veins and veinlets

The gangue has a mainly massive texture due to interlocking of fine- to coarse-grained anhedral quartz grains. Comb-texture, defined by quartz crystals oriented perpendicular to the vein walls, is also common for the gold-bearing veins irrespective of their attitude (Fig. 4a), and is the dominant texture of the SE-NW veinlets. This texture

Table 1. Metallic composition of representative mined and crushed ore

Cu	0.36 %	**Au**	9.7 g/t
Zn	0.13 %	**Ag**	21.0 g/t
As	60 g/t	**Hg**	0.24 g/t

Values determined by the Centre de Recherches Minérales (CRM) from a composite sample of vein and stratabound ore styles.

indicates open space filling (e.g., Dowling and Morrison, 1989). The sulfide assemblage within the gold-bearing veins displays three main mesoscopic textures: (1) net texture, where sulfides surround mm-scale quartz crystals, (2) massive cm-scale lenses within the quartz matrix, and (3) mm-thick bands of massive sulfides along the vein contacts.

Wallrock alteration

Most gold-bearing veins lack visible wallrock alteration. Where developed, alteration defines an irregular mm-scale envelop of sericite and/or chlorite at the contact between the vein and the host rock. Mineralized QFP felsic dikes are affected by intense and pervasive sericitic alteration. The QFP dikes are preferentially sericitized relative to the surrounding wallrock; this alteration phenomenon is developed at the deposit scale. The SE-NW veinlets have margins characterized by a 1-2 cm wide band of chloritic alteration in which a subvertical planar fabric (Sp) is generally well-developed. No significant visible alteration occurs in association with the stratabound ore style.

Geometry of the orebody

Gold mineralization with economic potential is mainly restricted to the volcano-sedimentary succession bounding the dacitic intrusion (Figs. 2a, 2b). At the mine-scale, mineralized zones are scattered within a 1 km^2 surface area (Fig. 2a). Physical characteristics of the mineralized zones are summarized in Table 2.

For the gold-bearing veins, there is a substantial difference in attitude and size depending on their position relative to the dacitic intrusion (Table 2). North of the dacitic intrusion, the veins strike mainly E-W with a steep dip (> 75°) to the south. Their lateral extent ranges from 100 to 200 m with a vertical extent in excess of 700 m, yielding a ratio (lateral/vertical) of about 1:7 (Figs. 2a, 2b). South of the dacitic intrusion, the vein

Table 2. Characteristics of different ore styles relative to the dacitic intrusion.

Geographic position relative to the dacitic intrusion		Ore style	Strike and dip	Size (lateral x vertical)*	Ore control	Example
	South	Gold-bearing vein	N-S with 45° E dip	100-200 m x 200-300 m	Fault and polygonal joint array	20S, 10, 1, 3
			E-W with 85° S dip	50-100 m x 100-150 m		A, NW
			NW-SE with 50° NE dip	75 m x 75 m		3S
			SW-NE with 40° SE dip	75 m x > 100 m		3W
	North	Gold-bearing vein	E-W with > 75° S dip	150 m x > 700 m	Stratigraphic contact	20E
					Synvolcanic fault	30, 40
	Both North and South	Stratabound	E-W with 75° S dip	100-200 m x 400 m	Lithological unit	H, I, 15, 20W
		Veinlet arrays	SE-NW with 75° NE dip	> 10 m x > 10 m	Fracture	Uneconomic
		Multiple veining	QFP felsic dike attitude: SE-NW with 75° NE dip	Unknown extent within dikes	Complex fracturing in a specific rock type	Uneconomic

* Measured on longitudinal sections parallel to gold-bearing zones

geometry is more complex with four main sets of gold-bearing veins (Table 2 and Fig. 7). Some of these veins display a progressive change in attitude, and interbranch with other vein sets (Fig. 7). Overall, these veins have smaller dimensions, ranging from 50 to 200 m in both lateral and vertical extent (Figs. 2a, 2b, 7), yielding a ratio close to 1:1. Stratabound ore, SE-NW veinlet arrays and mineralized QFP dikes also occur on both sides of the dacitic intrusion, but there is no significant variation in size and attitude relative to their position at the mine-scale (Table 2).

Relationships between ore styles

Although there are different sets of gold-bearing veins, all the veins have the same mineralogical composition. Branching and merging between different sets of gold-bearing veins is also observed (Figs. 5a, 7) indicating that these veins, regardless of their attitude, result from the same mineralizing episode. As the different ore styles share the same gangue and sulfide content, and relative proportion, a common origin can be proposed for all ore styles. Furthermore, observed transitions from gold-bearing veins to stratabound ore are also consistent with a single, albeit prolonged and episodic, mineralizing system. In the case of the H and NW zones, the lateral transition in ore style is sharp and coincides with the intrusive contact of the dacitic body (Fig. 2a). In the case of the 20W and 20E zones, the transition from a single gold-bearing vein to the stratabound ore is progressive (Fig. 6).

ORE CONTROLS

Four main types of ore controls have been established and are detailed below: (1) lithological units, (2) stratigraphic contacts, (3) synvolcanic faults, and (4) preexisting joints. At the deposit scale, a specific distribution of the types of ore controls was also recognized (Table 2). North of the dacitic intrusion, stratigraphic contacts and faults are the

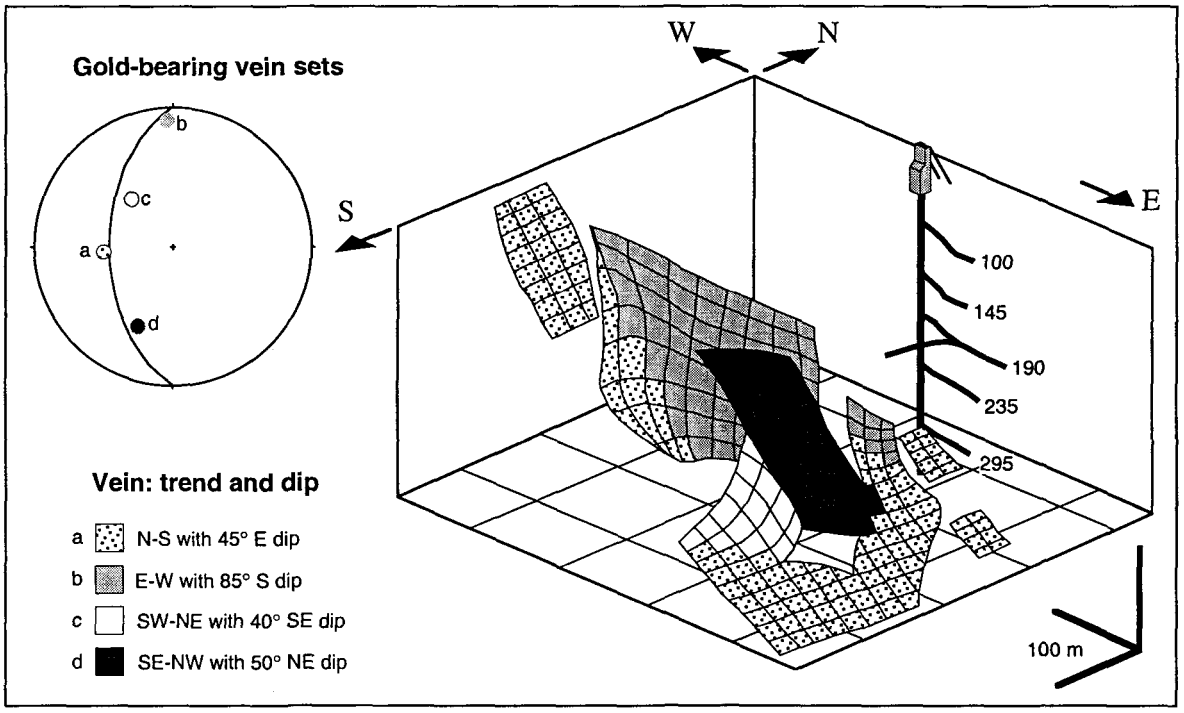

Figure 7. 3D projection of the gold-bearing vein network, south of the dacitic intrusion. Note the cylindrical distribution of poles to the main gold-bearing vein sets on the stereoplot, which is compatible with the polygonal joints (Fig. 9).

dominant ore controls whereas in the south, fractures in mafic sills control the vein emplacement.

Lithological units

Stratabound ore represents an unequivocal example of lithological ore control. Subconcordant gold-bearing veinlets and the sulfide replacement layers involve focusing of the mineralizing fluid by bedding-controlled permeabilities within the sedimentary horizons. The veining in the QFP dikes is another example of gold mineralization controlled by a specific rock type.

Stratigraphic contacts

Lateral and vertical transition of ore styles is a ubiquitous feature of mineralized zones controlled by the stratigraphic contacts. Throughout the mapped stopes, mineralization is in some parts stratabound and in other parts vein-dominated. This transition in ore style depends mostly on the presence or absence of sedimentary lenses at the boundary of the mafic sills. Several vein branches and mineralized sedimentary horizons (stratabound ore) emerging from the main zone were also mapped, implying that mineralizing fluids were focused within the heterogeneous volcano-sedimentary sequence by discontinuities with higher permeability. The 20W-20E zone exhibits typical features of stratigraphic control (Fig. 6). At the eastern end of the stope, a gold-bearing vein occurs at the interface between a mafic sill and a pillow breccia. In the central part, the vein style progressively changes to stratabound ore toward the west as sedimentary lenses appear and become wider and more continuous.

Synvolcanic faults

The 30 zone, which occurs 50 m north of the 20W-20E zone (Fig. 2a), is the best example of fault-controlled, gold-bearing vein mineralization. This vein is sharply defined and is hosted within the basaltic flow unit. The vein dips less steeply than the volcano-sedimentary sequence (Fig. 2b), and hence it is hosted by two different volcanic facies, pillow lava in the upper levels of the mine (190 and 235) and massive flow at greater depth (295, 355 and 415). This vein is also remarkably planar over its entire lateral and vertical extensions. Apparent controlling features are not obvious along the whole vein. However, crosscutting relationships between subvertical QFP and FP dikes indicate that the mineralizing fluids were focused within a pre-existing fracture (Fig. 8). Early FP dikes are clearly cut by the gold-bearing vein, whereas the QFP dikes are not affected by offset, but are mineralized. Such a relationship indicates the following sequence: (1) FP injection, (2) faulting and displacement of the FP dikes (movement unknown), (3) QFP injection, and (4) mineralization of the pre-existing fault. Since faulting occurred before the QFP injection, this ore controlling structure is considered as a synvolcanic fault. Furthermore, as the QFP felsic dikes do not show relative offset, movement along the fault during and after mineralization appears negligible.

Preexisting joints

All the gold-bearing veins located south of the dacitic intrusion occur within mafic sills and display sharp contacts and locally sharp angular changes in vein attitude implying that veins are controlled by preexisting fractures. A polygonal joint array is, in fact, weakly to moderately developed in the mafic sills. It is defined by a network of interconnected and chlorite-coated joints that divide the rock into cm-scale columns that strike E-W with a moderate plunge to the east, i.e., subparallel to the volcano-sedimentary strata. A stereoplot

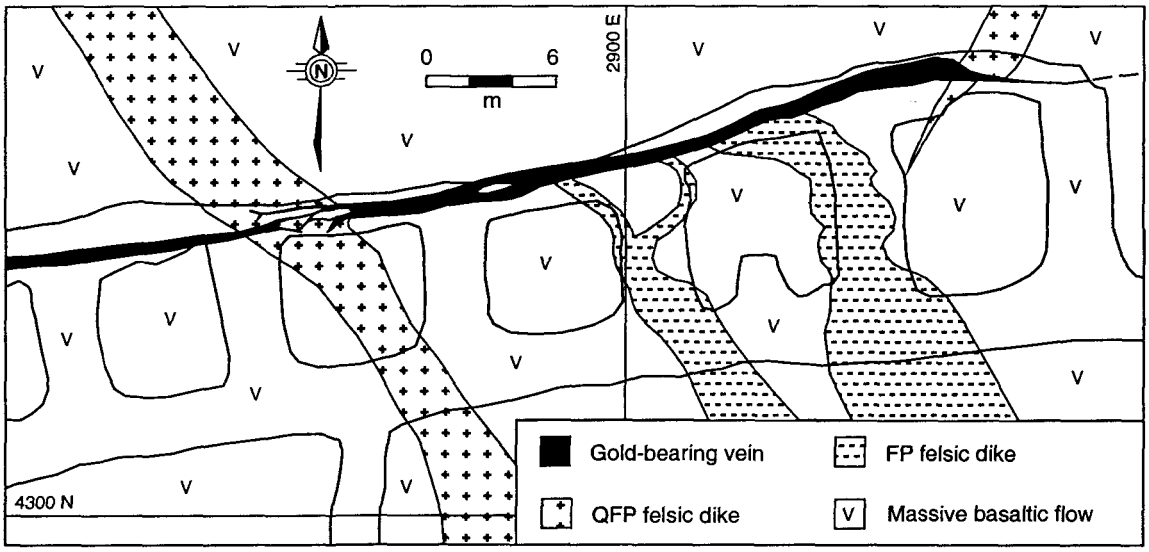

Figure 8. Simplified geological map of part of the 30 vein at level 355, showing crosscutting relationships between FP and QFP dikes and the gold-bearing vein.

of the poles to the joints displays a cylindrical distribution, where the joint intersection lines coincide with the calculated pole (Fig. 9). This polygonal pattern results either from poorly developed sets of contraction fractures related to cooling of mafic sills, or a brittle deformational event. The cooling hypothesis is preferred because a brittle event cannot explain the selective fracturing solely within the mafic sills south of the dacitic body, whereas the unusual attitude of contraction joints can be the result of perturbed cooling conditions.

Whatever its origin, this joint pattern has played a key role for gold-bearing vein emplacement at both the deposit- and vein-scale. At the deposit scale, the geometry of the gold-bearing veins is compatible with the polygonal joint array. The poles to the four main sets of gold-bearing veins plot along the cylindrical distribution of the joint array, and intersection lines between the vein sets are colinear with the column axes (Figs. 7, 9). Figure 10 shows an example of vein-scale control where a branch of the A vein is controlled by polygonal joints. A stereoplot of poles to the vein contacts displays a cylindrical distribution compatible with the polygonal joint array (Fig. 10). Although this example supports local joint-control, the main segments of gold-bearing veins are continuously planar, implying a dominantly planar rather than discontinuous joint-control. Fault-control is indicated by local offsets (< 3m) of markers (sedimentary horizons and FP dikes) along the four main sets of veins. The time of faulting is constrained to an event prior to vein emplacement since no evidence of movement was observed at the vein contacts. In fact, joint-control only occurs at the lateral ends of the gold-bearing veins (Figs. 5b and 10), where the main controlling fault dissipates and mineralizing fluids spread into adjacent joints. From these deposit- and vein-scale relationships, it is inferred that the polygonal joint array served as ground preparation for the successive faulting and gold mineralizing events.

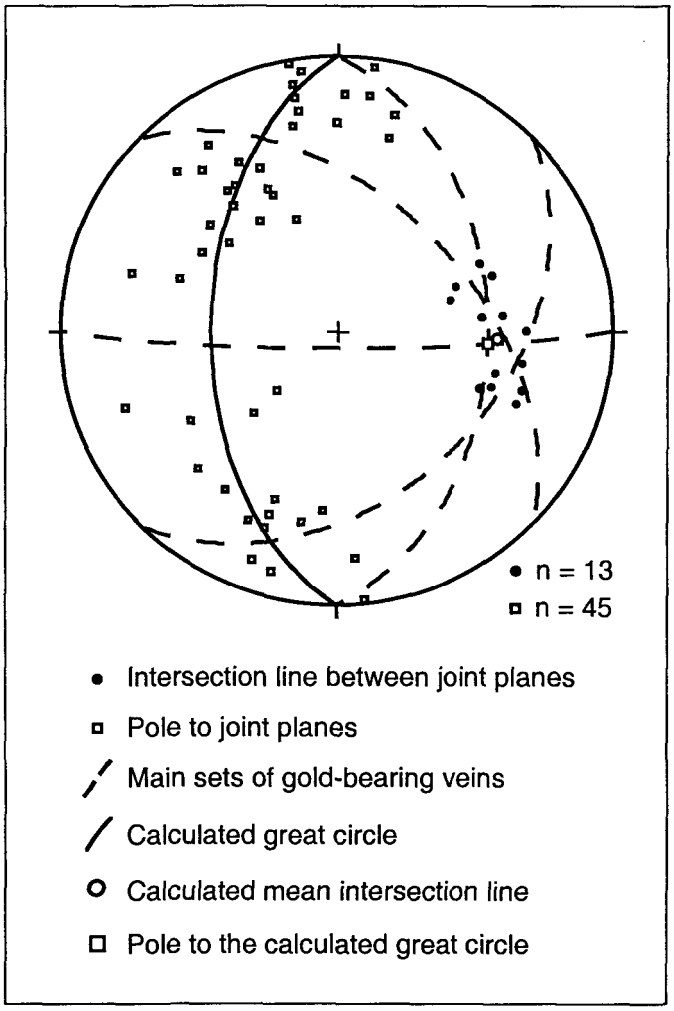

Figure 9. Equal area projection (lower hemisphere) of the poles to polygonal joints, their intersection lines, and the four main gold-bearing vein sets. The intersection lines between the gold-bearing vein sets are colinear with the intersection lines defined by the polygonal joints.

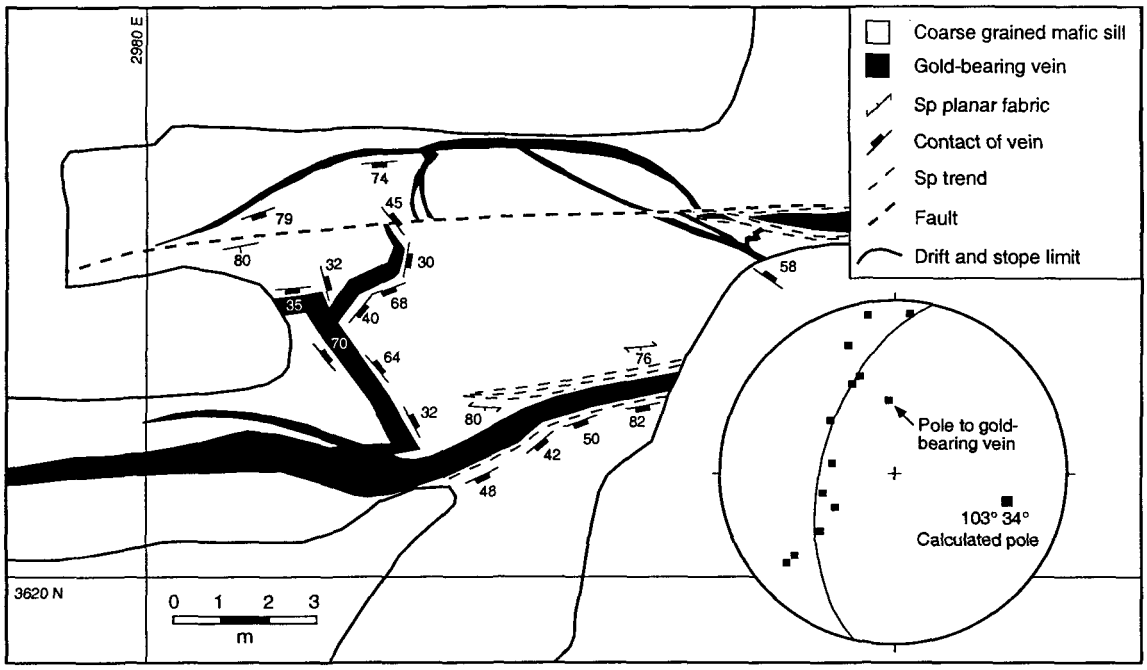

Figure 10. Detailed geological map of the eastern end of the A vein showing the structural elements and branching of a gold-bearing vein. Note the cylindrical distribution of poles to the vein branches.

RELATIVE TIMING OF THE GOLD MINERALIZATION

Evidence for pre-ductile deformation of the gold mineralization is presented here based on (1) the lack of structural compatibility between the orebody and ductile deformation, and (2) various crosscutting relationships.

Lack of structural compatibility

For shear-related Archean gold deposits, numerous studies have established the temporal and structural links between gold mineralization and regional deformation (e.g., Robert and Brown, 1986; Groves et al., 1989; Hodgson and Hamilton, 1989; Robert, 1990b). In such cases, the bulk strain axes of the gold-bearing vein network are commonly compatible with those of the regional penetrative deformation (e.g., Robert and Brown, 1986; Poulsen and Robert, 1989; Robert, 1990b). For complex vein networks, layer anisotropies induced by competency contrasts (e.g., dike contacts, compositional layering) have been emphasized as the main controls for shear and vein developments (e.g., Dubé et al. 1989; Belkabir et al., 1993).

In the Géant Dormant deposit, the geometry of the complex gold-bearing vein network located south of the dacitic intrusion is inconsistent with the bulk ductile deformation (Fig. 11). Considering the deformation and the host sequence characteristics, vein emplacement coeval with ductile deformation should have been favored (1) in sedimentary horizons, where strain is concentrated, (2) along felsic dike contacts that represent favorable subvertical layer anisotropies, and (3) within subhorizontal fractures related to the vertical elongation. Conversely, veins defining the complex network are hosted within unstrained mafic sills, veins expected along felsic dikes are absent, and subhorizontal fractures are filled with barren calcite. Furthermore, the typical comb-texture of the SE-NW veinlets gives a subhorizontal extension direction which is structurally

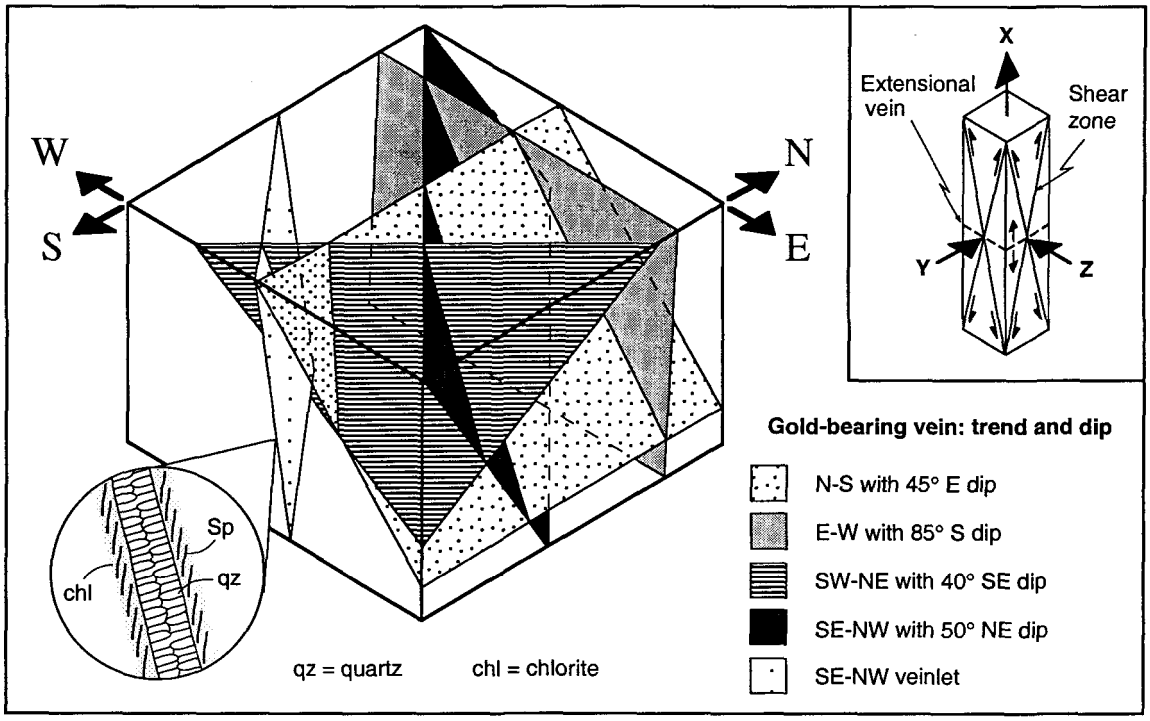

Figure 11. Schematic 3D representation of attitudes of gold-bearing vein within mafic sills south of the dacitic body. The circled inset shows the typical comb-texture of the SE-NW veinlets, which indicates a subhorizontal extension direction. The diagram in the square inset (from Poulsen and Robert, 1989) shows the expected geometry of the orebody for a shear-related Archean gold deposit developed within isotropic rock and affected by vertically dominated bulk strain. The lack of structural compatibility between the gold-bearing veins and the vertically dominated bulk strain is detailed in the text.

incompatible with the ductile deformation (Fig. 11). This lack of structural compatibility constraints the mineralizing event to a period which was pre-deformation or post-peak of deformation.

Crosscutting relationships

Evidence that the ductile deformation systematically overprints all the ore styles includes: (1) Sp fabric that surrounds and transects the gold-bearing veins (where Sp is developed) (Fig. 12a), (2) crosscutting of the gold-bearing veins and veinlets by subhorizontal extensional calcite veinlets related to the vertical tectonic elongation (Figs. 12a, 12b), (3) boudinaging in sections of the veins and veinlets (Fig. 12b), and (4) folded veins and veinlets with Sp axial planar fabric (Fig. 12b). Such observations indicate that the gold mineralization is either pre- or syn-deformation. As the vein network lack structural compatibility with the ductile deformation, a syn-deformational origin of the gold mineralization is unlikely. In addition, the systematic crosscutting of the gold-bearing veins by the hornblende-rich dikes, which are affected by the Sp fabric (Figs. 13a, 13b), clearly constrains the mineralizing event to a period prior to the ductile deformation. Therefore, although the absolute time of gold mineralization is unknown, it occurred prior to the regional deformation.

DISCUSSION

Evidence for a volcanic-related origin of the gold mineralization

From the relative timing established so far, the gold mineralization could range from volcanic-related (i.e., introduced in close temporal association with the last pulse of felsic magmatism) to early orogenic (i.e., introduced at a stage prior to deep burial, metamorphism and ductile deformation). These time periods imply distinctly different

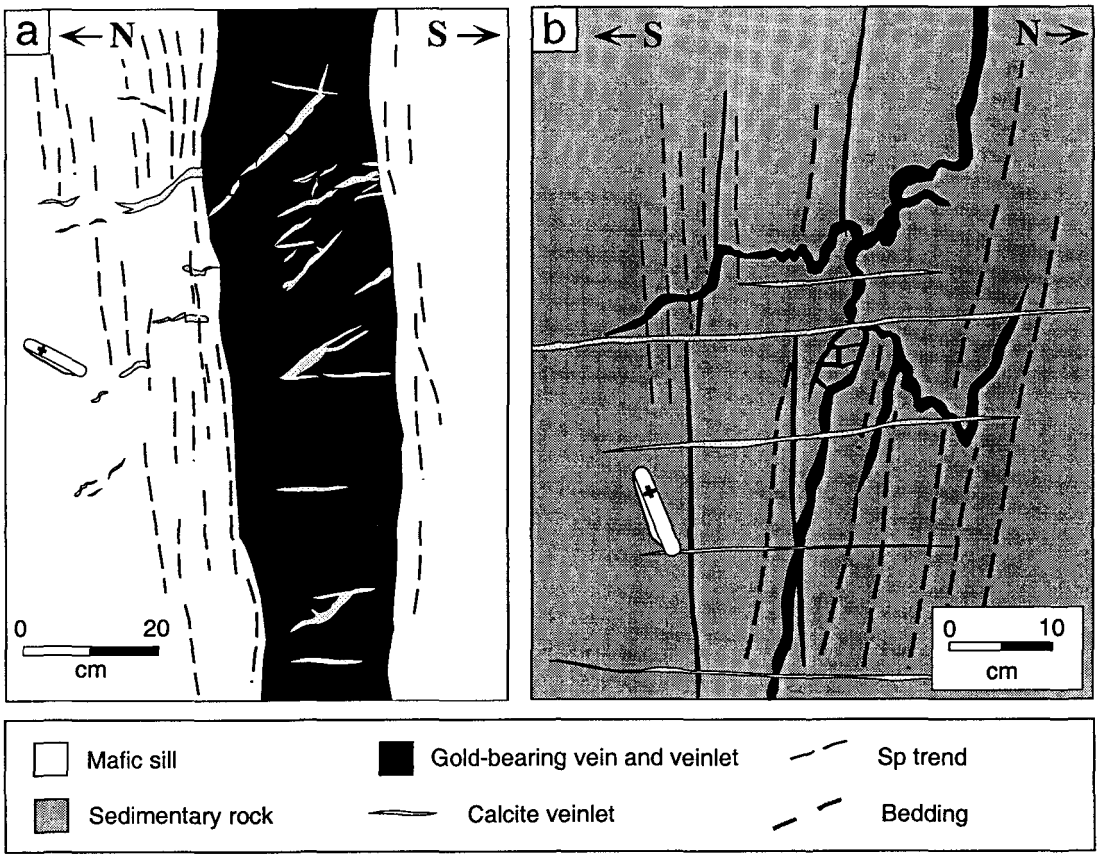

Figure 12. Structural characteristics of gold-bearing veins and veinlets (sketches from photographs). (a) Subvertical segment of the 20 vein showing vein-parallel Sp fabric and subhorizontal extensional calcite veinlets cutting the vein. Vertical view, from stope C-35-20-E. (b) Folded gold-bearing veinlets hosted by sedimentary rock. The veinlets oblique to the Sp fabric are folded whereas those parallel to the fabric are boudinaged. Note the systematic crosscutting of the folded and boudinaged veinlets by subhorizontal extensional calcite veinlets. Vertical view from the western end of the 30 vein, level 190.

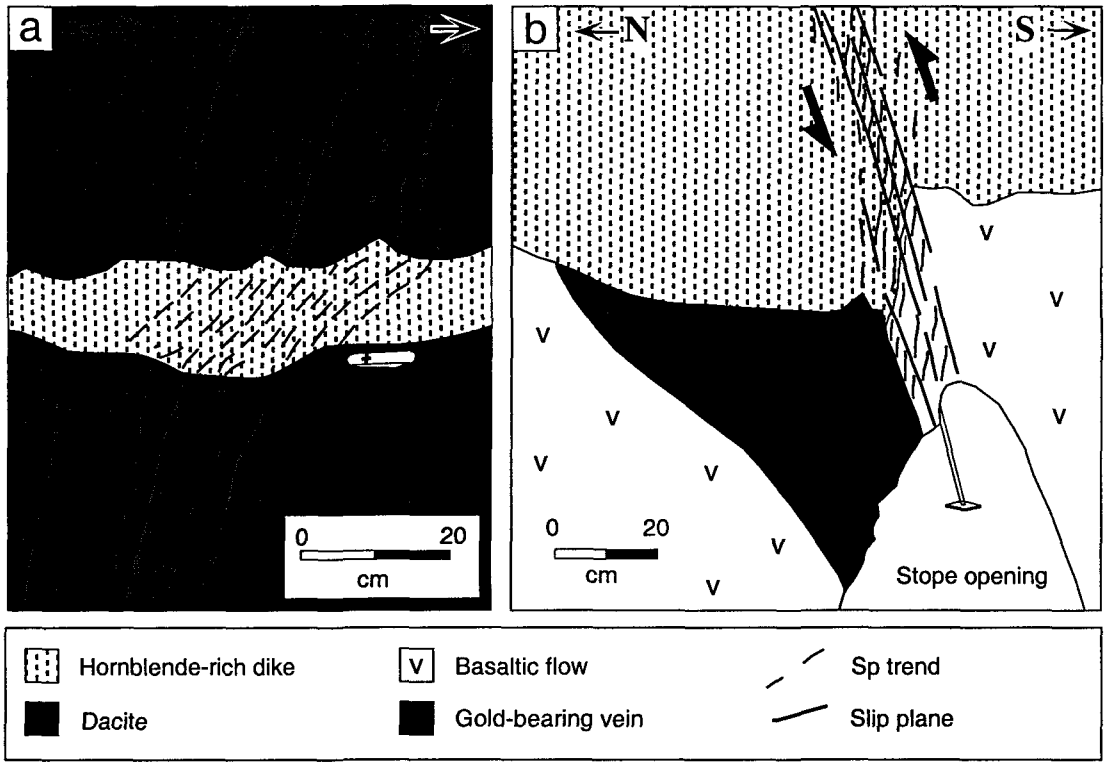

Figure 13. Structural characteristics of gold-bearing veins and veinlets (sketches from photographs). (a) Mafic hornblende-rich dike cutting gold-bearing boudinaged veinlets. The Sp fabric cuts across the mafic dike. Vertical view, level 235, close to the NW vein. (b) Mafic hornblende-rich dike cutting gold-bearing vein. The subvertical Sp fabric and the slip planes cut across the mafic dike and indicate dominate reverse movement, compatible with regional folding effects. Vertical view of the 30 vein from stope C-41-30-2900.

environments that can be examined to assess the origin of the gold mineralization. For a volcanic origin, it is likely that strata initially were subhorizontal and that the enclosing rocks were relatively warm with a disturbed geothermal gradient (high heat flow). For an early orogenic origin, the host environment is constrained by the attributes of the late hornblende-rich mafic dikes. Their chilled margins and ubiquitous stepped contacts suggest a colder environment during their emplacement. With these constraints, the origin of the deposit can be addressed on the basis of (1) the nature of the ore controls, (2) the mineralized QFP dikes, and (3) the geometry of the orebody.

The primary permeabilities that are observed to control the gold mineralization are compatible with a volcanic-related origin. Crosscutting relationships clearly indicate that some, if not all, of the fractures that control the vein emplacement were developed during the volcanic evolution of the host sequence (Fig. 8). Although the time of fracture development is not directly related to the time of gold mineralization, it is at least an indication that mineralization could be as old as the controlling fractures.

The selective mineralization and alteration of the QFP dikes argue in favor of a genetic link between QFP felsic magmatism and gold mineralization. In fact, it is unlikely that this ore style is solely a consequence of the rheological competence of the QFP dikes, since the older FP dikes, which have similar attitude and competence, are not mineralized or altered.

The geometry of the orebody, which is increasingly complex from north to south of the dacitic intrusion, is best explained as a consequence of original stratigraphic position. Because the strata are tilted along an E-W subvertical axis, the deposit, as shown on the map, represents a 1 km cross-section through the volcanic pile. The increase in complexity, which coincides with the younging direction of the strata (i.e., with proximity to the paleosurface), is developed within rocks of similar mechanical behavior at the deposit

scale. Such a relationship is expected in shallow epigenetic deposits where increased complexity of vein networks is related to diminishing confining pressure closer to the paleosurface. Additionally, the open space filling textures recorded in variously oriented veins and veinlets at Géant Dormant imply sustained opening of diverging fractures that can best be explained by variations of the stress field during the mineralizing period.

The features mentioned above (1 to 3) are hence compatible with a volcanic-related origin. It is also noteworthy that these features are commonly associated with volcanic-related quartz-bearing, gold and silver veins in recent volcanic terrains (i.e., low-sulfidation epithermal deposits) as discussed by Gaboury (1996). Other evidence supporting a volcanic-related origin includes: (1) the high silver content of the veins, (2) the sulfide assemblage of the veins, which is typical of Archean massive sulfide deposits (e.g., Chartrand and Cattalani, 1990), and (3) the weak vein alteration which suggests temperature equilibrium between warm host rocks and mineralizing fluids (high heat flow environment). Therefore, volcanic dynamic conditions, with a disturbed geothermal gradient and fluctuating stress field, emerge as the most likely environment for the observed characteristics of the deposit. A recent analog of a complex orebody related to the volcanic evolution of its host rocks is documented at the Emperor mine in Fiji (Anderson and Eaton, 1990).

Implications for gold exploration

The specific relationship between deformation and mineralization is one of the most important criteria to establish, because penetrative deformation can either directly control the emplacement of the mineralization or affect its initial geometry. In the former case, characteristics of the bulk penetrative deformation can be used to predict the strike and plunge of the orebodies (Poulsen and Robert, 1989; Robert and Poulsen, 1991). In the latter

case, (for post-mineralization deformation) it may be necessary to reconstruct the initial geometry of the orebodies in order to establish the ore controls (e.g., Gaboury et al., 1996). Furthermore, for highly deformed deposits, characteristics of the superimposed deformation can also be used to predict the spatial distribution and the resulting geometry of the orebodies (e.g., Robert et al., 1990; Tourigny et al., 1993).

For the Géant Dormant deposit, the characteristics of the ductile deformation are of no special importance for exploration purposes, as the regional deformation overprint is weak. Instead, exploration should be focused towards primary permeabilities that could have channeled the mineralizing fluids, including sedimentary units, lithological contacts and synvolcanic fractures. At a larger scale, the example of Géant Dormant opens up the possibility of finding gold mineralization away from crustal-scale faults and within undeformed parts of Archean greenstone belts. Distinctive features responsible for the gold mineralization remain to be established, but the felsic intrusive complex appears to have played a key role in concentrating the mineralization at the the scale of the deposit.

Similar gold deposits could also be present in intensely strained areas where deformation has obliterated the primary features and produced apparent "shear-related vein" relationships (Fig. 4d). Such artifacts can lead to unsuccessful exploration strategies at both mine- and district-scale. Table 3 lists a number of contrasting characteristics between true Archean shear-related gold deposits and the volcanic-related Géant Dormant deposit. Some of these characteristics can be used empirically to distinguish among shear-related gold deposits and to define a volcanic-oriented exploration program. Further investigations will establish geochemical characteristics of the host rocks and detailed features of the mineralization in order to develop a syn- to late-volcanic metallogenic model to serve as a guide for exploration.

Table 3. Contrasting characteristics of the volcanic-related Géant Dormant deposit and shear-related Archean gold deposits.

Characteristics	Volcanic-related: Géant Dormant	Shear-related Archean gold deposits
Au / Ag	< 1 (≈ 0.5: Table 1)	1 -10
Sulfide content	High Po, Py, Cp, Sp content	Low to moderate Py, Po, Asp content
Metal content	Cu, Zn rich	Cu, Zn poor
Alteration	Sericite / chlorite	Carbonate, micas K, albite, chlorite
Vein texture	Massive, comb quartz	Laminated or massive
Gangue material	Carbonate poor	Mostly carbonate rich
Ore control	Volcanic-related	Orogenic-related (shear-zone)
Vein termination	Multi-branching veinlets (Fig. 5b)	Pinch out, horsetail and sigmoidal veins
Geometry	Increasing complexity related to decreasing paleodepth	No significant vertical variation at the deposit scale, up to 2 km depth.
Relation to deformation	Orebody lack structural compatibility with *regional deformation*	Orebody structurally compatible with *regional deformation*

CONCLUSION

This field-based study demonstrates that the quartz-sulfide-rich gold-bearing veins and the other associated ore styles at the Géant Dormant mine developed prior to bulk ductile deformation. Timing of mineralization and its spatial relationship to the volcano-sedimentary sequence suggest that the mineralization has a volcanic-related origin, an interpretation supported by (1) the primary nature of the ore controls, (2) the association in space and time of the mineralization and the QFP felsic dikes that represent the last pulse of felsic magmatism, and (3) the increasingly complex geometry of the gold-bearing veins from deep to shallower paleodepths that is consistent with volcanic-related epigenetic mineralization.

The foregoing genetic model for the Géant Dormant deposit has important implications for exploration. First, exploration for this type of gold deposit must be guided by volcanic-related controls within the volcano-sedimentary sequence, as opposed to shear-related features. Second, because extensive deformation is not a required feature, the potential exists for comparable gold deposits in less deformed parts of Archean greenstone belts, which have been traditionally considered as infertile gold terrains.

Acknowledgments

This paper represents part of an ongoing Ph. D. thesis by the first author. The authors express their sincere thanks to Cambior Inc. for their important scientific collaboration, access to unpublished information, logistical support and permission to publish this paper. Our thanks are extended to geologists from the Ministère des Ressources naturelles du Québec at Val d'Or, Cambior Inc, Aurizon Mines Ltd and the Université du Québec à Chicoutimi for stimulating discussions in the field. H. Rasmussen provided dedicated and excellent field assistance. The manuscript has benefited from constructive criticism by M.I.

Legault, E.H. Chown, J. Moorhead and by EMG journal reviewers (C. McCuaig and an anonymous). T.J. Barrett (editor-in chief) is also acknowledged for the careful revision of the final version. Financial support from the Ministère des Ressources naturelles du Québec, Cambior Inc and from the Natural Sciences and Engineering Research Council of Canada (through a postgraduate scholarship to D.G.) are acknowledged with gratitude.

References

ANDERSON, W. A. and EATON, P.C., 1990. Gold mineralisation at the Emperor Mine, Vatakoula, Fiji. Journal of Geochemical Exploration, 36, p. 267-296.

BARRIE, C. T., LUDDEN, J. N. and GREEN, T. H., 1993. Geochemistry of volcanic rocks associated with Cu-Zn and Ni-Cu deposits in the Abitibi Subprovince. Economic Geology, 88, p. 1341-1358.

BELKABIR, A., ROBERT, F., VU, L. and HUBERT, C., 1993. The influence of dikes on auriferous shear zone development within granitoid intrusions: the Bourlamaque pluton, Val d'Or district, Abitibi greenstone belt. Canadian Journal of Earth Sciences, 30, p. 1924-1933.

BERTHÉ, D., CHOUKROUNE, P. and JEGOUZO, P., 1979. Orthogneiss, mylonite and non-coaxial deformation of granites: the example of the South Armorican Shear Zone. Journal of Structural Geology, 1, p. 31-42.

CHARTRAND, F., 1989. The Akasaba gold deposit. In: Archean gold deposits in the Rouyn-Noranda, Val d'Or and Chibougamau areas. Edited by A. Simard and F. Chartrand. Geological Association of Canada, Mineralogical Association of Canada, Field Trip A7 guidebook, p. 1-13.

CHARTRAND, F. and CATTALANI, S., 1990. Massive sulfide deposits in Northwestern Quebec. In: The Northwestern Quebec Polymetallic Belt. Edited by: M. Rive, P. Verpaelst, Y. Gagnon, J. M. Lulin, G. Riverin and A. Simard. The Canadian Institute of Mining and Metallurgy, Special Volume 43, p. 77-91.

CHOWN, E. H., DAIGNEAULT, R., MUELLER, W. and MORTENSEN, J. K., 1992. Tectonic evolution of the Northern Volcanic Zone, Abitibi belt, Quebec. Canadian Journal of Earth Sciences, 29, p. 2211-2225.

COLVINE, A. C., 1989. An empirical model for the formation of Archean gold deposits: products of final cratonization of the Superior province, Canada. In: The Geology of Gold Deposits: The Perspective in 1988. Edited by R. R. Keays, W. R. H. Ramsay and D. I. Groves. Economic Geology, Monograph 6, p. 37-53.

DAIGNEAULT, R. and ARCHAMBAULT, G., 1990. Les grands couloirs de déformation de la Sous-province de l'Abitibi. In: The Northwestern Quebec Polymetallic Belt. Edited by: M. Rive, P. Verpaelst, Y. Gagnon, J. M. Lulin, G. Riverin and A. Simard. The Canadian Institute of Mining and Metallurgy, Special Volume 43, p. 43-64.

DOSTAL, J. and MUELLER, W., 1992. Archean shoshonites from the Abitibi greenstone belt, Chibougamau (Québec, Canada): geochemistry and tectonic setting. Journal of Volcanology and Geothermal Research, 53, p. 145-165.

DOWLING, K. and MORRISON, G., 1989. Application of quartz textures to the classification of gold deposits using North Queensland examples. In: The Geology of Gold Deposits: The Perspective in 1988. Edited by R. R. Keays, W. R. H. Ramsay and D. I. Groves. Economic Geology, Monograph 6, p. 342-355.

DUBÉ, B., POULSEN, H. and GUHA, J., 1989. The effects of layer anisotropy on auriferous shear zones: the Norbeau mine, Québec. Economic Geology, 84, p. 871-878.

GABOURY, D. 1996. Environnment épithermal sous-marin des veines aurifères de quartz et de sulfures à la mine Géant Dormant, Sous-province de l'Abitibi. APGGQ-Chicoutimi 1996. Program and Abstracts, p. 78-84.

GABOURY, D., DUBÉ, B., LAFLÈCHE, M., R. and LAUZIÈRE, K., 1996. Geology of the Hammer Down mesothermal gold deposit, Newfoundland Appalachians, Canada. Canadian Journal of Earth Sciences, 33, p. 335-350.

GABOURY, D., DAIGNEAULT, R. et COUTURE, J-F. 1998. La mine Géant Dormant, Abitibi: un exemple de minéralisation aurifère volcanogène de type "veines de quartz". Ministère des Ressources Naturelles du Québec. In press.

GROVES, D. I., BARLEY, M. E. and HO, S. E., 1989. Nature, genesis and tectonic setting of the mesothermal gold mineralization in the Yilgarn block, Western Australia. In: The Geology of Gold Deposit: The Perspective in 1988. Edited by Reid R. Keays, W. R. H. Ramsay and D. I. Groves. Economic Geology, Monograph 6, p. 71-85.

HOCQ, M., 1990. Carte lithotectonique des Sous-Provinces de l'Abitibi et du Pontiac. Ministère des Ressources Naturelles du Québec. Carte No. 2092 A, Publication DV 89-04.

HODGSON, C. J. and HAMILTON, J. V., 1989. Gold mineralization in the Abitibi greenstone belt: End-stage result of Archean collisional tectonics? In: The Geology of Gold Deposits: The Perspective in 1988. Edited by R. R. Keays, W. R. H. Ramsay and D. I. Groves. Economic Geology, Monograph 6, p. 86-100.

KERRICH, R. and WYMAN, D., 1990a. Geodynamic setting of mesothermal gold deposits: An association with accretionary tectonic regimes. Geology, 18, p. 882-885.

KERRICH, R. and WYMAN, D., 1990b. Late evolution of greenstone belts and gold deposits. In: Greenstone gold and crustal evolution. Edited by F. Robert, P.A. Sheahan and S.B. Green. Nuna Conference, Val d'Or. Geological Association of Canada, Mineral deposits Division, p. 91-94.

KERRICH, R. and CASSIDY, K. F., 1994. Temporal relationships of lode gold mineralization to accretion, magmatism, metamorphism and deformation - Archean to present: A review: Ore Geology Reviews, 9, p. 263-310.

KIRKHAM, R. V., PILOTE, P., SINCLAIR, W. D., ROBERT, F. and DAIGNEAULT, R., 1995. Clark Lake porphyry Cu-Mo (-Au) deposit, Chibougamau, Quebec, Canada - Preserved island-arc sequence. Precambrian '95, Program and Abstracts, p. 296.

LARSEN, J. E. and HUTCHINSON, R. W., 1993. The Selbaie Zn-Cu-Ag deposits, Quebec, Canada: An example of evolution from subaqueous to subaerial volcanism and mineralization in an Archean caldera environment. Economic Geology, 88, p. 1460-1482.

LESHER, C. M., GOODWIN, I. H., CAMPBELL, I. H. and GORTON, M.P., 1986. Trace-element geochemistry of ore-associated and barren, felsic metavolcanic rocks in the Superior Province, Canada. Canadian Journal of Earth Sciences, 23, p. 222-237.

MAGNAN, M., DAIGNEAULT, R., ROBERT, F. and PILOTE, P., 1995. Intrusion-related Au-Cu-Ag sulfide-rich veins in the Archean Doré Lake complex, Chibougamau, Québec. Precambrian '95, Program and Abstracts, p. 296.

MARQUIS, P., BROWN, A. C., HUBERT, C. and RIGG, D. M., 1990. Progressive alteration associated with auriferous massive sulfide bodies at the Dumagami mine, Abitibi greenstone belt, Québec. Economic Geology, 85, p. 746-764.

MORASSE, S., WASTENEYS, H. A., CORMIER, M., HELMSTAEDT, H. and MASON, R., 1995. A pre-2686 Ma intrusion-related gold deposit at the Kiena mine, Val d'Or, Québec, Southern Abitibi Subprovince. Ecomonic Geology, 90, p. 1310-1321.

MORTENSEN, J. K., 1993. U-Pb geochronology of the Eastern Abitibi Subprovince. Part 1: Chibougamau-Matagami-Joutel region. Canadian Journal of Earth Sciences, 30, p. 11-28.

MUELLER, W. and DONALDSON, J. A., 1992. Development of sedimentary basins in the Archean Abitibi Belt, Canada: An overview. Canadian Journal of Earth Sciences, 29, p. 2249-2265.

PICARD, C. and PIBOULE, M., 1986. Pétrologie des roches volcaniques du sillon de roches vertes archéennes de Matagami-Chibougamau à l'ouest de Chapais (Abitibi est, Québec). 1. Le Groupe basale de Roy. Canadian Journal of Earth Sciences, 23, p. 561-578.

PILOTE, P., 1989. Géologie de la région de Casa-Berardi, Dieppe, Collet et Laberge. Ministère des Ressources Naturelles du Québec, MB 89-43.

PILOTE, P., DION, C., CIMON, J., KIRKHAM, R., ROBERT, F., SINCLAIR, W. D., DAIGNEAULT, R. et MAGNAN, M., 1994. Les minéralisations de type Cu-Mo-Au et les gisements Cu-Au filoniens du lac Doré, Chibougamau, processus hydrothermaux

distincts ou évolution d'un même événement minéralisateur? Séminaire d'information sur la recherche géologique. Programme et résumés, DV-94-09, p. 18.

PILOTE, P., KIRKHAM, R., ROBERT, F., SINCLAIR, W. D. et DAIGNEAULT, R., 1995. Développement d'un district à minéralisation de type Cu-Au (Mo) porphyrique dans la région de Chibougamau et implications métallogéniques. Séminaire d'information sur la recherche géologique. Programme et résumés, DV-95-04, p. 14.

POULSEN, K. H. and ROBERT, F., 1989. Shear zones and gold: practical examples from southern Canadian Shield. In: Mineralization and shear zones. Edited by J. T. Bursnall. Geological Association of Canada, Short Course Notes 6, p. 239-266.

ROBERT, F., 1990a. An overview of gold deposits in the Eastern Abitibi Subprovince. In: The Northwestern Quebec Polymetallic Belt. Edited by: M. Rive, P. Verpaelst, Y. Gagnon, J. M. Lulin, G. Riverin and A. Simard. The Canadian Institute of Mining and Metallurgy, Special Volume 43, p. 93-105.

ROBERT, F., 1990b. Structural setting and control of gold-quartz veins of the Val d'Or area, southeastern Abitibi Subprovince. In: Gold and Base Metal Mineralization in the Abitibi Subprovince, Canada, with emphasis on the Quebec segment. Edited by S. E. Ho, F. Robert and D. I. Groves. University of Western Australia. Publication 24, p. 167-209.

ROBERT, F. and BROWN, A. C., 1986. Archean gold-bearing quartz veins at the Sigma Mine, Abitibi greenstone belt, Québec: Part I. Geologic relations and formation of the vein system. Economic Geology, 81, p. 578-592.

ROBERT, F., BROMMECKER, R. and BUBAR, D. S., 1990. The Orenada zone 4 deposit: Deformed vein-type gold mineralization within the Cadillac tectonic zone, SE of Val d'Or. In: The Northwestern Quebec Polymetallic Belt. Edited by: M. Rive, P. Verpaelst, Y. Gagnon, J. M. Lulin, G. Riverin and A. Simard. The Canadian Institute of Mining and Metallurgy, Special Volume 43, p. 255-268.

ROBERT, F. and POULSEN, K. H., 1991. Practical application of structural analysis of lode gold deposits. In: Structural Geology in Mining and Exploration. University of Western Australia, publication 25, p. 154-157.

SINCLAIR, W. D., PILOTE, P., KIRKMAN, R. V., ROBERT, F. and DAIGNEAULT, R., 1994. A preliminary report of porphyry Cu-Mo-Au and shear-hosted Cu-Au deposits in the Chibougamau area, Quebec. In: Current Research 1994-C; Geological Survey of Canada, p. 303-309.

TOURIGNY, G., BROWN, A. C., HUBERT, C. and CRÉPAUX, R., 1989. Synvolcanic and syntectonic gold mineralization at the Bousquet mine, Abitibi greenstone belt. Economic Geology, 84, p. 1875-1890.

TOURIGNY, G., DOUCET, D. and BOURGET, A., 1993. Geology of the Bousquet 2 mine: An example of a deformed, gold-bearing polymetallic sulfide deposit. Economic Geology, 88, p. 1578-1597.

WYMAN, D.A. and KERRICH, R., 1993. Archean shoshonitic lamprophyres of the Abitibi Subprovince, Canada: petrogenesis, age, and tectonic setting. Journal of Petrology, 34, p. 1067-1109.

CHAPITRE 3

Evolution from seafloor-related to sulfide-rich quartz vein-type gold mineralization during deep submarine volcanic construction: The Géant Dormant gold mine, Archean Abitibi Belt, Canada

Ce chapitre représente la version intégrale d'un article publié en 1999 dans le Journal *Economic Geology*, Volume 94, page 3-21, par Gaboury et Daigneault.

Abstract

The Géant Dormant (Sleeping Giant) mine is a vein-type gold deposit which contrasts with Archean shear-related (mesothermal) deposits by the pre-ductile deformation timing of the quartz gold-bearing veins and by their high sulfide content. Gold mineralization is centered about a felsic complex which intrudes a volcano-sedimentary succession composed of mafic sills, interbedded pelagic sediments and mafic pillowed and felsic lavas. The felsic complex includes a dacitic subvolcanic dome and a swarm of polyphase felsic FP and QFP dikes. All felsic rocks are cogenetic and have calc-alkalic affinity ($Zr/Y \approx 12$) whereas all mafic rocks, including post-mineralization dikes, are cogenetic and tholeiitic ($Zr/Y \approx 2.5$). Strata were built from two different volcanic sources: a proximal felsic and a distal mafic one in a deep submarine setting (> 3150 m). Three successive mineralizing events are recognized: (1) a seafloor-related gold poor event, characterized by sericite, chlorite, and quartz alteration with disseminations and stringers of gold-bearing pyrrhotite and chalcopyrite affecting rocks of paleo-seafloor origin, (2) an autometasomatic event affecting only the dacitic dome, expressed by chloritization and dissemination of auriferous pyrite, and (3) quartz-sulfide vein-style gold mineralization, with only weak chlorite-sericite or no altered selvages.

The gold-bearing vein network was formed during the last stage of a four-stage volcanogenic hydrothermal system as indicated by the parallelism between volcanic and hydrothermal evolutionary patterns. At Stage 1, diffuse seafloor-related hydrothermal fluids altered and mineralized lavas and Fe-rich sediments. Stage 2 involves the sealing of the hydrothermal system by injection of a 1 km thick stack of impermeable mafic sills.

During Stage 3, the mineralizing system was reactivated by the emplacement of the dacitic dome. Stage 4 involves injection of QFP dikes along active synvolcanic faults. These dikes served as conduits for the ascension of mineralizing fluids through the volcanic pile. Gold, and related quartz and sulfides, precipitated in open fractures developed mainly in mafic rocks near QFP dikes. Vein formation is a consequence of the specific two-source volcanic pile. The exogenic voluminous mafic sills disturbed the evolution of a volcanogenic hydrothermal system related to the felsic center. Renewed felsic activity generated fractures for vein formation, enhanced by pressurization of mineralizing fluids at near lithostatic pressure within the impermeable host sequence. Gold enrichment from Stage 1 to Stage 4 is consistent with the proposed evolution and likely related to boiling of the mineralizing fluids during vein formation.

Résumé

La minéralisation aurifère filonienne à la mine Géant Dormant diffère de celle des gîtes filoniens archéens classiques par la formation des veines précoce par rapport à la déformation ductile régionale et par leur fort contenu en sulfures. La minéralisation est centrée sur un complexe felsique recoupant une séquence volcano-sédimentaire, composée de filons-couches mafiques interlités avec des sédiments et des laves mafique et felsique. Un dôme dacitique et des essaims de dykes de FP et de QFP composent le complexe felsique. Les roches felsiques sont calco-alkalines (Zr/Y≈12) et cogénétiques, alors que celles mafiques sont tholéiitiques (Zr/Y≈2,5) et sont également cogénétiques entre elles. L'empilement volcanique a été construit de manière séquentielle en milieu sous-marin profond (> 3 150 m) à partir de deux sources magmatiques: une source felsique proximale et une mafique distale. Trois événements successifs de minéralisation aurifère ont été identifiés: (1) une minéralisation volcanogène précoce manifestée par l'altération (chlorite, séricite, quartz) et la sulfurisation (filonnets et disséminations de pyrrhotite et chalcopyrite) des roches du paléo-fond océanique; (2) la chloritisation et la pyritisation internes du dôme dacitique résultant d'un processus autométasomatique; et (3) les veines aurifères sans, ou avec seulement une faible altération hydrothermale (chlorite-séricite).

Les veines résultent de l'épisode final d'un système volcanogène comportant quatre stades évolutifs. Le Stade 1 implique l'altération et la minéralisation des roches du paléo-fond océanique. Au Stade 2, l'injection des filons-couches mafiques (~1 km) entraîne le colmatage du système hydrothermal. Le Stade 3 correspond à l'introduction du dôme et à la reprise de l'activité hydrothermale. Le Stade 4 implique l'injection des dykes de QFP qui,

subséquemment, ont servi de conduits hydrothermaux. Les veines résultent du remplissage hydrothermal de fractures développées à proximité des dykes de QFP. La formation des veines est conséquente à la construction séquentielle de l'édifice volcanique à partir des deux sources. L'injection des filons-couches a perturbé l'activité hydrothermale associée au centre felsique. La reprise du magmatisme felsique a généré des fractures pour la formation des veines, qui a été favorisée également par la pressurisation lithostatique des fluides au sein d'un milieu imperméable. L'enrichissement en or, du Stade 1 au Stade 4, résulte de l'évolution intrinsèque du système, étant relié à l'ébullition des fluides lors de la formation des veines.

INTRODUCTION

The diversity of Canadian Archean gold deposits and their differing times of formation relative to volcanism, magmatism and ductile deformation have been discussed by Robert and Poulsen (1997) and Robert et al. (1997). Of the various types recognized, the sulfide-rich gold-bearing quartz vein is a significant one which remains enigmatic in origin. Formation of sulfide-rich gold-bearing quartz veins prior to regional ductile deformation is documented for some deposits such as Copper Rand (Magnan et al., 1995) and Géant Dormant (Gaboury et al., 1996), thus precluding a metamorphogenic origin. The Géant Dormant deposit is specially suited to address the genetic problem because gold-bearing veins are hosted within a weakly deformed volcano-sedimentary sequence where primary relationships are well preserved.

This paper documents the evolution of the volcanic pile and its associated hydrothermal system. Field, petrographic and geochemical data define the volcanic evolution and its submarine setting. Hydrothermal events are characterized by field distribution, sulfide and alteration assemblages, and mass balance calculations of altered host rocks. On the basis of the chronological and geometric relationships between volcanic and hydrothermal events, gold-bearing veins are interpreted as the last stage of a volcanogenic hydrothermal system which evolved from gold-poor seafloor-related to gold-rich vein-type mineralization during deep water volcanic construction. Mechanisms for vein formation and gold enrichment in this setting are discussed as well as the exploration significance of the proposed genetic model.

REGIONAL GEOLOGY

The Géant Dormant deposit is hosted within the first volcanic cycle of the Northern Volcanic Zone of the Archean Abitibi Subprovince (Chown et al., 1992), which is part of

the Superior Province of the Canadian Shield. The first volcanic cycle corresponds to an extensive subaqueous basalt plain with scattered felsic volcanic edifices, interstratified with or overlain by sedimentary assemblages. The 1 to 3 km thick basaltic assemblage (Chown et al., 1992) is dominantly composed of massive, pillowed and brecciated tholeiitic volcanic rocks (Picard and Piboule, 1986), with minor chert, iron formation and volcaniclastic rocks (Mueller and Donaldson, 1992a; Pilote, 1989). U-Pb dating of felsic centers indicate a time interval of 2730-2720 Ma (Mortensen, 1993). The volcano-sedimentary sequence is intruded by voluminous synvolcanic diorite-tonalite-leucotonalite plutons (Chown et al., 1992). The Northern Volcanic Zone is interpreted as a coherent assemblage, initially formed from a diffuse and immature arc (Chown et al., 1992). Between 2708 to 2685 Ma, rocks were affected by a N-S orogenic shortening event, comprised of a succession of several tectonic pulses (Chown et al., 1992), which have generated the following structural features: (1) E-W trending, subvertical, regional folds with an axial planar schistosity (Sp: for principal surface), (2) major E-W trending, 1 to 4 km wide reverse shear zones of regional extent, such as by the Laflamme fault (Fig. 1) and, (3) 1 to 5 km wide, NW-SE trending deformation zones such as the Harricana fault (Fig. 1).

GEOLOGY OF THE DEPOSIT

The Géant Dormant (Sleeping Giant) mine is a gold-bearing quartz and sulfide vein deposit located in northwestern Québec, between Matagami and Amos (Fig. 1). As of January 1998, production had attained 1.2 million metric tons at 8.9 g/t Au, with reserves in all categories of 580 000 tons at 11.2 g/t Au. Gold mineralization is hosted by a volcano-sedimentary succession which is intruded by a felsic complex and transected by post-mineralization mafic dikes (Fig. 2). The volcano-sedimentary succession is composed

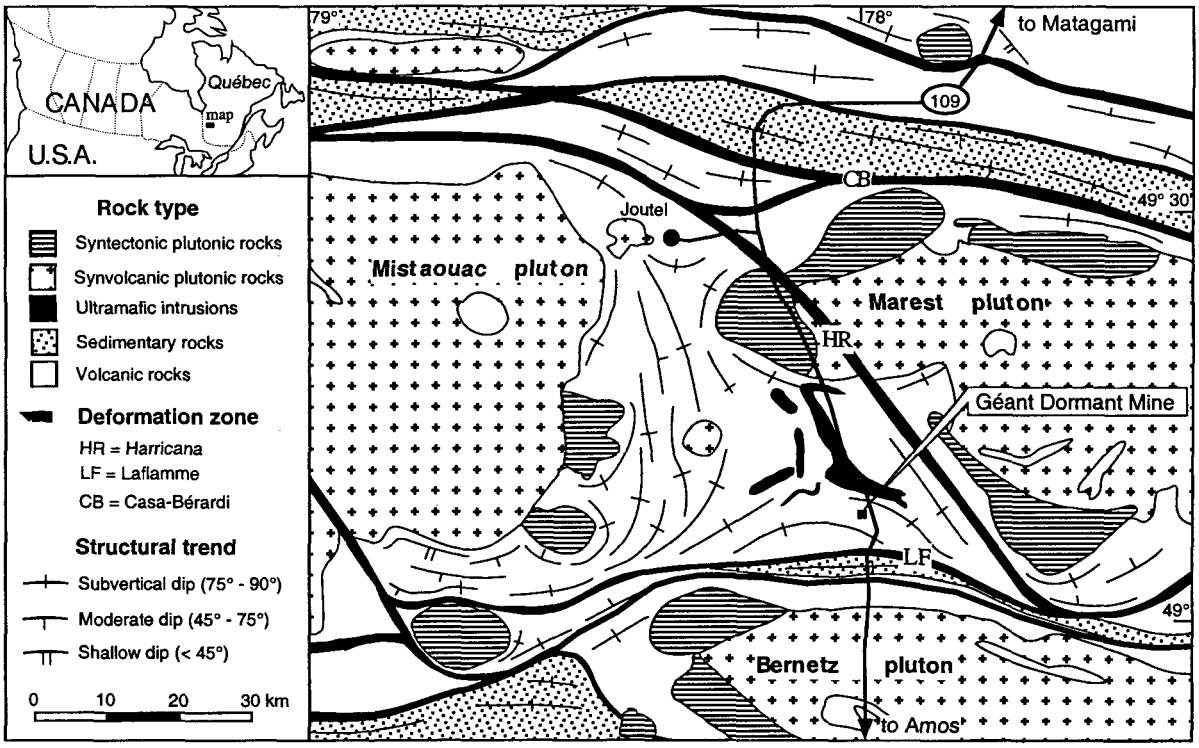

Figure 1. Simplified geological map of the mine district showing the location of the Géant Dormant gold deposit. Map modified from Hocq (1990) and Chown et al. (1992).

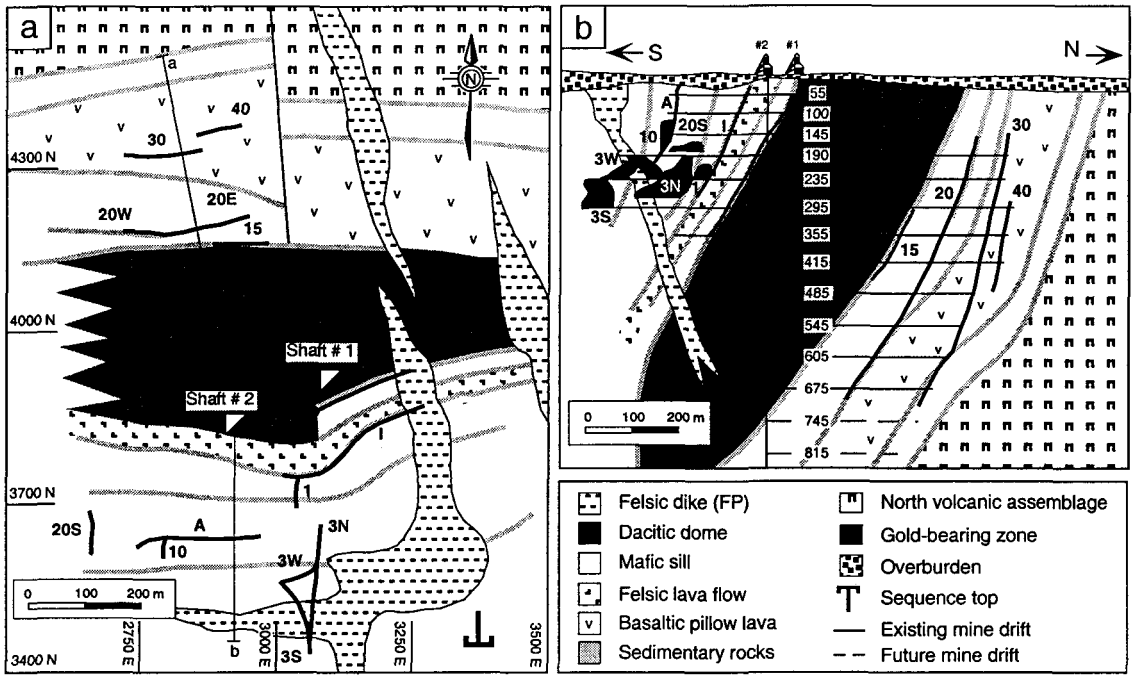

Figure 2. Characteristics of the mine sequence. (a) Simplified geological plan of the Géant Dormant mine area. (b) Idealized vertical N-S cross section. Various gold-bearing zones are labeled: A, 10, 40, etc. Modified from Cambior.

of mafic sills, interbedded sediments and flows of mafic pillowed and felsic lavas (Fig. 3). The felsic complex includes a dacitic body and a swarm of felsic porphyritic FP and QFP dikes. The post-mineralization dikes include two different generations: early aphanitic mafic and late hornblende-rich dikes. The 1.5 km thick host volcano-sedimentary sequence lies conformably on a basaltic pile (pillowed and massive lavas, dikes and sills) referred as the North volcanic assemblage, and it is structurally overlain by another sequence of basaltic lavas referred as the South volcanic assemblage (Fig. 3). Mafic rocks within the host sequence are geochemically different from mafic rocks in the North and South volcanic assemblages (Gaboury, 1996). All rock types have been metamorphosed to lower greenschist facies.

Volcanic strata (S0) strike predominantly E-W and dip steeply south, forming a normal homoclinal stratigraphic succession (Fig. 2). Weakly penetrative subvertical E-W trending Sp schistosity affects all rock types locally, including the hornblende-rich dikes, but internal deformation within the tilted sequence is weak and heterogeneous (Gaboury et al., 1996). Structural relationships between planar fabrics (S0-Sp), indicate that the host sequence is on the northern limb of an east-trending regional syncline with a subhorizontal axis (Gaboury et al., 1996).

Sedimentary rocks

Sedimentary units, enclosed between two mafic sills (Fig. 3), range from a few cm to 10 m thick, averaging 2 m, and consist of mixed beds of fine-grained volcaniclastic rock, chert and magnetite-rich iron formation (Algoma type: Gross, 1980). Sedimentary rocks are characterized by thin beds (< 4 cm) and parallel laminations. Local flame textures and graded bedding indicate southward younging of the sedimentary succession (Fig. 4a). Fine grains of quartz and euhedral plagioclase (< 1 mm) suggest a local felsic volcanic source.

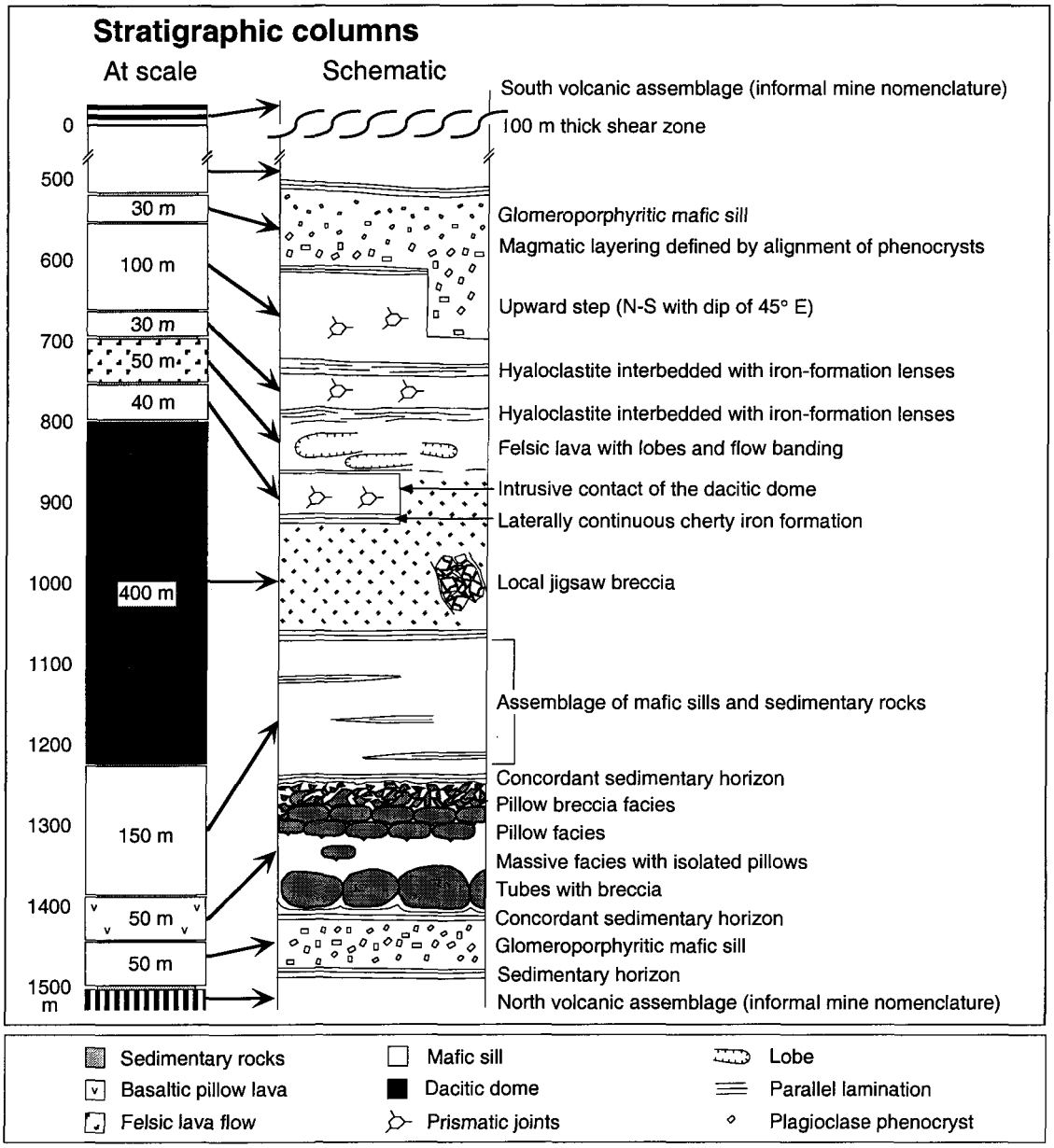

Figure 3. Stratigraphic column for the hosting sequence and schematic column along line a-b of Fig. 2a (0-500 m, data from drill cores; 500-1500 m, data from mapping at level 190.

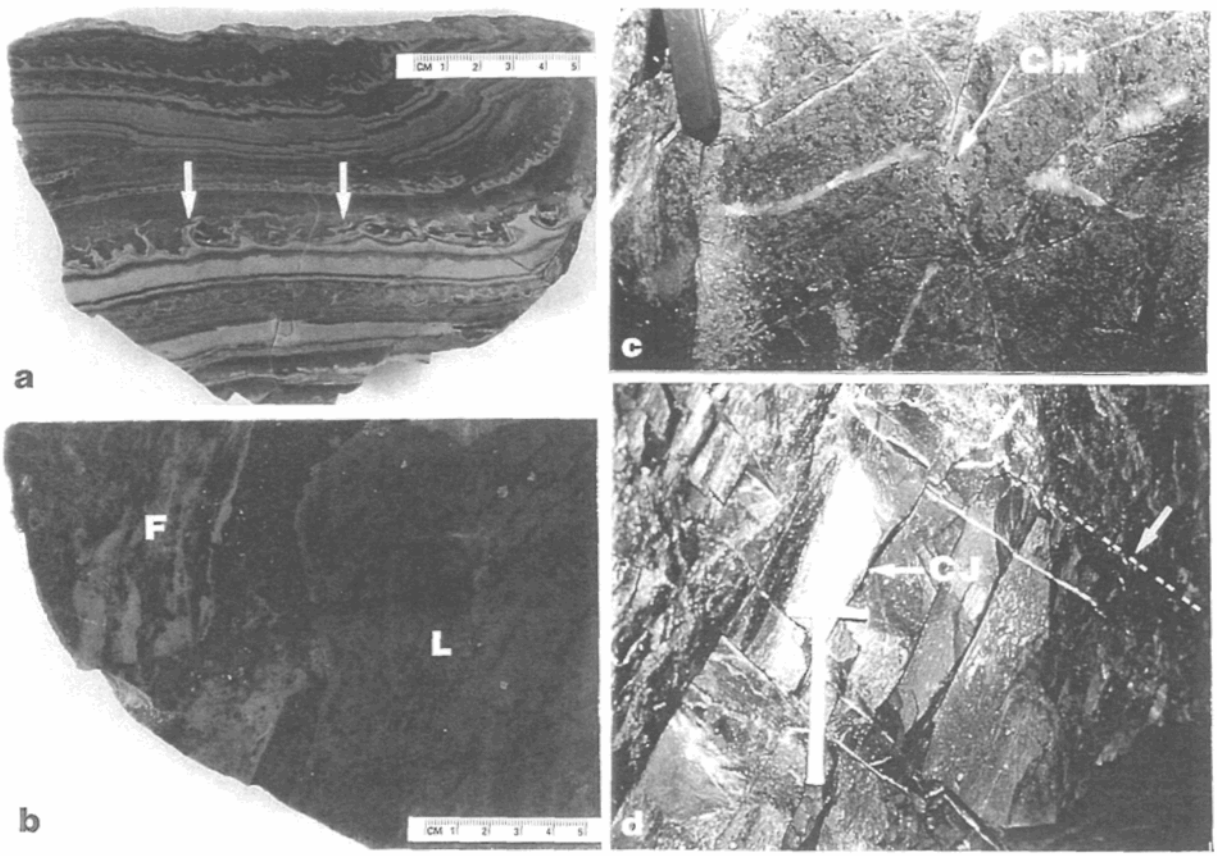

Figure 4. Field and slab photographs of the main lithological features. (a) Flame texture in fine grained volcaniclastite rock (arrows). (b) Fragmental aspect of the lava flow, (F) fragmental and (L) lobate facies. (c) Typical spotty aspect of the dacite induced by chloritization (Chl). Pocket knife as scale. (d) Columnar joints (CJ) developed within a post-mineralization tholeiitic mafic dike. The dashed line shows the dike contact.

The euhedral plagioclase shape implies minimal traction transportation or reworking of the volcaniclastite which is, together with parallel laminations and interbedded chemical sediments, compatible with a low energy, deep water environment of sedimentation.

Basaltic lava flow

The basaltic flow is aphanitic, locally plagioclase-phyric (< 1 cm) and slightly amygdaloidal (< 1%). This flow, 50 m in thickness, exhibits a southward succession of tube, massive lava, pillows and pillow breccia (Fig. 3) which, together with well-preserved pillow configurations, indicates younging to the south (Dimroth et al., 1978). The pillows are less than 1 m in diameter (basal tubes reach 10 m) with chilled margins 2-4 cm thick and with locally abundant hyaloclastic inter-pillow material. This flow is conformably interbedded at its base and top with sedimentary rocks (Fig. 3) and includes local intra-flow sedimentary lenses.

Felsic lava flow

The felsic lava flow is aphanitic with up to 15% quartz phenocryst (< 2 mm) (Fig. 5). It is about 50 m thick and lies conformably on a thin sedimentary horizon (Fig. 3). This flow includes various volcanic facies, such as fragmental, lobate-massive and tuffaceous, defining a flow facies assemblage facing toward the south. The fragmental facies occurs mainly at the base. It is composed up to 15% of angular to sub-angular cherty fragments, some with flow banding, ranging in size from 0.5 to 30 cm (Fig. 4b). The massive facies includes 1-2 m wide lobes of massive lava locally surrounded by flow banding. The massive and fragmental facies are transitional at the top to a sedimentary horizon which includes the tuffaceous facies. The tuffaceous facies corresponds to a 4 m thick massive horizon of cherty and aphanitic clastic material, characterized by a distinct beige color

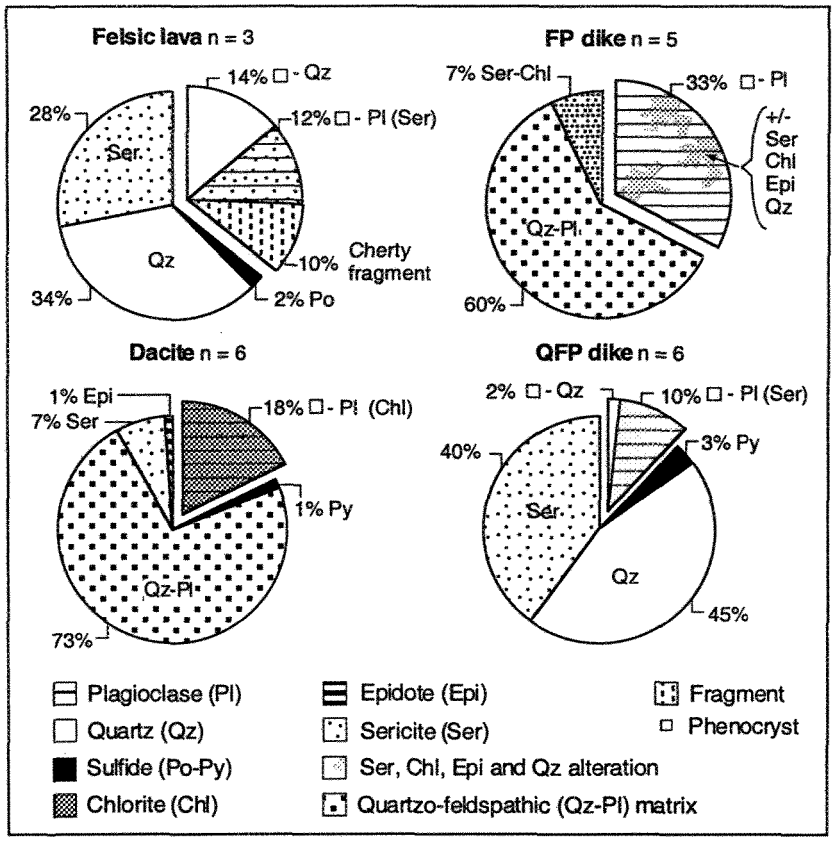

Figure 5. Pie diagrams illustrating petrographic features of felsic rocks. The offset part illustrates the proportion of phenocrysts and fragments (if present). The overprinted shade on plagioclase and matrix portions indicates the nature and extent of alteration. Felsic rocks are characterized by specific primary composition and alteration assemblage.

produced by a strong sericitization. This horizon is interbedded with discontinuous lenses of magnetite iron-formation (Fig. 3). The tuffaceous facies and interbedded sedimentary rocks are isolated from the lobate-massive facies by mafic sills (Fig. 3). This facies is interpreted to represent sedimented fine hyaloclastite at the top of the felsic flow lava (cf. de Rosen-Spence et al., 1980).

Mafic sills

Mafic sills, 1 to 100 m in thickness, are an ubiquitous feature in the mine environment (Fig. 3). They are aphanitic to medium-grained, devoid of vesicles or amygdules and locally plagioclase-phyric. Some are characterized by a glomeroporphyritic texture, defined by 20-30% of cm-scale plagioclase phenocrysts. Mafic sills are generally characterized by planar and bedding-concordant contacts with sedimentary horizons. Their intrusive nature is evidenced by: (1) internal symmetrical grain size decreasing toward both contacts in thicker sills, (2) presence of angular enclaves of sedimentary rocks within sills (Fig. 6a), (3) sedimentary beds cut by adjacent sills and, (4) dike injections of mafic material into adjacent sedimentary horizons (Fig. 6a). South of the dacitic body, four main mafic sills display lateral and vertical continuity over more than 400 m without any off-set (Figs. 2a, 3). In the northern part, the mafic sill complex is more heterogeneous and probably represents fingering typical of lateral sill termination (Figs. 2a, 3). Except for a stratigraphic upward step of a glomeroporphyritic sill (Fig. 3), no crosscutting feeder dike was mapped within the mine, or identified from drill cores.

Dacitic dome

The central dacite is aphanitic, homogeneous and characterized by 10-30% of mm-scale chlorite spots (Fig. 4c). The dacite forms a 400 m-wide lenticular body injected

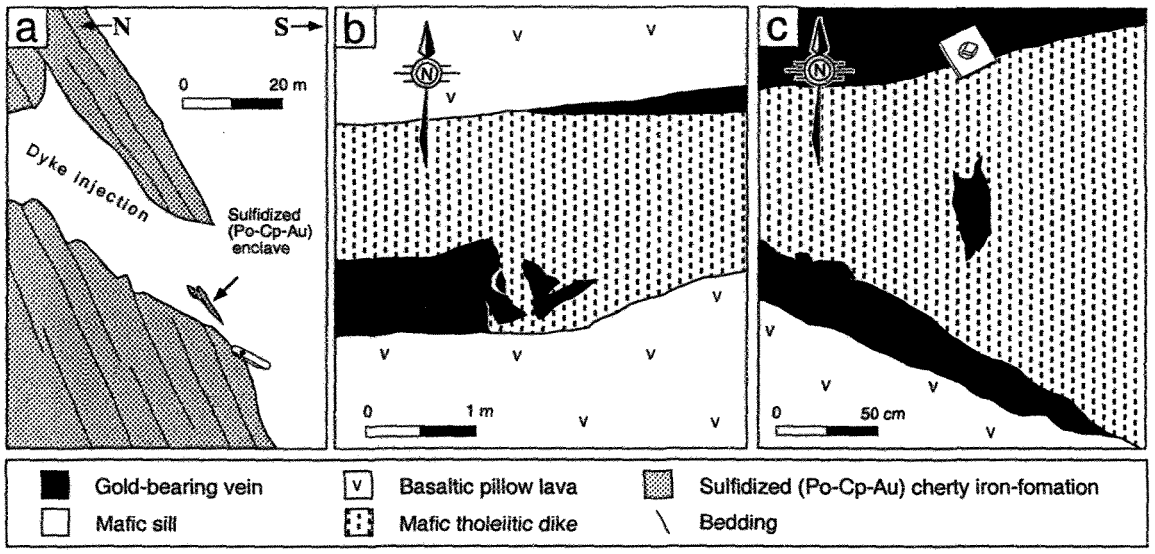

Figure 6. Sketches from photographs showing crosscutting relationships. (a) Discordant injection of sill material into mineralized (pyrrhotite-chalcopyrite) iron-formation with sulfidized (pyrrhotite) enclave. Vertical view from the zone H, level 190. (b) Mafic tholeiitic dike cutting gold-bearing vein and (c) enclave of gold-bearing vein within mafic tholeiitic dike. View of the roof of the 20 zone, stope 54-20-west.

subconformably into the sill-sediment complex (Fig. 2), which extends laterally for over 1 km. Lateral termination is expressed by progressive eastward closure and sill-sediment interstratification westward (Fig. 2a). Basal and upper contacts are planar and unbrecciated. Except for a local jigsaw breccia, defined by angular and sub-rounded cm-scale fragments contained in a chloritic matrix, the dacite is characteristically massive. The intrusive nature of this body is indicated by: (1) the crosscutting of a mafic sill (Figs. 2a, 3), (2) the presence of sedimentary enclaves within the dacite, and (3) the lack of typical textures and facies associated with an eruptive felsic dome, like a carapace breccia and lateral wedge-shaped hyaloclastite and autobrecciated fragment deposits. This body is interpreted as an endogenic dome.

Felsic dikes

Felsic porphyry dikes crosscut both the volcano-sedimentary succession and the dacitic intrusion. Dikes are divided into two main groups on the basis of phenocryst contents (Fig. 5): plagioclase-phyric dikes (FP) and quartz and plagioclase-phyric dikes (QFP). The QFP dikes systematically crosscut the FP dikes and form tabular and laterally extensive injections, whereas the latter are more irregular. QFP dikes are commonly oriented SE-NW and dip steeply NE (Fig. 7). Individual dikes are generally less than 4 m wide; wider dikes are generally composite intrusions of FP and QFP. Local offsets of sill-sediment contacts along SE-NW oriented QFP dikes (Fig. 7), without any evidence of late faulting at QFP contacts, suggest that these dikes were injected within pre-existing synvolcanic faults. This interpretation is coherent with the tabular and continuous nature of these intrusions.

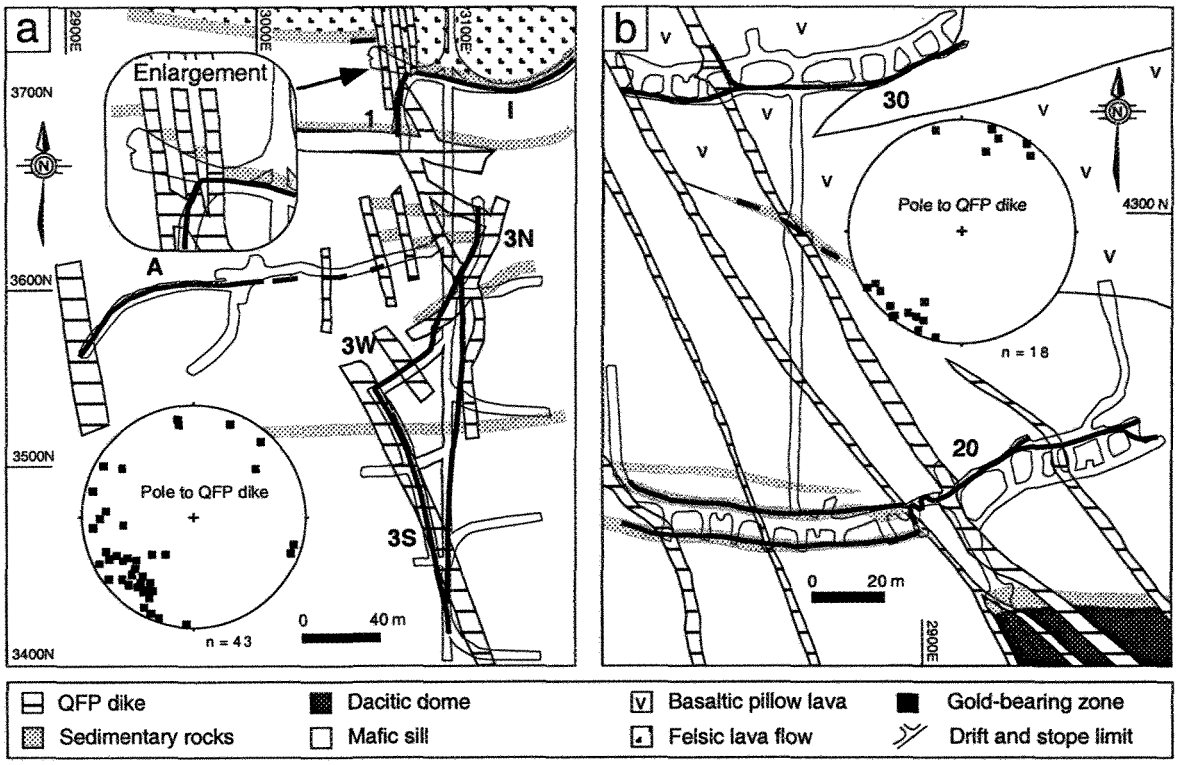

Figure 7. Geological maps from level 235 showing QFP dike distribution and their spatial association with the gold-bearing zones. (a) Mineralized zones located south of the dacitic dome. The enlargement shows displacement of a sedimentary horizon along QFP dikes, which represents evidence of dike injections along synvolcanic faults. (b) Mineralized zones 20 and 30 located north of the dacitic dome. Note the crosscutting sill intruding the pillow lava flow. Zones 15 and 40 are not developed at this level but their vertical projection plots within the corridor defined by the QFP dike swarm.

Post-mineralization mafic dikes

The first generation of mafic dikes is characterized by features indicating rapid cooling, such as aphanitic texture with conchoidal fractures, columnar joints perpendicular to wall rock (Fig. 4d) and jigsaw-fit breccia along contacts. Similar features documented in felsic dikes are interpreted as evidence for shallow-level subvolcanic emplacement (Mueller and Donaldson, 1992b). These dikes are about 2 m wide. They strike subparallel to the mafic sill complex and locally converge toward some gold-bearing veins, to follow and crosscut them (Fig. 6b, c). The second generation of mafic dikes consists to fine- to coarse-grained dikes, containing 40 to 60% euhedral hornblende phenocrysts. These dikes (< 10 m wide) display variable attitudes, locally well-developed chilled margins and step-shaped contacts.

LITHOGEOCHEMISTRY

The geochemical study on the various rocks was undertaken to characterize both igneous signatures and hydrothermal alteration. Igneous signature is defined using elements considered as relatively immobile during all but the most severe hydrothermal alteration, such as Zr, Ti, Al, Nb and Rare-Earth Elements (REE) (e.g., MacLean and Kranidiotis, 1987; Bienvenu et al., 1990).

Mafic rocks

Mafic rocks are homogeneous (Table 1 and Fig. 8). These rocks have a basaltic composition according to the Zr/Ti vs Nb/Yb plot (Fig. 8a) with a tholeiitic affinity as indicated by the Y vs Zr and Th/Yb vs Ta/Yb plots (Fig. 8b, c). Mafic rocks are characterized by relatively flat REE and HFSE patterns, expressed by $[La/Yb]_N$ (normalized to chondrite value of Thompson et al., 1984) values of 0.6 - 1.9 and by small

Table 1. Geochemical characteristic of the various rock types

	Mafic sill		Pillow lava		Mafic dike		Felsic lava		Dacitic dome		FP dike		QFP dike		Shosho. dike	
	X	SD	X	SD	X	SD	X	SD	X	SD	X	SD	X	SD	X	SD
XRF	n = 94		n = 8		n = 4		n = 8		n = 11		n = 28		n = 13		n = 9	
SiO2 (%)	46.65	1.32	46.81	1.65	46.45	2.82	65.54	6.84	66.94	5.30	64.35	5.56	67.90	3.43	42.46	3.45
TiO2	0.86	0.10	0.81	0.03	1.08	0.13	0.47	0.27	0.38	0.17	0.56	0.24	0.35	0.13	0.68	0.20
Al2O3	14.42	0.80	14.25	0.48	14.95	0.59	13.44	1.61	13.39	2.32	14.44	1.25	13.72	0.75	9.75	1.09
Fe2O3	12.21	0.93	11.66	1.15	14.37	2.31	5.22	2.33	4.68	1.65	5.10	1.87	3.40	1.53	9.39	1.11
MnO	0.19	0.02	0.20	0.03	0.18	0.02	0.06	0.03	0.06	0.02	0.06	0.02	0.06	0.03	0.18	0.02
MgO	7.51	1.05	5.41	1.14	6.98	0.14	1.75	1.24	1.48	0.75	1.70	0.93	0.93	0.43	11.92	2.99
CaO	9.89	1.12	11.38	1.33	7.21	2.06	3.48	1.45	3.06	1.34	3.52	0.93	3.52	1.13	12.44	4.76
Na2O3	1.37	0.49	1.04	0.46	1.45	0.67	2.49	1.19	2.75	1.84	2.60	1.38	1.45	1.41	1.26	0.88
K2O	0.41	0.41	0.22	0.42	0.59	0.99	2.24	0.69	2.00	1.04	2.19	0.94	3.13	0.83	0.56	0.28
P2O5	0.04	0.02	0.02	0.01	0.06	0.03	0.10	0.07	0.07	0.04	0.12	0.07	0.07	0.04	0.52	0.11
LOI	6.27	2.52	8.13	2.45	6.57	2.18	4.73	0.98	4.65	1.43	4.97	1.64	5.29	1.32	10.34	5.21
Total	99.83	0.68	99.90	0.51	99.73	0.32	99.24	0.67	99.45	0.61	99.61	0.76	99.81	0.68	98.71	3.32
Sr (ppm)	122	47	142	59	157	84	142	97	105	72	127	93	73.31	33.10	580	288
Rb	21	16	17	18	47	62	67	31	65	28	70	28	87.38	19.75	21	14
Nb	3	1	4	0	4	1	8	2	9	3	8	2	6.92	2.90	5	2
Y	21	3	20	2	24	10	20	8	19	12	16	4	10.85	3.34	19	4
Zr	56	7	58	3	65	11	189	48	181	55	162	18	141.54	17.25	161	31
INAA	n = 21		n = 3		n = 3		n = 6		n = 6		n = 6		n = 2		n = 6	
Hf	1.4	0.2	1.2	0.2	1.6	0.4	4.8	1.3	3.7	0.9	3.6	0.4	3.8	0.4	3.0	0.8
Ta	0.2	0.1	0.3	0.2	0.1	0.0	0.6	0.2	0.6	0.2	0.7	0.3	0.4	0.0	0.3	0.2
Th	0.1	0.0	0.1	0.0	0.2	0.0	2.3	1.1	2.2	0.6	2.0	0.4	2.4	0.0	3.4	1.7
La	2.8	1.0	2.4	0.2	4.2	0.1	19.8	5.5	16.5	4.8	17.3	2.1	20.5	4.9	44.2	13.7
Ce	7.0	2.4	6.3	0.6	9.5	0.7	40.2	10.8	33.7	10.9	35.7	5.0	41.0	12.7	109.6	35.6
Nd	5.0	2.1	6.0	1.0	6.0	1.4	18.5	4.6	14.0	5.2	15.3	2.9	14.0	7.1	65.0	18.7
Sm	2.1	0.4	1.9	0.1	2.5	0.1	4.1	1.1	2.9	0.9	3.2	0.7	2.7	0.7	13.0	3.4
Eu	0.8	0.2	0.7	0.1	0.9	0.1	0.9	0.3	0.7	0.1	0.9	0.2	0.7	0.1	3.0	0.9
Tb	0.5	0.1	0.4	0.1	0.7	0.2	0.5	0.1	0.3	0.1	0.3	0.1	0.3	0.0	0.9	0.1
Yb	2.1	0.3	1.9	0.2	3.0	1.1	1.9	0.9	1.1	0.7	1.2	0.2	0.9	0.3	1.2	0.4
Lu	0.3	0.1	0.3	0.0	0.4	0.2	0.3	0.1	0.2	0.1	0.2	0.0	0.1	0.1	0.2	0.0

X=average, SD=standard deviation, LOI= loss on ignition, XRF= X-ray Fluorescence, INAA= instrumental neutronic activation analysis

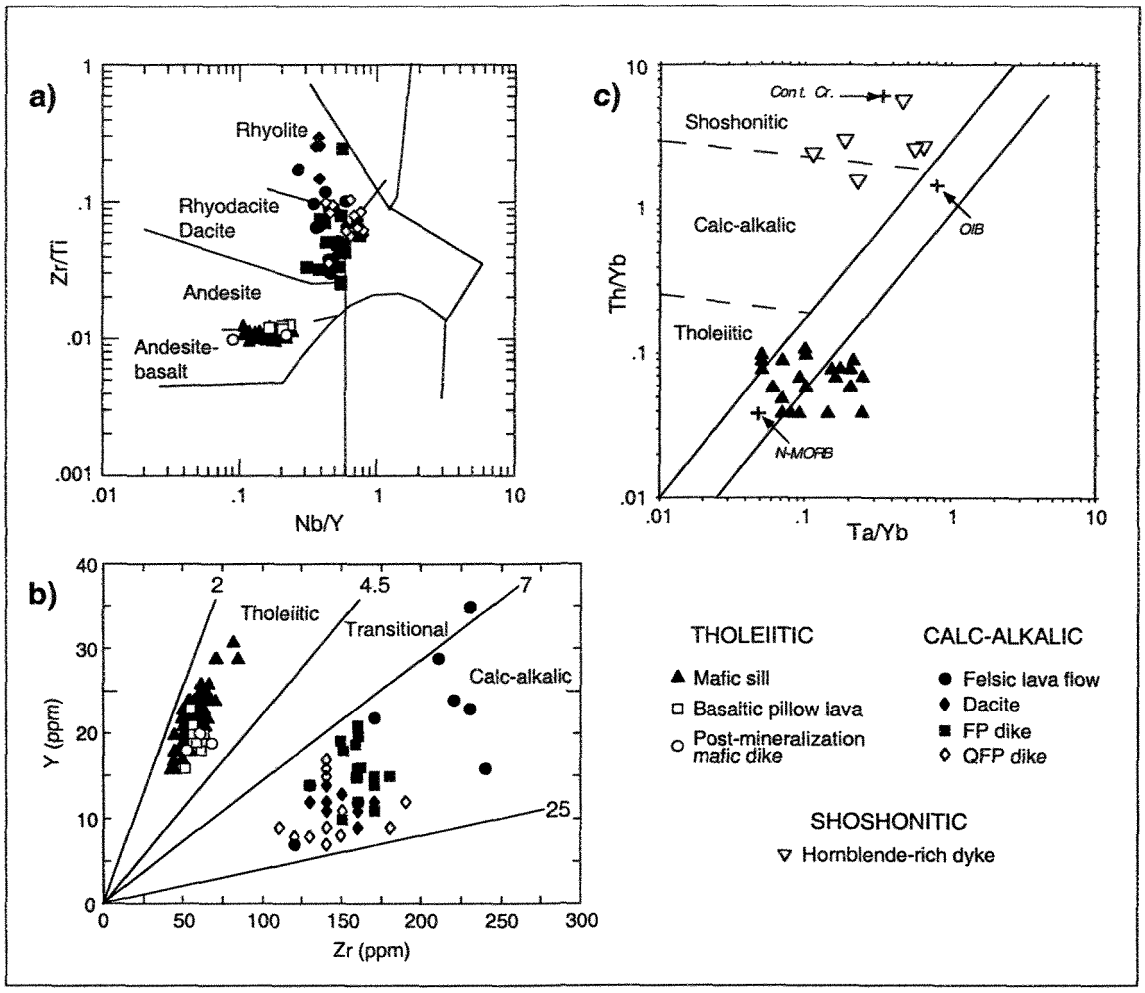

Figure 8. Geochemical discrimination diagrams. (a) Zr/Ti vs Nb/Yb plot (Winchester and Floyd, 1977). (b) Y vs Zr plot (Barrett and MacLean, 1994). (c) Th/Yb vs Ta/Yb plot (Pearse, 1983).

negative Hf and Ti anomalies (Fig. 9). The REE and HFSE abundance is under 11x chondrite, indicating that these rocks are relatively primitive and weakly fractionated by low pressure differentiation processes. The REE-HFSE signature of these tholeiites is typical of first volcanic cycle basalts (Picard and Piboule, 1986).

Felsic rocks

The felsic rocks range in composition from dacite to rhyolite according to the Zr/Ti vs Nb/Yb plot (Fig. 8a) and are calc-alkalic based on the Y vs Zr plot (Fig. 8b). These rocks are enriched in LREE (Fig. 9) as expressed by a mean value of $[La/Yb]_N$ = 11.6. They are also depleted in Ti, Ta and Nb relative to REE of similar incompatibility (Fig. 9). These geochemical data, taken together, imply that the degree of differentiation is high. The geochemical signature of these rocks is comparable to Archean volcanic felsic rocks of group FII (Lesher et al., 1986) and group III (Barrie et al., 1993) from the Abitibi belt.

Post-mineralization mafic dikes

The first generation is comparable to the mafic volcanic rocks, having a tholeiitic basaltic composition (Fig. 8a, b), a flat REE and HFSE pattern ($[La/Yb]_N$ values of 0.8 - 1.3), small negative Hf anomaly and REE and HFSE abundance under 11x chondrite (Fig. 9). The hornblende-rich dikes are shoshonitic based on the Th/Yb vs Ta/Yb plot (Fig. 8c). These rocks are characterized by a high degree of LREE fractionation, as expressed by a mean value of $[La/Yb]_N$ = 26.8 and by depletion of Ti, Hf, Zr, Ta and Nb relative to REE of similar incompatibility (Fig. 9). The shoshonitic geochemical signature of these dikes is similar to that of Archean lamprophyres (Wyman and Kerrich, 1993) and shoshonitic volcanic rocks of the Chibougamau area (Dostal and Mueller, 1992).

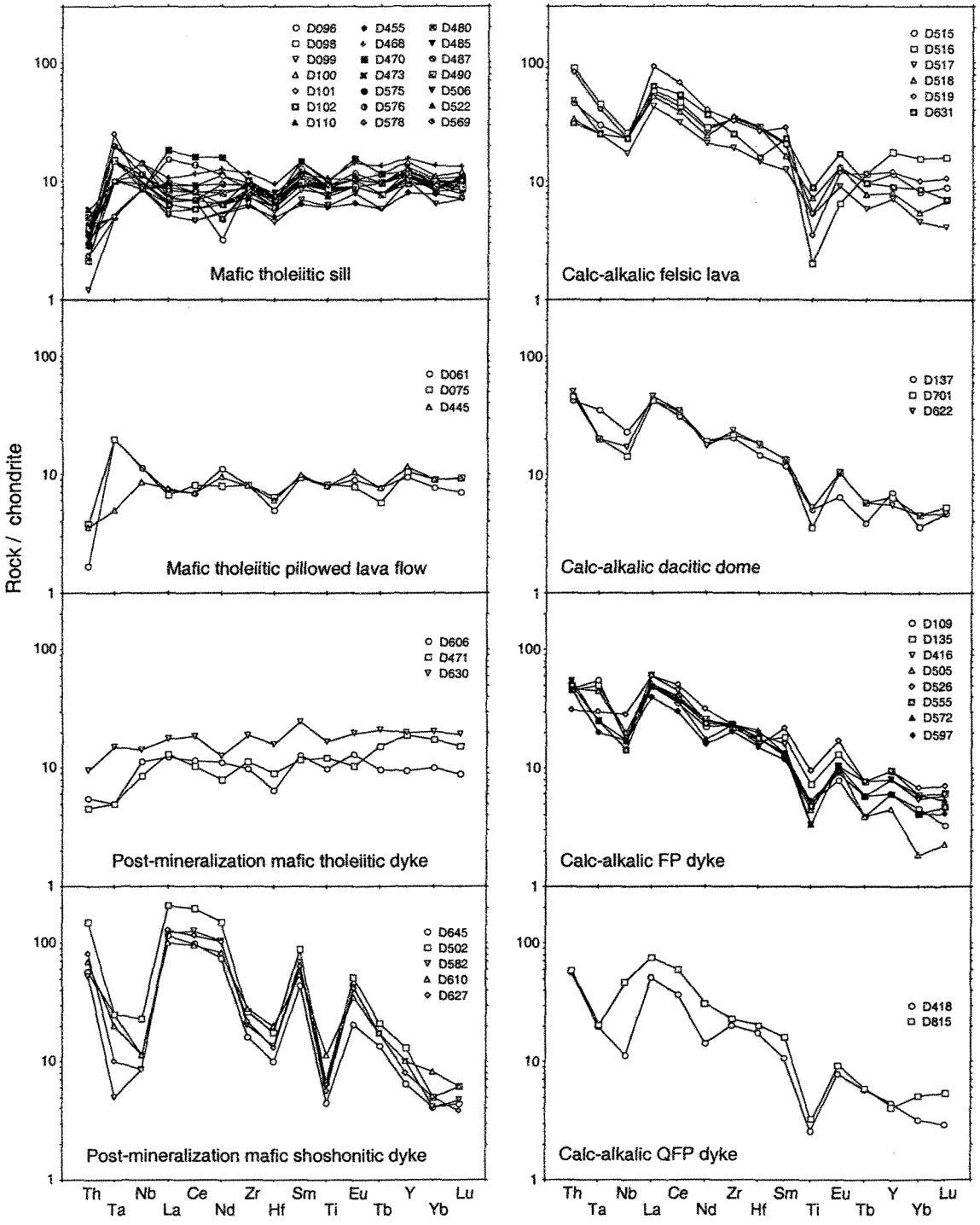

Figure 9. Chondrite normalized REE-HFSE plot for the various rocks. Normalizing values after Thompson et al. (1984).

VOLCANISM AND MAGMATISM

Construction of the volcanic pile

Volcanic rocks and related intrusions define two main stages of emplacement: seafloor volcanism and sedimentation, and felsic complex intrusion. The seafloor stage includes rocks strictly formed on the paleo-seafloor, as sedimentary rocks and mafic and felsic lava flows, and later mafic sill injections. Basaltic lava was extruded first, followed by felsic lava according to their relative stratigraphic position (Fig. 3). Felsic and basaltic lavas formed during continuous sedimentation as indicated by their interstratification with sediments. Later intrusion of mafic sills is indicated by crosscutting of pillowed (Fig. 7b) and felsic lava flows (Fig. 3). The planar and concordant nature of sill contacts, absence of peperite and angular sedimentary enclaves within sills implies that sediments were partly to totally indurated or consolidated during sill introduction (cf. Kokelaar, 1982). However, south of existing mine drifts (i.e., closer to the paleosurface), drill cores display irregular and peperitic-like contacts between mafic sills and sediments (Gaboury, 1996). Considering that sills are commonly introduced successively upward into the sedimentary pile (Einsele, 1985; 1986), these irregular contacts suggest that later and upper sills reached the wet and unconsolidated upper portion of the sedimentary pile. The felsic complex formation is well constrained by crosscutting relationships which imply the initial formation of the dacitic dome, followed by multiphase injections of FP dikes, and later introduction of QFP dikes along synvolcanic faults.

U-Pb zircon dating realized at the Royal Ontario Museum (see Morasse et al., 1995 for technical procedures) yields an age of 2722 ± 2 Ma for the QFP dikes (Fig. 10). This age brackets the end of felsic magmatism at a period consistent with the known age of the first volcanic cycle (2730-2720 Ma).

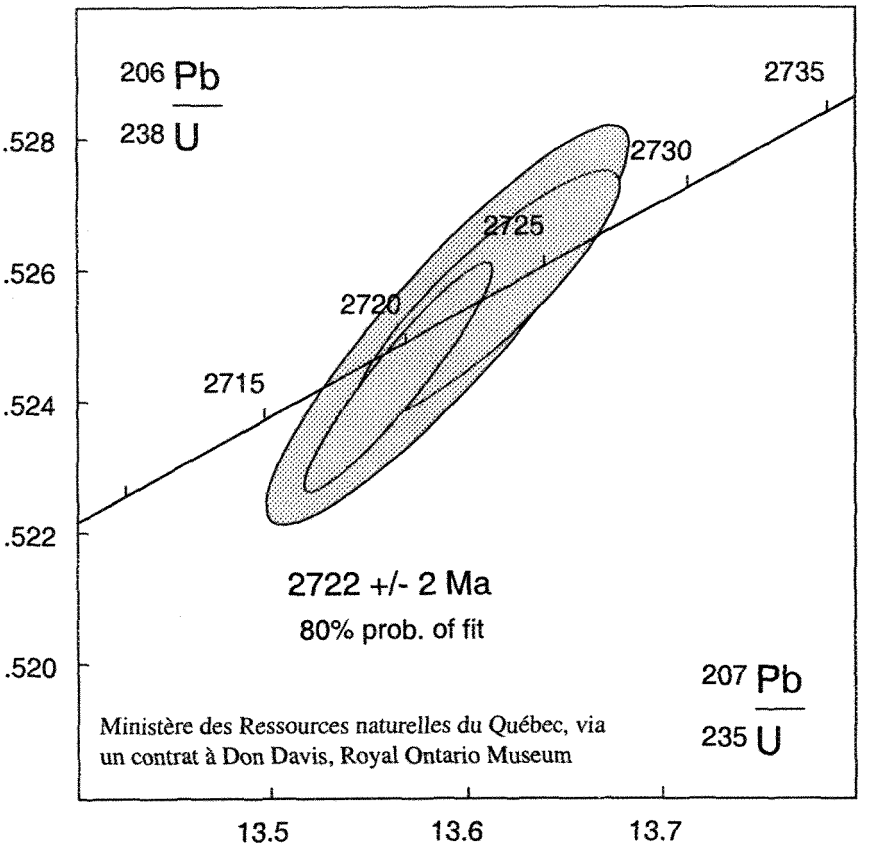

Figure 10. U-Pb concordia diagram of abraded zircon analyses from a QFP dike. Ellipses represent 2σ uncertainty in U-Pb isotope ratios.

Magmatic sources

Geochemistry of the various rocks, except for the late shoshonitic dikes, defines two distinct groups: mafic tholeiitic and felsic calc-alkalic rocks (Fig. 8b). In each group, the various rock types are characterized by similar REE-HFSE profiles (Fig. 9) suggesting that all calc-alkalic felsic rocks are cogenetic and all mafic tholeiitic rocks, including post-mineralization tholeiitic dikes, are also cogenetic. Considering the mutual crosscutting relationships between mafic and felsic rocks (Figs. 11, 12), a cyclic differentiation of an unique magmatic source is unlikely. The crosscutting features are best explained by sequential pulses of volcanic products originating from two different magmatic sources. This two-source interpretation is also consistent with the lack of transitional rock in the volcanic pile and the specific differentiation trend for each group (Fig. 8b).

Relative proximity of volcanic centers

The interpretation of bimodal volcanism from two different magmatic sources implies the existence of two different and spatially isolated volcanic centers. Some features indicate the relative proximity of these volcanic centers. For felsic volcanism, which forms relatively small and laterally restricted edifices, the dacitic dome and the abundance of FP and QFP dikes are features indicating the proximity of the felsic center (e.g., Cas, 1992; Mueller and Donaldson, 1992b; Gibson et al., 1997). For mafic volcanism, which constitute large, multi-centers, and laterally extensive edifices (e.g., Bloomer et al., 1989; Chown et al., 1992), it is difficult to determine precisely the position with respect to the edifices. The lack of feeder dikes associated with the mafic sills suggests, by comparison with the felsic volcanism, a more distal environment. The laterally extensive nature of mafic sills relative to their feeder position, defined by great lateral extension compared to thickness (300:1, Leaman, 1995), is also consistent with a more distal volcanic center.

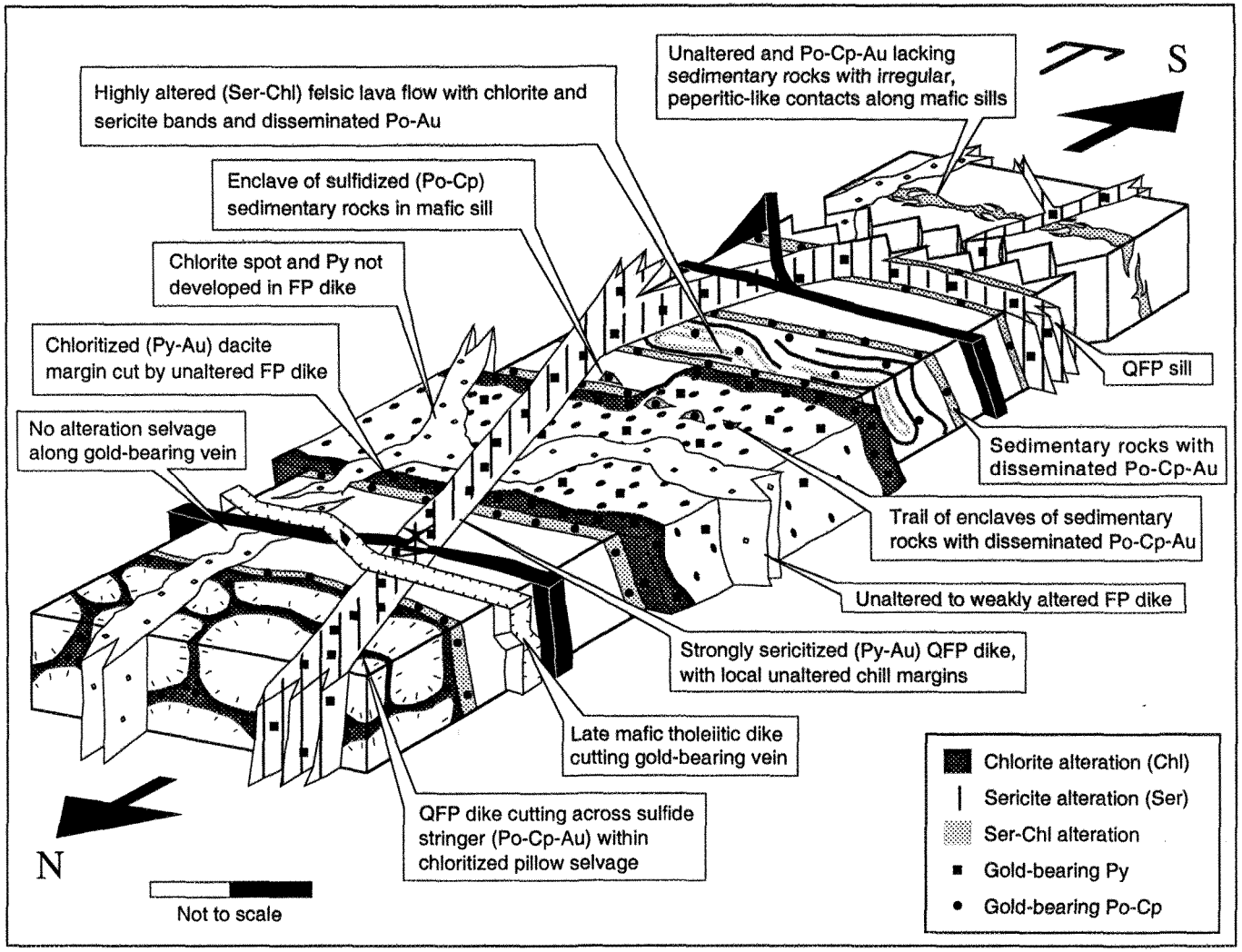

Figure 11. Schematic 3D representation of the spatial distribution and systematic crosscutting relationships of various rocks, alteration and mineralization throughout the host sequence.

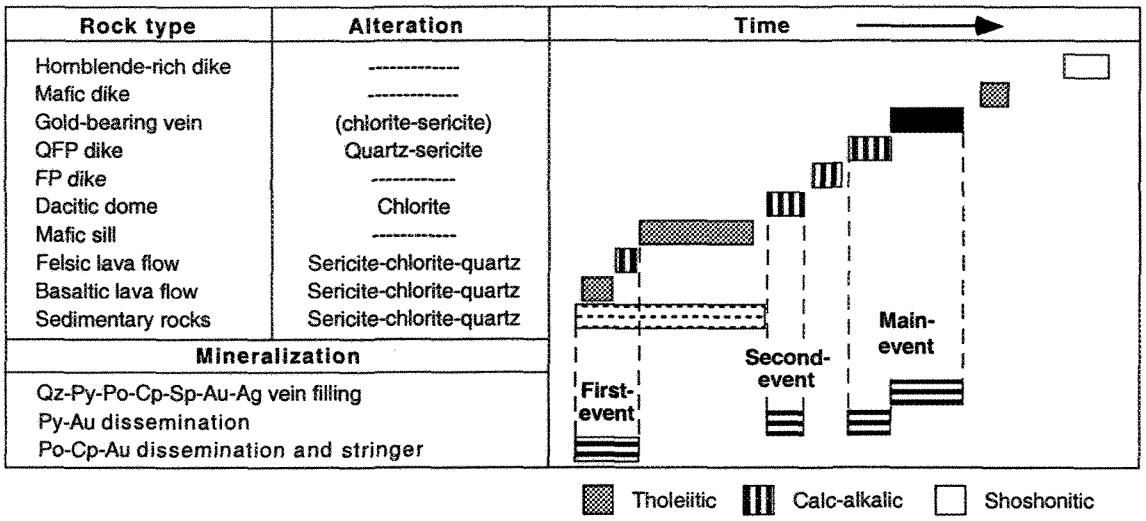

Figure 12. Chronologic relationships between rocks, alteration and mineralization.

Therefore, construction of the host volcanic pile is best explained by sequential pulses from two different volcanic centers: a proximal felsic center and a more distal mafic center.

Water depth constraints

Submarine volcanic products vary with water depth due to pressure exerted by the water column, which can (1) inhibit volatile expansion (boiling) and limit explosive fragmentation (McBirney, 1963) and vesicle formation (Spark, 1978) and (2) contribute significantly to the total pressure exerted on magma, thus favoring lateral magma movement (sill formation) rather that vertical magma movement leading to an eruption (cf. Walker, 1989; McPhie, 1993). Volatile expansion is limited by the critical point of pure water (2.16×10^7 Pa), which corresponds to a confining pressure exerted by at least 3 150 m of seawater (Bischoff and Rosenbauer, 1984). This value is generally considered as the maximum depth for explosive eruptions (Gibson et al., 1997).

The lack of evidence for explosive felsic volcanism and the low (< 1%) vesicle or amygdule content (Jones, 1969; Moore and Schiling, 1973) of volcanic rocks suggest a deep water setting, probably below or close to the 3 150 m limit. This setting is compatible with the pelitic nature of sediments and presence of Algoma-type iron-formations (Mueller and Donaldson, 1992a; Eriksson et al., 1994). A deep water setting is also consistent with the abundance of sill-like intrusive volcanic rocks (mafic sills and dacitic dome), as exemplified by the deep water (3 300 m) sill-sediment complex of the Escanaba Trough (Zierenberg et al., 1993).

Reconstructed architecture of the host sequence

Considering the deformed host sequence, the mine plan (Fig. 2a) can be viewed as a true cross-section through the volcanic pile. In detail, a 75° northward rotation along an E-

W subhorizontal axis, corresponding to strata dip and fold axis respectively, allows the reconstruction of subhorizontal surfaces and the determination of the initial attitudes of crosscutting planar elements such as QFP dikes and gold-bearing veins (see below). The reconstructed E-W cross-section of the deposit (Fig. 13) illustrates the spatial association between the dacite dome, QFP dikes and gold-bearing veins at mine-scale, emphasizing that gold-mineralization is distributed around a felsic center.

HYDROTHERMAL EVENTS

Three successive mineralizing events are recognized, based on crosscutting relationships, but only the last is economically significant. Each event affects specific rock types and is characterized by particular styles, sulfide assemblages, alterations and gold grades (Fig. 12). Special emphasis was given to the timing of the main mineralizing event due to its genetic significance.

First mineralizing event

The first event is characterized by dissemination and stringers of auriferous (1-3 g/t Au: Cambior, unpub. data) of monoclinic pyrrhotite and chalcopyrite (pyrrhotite: chalcopyrite = 20:1) with chlorite, sericite and quartz alteration. In pillow lava, mineralization occurs as stringers concentrated around pillow selvages, forming up to 20% of the entire rock (Fig. 14a). Gold occurs as minute inclusions in pyrrhotite (Fig. 14b). Intense muscovite-sericite alteration imparts a beige color to the lava. It is best developed at the top of the pillow lava flow and it is crosscut by the #30 gold-bearing vein (Fig. 15). Mass balance calculations indicate loss of Fe_2O_3 and MgO compared to an unaltered pillow lava sample (Fig. 16). In sedimentary rocks, first event mineralization occurs as disseminations and as replacement of magnetite-rich beds. Distinctive alteration occurs as

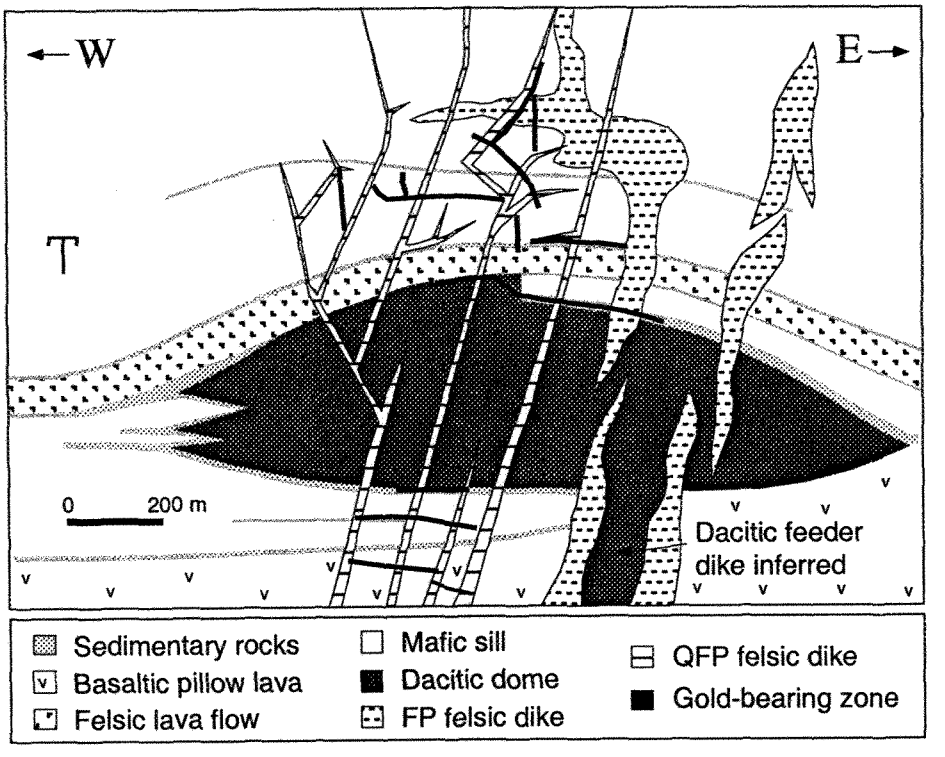

Figure 13. Reconstructed E-W cross-section of the volcanic sequence before tilting related to the ductile regional deformation.

Figure 14. Photographs of the main mineralizing features. (a) Typical stringer of gold-bearing pyrrhotite-chalcopyrite (Po) occurring in the selvage of pillow lava (P). (b) Photomicrograph of gold (Au) inclusion in pyrrhotite (Po) with a chalcopyrite grain (Cp) of the first mineralizing event. (c) Discordant chlorite and sericite (arrows) alteration superposed on sedimentary rocks, pocket knife for scale. (d) Gold-bearing pyrite (Py) plating joints in pervasively chloritized dacite. Pyrite aggregates (Py) are crosscut by a younger quartz-sulfide veinlet (V) related to the main mineralizing event. Note that both mineralization styles are overprinted by the ductile deformation. (e) Typical gold-bearing quartz (Qz) and sulfide (Py) vein occuring in mafic sill. Dashed lines show the sharp contacts. (f) Typical stratabound mineralization style showing both quartz-sulfide veinlets (V) and concordant parallel layers of massive pyrite (Py).Fig. 4. Slabs of typical styles of gold mineralization preceding vein formation. (a) Typical stringer of gold-bearing monoclinic pyrrhotite (Po) with trace of chalcopyrite occurring in the selvages of pillow lava related to the first mineralizing event. (d) Disseminated gold-bearing pyrite (Py) in pervasively chloritized dacite related to the second mineralizing event. Pyrite aggregates (Py) are crosscut by a younger quartz-sulfide veinlet (V) related to the main mineralizing event. Note that the veinlet and pyrite aggregates are overprinted by the ductile deformation.

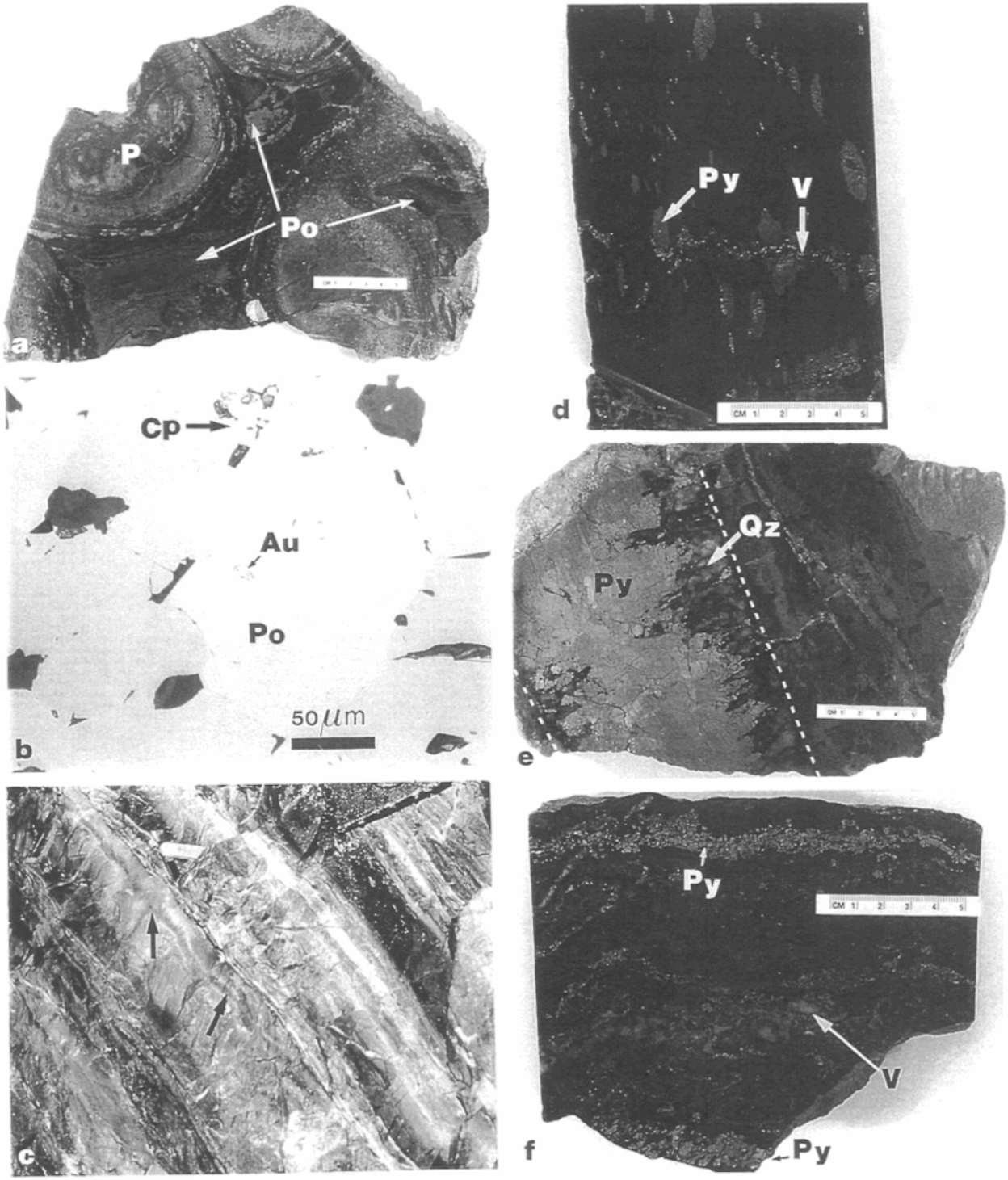
P
Po
a
Cp
Au
Po
50 μm
b
c
Py
V
d
Qz
Py
e
Py
V
Py
f

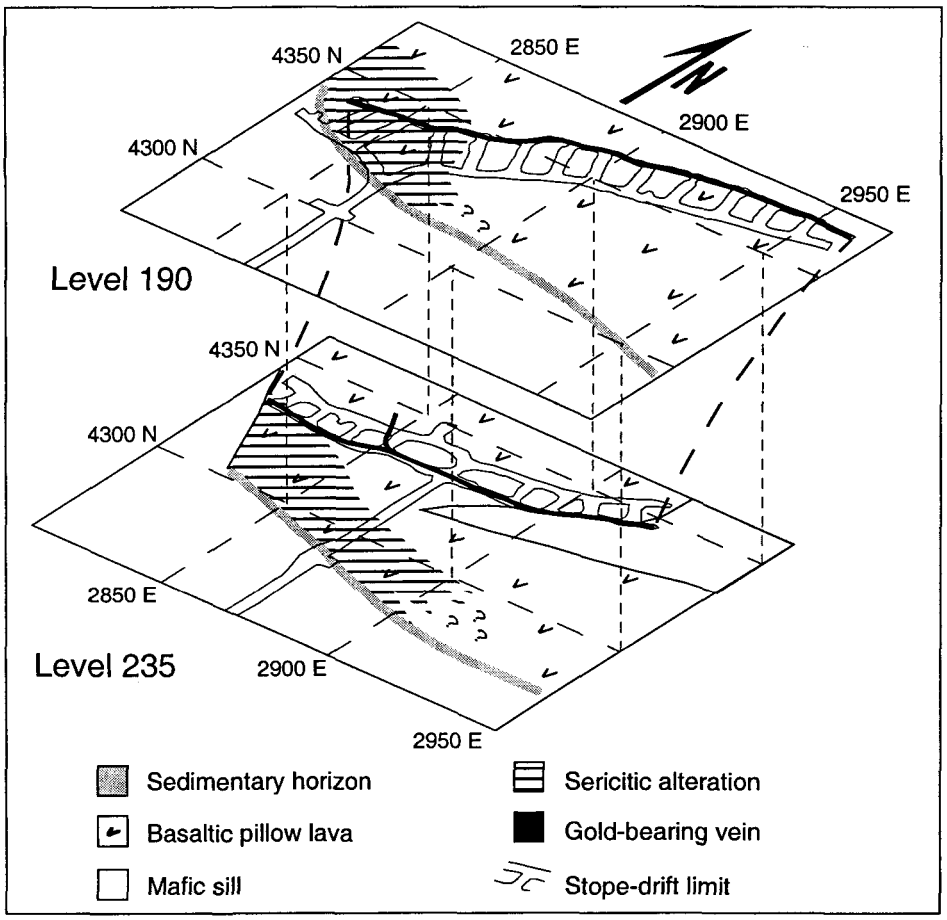

Figure 15. Spatial distribution of sericitic alteration developed along flow top at levels 190 and 235.

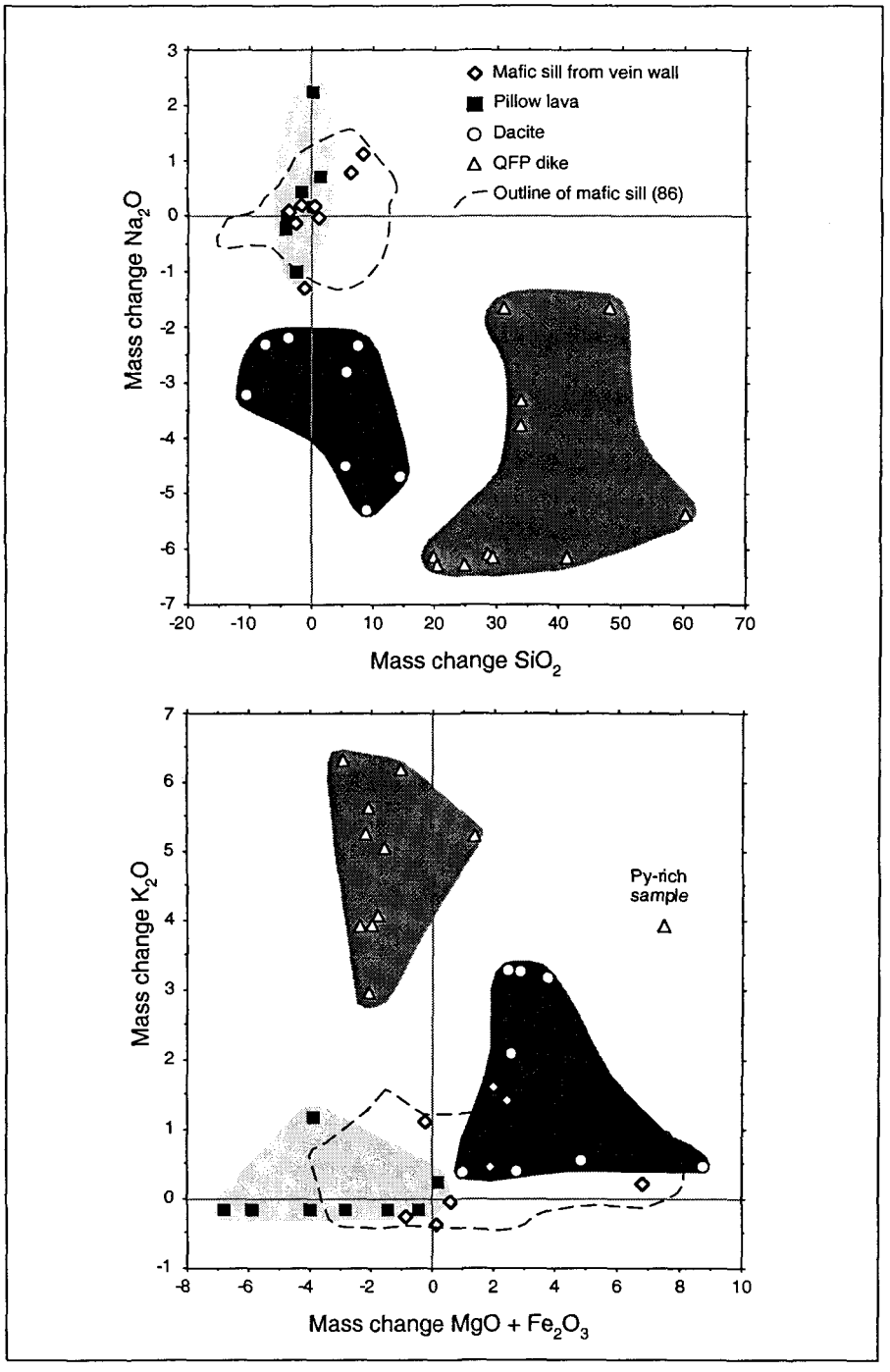

Figure 16. Plots of calculated mass change, using a single unaltered precursor and Zr as immobile monitor element (MacLean and Kranidiotis, 1987; MacLean, 1990). (a) Na_2O versus SiO_2 and (b) K_2O versus $MgO+Fe_2O_3$. Each rock type is characterized by a specific alteration. Note that samples from the selvages of gold-bearing vein plot within the cluster of 86 mafic sills. Mass changes are in absolute wt%.

mm- to cm-wide chloritic and sericitic bands that mimic the primary bedding (Fig. 14c). Pervasive quartz alteration accounts for the high silica content of some volcaniclastic deposits. The felsic lava flow is characterized by disseminated pyrrhotite (< 2%) and by strong sericitic alteration which has destroyed all plagioclase in the rock (Fig. 5). Chlorite alteration occurs as bands overprinting original flow-banding.

First event mineralization and alteration affected rocks formed on the paleo-seafloor (Fig. 11). The early timing of this event is constrained by crosscutting relationships. Sulfide stringers within pillow lava are clearly cut by younger FP and QFP dikes (Figs. 11, 17). Mafic sills lack any evidence of this first mineralizing event. Alteration is visually absent and mass balance calculation plots display a cluster of 86 samples indicating that mafic sills are effectively devoid of significant alteration (Fig. 16). Furthermore, enclaves of sulfidized (pyrrhotite-chalcopyrite) sediments in some mafic sills (Figs. 6a, 11) clearly constrain this mineralizing event to a period prior to mafic sill injection.

Second mineralizing event

The second mineralizing event involves chloritic alteration and auriferous pyritic mineralization of the dacite dome (Fig. 11). Alteration and mineralization are zoned within the dome. Pervasive chloritization, inducing a homogenous black color, and associated joint-plating of gold-bearing pyrite (< 10 %) occur mainly at the top and base of the dome (Fig. 14d). This pervasive alteration grades progressively inward to a spotty chloritic alteration and associated disseminated pyrite (< 3%). Chlorite forms up to 30% of the rock, occurring as mm-wide spherical replacement patches (Fig. 4c) of plagioclase phenocrysts. Gold values associated with this event are erratic, and range from nil to locally up to 20 g/t

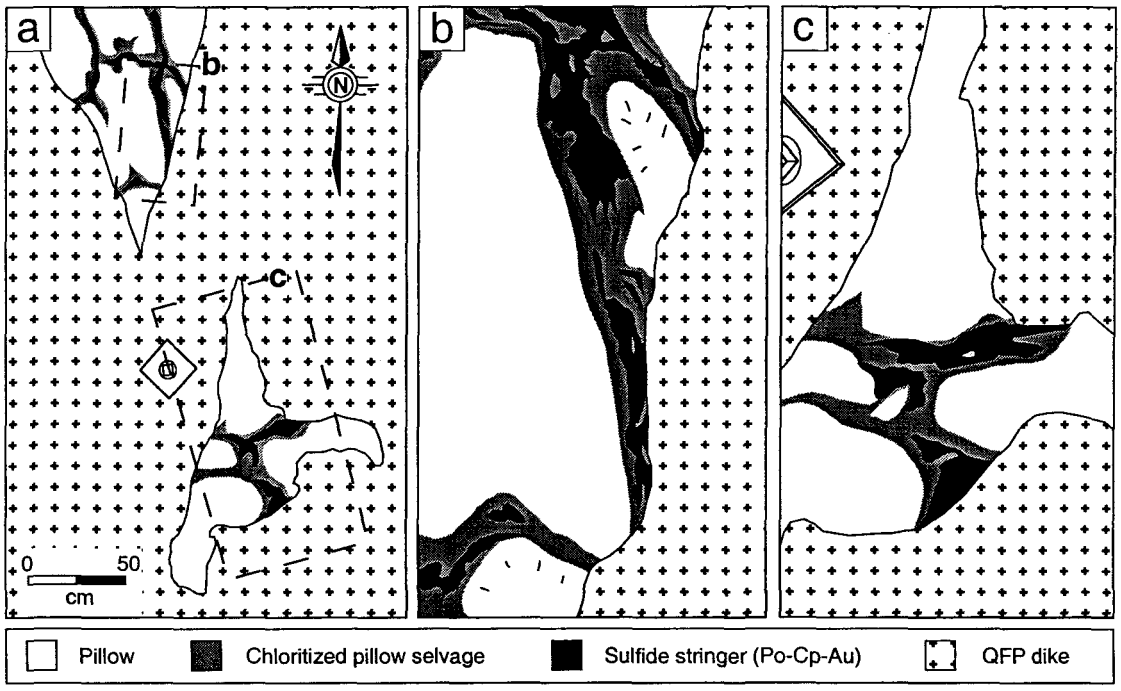

Figure 17. Sketches from photographs showing a QFP dike crosscutting pyrrhotite-chalcopyrite stringer mineralization in pillow lava. (a) Overview showing an enclave of pillow lava within the QFP dike. (b, c) Detailed views. View of the roof of the drift along the 20 zone, level 485.

(Cambior, unpub. data). The chloritization correlates with a gain of Fe_2O_3 and MgO, ($\pm$ K_2O), and loss of Na_2O (Fig. 16).

The second mineralizing event is separated from the first event by a period of mafic sill injection. The second event, which only affects the dacitic dome and not the surrounding mafic sills, is interpreted to be the result of an autometasomatic mineralizing process related to dome emplacement and cooling, because later FP dikes, which crosscut the dome, are neither altered nor mineralized (Fig. 11). Since these dikes are petrographically (Fig. 5) and geochemically (Fig. 9) similar to the dacite, it is unlikely that they could have been unaffected by this mineralizing event.

Main mineralizing event

The main event hydrothermal activity leads to the formation of gold-bearing quartz and sulfide veins and associated stratabound ore as well as mineralization and alteration within QFP dikes (Fig. 11). Gold-bearing veins (Fig. 14e) are generally massive, have an average thickness of 50 cm and are rich in gold (commonly >100 g/t Au). The vein contacts range from sharp, planar and free of surrounding planar fabric, to locally undulose and schistose. Vein geometry, especially south of the dacitic dome, is complex (Fig. 2) and composed of four main sets: (1) E-W steeply (70-85°) S dipping, (2) N-S moderately (45°) E dipping, (3) SE-NW moderately (50°) NE dipping, and (4) SW-NE moderately (40°) SE dipping (Gaboury et al. 1996). Interbranching of main vein sets is a common phenomenon (Fig. 11). Gangue minerals are dominated by quartz with minor amounts of calcite, chlorite, sericite and metamorphic actinolite. Sulfide content of pyrite, hexagonal pyrrhotite, chalcopyrite and sphalerite ranges from 5% to 80%, with an average of 25%. Gold occurs mainly as μm-scale inclusions in all sulfides and in smaller amounts as fine fracture fillings in pyrite. Veins are characterized by open-space filling textures (Gaboury

et al., 1996) which, together with features such as bridge stud (cf. Foxford et al., 1995), indicate formation by extensional fracturing. Stratabound ore consists of gold-bearing segments of sedimentary horizons, where mineralization occurs as subconcordant, mm- to cm-wide quartz-sulfide veinlets (Fig. 14f), identical to main gold bearing veins, and concordant, parallel layers of massive pyrite (Gaboury et al., 1996). Gold-bearing veins are mainly developed within and at contacts between mafic sills. Stratabound ore formation depends on the presence of sedimentary lenses at the mineralized boundary of the mafic sills. Alteration related to vein and veinlet formation is weak to absent; where developed it corresponds an irregular mm-scale envelop of sericite and/or chlorite. The weakness of the alteration is also indicated by the inconclusive mass change variations of mafic sill samples from vein walls (Fig. 16).

Mineralization within the QFP dikes occurs as multiple, mm-wide quartz and sulfide veinlets and disseminated auriferous pyrite. An intense and pervasive quartz and sericite alteration affects these dikes (Figs. 5, 11). This alteration is restricted to the dikes. Local sericitic veinlets cutting unaltered margins indicate that alteration was related to fracture-induced permeabilities. Mass balance calculations indicate SiO_2 and K_2O gains and loss of Na_2O (Fig. 16). This alteration-mineralization within QFP dikes is a ubiquitous phenomenon developed at the deposit scale (Fig. 11). Systematic QFP assays have revealed erratic gold grades ranging from nil to over than 100 g/t Au (Cambior, unpub. data).

Timing of the main mineralizing event

The absolute timing of the main mineralizing event remains to be established. However, evidence for a volcanic-related timing is presented below based on crosscutting and geometrical relationships.

The main mineralizing event overprints the QFP dikes whereas tholeiitic mafic dikes crosscut gold-bearing veins (Fig. 6b, c). These mafic dikes are interpreted as cogenetic with hosting mafic sills and display features typical of shallow subvolcanic dikes. Such relationships constrain this mineralizing event after the end of the 2722 ± 2 Ma felsic calc-alkalic activity but before the end of the mafic tholeiitic magmatism.

This volcanic-related timing implies that the actual geometry of the gold-bearing vein network results from the tectonic tilting affecting the whole sequence. Such tilting can be ascertain by comparing the geometrical features associated with both, the actual (Fig. 18a) and the reconstructed (untilted) vein networks (Fig. 18b). For the actual network, veins and QFP dikes are characterized by numerous directions and dips (Fig. 18a), whereas for the reconstructed network, untilted veins and dikes show a more coherent system characterized by a similar direction with only variable dips (Fig. 18b). Additionally, the poles to the main vein sets, which correspond to the opening extensional vector, all lie in an inclined plane for the actual (Fig. 18c) and in a vertical plane for the reconstructed vein network (Fig. 18d). Such a projection of poles into a plane indicates that two of the three vectors defining the stress field are close to the same magnitude, a feature accounting for the interbranching of the main veins. It is noteworthy that the rotated geometry becomes a coherent system compatible with a vertical attitude of the principal stress axis $\sigma 1$ (Fig. 18d). Such a vertical $\sigma 1$ attitude accounting for the lithostatic load is expected for vein networks developed at shallow crustal level. Consequently, the vein network is geometrically more coherent when considered rotated back, implying that it is folded as the host strata. Additionally, the increasingly complex geometry of the vein network from north to south (Fig. 2) is also consistent with a tilted network initially formed in shallow crustal level, where increased complexity of vein network is related to diminishing confining pressure closer to the paleosurface (Gaboury et al., 1996).

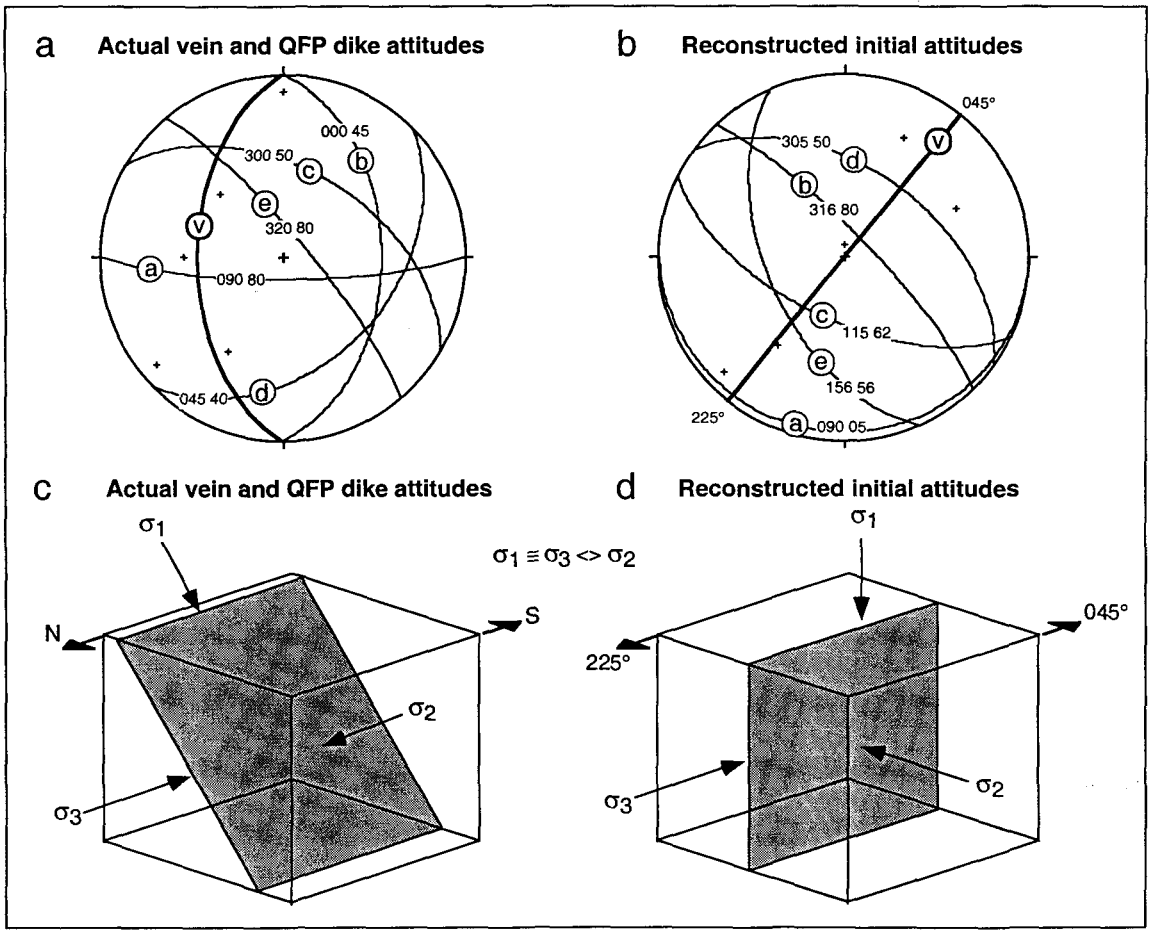

Figure 18. Structural features of veins and QFP dikes. Equal area projections (lower hemisphere) of (a) actual and (b) reconstructed (untilted) main vein and QFP dike attitudes (vein data from Gaboury et al., 1996). The reconstructed attitude results from a 75° northward rotation along an E-W subhorizontal axis, corresponding to the strata dip and fold axis. For reference, main gold-bearing veins are labeled a, b, c, d, whereas e corresponds to QFP dike. The V plane is defined by the poles to the main veins and QFP dikes. Actual (c) and reconstructed (d) stress fields to account for the V plane.

All together, these crosscutting and geometric features are consistent with a gold-bearing vein formation occurring after the end of the felsic magmatism, in an original volcanic setting, in shallow crustal level, and in an extensional tectonic regime.

GENETIC MODEL

A four-stage model is proposed to account for the three successive mineralizing events, based on the parallelism between relative chronology of volcanic and hydrothermal activities (Fig. 12). At Stage 1, diffuse seafloor-related hydrothermal fluids altered and mineralized lavas and sediments lying at the top of the North volcanic assemblage (Fig. 19a). Stage 2 involves the sealing of the hydrothermal system at the base of the newly formed, altered and mineralized seafloor sequence (Fig. 19b) by the sequential injection of a 1 km thick stack of mafic sills into altered, mineralized and hydrothermally indurated sediments (Fig. 19b). Declining hydrothermal activity induced by sill injections is consistent with the lack of alteration and mineralization and presence of peperite-like textures within sedimentary horizons at the upper stratigraphic levels. These features suggest that first sills were injected within sediments indurated by Stage 1 hydrothermal activity, as documented at Middle Valley (Goodfellow and Zierenberg, 1997), whereas later upwardly introduced sills encountered newly deposited, unaltered, unmineralized, wet sediments (Fig. 19b). Stage 3 involves reactivation of the mineralizing system during emplacement of the felsic dome, as expressed by the autometasomatic chloritization and auriferous pyrite mineralization (Fig. 19c). Stage 4 includes FP and QFP injections and subsequent hydrothermal activity. QFP dikes were injected along active synvolcanic faults which induced fracturing within the cooling dikes. These dikes, which are the only planar features cutting across the whole sequence and linking all veins together, served as conduits for the ascent of mineralizing fluids at different levels within the volcanic pile.

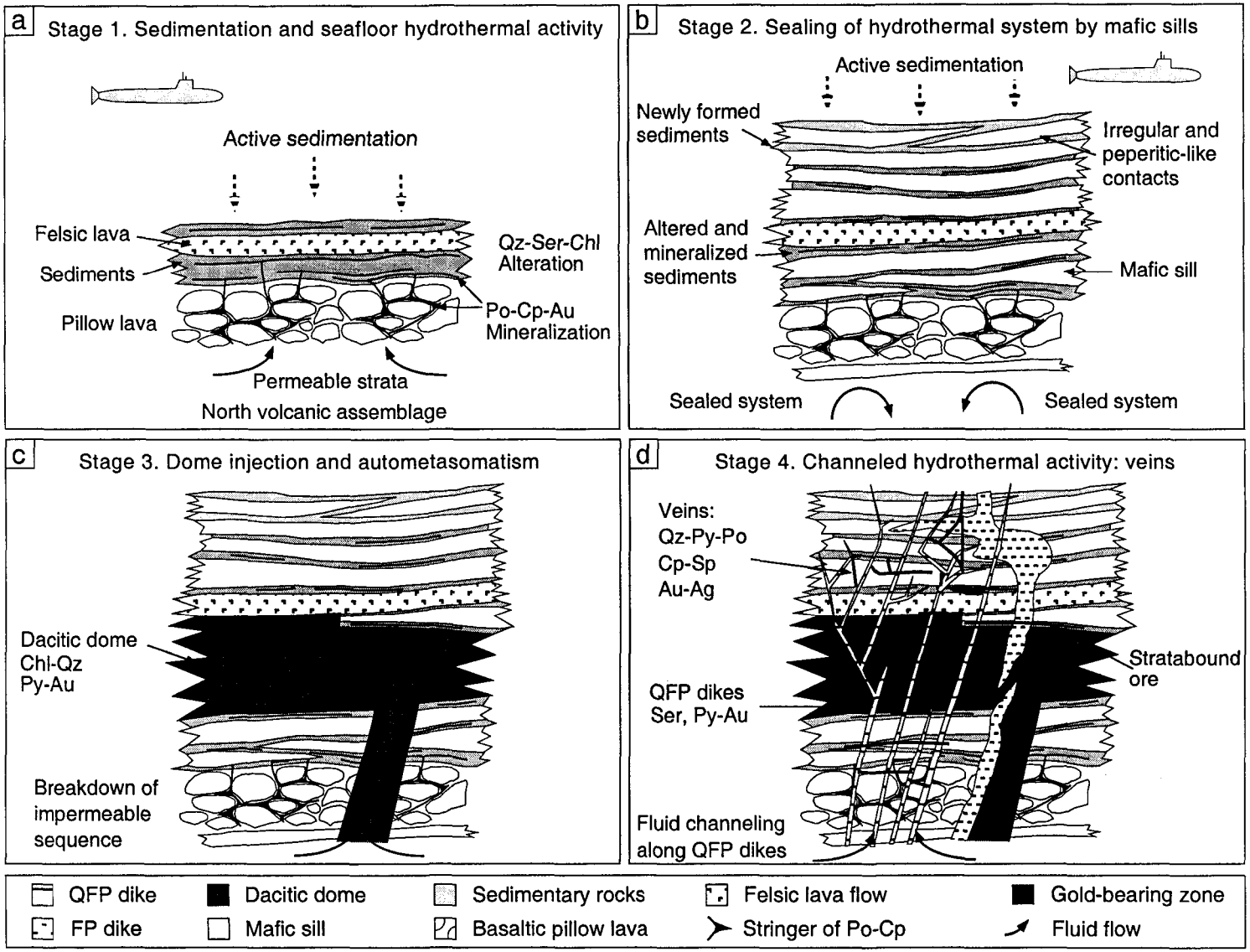

Figure 19. Schematic four-stage genetic model. Refer to figure 13 for geometrical relationships.

Gold, quartz and sulfides precipitated in open fractures developed mainly in mafic rocks close to QFP dikes, throughout the volcanic pile (Fig. 19d).

DISCUSSION

Evolving Volcanogenic System

The proposed model accounts for most of the volcanic and hydrothermal features, but the possibility that each mineralizing event represents isolated and unrelated events cannot be strictly ruled out because of the lack of absolute ages for each mineralizing event. However, the following criteria support the genetic link between the mineralizing events: (1) the coherence between the relative timing of the volcanic and hydrothermal activities (Fig. 12), (2) the similarity of hydrothermal features from the three successive mineralizing events, and (3) the alteration and sulfide assemblages of gold-bearing veins which are typical of volcanogenic Archean polymetallic mineralization. Furthermore, the possibility that the main event results from an overprinting mesothermal-related event (cf. Hodgson, 1993; Robert, 1995) can be ruled out on the basis of the volcanic-related timing and the inferred shallow crustal level of vein formation.

Vein formation

Vein formation requires fluid channeling along fractures and favorable conditions for precipitating gangue and ore minerals under hydrostatic to lithostatic fluid pressures (Jébrak, 1992; Peters, 1993). In a submarine setting, the water column directly influence the fluid pressure conditions. In shallow water (< 1 000 m) and permeable volcanic rocks, fluids flow under hydrostatic pressure, whereas lithostatic conditions occur in deep water and more impermeable volcanic rocks (Gibson et al., 1997). In shallow water settings, quartz-sulfide veins characterized by typical epithermal textures are documented at the

Archean Zn-Cu-Ag-Au Selbaie Mine (Larson and Hutchinson, 1993) and at the Jurassic Au-Ag-Cu-Zn Eskay Creek Mine (e.g., Roth et al., 1997). These veins occur stratigraphically below stratabound ore and are interpreted as ore feeder structures. Vein formation is related to boiling of ascending mineralizing fluids and these deposits are interpreted as submarine equivalents of epithermal deposits on land (Hannington et al., 1997). In deep water settings, vein formation is constrained by high bathymetric confining pressure, which inhibits boiling of ascending fluids within the conduits, thus favoring seafloor ore precipitation (cf. Herzing and Hannington, 1995).

At the Géant Dormant mine, presence of gold-bearing veins is not easily reconcilable with the interpreted deep water setting. At least three features are distinct from typical VMS volcanic setting, and interpreted to be relevant for vein formation: (1) the two-source volcanic pile, (2) the thickness of the pile generated by sill injection and, (3) the lack of synvolcanic faults cutting across the whole mafic sill succession. Considering the relative timing between gold mineralizing events and felsic intrusive rocks (Fig. 12), it is obvious that they are intimately related, indicating that the hydrothermal system is genetically associated to the proximal felsic volcanic center. Hence, the sealing effect related to mafic sill injection must be considered as an exogenic perturbing event in respect to the evolution of the hydrothermal system. Lack of synvolcanic faults combined with the impermeable nature of mafic sills suggests that the > 1 km thick sequence was devoid of structural permeability necessary to channel mineralizing fluids from the base of the sill stack toward the top of the growing volcanic pile during and after the mafic sill event (Stage 2). Later, veins formed in the sill-sediment sequence following fracturing induced by renewed felsic activity.

Constraints for vein formation are indicated by the following relationships. The dominant initial subhorizontal attitudes of veins (Figs. 2, 18b) suggests that most veins, if

not all, do not represent feeder conduits for the seafloor. It also indicates that vein formation is related to fluid pressurization above or close to the lithostatic pressure. Hence, it is proposed that altered and mineralized QFP dikes acted as conduits for fluid venting at seafloor. Fluctuation of the weak QFP dike permeability, likely triggered by tectonic subsiding events, promoted fluid pressurization in the impermeable host pile. Pressurization leads to vein formation by extensional opening along favorably oriented pre-existing faults and fractures, and lithological contacts close to QFP dikes. Once fluid pressure exceeded the impermeability limit of the QFP dikes (close to lithostatic pressure), fluid circulation along QFP dikes was reestablished, venting at seafloor resumed and fluid accumulated in fractures (veins) were drained, thus favoring mineral precipitation in the veins. Episodic formation of different veins at different levels is suggested by crosscutting relationships of multiple quartz-sulfide veinlets within altered and mineralized QFP dikes (Gaboury et al., 1996). This vein formation scenario is similar to the fault-valve model (Sibson et al., 1988) proposed for mesothermal vein systems, but the extensional regime and the shallower crustal level are significant differences.

Gold-rich volcanogenic system

Gold content of the Stage 4 veins is at least 10 times greater than average grade of VMS deposits in the Abitibi belt (cf. Chartrand et Cattalini, 1990), whereas gold grade related to seafloor Stage 1 is quite typical of VMS deposits. Gold enrichment can be due to an inherent gold-rich fluid and/or highly efficient mechanism for precipitation and concentration of gold (Hannington et al., 1997). Comparing Stage 4 to Stage 1, two main geological features are different: the abundance of felsic calc-alkalic intrusive rocks and the fracture filling style of the gold-mineralization.

Modern gold-rich VMS are associated with calc-alkalic felsic rocks in immature back arcs, spreading centers and rifts, such as the Lau basin, Okinawa trough, Manus basin and western Woodlark basin (Herzing et al., 1993). In this setting, two features are invoked to account for gold enrichment: (1) favorable chemistry of mineralizing fluids resulting from buffering with felsic calc-alkalic rocks (Herzing et al., 1993; Herzing and Hannington, 1995), and (2) direct magmatic contribution of a gold-rich aqueous solution during crystallization of a felsic magma (Sillitoe, 1989; 1995). For the Géant Dormant deposit, the obvious spatial and temporal associations between calc-alkalic felsic rocks and gold mineralization (Figs. 12, 13) are permissive evidence for suggesting that buffering and magmatic gold contribution are plausible features to account for gold-enrichment at Stage 4.

The Stage 4 gold-mineralization, by its fracture filling nature, indicates different physical conditions for gold precipitation compared to the seafloor Stage 1. For some VMS-related and shallow submarine epithermal deposits, boiling is commonly invoked as the prominent mechanism for gold precipitation (Hannington et al., 1997). In a submarine setting, boiling is limited by the confining bathymetric pressure, since mineralizing fluids and seawater define an "open system". Thus, boiling of mineralizing fluids at a temperature lower than 350° C is limited to water depth < 1 500 m (Hannington et al., 1997).

Although, no direct evidence confirms the following boiling hypothesis, it is interesting to discuss it in the light of the proposed model in order to draw comparison with the volcanogenic exhalative counterpart. For the Géant Dormant, the inferred water depth is much greater than the boiling limit. This is consistent with the low gold content of the Stage 1 which is typical of VMS deposits formed in deep water setting. In addition, Stage 4 gold-bearing veins lack typical texture indicating low confining pressure at which boiling generally occurs (Buchanan, 1981), such as cockade, colloform and crustiform textures (cf.

Dong et al., 1995). This also eliminates the possibility of a tectonic uplift or sea level drop during vein formation. Therefore, boiling in an "open system" appears incompatible with volcanic and vein characteristics.

Since boiling is pressure dependent, significant fluid pressure drops can occur momentarily in a "closed system" due to fracture opening and vein formation (Sibson et al., 1988). Since an increase of fracture area of one order of magnitude causes two orders of magnitude decrease in fluid pressure (Zucrow and Hoffman, 1976; Kieffer, 1984), such a pressure drop can be sufficient to generate boiling, even at lithostatic conditions (Helgeson and Lichtner, 1987) and to precipitate gold and related quartz and sulfides.

According to Skinner (1979), in addition to boiling, there are three other causes of mineral precipitation: (1) decrease in temperature, (2) chemical changes due to hydrothermal alteration, and (3) chemical changes due to fluid mixing. Considering the volcanic setting and vein characteristics, all these three causes can be ruled out. A decrease in temperature, except for the one induced by boiling, appears to be unlikely considering the lack of mineral zoning at the deposit scale. The weak to absent hydrothermal alteration associated with the veins is inconsistent with a chemical change of the fluid nature by fluid-rock interactions. Moreover, the weak alteration combined with the impermeable nature of mafic sills appears inconsistent with fluid mixing, which occurs commonly in hydrostatic conditions (Rosenberg et al., 1993). Therefore, boiling appears to be the most likely mechanism for precipitation of gold and other minerals during vein formation.

CONCLUDING REMARKS

The Géant Dormant gold deposit is an example of volcanogenic gold-bearing veins formed in a thick sequence of mafic sills and sediments, following the sealing of a pre-established volcanogenic hydrothermal system. The proposed model involves a specific

volcanic evolution which is unusual compared to classic VMS settings. However, this demonstrates that some variations on a well-established model can lead to different styles and metal contents of mineralization, and consequently to a different exploration strategy. The most significant outcome is the recognition that gold-rich volcanogenic systems are not limited to shallow water settings, as suggested by the boiling limit of mineralizing fluids under bathymetric confining pressure in an "open system". In a deep water setting, gold precipitation by boiling can occur only in a "closed system" isolated from the confining pressure. Subvolcanic vein formation is an efficient mechanism to achieve intermittent "closed system" conditions and generate fluid boiling. Fluid pressurization to lithostatic level is necessary to form veins in a deep water setting. This requires an impermeable host sequence which is uncommon in VMS settings. Since volcanic and hydrothermal vents are commonly associated (e.g., Gibson et al., 1997), an efficient sealing over an active VMS system is unlikely due to the permeable nature of flows and to reactivation of faults. Where systems are sealed, subsidence following eruptive activities generally leads to vertical stacking of VMS lenses along ore feeder faults (e.g., Gibson and Watkinson, 1990). Hence, because of the genetic association between volcanism, subsidence and hydrothermal activity, generation of conduits to keep fluids venting at seafloor can be considered as a self-sustaining process. An independent volcanic event, unrelated to the volcanic center where mineralizing activity is in progress, is necessary to generate an impermeable overlying sequence, such as thick sill succession. The bedding-parallel anisotropies related to a sill-sediment complex are also important to enhance subhorizontal vein development (Gaboury et al., 1996). Bimodal sill-sediment complexes appear thus to be prospective environments for volcanogenic-related vein-style gold mineralization.

Acknowledgments

The authors express their sincere thanks to Cambior Inc., Aurizon Mine Ltd. and the Ministère des Ressources naturelles du Québec for their scientific collaboration and financial support. P. Pilote is thanked for the realization of the U-Pb zircon age under contract given by the Ministère des Ressources naturelles du Québec. Our thanks are extended to numerous geologists for stimulating discussions, especially C. Gobeil (Cambior), and to the mine staff for their generous assistance to the first author during four consecutive summers. The manuscript has benefited from constructive criticism by A. L. Smith, G. Beaudoin, W. Mueller, E.H. Chown and by two *Economic Geology* reviewers. The Natural Sciences and Engineering Research Council of Canada (NSERC) and the Fonds pour la Formation de Chercheurs et d'Aide à la Recherche (FCAR) also financed the project through Ph.D. postgraduate scholarships to the first author.

References

Barrett, T.J. and MacLean, W.H., 1994, Chemostratigraphy and hydrothermal alteration in exploration for VHMS deposits in greenstones and younger volcanic rocks. In: Alteration and alteration processes associated with ore-forming systems. Edited by: D.R. Lentz. Geological Association of Canada, Short Course Handbook, v. 11, p. 433-467.

Barrie, C.T., Ludden, J.N. and Green, T.H., 1993, Geochemistry of volcanic rocks associated with Cu-Zn and Ni-Cu deposits in the Abitibi Subprovince: Economic Geology, 88: 1341-1358.

Bienvenu, P., Bougault, H., Joron, J.L., Treuil, M., and Dmitriev, L., 1990, MORB alteration; rare-earth element/non-rare earth hygromagmaphile element fractionation: Chemical Geology, V. 82, p. 1-14.

Bischoff, J.L. and Rosenbauer, R.J., 1984, The critical point and two phase boundary of seawater, 200-500° C: Earth and Planetary Science Letters, v. 68, p. 172-180.

Bloomer, S.H., Stern, R.J. and Smoot, N.C., 1989, Physical volcanology of the submarine Mariana and Volcano arcs: Bulletin of Volcanology, v. 51, p. 210-224.

Buchanan, L.J., 1981, Precious metal deposits associated with volcanic environments in the Southwest: Arizona Geological Society Digest, v. 14, p. 237-262.

Cas, R., 1992, Submarine volcanism: eruption styles, products, and relevance to understanding the host-rock successions to volcanic-hosted massive sulfide deposits: Economic Geology, v. 87, p. 511-541.

Chartrand, F. and Cattalani, S., 1990, Massive sulfide deposits in Northwestern Quebec: Canadian Institute of Mines and Metallurgy, Special Volume 43, p. 77-91.

Chown, E.H., Daigneault, R., Mueller, W. and Mortensen, J.K., 1992, Tectonic evolution of the Northern Volcanic Zone, Abitibi belt, Quebec: Canadian Journal of Earth Sciences, v. 29, p. 2211-2225.

de Rosen-Spence, A.F., Provost, G., Dimroth, E., Gochnauer, K and Owen, V., 1980, Archean subaqueous felsic flows, Rouyn-Noranda, Quebec, Canada, and their Quarternary equivalents: Precambrian Research, v. 12, p. 43-77.

Dimroth, E., Cousineau, P., Leduc, M. and Sanschagrin, Y., 1978, Structure and organization of Archean subaqueous basalt flows, Rouyn-Noranda area, Quebec, Canada: Canadian Journal of Earth Sciences, v. 15, p. 902-918.

Dong, G., Morrison, G. and Jaireth, S., 1995, Quartz textures in epithermal veins, Queensland - Classification, origin, and implication: Economic Geology, v. 90, p. 1841-1856.

Dostal, J. and Mueller, W., 1992, Archean shoshonites from the Abitibi greenstone belt, Chibougamau (Québec, Canada): geochemistry and tectonic setting: Journal of Volcanology and Geothermal Research, v. 53, p. 145-165.

Einsele, G., 1985, Basaltic sill-sediment complexes in young spreading centers: Genesis and significance. Geology, v. 13, p. 249-252.

Einsele, G., 1986, Interaction between sediments and basalt injections in young Gulf of California-type spreading centers: Geologische Rundschau, v. 75, p. 197-208.

Eriksson, K.A., Krapez, B. and Fralick, P.W., 1994, Sedimentology of Archean greenstone belts: signatures of tectonic evolution: Earth-Science Review, v. 37, p. 1-88.

Foxford, K.A., Nicholson, R., Hebblethwaite, R.P.B. and Polya, D.A., 1995, Conceptual methods for modelling systems of mineralized echelon veins: Examples from Southern England and Portugal: Exploration and Mining Geology, v. 4, p. 285-296.

Gaboury, D., 1996, Potentiel et cibles pour les SMV sur la propriété Géant Dormant, Abitibi. Consulting report for Cambior, Orbitacle, Cahier 96-02, 42 p.

Gaboury, D., Daigneault, R., Tourigny, G. and Gobeil, C., 1996, An Archean volcanic-related gold-sulfide-quartz vein orebody: the Géant Dormant mine, Abitibi Subprovince, Québec, Canada: Exploration and Mining Geology, v. 5, p. 197-213.

Gibson, H.L. and Watkinson, D.W., 1990, Volcanogenic massive sulphide deposits of the Noranda cauldron and shield volcano, Québec: Canadian Institute of Mines and Metallurgy, Special volume 43, p. 119-132.

Gibson, H.L., Morton, R.L. and Hudak, G.J., 1997. Submarine volcanic processes, deposits and environments favorable for the location of volcanic-associated massive sulfide deposits. In: Volcanogenic-associated massive sulfide deposits: Processes and examples in modern and ancient settings. Edited by: C.T. Barrie and M.D. Hannington. Geological Association of Canada, Short Course Handbook, v. 13, p. 13-51.

Goodfellow, W.D. and Zierenberg, R.A., 1997, Genesis of massive sulfide deposits at sediment-covered spreading centers. In: Volcanogenic-associated massive sulfide deposits: Processes and examples in modern and ancient settings. Edited by: C.T. Barrie and M.D. Hannington. Geological Association of Canada, Short Course Handbook, v. 13: 183-214.

Gross, G.A., 1980, A classification of iron formations based on depositional environments: Canadian Mineralogist, v. 18, p. 215-222.

Hannington, M.D., Poulsen, K.H., Thompson, J.F.H. and Sillitoe, R.H., 1997, Volcanogenic gold and epithermal-style mineralization in the VMS environment. In. Volcanogenic-associated massive sulfide deposits: Processes and examples in modern

and ancient settings. Edited by: C.T. Barrie and M.D. Hannington. Geological Association of Canada, Short Course Handbook, v. 13,.p. 183-214.

Helgeson, H.C. and Lichtner, P.C., 1987, Fluid flow and mineral reactions at high temperatures and pressures: Geological Society of London Journal, v. 144, p. 313-326.

Herzing, P.M. and Hannington, M.D., 1995, Polymetallic massive sulfides at modern seafloor: a review: Ore Geology Reviews, v. 10, p. 95-115.

Herzing, P.M., Hannington, M.D., Fouquet, Y., Von Stackelberg, U. and Peterson, S., 1993, Gold-rich polymetallic sulfides from the Lau back arc and implications for the geochemistry of gold in sea-floor hydrothermal system of the southwest Pacific: Economic Geology, v. 88, p. 2182-2209.

Hocq, M., 1990, Carte lithotectonique des Sous-Provinces de l'Abitibi et du Pontiac. Ministère des Ressources Naturelles du Québec. Map No. 2092 A from report DV 89-04.

Hodgson, C.J., 1993, Mesothermal gold deposits. In: Mineral deposit modeling. Edited by: R. V. Kirkham, R.V., Sinclair, W.D., Thorpe R.I., Duke J.M. Geological. Association of Canada, Special Volume 40, p. 635-678.

Jébrak, M., 1992, Les textures intra-filoniennes, marqueurs des conditions hydrauliques et tectoniques: Chroniques de la Recherche Minière, v. 506, p. 25-36.

Jones, J,G., 1969., Pillow lavas as depth indicators: American Journal of Sciences, v. 267, p. 181-195.

Kieffer, S.W., 1984, Factors governing the structures of volcanic jets. In: Explosive volcanism: inception, evolution and hazards, Washington, D.C., National Academy Press, p. 143-157.

Kokelaar, B.P., 1982, Fluidization of wet sediments during emplacement and cooling of various igneous rocks: Journal of the Geological Societey of London, v. 139, p. 21-33.

Larsen, J.E. and Hutchinson, R.W., 1993, The Selbaie Zn-Cu-Ag deposits, Quebec, Canada: An example of evolution from subaqueous to subaerial volcanism and mineralization in an Archean caldera environment: Economic Geology, v. 88, p. 1460-1482.

Leaman, D.E., 1995, Mechanics of sill emplacement: comments based on the Tasmanian dolerites: Australian Journal of Earth Sciences, v. 42, p. 151-155.

Lesher, C.M., Goodwin, A.M., Campbell, I.H. and Gorton, M.P., 1986, Trace-element geochemistry of ore-associated and barren, felsic metavolcanic rocks in the Superior Province, Canada: Canadian Journal of Earth Sciences, v. 23, p. 222-237.

MacLean, W.H., 1990, Mass change calculations in altered rock series: Mineralium Deposita, v. 25, p. 44-49.

MacLean, W.H. and Kranidiotis, P., 1987, Immobile elements as monitors of mass transfer in hydrothermal alteration: Phelps Dodge massive sulfide deposit, Matagami, Quebec: Economic Geology, v. 82, p. 951-962.

Magnan, M., Daigneault, R., Robert, F. and Pilote, P., 1995, Intrusion-related Au-Cu-Ag sulfide-rich veins in the Archean Doré Lake complex, Chibougamau, Québec: Precambrian '95, Program and Abstracts, p. 296.

McBirney, A.R., 1963, Factors governing the nature of submarine volcanism: Bulletin of Volcanology, v. 26, p. 455-469.

McPhie, J., 1993, The Tennant Creek porphyry revisited: A synsedimentary sill with peperite margins, Early Proterozoic, Northern Territory: Australian Journal of Earth Sciences, v. 40, p. 545-558.

Moore, J.G. and Schiling, J.G., 1973, Vesicles, water and sulfur in Reykjanes ridge basalts: Contribution to Mineralogy and Petrolology, v. 41, p. 105-118.

Morasse, S., Wasteneys, H. A., Cormier, M., Helmstaedt, H. and Mason, R., 1995, A pre-2686 Ma intrusion-related gold deposit at the Kiena mine, Val d'Or, Québec, Southern Abitibi Subprovince: Ecomonic Geology, v. 90, p. 1310-1321.

Mortensen, J.K., 1993, U-Pb geochronology of the eastern Abitibi Subprovince. Part 1: Chibougamau-Matagami-Joutel region: Canadian Journal of Earth Sciences, v. 30, p. 11-28.

Mueller, W. and Donaldson, J.A., 1992a. Development of sedimentary basins in the Archean Abitibi Belt, Canada: an overview: Canadian Journal of Earth Sciences, v. 29, p. 2249-2265.

Mueller, W. and Donaldson, J.A., 1992b, A felsic dyke swarm formed under the sea: the Archean Hunter Mine group, south-central Abitibi belt, Quebec, Canada: Bulletin of Volcanology, v. 54, p. 602-610.

Pearce, J.A., 1983, Role of the subcontinental lithosphere in magma genesis at active continental margins. In: Continental basalts and mantle xenoliths. Edited by: C. J. Hawkesworth and M. J. Norry. Shiva, Cheshire, United Kingdom, p. 230-249.

Peters, S.G., 1993, Nomenclature, concepts and classification of oreshoots in vein deposits: Ore Geology Reviews, v. 8, p. 3-22.

Picard, C. and Piboule, M., 1986, Pétrologie des roches volcaniques du sillon de roches vertes archéennes de Matagami-Chibougamau à l'ouest de Chapais (Abitibi est, Québec). 1. Le Groupe basal de Roy: Canadian Journal of Earth Sciences, v. 23, p. 561-578.

Pilote, P., 1989, Géologie de la région de Casa-Berardi, Dieppe, Collet et Laberge. Ministère des ressources naturelles du Québec, report MB 89-43.

Robert, F., 1995, Quartz-carbonate vein gold. In: Geology of the Canadian mineral deposit types. Edited by O.R. Eckstrand, W.D. Sinclair and R.I. Thorpe. Geological Survey of Canada, Geology of Canada no. 8, p. 350-366.

Robert, F. and Poulsen, K.H., 1997, World-class Archaean gold deposits of Canada: An overview: Australian Journal of Earth Sciences, v. 44, p. 329-352.

Robert, F., Poulsen, K.H. and Dubé, B., 1997, Gold deposits and their geological classification. In: Proceedings of Exploration 97: Fourth Decennial International Conference on Mineral Exploration. Edited by A.G. Gubins, p. 209-220.

Rosenberg, N.D., Spera, F.J. and Haymon, R.M., 1993, The relationship between flow and permeability field in seafloor hydrothermal systems: Earth and Planetary Science Letters, v. 116, p. 135-153.

Roth, T., Thompson, J.F.H. and Barrett, T.J., 1997, The precious metal-rich Eskay Creek deposit, northwestern British Colombia. In: Volcanogenic-associated massive sulfide deposits: Processes and examples in modern and ancient settings. Edited by: C.T. Barrie

and M.D. Hannington. Geological Association of Canada, Short Course Handbook, v. 13, p. 367-385.

Sibson, R.H., Robert, F. and Poulsen, K.H., 1988. High-angle reverse faults, fluid-pressure cycling and mesothermal gold-quartz deposits: Geology, v. 16, p. 551-555.

Sillitoe, R.H., 1989, Gold deposits in western Pacific island arcs: The magmatic connection: Economic Geology Monograph 6, p. 274-291.

Sillitoe, R.H., 1995, The influence of magmatic-hydrothermal models on exploration strategies for volcano-plutonic arcs. In Magmas, Fluids, and Ore Deposits. Edited by: J.F.H. Thompson. Mineralogical Association of Canada, Short Course Handbook, v. 25 p. 511-525.

Skinner, B.J., 1979, The many origins of hydrothermal mineral deposits. In: Geochemistry of Hydrothermal Ore Deposits, Edited by: Barnes, H.L., Wiley Intersciences, New York, p. 1-21.

Spark, R.S.J., 1978, The dynamics of bubble formation and growth in magmas: A review and analysis: Journal of Volcanology and Geothermal Research, v. 3, p. 1-37.

Thompson, R.N., Morrison, M.A., Hendry, G.L. and Parry, S.J., 1984, An assessment of the relative role of crust and mantle in magma genesis: an elemental approach: Philosophical Transactions of the Royal Society of London, v. A310, p. 549-590.

Walker, G.P.L., 1989, Gravitational (density) controls on volcanism, magma chambers and intrusions: Australia Journal of Earth Sciences, v. 36, p. 149-165.

Winchester, J.A. and Floyd, P.A., 1977, Geochemical discrimination of different magma series and their differentiation products using immobile elements: Chemical Geology, v. 20, p. 325-343.

Wyman, D.A. and Kerrich, R., 1993, Archean shoshonitic lamprophyres of the Abitibi Subprovince, Canada: petrogenesis, age, and tectonic setting: Journal of Petrology, v. 34, p. 1067-1109.

Zierenberg, R.A., Koski, R.A., Morton, J.L., Bouse, R.M. and Shanks III, W.C., 1993, Genesis of massive sulfide deposits on a sediment-covered spreading center, Escanaba trough, southern Gorda ridge: Economic Geology, v. 88, p. 2069-2098.

Zucrow, M.J. and Hoffman, J.D., 1976, Gas Dynamics, v. 1, New York, Wiley, 784 p.

CHAPITRE 4

Constraints on the evolution of a hydrothermal system from REE and trace-elements of sulfides: Example from the Géant Dormant gold mine, Archean Abitibi Belt, Canada

Ce chapitre représente la version intégrale d'un article soumis pour publication dans la revue *Canadian Mineralogist* par Gaboury et Daigneault.

Abstract

At the Géant Dormant gold mine, located in the Archean Abitibi greenstone belt, the host sequence recorded three successive mineralizing events ranging in time from sulfidic seafloor-related to quartz sulfide-rich vein-type gold mineralizations. Rare earth elements (REE) and selected trace-elements (Au, Ag, As, Co, Cr, Ni, Sb and Se) of monomineralic sulfide concentrates of pyrite, pyrrhotite, chalcopyrite and sphalerite, analyzed by instrumental neutronic activation, were used to characterize the various mineralizing events and to interpret the causes of temporal evolution of the hydrothermal system. Chondrite-normalized REE patterns are specific for end-member mineralizing events whereas trace-element contents define coherent evolutive trends. The seafloor-related pyrrhotites have weakly fractionated REE patterns with negative Ce anomalies, high Ni and Co and low Au and Ag concentrations. This signature is consistent with the hydrothermal leaching of trace-elements from ferro-magnesian minerals in underlying basaltic rocks, and mixing with oxidizing seawater during subseafloor sulfide precipitation. Sulfides in the veins are characterized by low Ni and Co, high Au and Ag concentrations. The REE signatures, with strong fractionations of light REE and positive Eu anomalies, compare with those of mature volcanogenic fluids venting on seafloors, induced by the leaching of trace-elements from plagioclase in basaltic rock source. The geochemical data are compatible with the evolution of a volcanogenic hydrothermal system, involving the transition from ferro-magnesian to plagioclase as the main mineral sources for the leached metals. Results of this study demonstrate the usefulness of the trace-elements of sulfides as tracers of the hydrothermal system evolution. For the exploration, the proposed approach has the potential to be used as a tool for vectoring the search of massive sulfide deposits on land.

Résumé

À la mine Géant Dormant, située dans la ceinture de roches vertes archéennes de l'Abitibi, les roches encaissantes ont enregistré trois événements de minéralisation aurifère. Ceux-ci s'échelonnent dans le temps d'une sulfurisation volcanogène précoce à des veines de quartz riches en sulfures. Le contenu en éléments des terres rares (ÉTR) et en éléments traces (Au, Ag, As, Co, Cr, Ni, Sb et Se) de concentrés monominéraliques de pyrite, de pyrrhotite, de chalcopyrite et de sphalérite a été analysé par activation neutronique. La concentration de ces éléments a été utilisée pour caractériser chacun des événements dans le but de préciser l'évolution temporelle du système hydrothermal et d'en interpréter ces causes. Les spectres normalisés des ÉTR sont spécifiques pour le premier et le dernier des événements de minéralisation, alors que la concentration de certains éléments traces définit une tendance évolutive. La pyrrhotite précoce et volcanogène se caractérise par des spectres en ÉTR faiblement fractionnés avec des anomalies négatives en Ce et par une concentration forte en Ni et Co, et faible en Au et Ag. Cette signature est cohérente avec le lessivage des éléments traces à partir de minéraux ferro-magnésiens des basaltes composant l'empilement volcanique sous-jacent, et avec le mélange entre les fluides hydrothermaux et l'eau de mer oxydante au site de précipitation des sulfures. Les sulfures des veines sont caractérisés par des contenus faibles en Ni et Co, mais élevés en Au et Ag, ainsi que par des fractionnements prononcés en ÉTR légères et des anomalies positives en Eu. La signature en ÉTR se compare à celle typique des systèmes volcanogènes matures et actifs, dominés par le lessivage des éléments traces dans les plagioclases des basaltes. Ces données s'intègrent au sein d'un modèle volcanogène qui a progressivement gagné en maturité. Les résultats de cette étude démontrent l'utilité des éléments traces des sulfures comme traceurs de l'évolution des systèmes hydrothermaux. Pour l'exploration, l'approche utilisée est potentiellement utilisable pour orienter et optimiser l'exploration dans les contextes volcanogènes.

INTRODUCTION

Sulfides are very common in hydrothermal precious and base metal deposits and are commonly the only metal-bearing minerals of economic significance. Sulfides contain significant levels of trace-elements, occurring as inclusions and stoichiometric and nonstoichiometric lattice substitutions (*e.g.*, Huston *et al.* 1995). Numerous studies have demonstrated their usefulness to: 1) discriminate different classes of ore deposits (*e.g.*, Loftus-Hills & Solomon 1967, Bralia *et al.* 1979, Roberts 1982), 2) characterize physical conditions of ore formation (*e.g.*, Graf 1977, Green *et al.* 1981, Phillips *et al.* 1988, Brill 1989, Huston *et al.* 1995), and 3) guide exploration (*e.g.*, Seccombe 1977, Roberts 1982). The preceding applications are based on the fact that hydrothermal sulfides record in part the fluid composition from which they precipitated. Hence, if various sulfidic events of an extinct hydrothermal system can be sampled, the trace-elements of sulfides may be used as tracers for monitoring the temporal evolution of the mineralizing system, and to serve as basis for interpreting the factors influencing its evolution.

The Géant Dormant gold mine is of special interest for this purpose, because the host sequence records the coeval evolution of its associated volcanogenic hydrothermal system (Gaboury & Daigneault 1999, Gaboury *et al.* 1999). In this paper, rare earth elements (REE) and selected trace-elements in pyrite, pyrrhotite, chalcopyrite and sphalerite concentrates are reported and used first to characterize the three successive mineralizing events. These events comprise gold-poor seafloor-related sulfidic mineralization, gold-poor dome hosted disseminated pyrite, and gold-rich quartz sulfide-rich veins (Gaboury & Daigneault 1999). Secondly, the geochemical data are used to monitor, and to discuss and interpret the causes of the evolution in time of the hydrothermal system. It is shown that the normalized REE patterns of sulfides from the seafloor and the veins are clearly distinct, whereas some trace-elements define coherent increasing or

decreasing time-related trends. The geochemical data are best integrated, on a comparative basis, as the result of the progressive maturation of a volcanogenic hydrothermal system. The conclusions of this study are also relevant for the exploration in volcanogenic environment on land, as the maturity evaluation of specific mineralizing events has the potential to be used as a vectoring tool.

GEOLOGICAL OUTLINE

Mine geology

The Géant Dormant mine, located within the 2730-2720 Ma Northern Volcanic Zone (Chown *et al.* 1992) of the Abitibi greenstone belt (Fig. 1), is a vein-type gold deposit (> 700 000 oz Au). The Géant Dormant deposit contrasts strongly with Archean mesothermal deposits of the Abitibi belt by the formation of veins prior to ductile deformation and regional metamorphism, and their high sulfide content (Gaboury *et al.* 1996). The gold mineralization is centered about a calc-alkalic felsic complex which intrudes a volcano-sedimentary succession composed of mafic tholeiitic sills, interbedded fine-grained volcaniclastic rocks, cherts and magnetite-rich iron-formations, and units of mafic tholeiitic pillowed and felsic calc-alkalic lavas (Fig. 2). The felsic complex includes a dacitic subvolcanic dome and a swarm of plagioclase-phyric (FP) and quartz and plagioclase-phyric (QFP) felsic dikes. Mafic tholeiitic and shoshonitic dikes crosscut the gold-bearing veins (Fig. 3). The strata, the felsic complex and the gold-bearing vein network were altogether tilted (Fig. 2b) during regional shortening events and all the rocks are metamorphosed to greenschist facies. However, as the internal deformation within the tilted sequence is weak and heterogeneous, primary geometrical relationships and vein textures are commonly well preserved.

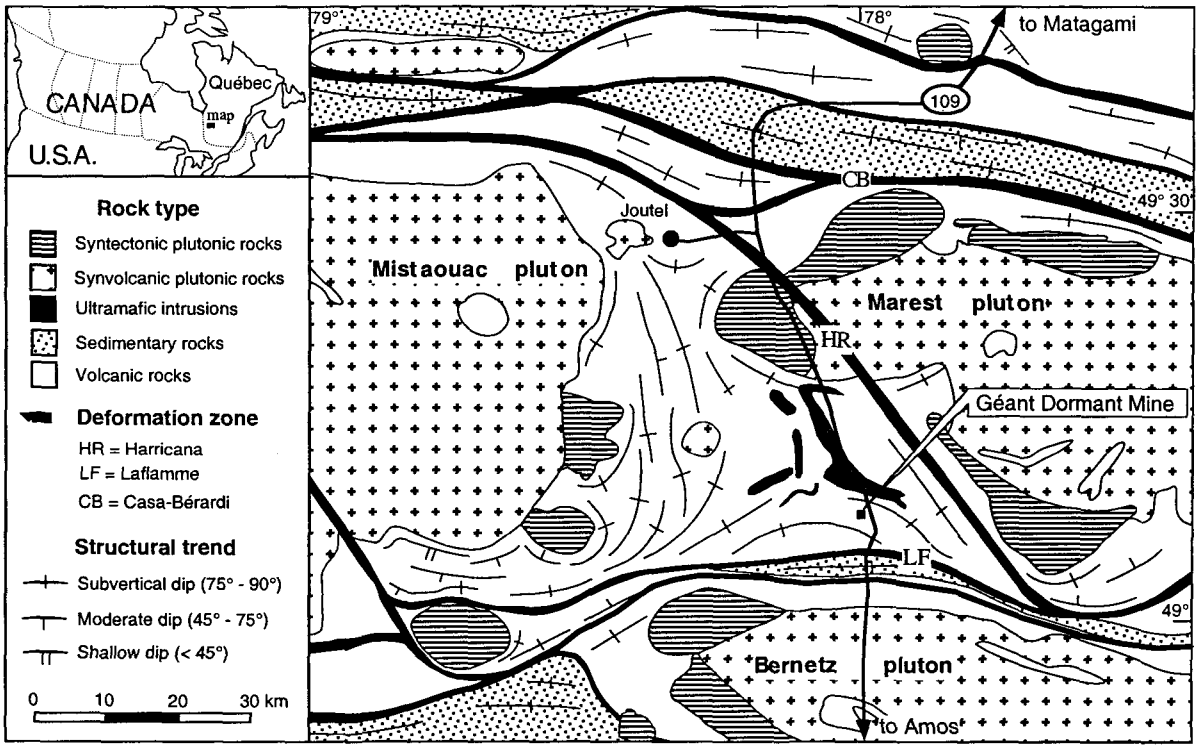

Figure 1. Location of the Géant Dormant mine in its regional context.

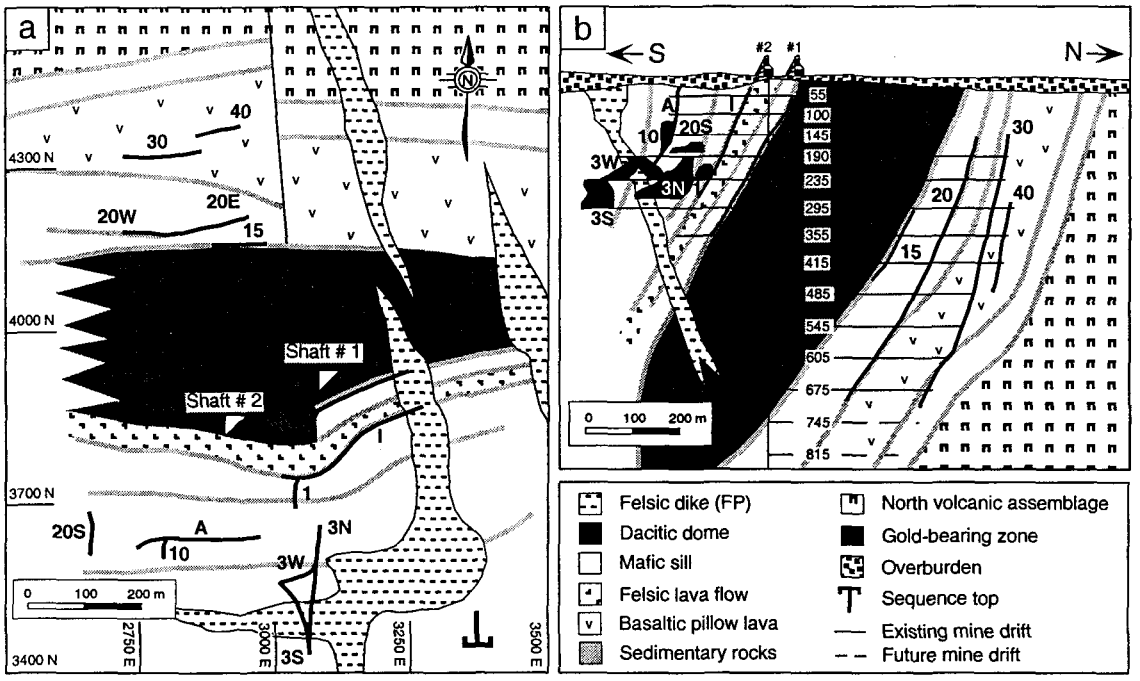

Figure 2. Characteristics of the mine sequence. (a) Simplified geological plan of the Géant Dormant mine area. (b) Idealized vertical N-S cross section. Various gold-bearing zones are labeled: A, 10, 40, etc. Modified from Gaboury and Daigneault (1998).

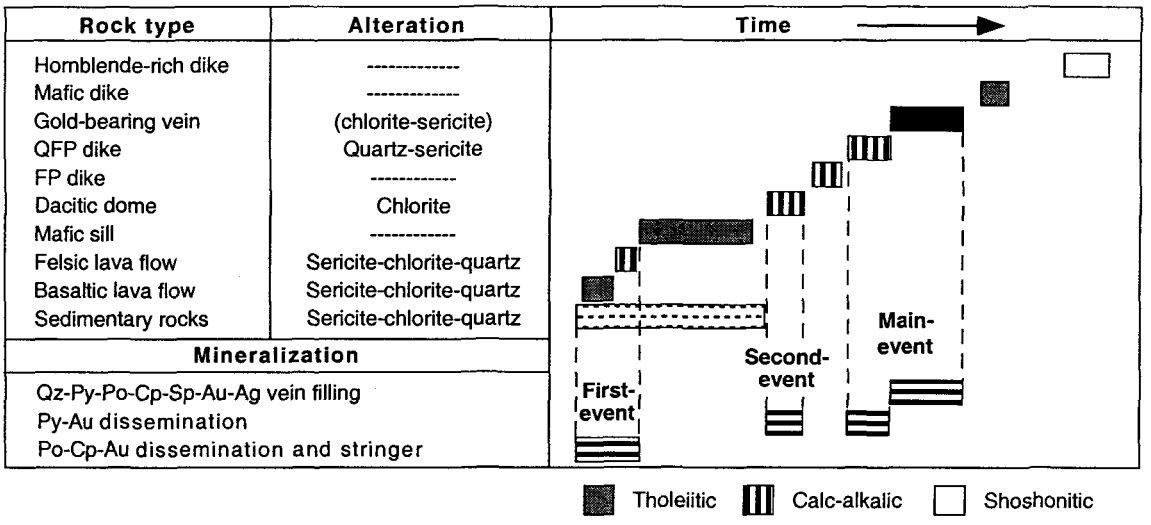

Figures 3. Chronological relationships between rocks, alteration and mineralization. Modified from Gaboury and Daigneault (1999).

Hydrothermal events

Gold-bearing veins were formed during the final stage of a four-stage volcanogenic hydrothermal system which evolved from seafloor-related to vein-style mineralization during volcanic construction (Gaboury & Daigneault 1999). The four-stage model includes three successive hydrothermal events (Fig. 3) characterized by a particular style, sulfide assemblage, alteration and gold grade (Table 1). This subdivision in three distinct events is based on systematic crosscutting relationships.

The first mineralizing event is an auriferous (< 3 g/t Au) pyrrhotite (95%) and chalcopyrite (5%) mineralization hosted by seafloor-related rocks, such as mafic pillowed and felsic lava flows and sedimentary rocks (Fig. 3). Sulfides form up to 20% of the rocks and occur as: stringers within pillow selvages, partial replacement of magnetite iron-formation beds, and disseminated in sedimentary rocks and felsic lava flow. This event is interpreted as subseafloor mineralization (Gaboury & Daigneault 1999). The second mineralizing event comprises disseminated auriferous gold-bearing pyrite (< 20%) within chloritized the dacitic rock. Pyrite and chlorite are restricted to the inner dacitic dome and are the product of hydrothermal activity which took place during dome emplacement and cooling (Fig. 3). Gold grade is low (< 1 g/t Au) with erratic values up to 20 g/t Au. The third and main mineralizing event comprises mineralization in QFP dikes and associated gold-bearing veins (Fig. 3). In QFP dikes, mineralization occurs as disseminated auriferous pyrite (< 5%) associated with intense and pervasive sericite and quartz alteration. Gold grade is similar to the disseminated pyrite in the dacite but with erratic values reaching > 100 g/t Au. Gold-bearing veins are generally massive, average 50 cm in thickness and are rich in gold (assays commonly > 100 g/t Au). Gangue minerals are dominated by quartz with minor amounts of chlorite, sericite, calcite and actinolite (Fig. 4). Sulfide content ranges from 5 to 80% with an average of 30%. Pyrite, pyrrhotite, chalcopyrite and

Table 1. Characteristics of each mineralizing event and representative samples

Event	Sulfide	Habit	Gangue[1]	Host rock[1]	Alteration[1]	Mass balance[1]	Sample
First	Po-Cp	Diss	Qz-Chl	Pillow lava	Chl in selvage	Loss: Fe-Mg	Po: R4, R5, R16
	Po-Cp	Diss	-------	Sediment	Chl-Ser-Qz	Gain: ? Loss: ?	Po: R15
Second	Py	Diss	-------	Dacitic dome	Weak to intense Chl	Gain: Fe-Mg-K Loss: Na	Py: R18, R19
Main	Py	Diss	-------	QFP dike	Intense Ser-Qz	Gain: Si-K Loss: Na	Py: R17, R18
	Py-Po-Cp-Sp	Vein	Qz-Chl Ser-Cal Act	Mafic sill	Nil to weak Ser-Chl	Gain: nil Loss: nil	Py: R6, (R8-12) Po: R1, R3 Cp: R2, (R13) Sp: (R14)

Py: pyrite
Po: pyrrhotite
Cp: chalcopyrite
Sp: sphalerite
Qz: quartz
Chl: chlorite
Ser: sericite
Cal: calcite
Act: actinolite
Diss: disseminated
Masse balance calculation for the alteration

[1] From: Gaboury and Daigneault, 1999

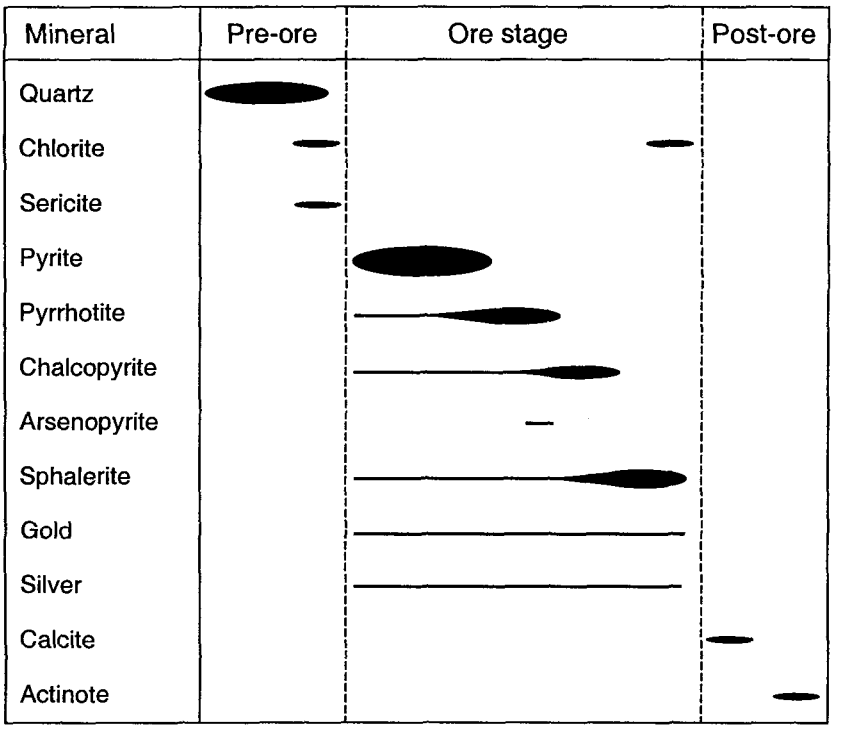

Figure 4. Paragenesis of filling minerals for gold-bearing veins.

sphalerite are the dominant sulfides, with minor amounts of arsenopyrite (Fig. 4). Altered and mineralized QFP dikes are spatially associated with gold-bearing veins and are interpreted as hydrothermal fluid feeder conduits for the vein system (Gaboury & Daigneault 1999).

Precious metal sitings

For the vein-style mineralization, gold and silver occur mainly as μm-scale inclusions in all the main sulfides (Figs. 5a, b) and as minor fine fracture fillings in pyrite (Fig. 5c). For disseminated sulfides, inclusions of gold and silver are uncommon (Fig. 5d), and microprobe data (Gaboury 1999) suggest that precious metals occur as "invisible gold and silver" in the sulfides (*e.g.*, Cook & Chryssoulis 1990).

SULFIDE ANALYSIS

Sample preparation

Representative, unstrained or only weakly deformed rock samples of the three mineralizing events come from the underground mine (Table 2). Between 1 to 3 grams of monomineralic sulfide concentrates were prepared (Table 2) for analysis by instrumental neutronic activation analysis (INAA). For the veins, segments of massive monomineralic sulfide were hammer sampled and hand crushed in a small agate mortar. Sulfide grains and fragments were hand picked under a binocular. Rock samples with disseminated sulfides were first fragmented by a porcelain crusher and then hand crushed to a fraction of about 1 mm in a porcelain mortar. Sulfides in the dust-free 1 mm fraction were separated from the silicates by settling using Methylene Iodide as heavy liquid and then washed with acetone. Successive stages of settling, involving progressive grain reduction of the sulfide precipitates by hand crushing in a small agate mortar, were necessary to remove most of the

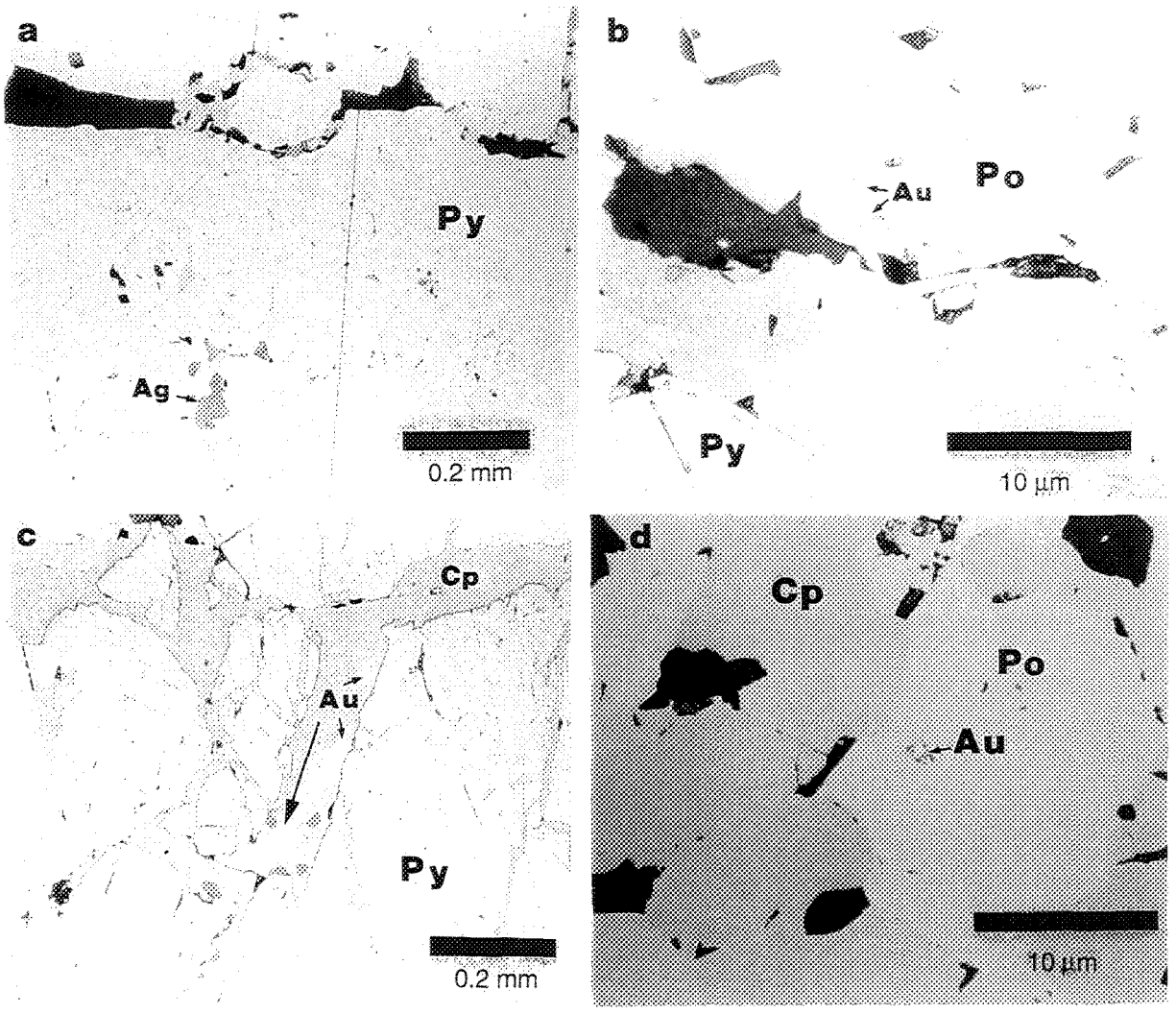

Figure 5. Photomicrographs (reflected natural light) of typical gold and silver occurrences in various sulfides. (a) Silver (Ag) inclusions in vein pyrite (Py). (b) Gold (Au) inclusions in vein pyrrhotite (Po). (c) Gold (Au) associated with chalcopyrite (Cp) as filling fracture in a vein pyrite (Py) grain. (d) Rare gold (Au) inclusion in pyrrhotite (Po) from pillow selvages.

Table 2. Location and characteristics of the analyzed sulfide samples

#	sulfide	Wt (g)	X(E)	Y(N)	Z	Occurence	Separation	% impurety
R1	Po	3.1086	3045	3500	230	Vein 3	Hand picking	< 1 % Qz
R2	Cp	2.7286	3045	3500	230	Vein 3	Hand picking	Tr Qz
R3	Po	2.4081	2910	4122	415	Vein 20	Hand picking	Tr Qz, < 2% Cpy
R4	Po	2.9459	2960	4180	545	Pillow selvages	Hand picking	< 1% Qz, < 1% Act
R5	Po	3.1761	2945	4080	605	Pillow selvages	Hand picking	< 1% Qz, < 1% Act
R6	Py	2.7628	3045	3500	230	Vein 3	Hand picking	Tr Qz
R7	Sp	2.1595	3045	3500	230	Vein 3	Hand picking	< 1% Qz, Tr Py
R8	Py	2.1109	3002	4210	338	Vein 20	Hand picking	< 1% Qz, Tr Sp
R9	Py	1.9284	2932	4225	245	Vein 20	Hand picking	< 1% Qz
R10	Py	2.5498	3100	3600	235	Vein 3	Hand picking	< 1% Qz, Tr Cp
R11	Py	2.4933	2909	4126	415	Vein 20	Hand picking	Tr Qz-Cp-Sp-Po
R12	Py	2.0395	3130	3500	295	Vein 3	Hand picking	< 1% Qz, Tr Cp-Sp
R13	Cp	1.7680	2909	4126	415	Vein 20	Hand picking	< 1% Qz
R14	Sp	1.0078	2909	4126	415	Vein 20	Hand picking	< 1% Qz, Tr Py, Cp
R15	Po	2.5006	2787	3755	190	Sediments	Settling	< 10% Qz
R16	Po	1.7441	2980	4237	355	Pillow selvages	Hand picking	Tr Cp
R17	Py	1.1254	2810	4337	235	QFP dike	Settling	< 15% Qz
R18	Py	1.5023	2725	3602	190	QFP dike	Settling	< 5% Qz
R19	Py	1.5780	3082	3780	190	Dacite	Settling	< 10% Qz
R20	Py	1.1691	2940	3830	485	Dacite	Settling	< 5 % Qz

Sample location refers to mine coordinates (m): X = longitude, Y = latitude and Z = depth, see figure 2
Abbreviation as Table 1.

silicates adhered to the sulfide surfaces. The purity of each sample was verified under a binocular microscope. It is generally better than 98% for hand picked sulfides and better than 85% for sulfides separated by settling (Table 2).

Analytical procedures

Twenty samples were analyzed by INAA at the Université du Québec at Chicoutimi facility following technical procedures described by Bédard & Barnes (1990), except for the following parameters. Samples R1-R7 were irradiated for 240 minutes and R8-R20 for 120 minutes. Two energy spectra were collected for samples R1-R7 at 8 days and 40 days after their irradiation. However, the second count has not improved the analytical precision. For samples R7 to R20, only one spectrum was collected between 7-8 days, and after 12 days for samples R8, R11 and R12 because of their high dead time during the first count.

Advantages and limitations of the method

The analysis of sulfide concentrates presents numerous advantages compared with microprobe applications. First, INAA yields a wide selection of analyzed elements, including REE, with detection limits better than those of ion and proton microprobes (Hoffman 1992). Second, as samples are composed of numerous grains, a single INAA analysis yields a better estimate of the overall composition of a sulfidic mineralizing event, compared to the average of potty microprobe analyses. Third, the method is particularly well-suited for the quantification of trace-elements occurring as inclusions, such as gold and silver.

Technically, the method suffers from limitations mainly related to sample preparation (Huston *et al.* 1995), such as: 1) the relatively large quantity of sample needed for analysis, 2) the difficulty related to the preparation of a pure concentrate, and 3) the

difficulty in separating different coexisting sulfidic phases. The veracity of an analyzed sulfide sample to represent adequately a mineralizing event is another limitation of the method. The analyzed sulfides should be the only, or the main phases containing the economic metals. This is common for hydrothermal base metal deposits because Cu, Zn and Pb occur as major constituents of sulfides, but it is less common for precious metal deposits. In the latter, gold and silver commonly occur as dissemination within the gangue minerals, being not associated or included within sulfidic phases. In the present case, gangue minerals are barren (Fig. 4) and gold and silver occur within the sulfides, indicating that the analyzed sulfides are representative of the mineralizing events.

RESULTS

The REE and selected trace-element (Au, Ag, As, Co, Cr, Ni, Sb and Se) concentrations are given in Tables 3 and 4 respectively. REE were determined in only 12 samples due to the low ΣREE abundance of sulfides (Table 3). Nevertheless, each mineralizing event is represented by REE signatures. Analytical results from the sample R7 of sphalerite are not included in the Tables 3 and 4, because of the poor quality of the collected energy spectrum (> 99% dead time).

To better assess the precision of the reported sulfide analyses, the standard deviations at specific concentrations of 5 CANMET precious metal standards (TDB-1, UMT-1, WPR-1, WMS-1, WGB-1) are presented in the Tables 3 and 4. The counting 1σ error of each determined analytical value is also reported. This error represents the minimum uncertainty of the analytical values.

Table 3. Selected REE of sulfide concentrates analyzed by INAA

#	La		Ce		Sm		Eu		Tb		Yb		Lu	
	ppm	±	ppm	±	ppm	±	ppm	±	ppm	±	ppm	±	ppm	±
R1	0.35	0.01	nd		0.052	0.005	0.08	0.03	<0.05		<0.05		0.005	0.002
R2	1.36	0.36	<2.7		0.03	0.01	0.16	0.06	nd		0.08	0.04	<0.01	
R3	0.39	0.01	<0.7		0.028	0.004	0.07	0.03	nd		nd		0.005	0.003
R4	0.56	0.02	0.6	0.3	0.367	0.004	0.12	0.05	0.15	0.04	0.15	0.03	0.022	0.003
R5	0.61	0.02	0.5	0.2	0.388	0.004	<0.09		0.15	0.04	0.15	0.03	0.033	0.005
R6	0.75	0.04	<3.8		0.11	0.02	0.22	0.09	<0.2		nd		0.03	0.01
R8	nd		nd		nd		nd		nd		nd		<0.2	
R9	0.52	0.05	nd		0.1	0.02	0.38	0.15	nd		nd		nd	
R10	0.81	0.03	nd		0.09	0.01	nd		nd		nd		nd	
R11	<0.5		nd		nd		nd		nd		nd		nd	
R12	2.3	0.3	nd		nd		nd		nd		<0.5		nd	
R13	<0.02		<1.7		nd		nd		nd		nd		nd	
R14	<0.2		nd		nd		nd		<0.9		<0.7		nd	
R15	6.9	0.04	12.5	0.5	0.964	0.004	0.42	0.04	0.15	0.02	0.39	0.03	0.029	0.005
R16	1.57	0.03	2.5	0.4	0.588	0.004	0.2	0.04	<0.06		0.3	0.03	0.039	0.005
R17	7.53	0.06	12.4	0.5	1.03	0.005	0.37	0.04	0.19	0.05	0.44	0.04	0.052	0.006
R18	46.3	0.13	92.6	0.8	6.65	0.008	1.11	0.07	0.69	0.06	1.74	0.05	0.227	0.007
R19	10.2	0.06	21.4	0.5	1.917	0.005	0.44	0.04	0.27	0.04	1.39	0.04	0.197	0.006
R20	10.1	0.07	19.4	0.6	1.614	0.006	0.38	0.04	0.25	0.05	1.00	0.04	0.080	0.006

±: 1σ counting error nd: not detected

	ppm	%	ppm	%	ppm	%	ppm	%	ppm	%	ppm	%	ppm	%
σ std	0.5	9	2	30	0.4	2	0.3	15	0.1	33	0.1	25	0.1	10
σ std	1.0	5	10	15	1.0	5	1.0	10	0.2	10	0.5	7	0.2	8
σ std	10.0	2	30	2	6.0	3	2.0	2	1.0	6	3.0	2	0.5	2

σ std: standard deviation at specific concentrations of CANMET precious metal standards (S-J. Barnes, Unpubl. data)

Table 4. Selected trace-elements of sulfide concentrates analyzed by INAA

#	Ag		As		Au		Co		Cr		Ni		Sb		Se	
	ppm	±	ppm	±	ppm	±	ppm	±	ppm	±	ppm	±	ppm	±	ppm	±
R1	86	0.7	3.9	0.2	9.5	0.004	51	0.2	11	0.6	110	10	1.4	0.02	20	0.5
R2	1389	2	5.1	0.4	63	0.01	10	0.2	5	1	<14		2.1	0.03	19	0.9
R3	125	0.9	18	0.2	22.0	0.006	51	0.02	16	0.6	64	17	0.8	0.2	8	0.6
R4	14	0.7	<0.7		0.99	0.002	900	0.6	10	0.5	929	19	nd		42	0.4
R5	14	0.7	<0.6		1.03	0.002	912	0.6	10	0.5	942	19	nd		42	0.5
R6	1049	3	2886	2	65	0.02	242	0.7	10	2	nd		1.9	0.07	18	2
R8	512	3	2759	14	540	0.1	396	1	14	3	88	31	3.3	0.2	15	3
R9	3697	7	3520	2	163	0.04	132	0.8	<9		136	46	16	0.1	45	3
R10	1171	3	1199	1	77.3	0.02	37	3	8	2	120	35	1.5	0.04	17	2
R11	746	3	19	4	294	0.06	757	1	8	2	1356	49	1.1	0.1	52	2
R12	651	2	3498	13	322	0.07	140	0.5	8	2	nd		1.1	0.1	11	1
R13	108	0.7	0.82	0.08	16.7	0.006	6	0.1	6	0.9	<44		0.4	0.01	21	0.8
R14	782	8	62	1	356	0.07	83	1	<21		nd		1.8	0.1	4	2.1
R15	30	0.6	0.26	0.06	0.40	0.001	229	0.4	9	0.4	43	10	<0.2		23	0.5
R16	2	0.6	0.14	0.07	0.48	0.001	755	0.8	10	0.6	712	26	<0.2		20	0.7
R17	245	1	404	0.5	0.41	0.001	196	0.5	11	0.7	75	14	nd		13	0.9
R18	656	2	1197	0.9	0.42	0.001	186	0.4	10	0.8	24	11	nd		11	0.9
R19	110	1	197	0.4	0.98	0.002	219	0.4	14	0.5	41	10	nd		14	0.6
R20	47	1	66	0.3	0.38	0.001	554	0.7	48	0.8	29	11	nd		33	0.8

±: 1σ counting error nd: not detected

	ppm	%	ppm	%	ppm	%	ppm	%	ppm	%	ppm	%	ppm	%	ppm	%
σ std	nd	?	1	20	0.001	30	30	3.0	10	30	100	10	0.1	25	2	30
σ std	nd	?	10	6	0.010	30	100	2.0	20	15	500	7	0.5	7	10	8
σ std	nd	?	20	5	0.030	20	1000	1.5	50	10	1000	5	2.0	4	100	2

σ std: standard deviation at specific concentrations of CANMET precious metal standards (S-J. Barnes, Unpubl. data)

REE patterns

REE patterns normalized to chondrite values (Thompson *et al.* 1984) are shown in the Figure 6. Three distinctive REE patterns characterize sulfides of specific habits and events. Pyrrhotite samples from pillow selvages (first event) are characterized by negative Ce anomalies and by slightly fractionated REE patterns (Fig. 6a), expressed by $[La/Lu]_N$ values of 2.1 to 4.1. The REE abundance is close to chondrite values. Samples of disseminated pyrite in dacite (second event) and in QFP dikes (main event), as well as a pyrrhotite sample in sedimentary rocks (first event) are enriched in light REE (Fig. 6b), as expressed by values of $[La/Lu]_N$ ranging from 5.4 to 24.6. These patterns are quite similar to the REE patterns of their altered host rock (Fig. 6b). Pyrite, chalcopyrite and pyrrhotite samples from gold-bearing veins (main event) are characterized by similar but incomplete patterns with REE abundance below or close to chondrite values (Fig. 6c). The $[La/Sm]_N$ ratios of 4.2 to 28.1, combined with the below detection limit concentrations of most heavy REE, suppose a strong fractionation of light REE. Positive Eu anomalies are indicated by the Eu/Sm ratios ranging from 1.5 to 5.3. These ratios are well above the value of 0.38 in chondrite.

Other trace-elements

Other trace-elements are presented as spidergrams normalized to Archean mafic rocks (Fig. 7). Diagrams expose patterns for each sulfide from specific mineralizing events and habits. These patterns show enrichment or depletion factors of the trace-elements relative to their normalizing value. Normalization to mafic rocks (Kerrich 1983) was chosen because it is the main rock type underlying the deposit (Gaboury & Daigneault 1999) and hence, the most likely metal source for the volcanogenic hydrothermal system.

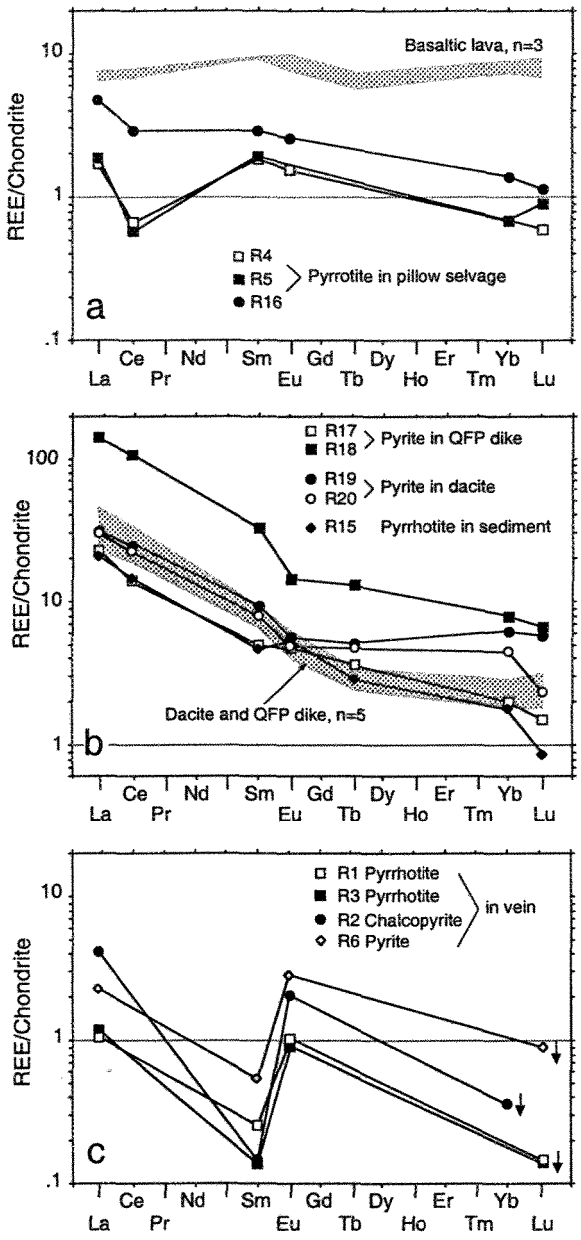

Figure 6. Chondrite normalized REE plots for the various sulfides relative to their habit and event. Normalizing values after Thompson et al. (1984). (a) Pyrrhotite samples from the pillow selvages (first event), characterized by a slight enrichment of light REE and negative Ce anomalies. (b) Samples of pyrite disseminated in dacite (second event) and in the QFP dikes (main event) showing strong light REE enrichment. Note the similarity between the REE patterns of the pyrite samples and those of the host rocks. A pyrrhotite sample from the sedimentary rocks (first event) shows also a similar REE pattern. (c) Partial REE patterns for the vein sulfides (main event) suggesting strong fractionations of light REE and positive Eu anomalies. Arrows indicate that the plotted values could be significantly lower due to the higher uncertainty (1s error) associated to the element of lower abundance. Host rock REE data from Gaboury and Daigneault (1999).

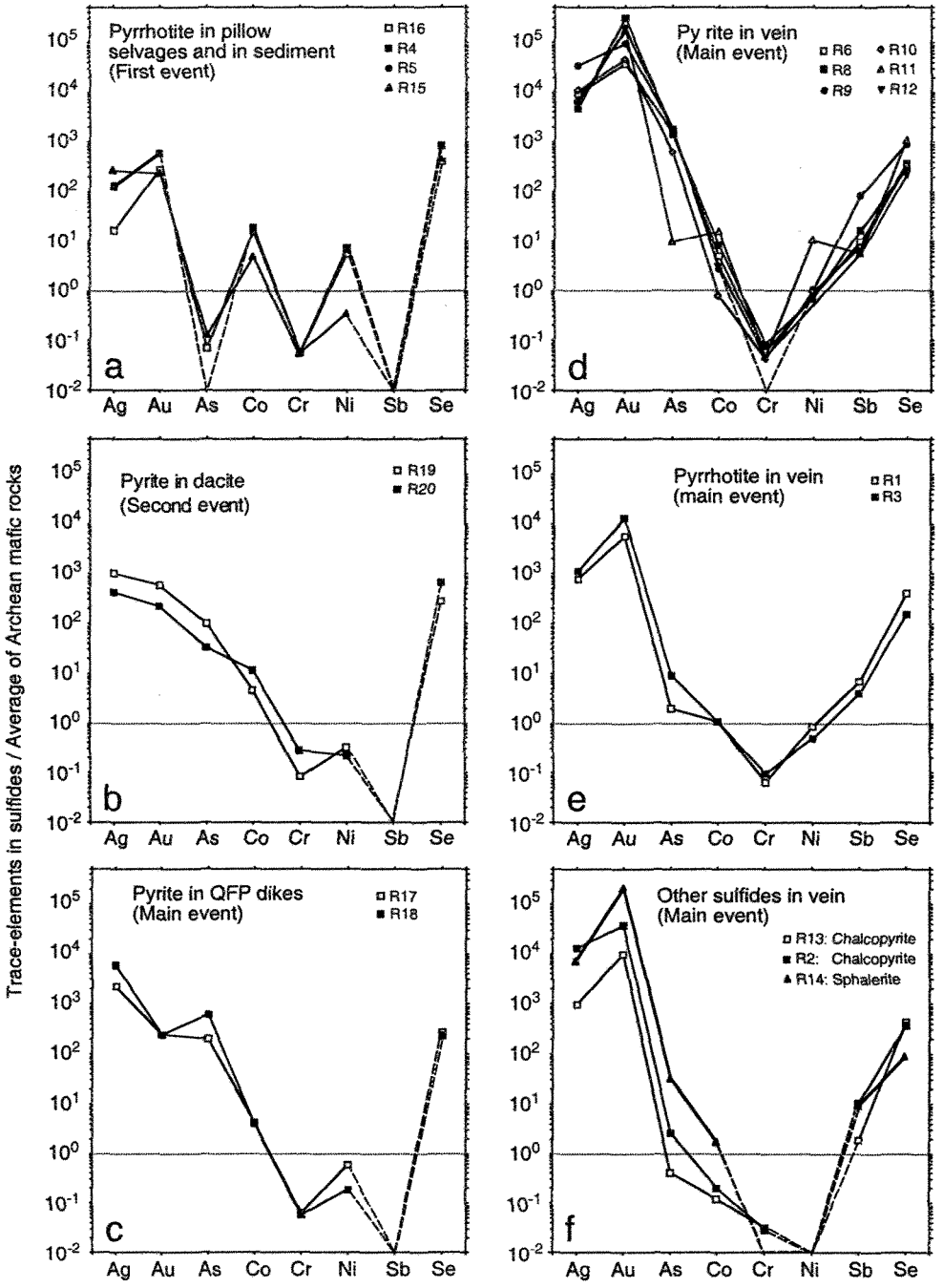

Figure 7. Spidergrams of selected trace elements normalized to average Archean mafic rocks (Kerrich, 1984) for the various sulfides, subdivided in terms of their habit and event. (a) VVV-shaped patterns for the pyrrhotite samples from the first mineralizing event. VV-shaped patterns for the disseminated pyrite in (b) the dacite (second mineralizing event) and in (c) the QFP dikes (main mineralizing event). V-shaped patterns for the vein sulfides, (d) pyrite, (e) pyrrhotite and (f) chalcopyrite and sphalerite, from the main mineralizing event. Elements below the detection limit are linked to others by dashed lines.

The patterns are surprisingly different considering the sulfide habits and events. Pyrrhotite samples from pillow selvages and sediment (first event) are characterized by VVV-like shaped patterns (Fig. 7a). Samples of pyrite disseminated in the dacite (second event) and in the QFP dikes (main event) have VV-like shaped patterns (Figs. 7b, c), whereas all the sulfides in veins (main event) have similar V-shaped patterns. On the other hand, the similarity between individual patterns for each defined shape supports indirectly the validity of the analytical results. This is particularly significant because used samples are scattered spatially in the mine. Samples from the veins, the QFP dikes and the dacite are located over 800 m, 700 m and 400 m apart, respectively (Table 2).

In detail, the normalized pattern shapes reflect the variable enrichments or depletions of As, Co, Ni and Sb. Other elements, Ag, Au and Se, are enriched in all the sulfides at various levels relative to their normalizing value, whereas Cr is systematically depleted (Fig. 7). The normalized content of Se and Cr is also similar for all the sulfides (Fig. 7). For pyrrhotite of the first mineralizing event, the VVV-shape reflects the depletion of As and Sb, and the enrichment of Co and Ni (Fig. 7a). For disseminated pyrite, the VV-shape express the depletion of Ni and Sb, whereas As and Co are respectively moderately and slightly enriched (Figs. 7b, c). For the vein sulfides, there are significant differences in As concentration relative to sulfide species (Figs. 7d, e, f) reflecting the crystal structure and the chemical composition of sulfides (see below). Overall, the v-shape is related to the Co and Ni contents which are close to their normalizing value, whereas As and Sb are enriched at various levels.

In order to visualize the trends of trace-element enrichments and depletions in a sequence, the various sulfide types versus the normalized average values of trace-elements are presented in the Figure 8. For pyrrhotite, a strong enrichment of Au, Ag, As, Sb, and a depletion of Ni and Co concentrations characterizes the vein samples compared to samples

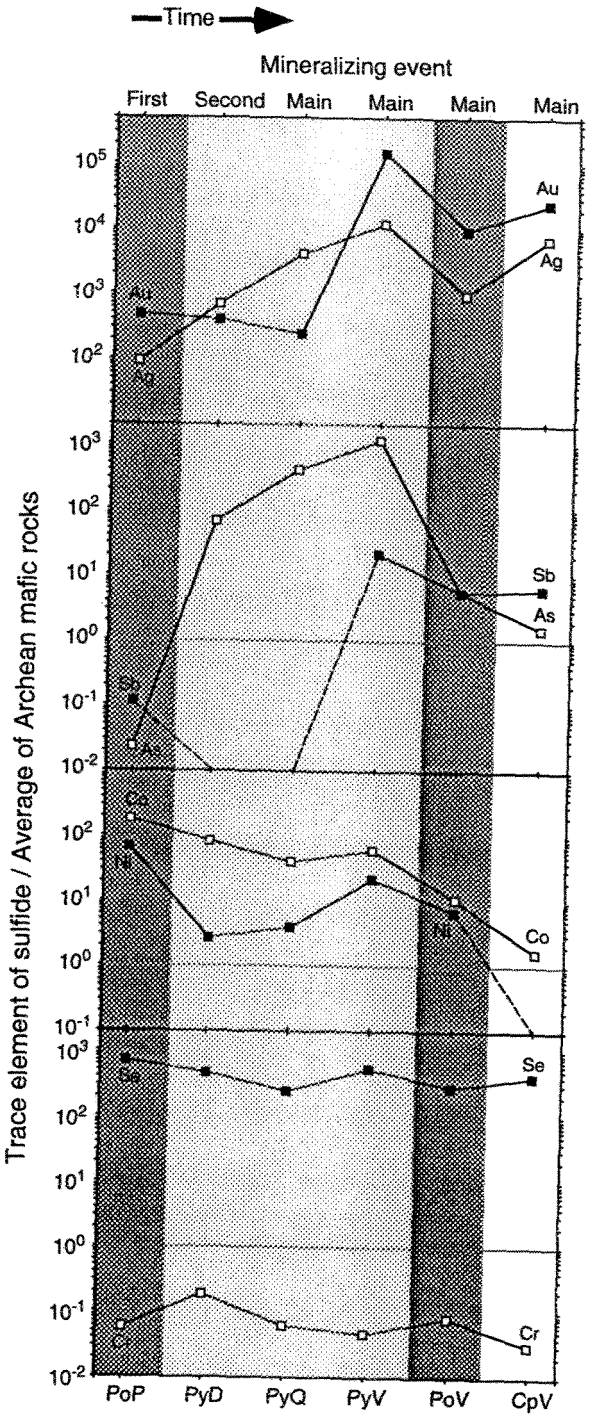

Figure 8. Diagram showing the trend of enrichment or depletion of trace elements in a time-related framework. Plotted data are the normalized average of trace elements. Grey-colored areas highlight the corresponding sulfide species for comparison. PoP: pyrrhotite in pillow selvages; PyD: pyrite disseminated in the dacite; PyQ: pyrite disseminated in QFP dikes; PyV, PoV and CpV: pyrite, pyrrhotite and chalcopyrite in vein respectively.

of the first mineralizing event. (Fig. 8). The pyrite samples record the change from the second (pyrite in dacite) to the main mineralizing event (pyrite in QFP dikes and in the veins). From these samples, a progressive and strong enrichment of Ag, As and Sb (Fig. 8) characterizes the temporal evolution from the second to the main mineralizing event. Gold is less abundant in pyrite from the QFP dikes than from the dacite. Gold is also strongly enriched in pyrite from veins by two orders of magnitude compared to other pyrite samples (Fig. 8). Other trace-elements in pyrite, such as Co, ± Ni, show insignificant variations. Combining the data from pyrrhotite and pyrite samples, these sulfides record, from the first to the main event, an overall increase of Au, Ag, As and Sb, and a decrease of Ni and Co.

DISCUSSION

Metamorphism influence on trace-element content

Regional greenschist metamorphism overprints the gold-bearing veins, as indicated by the overgrowth of radiating acicular actinolite in gold-bearing veins (Fig. 9a) and by the crosscutting of veins by metamorphozed mafic tholeiitic dikes. Metamorphic recrystallization of sulfides commonly leads to the loss of inclusions and remobilization of their metallic constituents such as gold and silver (Larocque & Hodgson 1995). Such a recrystallization phenomenon is observed in thin sections (Fig. 9b) from vein samples taken below the level 545 (545 m below the surface). Above this level, pyrite grains are subprismatic, cataclastic and rich in gold and silver inclusions (Fig. 5). Such a vertical zoning is interpreted be the result of the subhorizontal orientation of the regional metamorphic isograds, as documented in the Abitibi belt (Robert & Brown 1986, Powell *et al.* 1993, 1995, Larocque & Hodgson 1995). Hence, vein samples used in this study were taken above the level 545 (Table 2), to overcome the loss of trace-elements occurring as

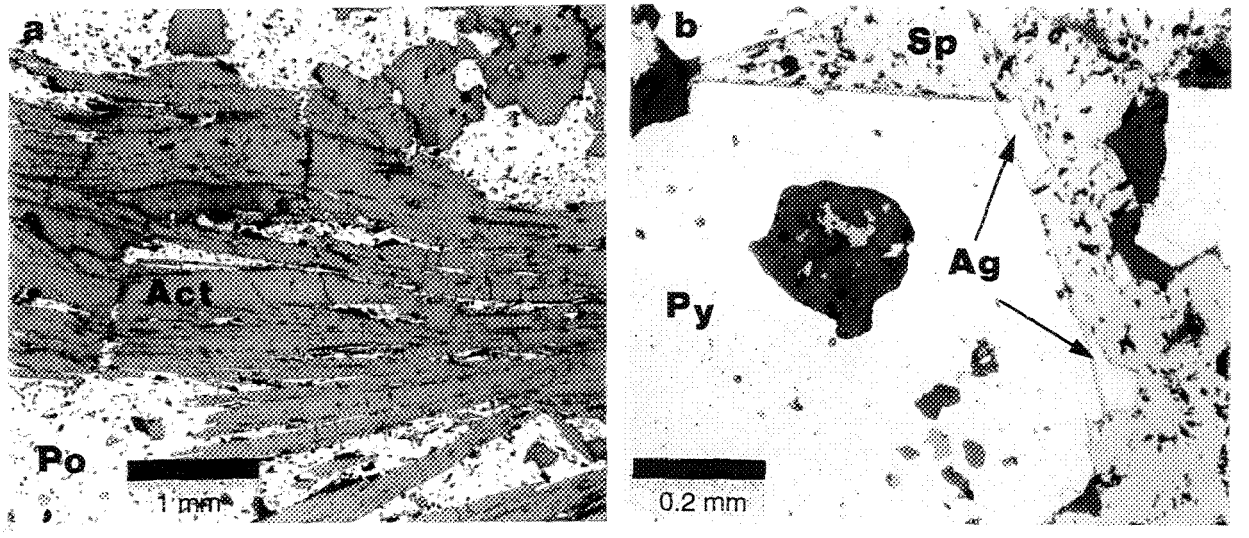

Figure 9. Photomicrographs (reflected natural light) showing the influence of the regional metamorphism. (a) Metamorphic overgrowth of acicular actinolite (Act) on pyrrhotite (Po) in a vein. (b) Recrystallized pyrite without visible gold and silver inclusion and with planar grain borders. Note the expelled silver (Ag) occurring along the border of the pyrite grain.

inclusions in sulfides. On the other hand, REE are generally considered as relatively immobile during the metamorphism (Grauch 1989).

Significance of REE patterns

According to Graf (1977), sulfides do not fractionate the REE pattern of the hydrothermal fluids during their precipitation. The fact that each sulfide event has a characteristic REE pattern is consistent with that statement. Therefore, REE patterns of sulfides may be considered as representative of the relative proportion of REE in the fluids involved during their precipitation.

The REE patterns of pyrrhotite in pillow selvages are characterized by a weak fractionation of light REE, low REE abundance and negative Ce anomaly (Fig. 6a). Low REE abundance is typical of hydrothermal sulfides because fluids generally carry low REE concentrations (*e.g.*, Michard 1989). The negative Ce anomaly is a typical feature of the modern seawater REE patterns (Elderfield & Greaves 1982), where Ce is separated from the rest of REE by oxidation of Ce^{3+} to Ce^{4+} (Fryer 1983). In general, Archean seawater is thought to be more reducing that modern seawaters, because of the lower atmospheric oxygen levels. However, the abundance of magnetite facies iron-formations may suggest that local Archean oxidizing submarine environments may have existed, as suggested by Manikyamba *et al.* (1993), where Ce would have occurred as the tetravalent state. Negative Ce anomalies are also reported from recent sulfide-sulfate volcanogenic precipitates and it is interpreted to reflect the mixing of high-temperature hydrothermal fluids with seawater (Barrett *et al.* 1990). Accordingly, the negative Ce anomalies of pyrrhotite samples from the pillow selvages may be explained by the Ce oxidation due to mixing of hydrothermal fluids with oxygenated seawater at the subseafloor site of pyrrhotite precipitation.

For the disseminated sulfides (Fig. 6b), the similarity between the REE patterns of sulfides and of their host rocks suggests that the REE patterns of sulfide are not representative of the initial REE concentrations of the fluids. This interpretation is supported by the high REE abundance of these sulfides. These anomalous REE patterns may be related to a problematic extraction of the sulfides or to an inherited REE signature due to the overprinting of preexisting minerals by sulfides. The former hypothesis seams unlikely because the samples with the highest impurity contents are those with the lowest REE abundance (Table 2). In addition, quartz is the dominant impurity (Table 2) and it is a poor REE host mineral (*e.g.*, Grauch 1989). Conversely, the latter hypothesis appears plausible because evidences of magnetite replacement by pyrite are commonly observed in thin sections (Fig. 10). Nevertheless, the REE patterns of these disseminated sulfides cannot be considered as representative of the initial REE concentrations of the hydrothermal fluids.

The REE patterns of the vein sulfides (Fig. 6c), although incomplete, can be compared with those of high-temperature hydrothermal fluids venting on seafloor (Michard *et al.* 1983, Michard & Albarède 1986, Michard 1989, Campbell *et al.* 1988) and their sulfidic precipitates (Barrett *et al.* 1990). These patterns are typically characterized by a strong positive Eu anomaly, low REE abundance and strong enrichment of light REE (Fig. 11). This distinctive pattern is also recorded in sulfides from preserved massive sulfide deposits on land (*e.g.*, Graf 1977, Barrett *et al.* 1991, Peter & Goodfellow 1996) and from syngenetic gold-bearing sulfides hosted by magnetite iron-formation (Siva Siddaiah *et al.* 1994). The similarity between the REE patterns of the vein sulfides and of the high-temperature volcanogenic fluids (Figs. 6c, 11) supports the inferred volcanogenic origin of the veins.

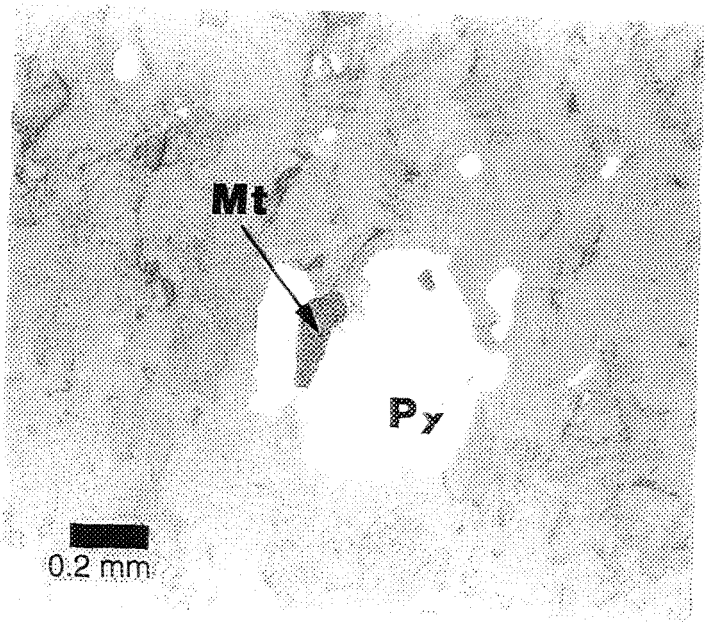

Figure 10. Photomicrograph (reflected natural light) showing the replacement of magnetite (Mt) by pyrite (Py) in altered QFP dikes.

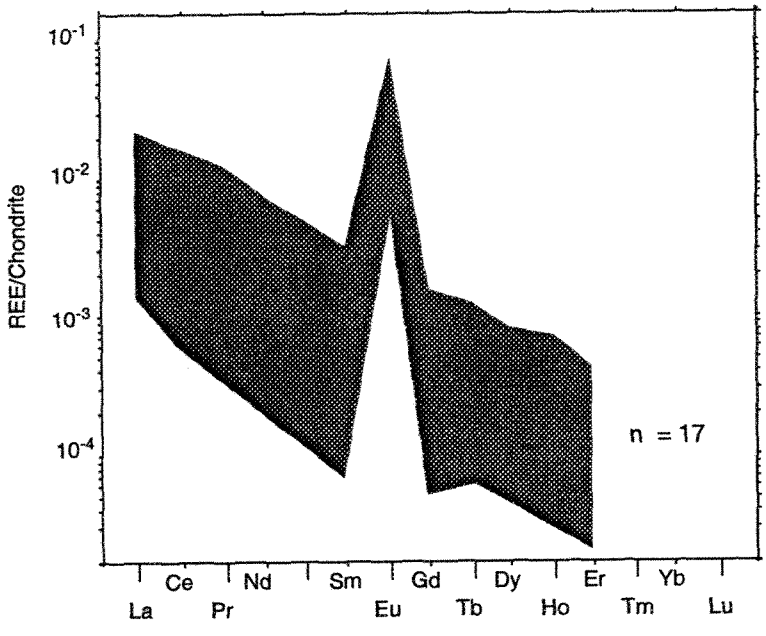

Figure 11. Chondrite-normalized REE plot for the end-member hydrothermal vent fluids from several sites in the modern oceans (Michard and Albarède, 1986; Klinkhammer et al., 1994).

Factors influencing trace-element content in sulfides

According to Vaughan and Craig (1978), the absolute concentration of any trace-element in sulfides may reflect: 1) the availability of the element in the hydrothermal solution from which sulfides were precipitated, 2) partitioning of an available element in hydrothermal solution between two or more coprecipitating sulfides, neither of which being saturated, 3) the saturation limit of a sulfide coexisting with a sulfide of that element, and 4) complex interactions of various sulfide components. For the present case, the three successive mineralizing events but the gold-bearing veins are essentially monomineralic, and the trace-element signatures of the vein sulfides (Figs. 6a, 7d, e, f) are overall quite similar. Hence, these considerations indicate that the trace-element concentrations in sulfides for the Géant Dormant deposit reflect mainly the composition of the mineralizing fluids (statement 1).

However, as hydrothermal systems are open-systems, the concentration of any trace-element in a specific sulfide should be viewed as a value which depends on 1) the absolute concentration of the element in the circulating hydrothermal solution, 2) the efficiency of the precipitating mechanisms of sulfides, and 3) the capacity of a precipitating sulfide to absorb a trace-element as inclusions or stoichiometric and nonstoichiometric substitutions in the lattice (*e.g.*, Huston *et al.* 1995). The precipitating mechanisms have a strong influence on the trace-element concentrations in sulfides because the various ligand-metal complexes have different stabilities. As example, sulfidation reactions destabilize essentially the bisulfide complexes, hence favoring the precipitation of metals transported by the S^{2-} ligand (Morrison *et al.* 1991). Inversely, a quick sulfide crystallization rate, induced by fluid boiling for example, favors trace-element trapping as inclusions. Conversely, slow crystallization conditions, induced by cooling or sulfidation for example, will enhance lattice substitutions.

The concentration of trace-elements in the hydrothermal fluids depends on the source minerals and the chemistry of hydrothermal fluids, because hydrothermal deposits form by leaching, transport and precipitation of metals. For the source minerals, constraints are imposed by the absolute abundance of a specific trace-element and its solubility, *i.e.*, its facility to be leached and transported in solution (Crerar *et al.* 1985). For the fluid, its own chemical characteristics (salinity, ligand abundance and type, pH, O and S fugacity, and temperature) and its degree of interaction with the source minerals (W/R ratio) are the main constraints. The Figure 12 summarizes schematically the various factors influencing the trace-element concentration of any sulfide.

Signification of trace-element content in sulfides

Unlike REE, trace-elements are sensitive at various levels to processes controlling their incorporation into hydrothermal sulfides, as discussed above. It is thus necessary to determine which trace-elements can be considered as the most insensitive to fractionation during sulfide precipitation and hence, the most representative of the initial composition of the hydrothermal fluids. This can be achieved by considering the documented solubility of the trace-elements in volcanogenic fluids and their siting in sulfides (Table 5). Nickel, Co and Se are considered as the most representative of the hydrothermal fluids, *i.e.*, the most insensitive to fractionation during precipitation of sulfides, because they occur as replacement of the major elements (Fe^{2+}, S^{2-}) in sulfides, and because they are common in volcanogenic sulfides. Thus, the Ni, Co and Se concentrations in sulfides reflect their initial concentration in the fluids. Gold, Ag, As and Sb are soluble in hydrothermal fluids and common in volcanogenic sulfides (Table 5). However, these trace-elements occur as lattice substitutions and as inclusions, implying that their concentration in sulfides are strongly influenced by the precipitating conditions, as discussed previously (Fig. 12).

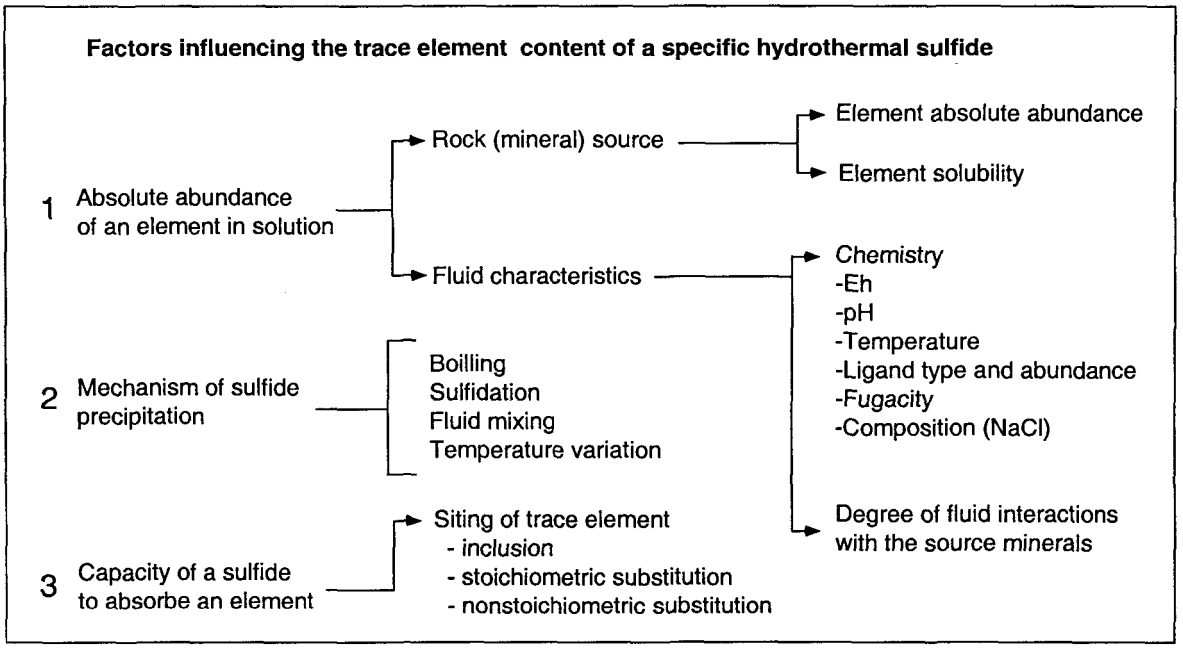

Figure 12. Schematic representation of the various factors influencing the trace element content in a sulfide.

Table 5. Solubility and siting of discussed trace elements in volcanogenic sulfides

Element*	Relative solubility[1]	Occurence in *volcanogenic* sulfides[2]	Siting: substitution[2]	
			nonstoichiometric	Stoichiometric
Au^{+}	High[3]	Common	Py, Po[4]	
Ag^{+}	High[3]	Common	Cp, Sp	
As^{3+}	moderate	Common	Py	
Co^{2+}	Moderate	Common		Replace Fe^{2+}
$Cr^{3+/6+}$	low	Uncommon	?	
Ni^{2+}	Moderate	Common		Replace Fe^{2+}
Sb^{3+}	Moderate	Common		
Se^{2-}	High	Common		Replace S^{2-}
$W^{4+/6+}$	low	Uncommon	?	

*The most common valence in geological systems[1]

[1]Crerar et al. (1985)
[2]Huston et al. (1995)
[3]Morrison et al. (1991)
[4]Cook and Chryssoulis (1990)

Therefore, the concentration of these trace-elements in sulfides partly reflects their initial concentration in the hydrothermal fluids. Finally, Cr cannot be considered as representative of the fluids because it is weakly soluble in volcanogenic fluids (Table 5).

Monitoring of the hydrothermal system evolution

The time-related variation trends of the trace-elements (Fig. 7) combined with the specific REE patterns of the end-member sulfidic events, indicate that the hydrothermal system evolved in time, a feature also suggested by the field relationships and the gold grades of the various mineralizing events. However, the evolution of a hydrothermal system cannot be quantitatively monitored based solely on trace-element data because of the numerous factors influencing the trace-element content in sulfides (Fig. 12). Even if many chemical characteristics of the mineralizing fluids can be estimated by fluid inclusion studies, such a quantitative approach is limited by the lack of valuable partitioning coefficient of liquid/mineral for most trace-elements. Additionally, analyses of trace-elements other than REE for potential source minerals, such as olivine, pyroxene or plagioclase, are also rare in the literature. Nevertheless, the evolving trends of the hydrothermal system can be approached empirically considering the main causes of variations in the hydrothermal metal budget, commonly invoked for volcanogenic systems, such as a progressive maturation of the convection cells and a possible magmatic contribution of metals.

As REE mainly reflects the hydrothermal fluid composition, the progressive maturation hypothesis can be first tested by comparing REE patterns. According to Klinkhammer *et al.* (1994), the typical REE pattern of high temperature hydrothermal fluids venting on seafloor (Fig. 11), results of the leaching of REE and other metals from plagioclase minerals (Fig. 13) in basaltic rocks. On this basis, sulfides from the gold-

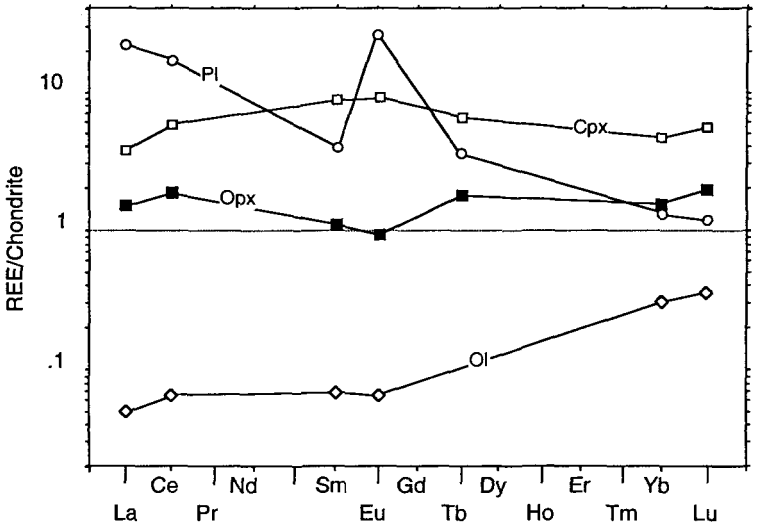

Figure 13. Chondrite normalized REE plot for representative mineral sources of leached trace elements. Plagioclase (Pl) from Phinney and Morrison (1990), olivine (Ol) from Arndt and Lesher (1992), clinopyroxene (Cpx) and orthopyroxene (Opx) from Irving and Fray (1984). Normalizing values after Thompson et al. (1984). Note the similitude between the REE patterns of the plagioclase and those of sulfides from gold-bearing veins. REE patterns of pyrrhotite in pillow selvages compare better with olivine and pyroxene.

bearing veins having comparable REE patterns (Fig. 5c) can be interpreted as the result of a mature hydrothermal system, dominated by plagioclase leaching. Conversely, the REE patterns of pyrrhotite samples from the first mineralizing event (Fig. 5a) compare better with the REE patterns of olivine and pyroxene (Fig. 13) rather than plagioclase. Hence, this pyrrhotite may reflect the hydrothermal leaching of ferro-magnesian minerals. Such an evolution from ferro-magnesian to plagioclase leaching in basaltic rocks was modeled as a normal maturation of a volcanogenic hydrothermal system (Graf 1977).

In order to test if the maturation hypothesis suggested by the REE patterns can account for the determined variation trends of the trace-elements, average analyses of Archean ultramafic and felsic rocks (Fig. 14) are used as database to approximate the composition of ferro-magnesian and plagioclase minerals respectively. From the Figure 14, it is expected that the Ni and Co concentrations will be higher in sulfides precipitated from a solution having leached ferro-magnesian minerals rather than plagioclase, whereas Se content should be constant. These expected results fit well with the decreasing trend of Co and Ni and the constant abundance of Se, recorded by sulfides from the first to the main mineralizing event (Fig. 8). Additionally, such a transition of source minerals is also consistent with the overall increasing trend of the trace-elements which are partly representative of the fluid composition (Au, Ag, As and Sb), as plagioclase becomes the inferred dominant leached source mineral (Figs. 8, 14). Thus, the maturation hypothesis well accounts for the REE signatures and for the variation trends of selected trace-elements.

Magmatic contributions of metals and fluids to volcanogenic hydrothermal systems are still a matter of debate (*e.g.*, de Ronde 1995, Yang & Scott 1996). A magmatic contribution is an attractive hypothesis to account for the significant Au-Ag enrichment in the veins. Selenium concentrations between 20-200 ppm in pyrite grains from massive sulfide deposits are interpreted as an evidence for magmatic contributions of Se and

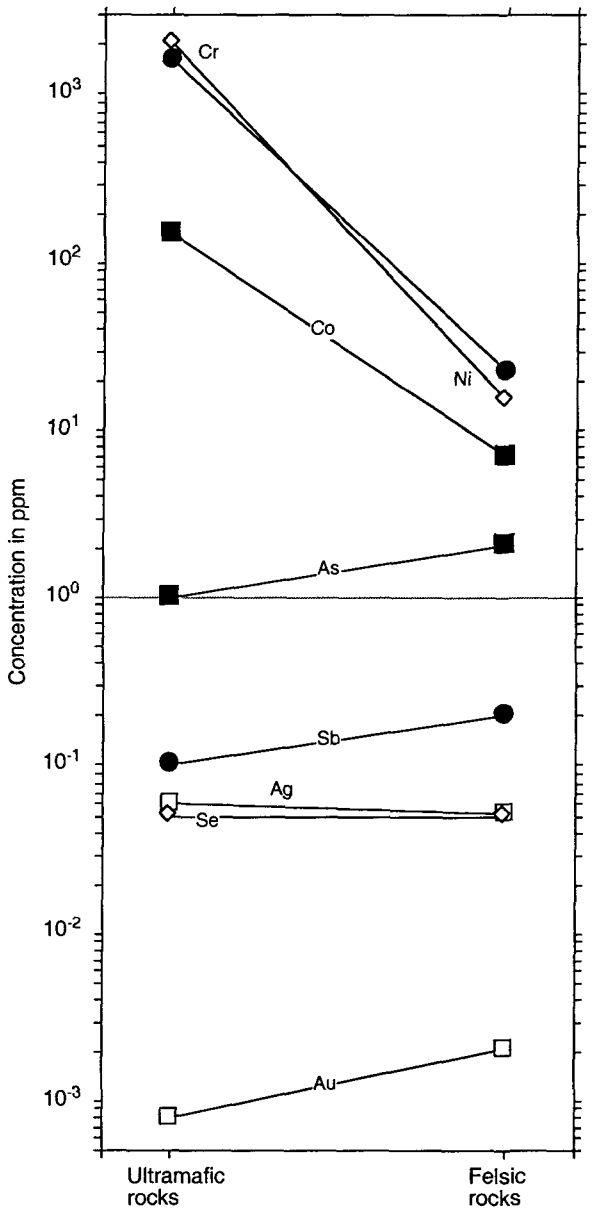

Figure 14. Average concentration of trace elements in Archean ultramafic and felsic rocks (Kerrich, 1983) showing the relative variations of element concentrations.

probably of S and some metals, such as gold and copper (Huston *et al.* 1995). Selenium concentrations of the various sulfides (Table 4) range from 4.3 to 52.0 with an average of 22.4. Although the Se average is close to the lower limit of the magmatic range, a magmatic contribution, only during the vein formation, can be ruled out based on the overall constant concentration of Se for all the mineralizing events (Figs. 7, 8). Nevertheless, a continuous magmatic contribution during all the mineralizing events cannot be discarded.

Gold and silver enrichment in veins

Because a magmatic contribution cannot account alone for the Au-Ag enrichment in the veins, other factors should be considered, such as a better precipitating mechanism or a more favorable fluid chemistry for gold and silver. As QFP dikes constitute hydrothermal fluid feeder conduits for the veins, a specific fluid chemistry appears unlikely, because gold and silver concentrations in pyrite from QFP dikes better compare with the other disseminated sulfides (Figs. 6, 7). Conversely, a different sulfide precipitating mechanism, between vein and disseminated sulfides, is suggested by the replacement nature of pyrite in QFP dikes (Fig. 10), indicating that sulfidation may be the dominant process leading to sulfide formation in these altered rocks. Such a sulfidation mechanism is consistent with the low concentration of Au-Ag, which is limited by the lattice substitution possibilities (Cook & Chryssoulis 1990). For the gold-bearing veins, a more efficient mechanism is suggested by the higher Ag-Au concentrations and the abundance of Au-Ag inclusions. These features may indicate a fast precipitation of sulfides and precious metals, which is consistent with a mechanism of boiling related to fluid pressure fluctuations during vein formation, as documented by Cole & Drummond (1986) and Morrison *et al.* (1991).

Implications for exploration

Considering the progressive maturation interpretation, the use of Ni and Co, and the REE contents in sulfides may have important implications for vectoring exploration in ancient volcanogenic systems. For example, common occurrences of disseminated sulfides in pillow lava selvages, which are indicative of hydrothermal activity, can be sampled and analyzed to determine if they are the product of an immature- or a mature-stage event. In the former case, it is expected that sulfides will have flat normalized REE patterns, devoid of Eu positive anomaly, with Co and Ni concentrations greater than their normalizing value. In such case, exploration should be focused in the upper stratigraphic levels, in the hope that the hydrothermal system attained maturation and economic significance. In the latter case, sulfides having fractionated light REE patterns with distinctive Eu anomalies, and depleted Ni and Co normalized concentrations, should be considered as the result of a mature hydrothermal system. Hence, exploration should be focused, either along the same stratigraphic horizon, or in the lower stratigraphic levels. In that case, the sampled sulfide occurrences may result from lateral or upward mineralizing fluid percolations, away from an economic deposit, through permeable lava flows, as documented at the Ansil Mine (Riverin *et al.* 1990).

CONCLUSIONS AND RECOMMENDATIONS

This study represents an attempt to use the trace-elements in sulfides as tracers for monitoring the hydrothermal evolution and to interpret its causes. The proposed methodology, using normalization to mafic rocks and spidergram presentation of trace-elements, proved it-self to be powerful for discriminating sulfides in terms of events and habits. This approach, combined with the use of REE, provides a framework to constrain the chemical variations in time of the hydrothermal system as a whole. The results

presented here were empirically modeled and interpreted as reflecting the progressive maturation of a volcanogenic hydrothermal system. Such a maturation corresponds to the transition in time from ferro-magnesian- to plagioclase-dominated mineral sources for the hydrothermal leaching of the various metals.

Despite that the approach has great potential, one should be aware of the numerous factors influencing the trace-element contents in the hydrothermal sulfides. In that sense, the modeling and the interpretation of the hydrothermal evolution remain empirical due to the lack, or the rarity, of fundamental data. Further studies are clearly needed to test the proposed approach in other geological contexts and to improve the interpretation aspect with better fundamental data on the trace-element behaviors in hydrothermal systems.

Acknowledgments

The authors express their sincere thanks to Cambior Inc., Aurizon Mine Ltd. and the Ministère des ressources naturelles du Québec for their important scientific collaboration and financial support during field seasons. Our thanks are extended to the mine staff for their generous assistance to the first author during four consecutive field seasons. R. Lechasseur and M. Lapointe are thanked for theirs advice with sample preparation and P. Bédard for is help with the INAA. The manuscript has benefited from constructive criticism at an early-stage by W. Mueller, J-C. Couture, S-J Barnes and R. Kerrich. The Natural Sciences and Engineering Research Council of Canada (NSERC) and the Fonds pour la Formation de Chercheurs et d'Aide à la Recherche (FCAR) also financed the project through Ph.D. postgraduate scholarships to the first author and NSERC grant to the second author.

References

ARNDT, N.T. & LESHER, C.M. (1992): Fractionation of REEs by olivine and the origin of Kambalda komatiites, Western Australia. *Geochim. Cosmochim. Acta* **56**, 4191-4204.

BARRETT, T.J., JARVIS, I. & JARVIS, K.E. (1990): Rare earth element geochemistry of massive sulfides-sulfates and gossans on the Southern Explorer Ridge. *Geology* **18**, 583-586.

BARRETT, T.J., MACLEAN, W.H., CATTALANI, S., HOY, L. & RIVERIN, G. (1991): Massive sulfide deposits of the Noranda area, Quebec. III. The Ansil mine. *Can. J. Earth Sci.* **28**, 1699-1730.

BÉDARD, L.P. & BARNES, S.J. (1990): Instrumental neutron activation analysis by collecting only one spectrum: Results for international geochemical reference samples. *Geostandards Newslett.* **14**, 479-484.

BRALIA, A., SABATINI, G. & TROJA, F. (1979): A revaluation of the Co/Ni ratio in pyrite: A geochemical tool in ore genesis problems. *Mineral. Deposita* **14**, 353-374.

BRILL, B.A. (1989): Trace-element contents and partitioning of elements in ore mine from the CSA Cu-Pb-Zn deposit, Australia. *Can. Mineral.* **27**, 263-274.

CAMPBELL, A., PALMER, M.R., KLINKHAMMER, G.P., BOWERS, T.S., EDMOND, J.M., LAWRENCE, J.R., CASEY, J.F., THOMPSON, G., RONA, P. & KARSUN, J.A. (1988): Chemistry of hot springs on the Mid-Atlantic Ridge. *Nature* **335**, 514-519.

CHOWN, E.H., DAIGNEAULT, R., MUELLER, W. & MORTENSEN, J.K. (1992): Tectonic evolution of the Northern Volcanic Zone, Abitibi belt, Quebec. *Can. J. Earth Sci.* **29**, 2211-2225.

COLE, D.R. & DRUMMOND, S.E. (1986): The effect of transport and boiling on Ag/Au ratios in hydrothermal solutions: a preliminary assessment and possible implications for the formation of epithermal precious-metal ore deposits. *J. Geochem. Explor.* **25**, 45-79.

COOK, N.J. & CHRYSSOULIS, S.L. (1990): Concentrations of "invisible gold" in the commun sulfides. *Can. Mineral.* **28**, 1-16.

CRERAR, D., WOOD, S., BRANTLEY, S. & BOCARSLY, A. (1985): Chemical controls on solubility of ore-forming minerals in hydrothermal solutions *Can. Mineral.* **23**, 333-352.

DE RONDE, C.E.J. (1995): Fluid chemistry and isotopic characteristics of seafloor hydrothermal systems and associated VMS deposits: Potential for magmatic contribution. *In* Magmas, fluids and ore deposits (J.F.H. Thompson, ed.). *Mineral. Ass. Can., Short Course Handbook* **23**, 479-510.

ELDERFIELD, H. & GREAVES, M.J. (1982): The rare earth elements in seawater. *Nature* **296**, 214-219.

FRYER, B.J. (1983): Rare earth elements in iron formations. *In* Iron formation: Facts and problems (A.F. Trendall ed.). Elsevier, Amsterdam, The Netherlands (345-358).

GABOURY, D. (1999): Origine volcanogène des veines aurifères riches en sulfures de la mine Géant Dormant, Abitibi, Québec. Ph.D. Thesis, Univ. du Québec à Chicoutimi, submitted.

GABOURY, D. & DAIGNEAULT, R. (1999): Evolution from seafloor-related to sulfide-rich quartz vein-type gold mineralization during deep submarine volcanic construction: The Géant Dormant gold mine, Archean Abitibi belt, Canada. *Econ. Geol.* **94**, 3-21.

GABOURY, D., DAIGNEAULT, R., TOURIGNY, G. & GOBEIL, C. (1996): An Archean volcanic-related gold-sulfide-quartz vein orebody: the Géant Dormant mine, Abitibi Subprovince, Québec, Canada. *Explor. Mining Geol.* **5**, 197-213.

GABOURY, D., DAIGNEAULT, R. & BEAUDOIN, G. (1999): Volcanogenic-related origin of sulfide-rich quartz veins: evidence from O and S isotope systematics at the Géant Dormant gold mine, Archean Abitibi belt, Canada. *Mineral. Deposita,* In press.

GRAF, J.L. (1977): Rare earth elements as hydrothermal tracers during the formation of massive sulfide deposits in volcanic rocks. *Econ. Geol.* **72**, 527-548.

GRAUCH, R.I. (1989): Rare earth elements in metamorphic rocks. *In* Geochemistry and Mineralogy of Rare Earth Elements (B.R. Lipin & G.A. McKay, eds.). Rev. Mineral. **21**, 147-167.

GREEN, G.R., SOLOMON, M., WALSHE, J.L. (1981): The formation of the volcanic-hosted massive sulfide ore deposit at Rosebery, Tasmania. *Econ. Geol.* **76**, 304-338.

HOFFMAN, E.L. (1992): Instrumental neutron activation in geoanalysis *J. Geochem. Explor.* **44**, 297-319.

HUSTON, D.L., SIE, S.H., SUTER, G.F., COOKE, D.R. & BOTH, R.A. (1995): Trace elements in sulfide minerals from Eastern Australian volcanic-hosted massive sulfide deposits: Part I. Proton microprobe analyses of pyrite, chalcopyrite, and sphalerite, and Part II. Selenium levels in pyrite: Comparison with δ34S values and implications for the source of sulfur in volcanogenic hydrothermal systems. *Econ. Geol.* **90**, 1167-1196.

IRVING, J.A. & FREY, F.A. (1984): Trace element abundances in megacrysts and their host basalts: constraints on partition coefficient and megacryst genesis. *Geochim. Cosmochim. Acta* **48**, 1201-1221.

KERRICH, R. (1983): Geochemistry of gold deposits in the Abitibi greenstone belt. *Can. Inst. Mining Metall., Spec. Vol.* **27**.

KLINKHAMMER, G.P., ELDERFIELD, H., EDMOND, J.M. & MITRA, A. (1994): Geochemical implications of rare earth element patterns in hydrothermal fluids from mid-ocean ridges. *Geochim. Cosmochim. Acta* **58**, 5105-5113.

LAROCQUE, A.C.L. & HODGSON, C.J. (1995): Effects of greenschist-facies metamorphism and related deformation on the Mobrun massive sulfide deposits, Québec, Canada. *Mineral. Deposita* **30**, 439-448.

LOFTUS-HILLS, G. & SOLOMON, M. (1967): Cobalt, nickel and selenium in sulphides as indicators of ore genesis. *Mineral. Deposita* **2**, 228-242.

MANIKYAMBA, C., BALARAM, V. & NAQVI, S.M. (1993): Geochemical signatures of polygenetic origin of a banded iron formation (BIF) of the Archaean Sandur greenstone belt (schist belt) Karnataka nucleus, India. *Precambrian Res.* **61**, 137-164.

MICHARD, A. (1989): Rare earth element systematics in hydrothermal fluids. *Geochim. Cosmochim. Acta* **53**, 745-750.

MICHARD, A. & ALBARÈDE, F. (1986): The REE content of some hydrothermal fluids. *Chem. Geol.* **55**, 51-60.

MICHARD, A., ALBARÈDE, F., MICHARD, G., MINSTER, J.-F. & CHARLOU, J.L. (1983): Rare earth elements and uranium in high-temperature solution from East Pacific Rise hydrothermal vent field (13°N). *Nature* **303**, 795-797.

MORRISON, G.W., ROSE, W.J. & JAIRETH, S. (1991): Geological and geochemical controls on the silver content (fineness) of gold-silver deposits. *Ore Geol. Rev.* **6**, 333-364.

PETER, J.M. & GOODFELLOW, W.D. (1996): Mineralogy, bulk and rare earth element geochemistry of massive sulphide-associated hydrothermal sediments of the Brunswick Horizon, Bathurst Mining Camp, New Brunswick. *Can. J. Earth Sci.* **33**, 252-283.

PHILLIPS, N., GROVES, D.I., AMARO, D., HALLBAUER, D.K. & FOTIOS, M.G. (1988): Morphology and trace-element compositions of pyrites from Kalgoorlie gold deposits: sensitive indicators of syndeformational fluid regimes and depositional processes. In Advances in understanding Precambrian gold deposits, volume 2. (S.E. Ho & D.I. Groves eds.). Univ. of Western Australia, Publ. **12**, 217-226.

PHINNEY, W.C. & MORRISON, D.A. (1990): Partition coefficients for calcic plagioclase: Implications for Archean anorthosites. *Geochim. Cosmochim. Acta* **54**, 1639-1654.

POWELL, W.G., HODGSON, C.J. & CARMICHAEL, D.M. (1993): Low-temperature metamorphism and its relationship to the Larder Lake-Cadillac Break, Matachewan area, Abitibi belt, Ontario, Canada. *J. Metamorphic Geol.* **11**, 165-178.

POWELL, W.G., CARMICHAEL, D.M. & HODGSON, C.J. (1995): Conditions and timing of metamorphism in the southern Abitibi greenstone belt, Quebec. *Can. J. Earth Sci.* **32**, 787-805.

RIVERIN, G., LABRIE, M., SALMON, B., CAZAVANT, A., ASSELIN, R. & GAGNON, M. (1990): The geology of the Ansil deposit, Rouyn-Noranda, Québec. *Can. Inst. Mining Metall., Spec. Vol.* **43**, 143-151.

ROBERT, F. & BROWN, A.C. (1986): Archean gold-bearing quartz veins at the Sigma Mine, Abitibi greenstone belt, Québec: Part I. Geologic relations and formation of the vein system. *Econ. Geol.* **81**, 578-592.

ROBERTS, F.I. (1982): Trace element chemistry of pyrite: A usefull guide to the occurence of sulfide base metal mineralization. *J. Geochem. Explor.* **17**, 49-62.

SECCOMBE, P.K. (1977): Sulphur isotope and trace element composition of stratiform sulphides as an ore guide in the Canadian shield. *J. Geochem. Explor.* **8**, 117-137.

SIVA SIDDAIAH, N., HANSON, G.N. & RAJAMANI, V. (1994): Rare earth element evidence for syngenetic origin of an Archean stratiform gold sulfide deposit, Kolar Schist Belt, South India. *Econ. Geol.* **89**, 1552-1566.

THOMPSON, R.N., MORRISON, M.A., HENDRY, G.L. & PARRY, S.J. (1984): An assessment of the relative role of crust and mantle in magma genesis: an elemental approach. *Phil. Trans. Royal Soc. London* **A310**, 549-590.

VAUGHAN, D.J. & CRAIG, J.R. (1978): Mineral chemistry of metal sulfides. Cambridge University Press, U.K.

YANG, K. & SCOTT, S.D. (1996): Possible contribution of a metal-rich magmatic fluid to a sea-floor hydrothermal system. *Nature* **383**, 420.

CHAPITRE 5

Volcanogenic-related origin of sulfide-rich quartz veins: evidence from O and S isotopes at the Géant Dormant gold mine, Abitibi belt, Canada

Ce chapitre représente la version intégrale d'un article en impression dans le Journal *Mineralium Deposita* par Gaboury, Daigneault et Beaudoin.

Abstract

The Géant Dormant gold mine is a sulfide-rich quartz vein gold deposit hosted by a volcano-sedimentary sequence and an associated felsic endogenous dome and dikes. The auriferous quartz-sulfide veins were preceded by two synvolcanic gold-bearing mineralizing events: early sulfidic seafloor-related and later disseminated pyrite in the felsic dome. This deposit differs from classical Archean auriferous quartz vein deposits by the low carbonate and high sulfide contents of the veins and by their formation prior to ductile penetrative deformation.

The $\delta^{18}O$ values of quartz associated with seafloor-related auriferous sulfides average 11.9 ± 0.6‰ (n = 3). The seafloor hydrothermal fluids had a $\delta^{18}O$ value of 3.2‰ calculated at 250°C. The oxygen isotope composition of quartz and chlorite from veins average 12.5 ± 0.3‰ (n = 20) and 5.9 ± 1.1‰ (n = 4) respectively. Assuming oxygen isotope equilibrium between quartz and chlorite, the veins formed at a temperature of ~275°C, which is consistent with the calculated temperature of 269 ± 10°C from chlorite chemistry. The gold-bearing fluids had a $\delta^{18}O$ value of 4.7‰ calculated at 275°C. The $\delta^{34}S$ values of sulfides from the three gold events range from 0.6 to 2.8‰ (n = 32) and are close to magmatic values. Sulfur isotope geothermometry constraints the sulfide precipitation in the gold-bearing veins at a temperature of ~350°C.

The similarity of the isotope data, the calculated $\delta^{18}O$ of the mineralizing fluids and the likely seawater fluid source suggest that the three mineralizing events are genetically related to a volcanogenic hydrothermal system. The high value of the auriferous fluids ($\delta^{18}O$ = 4.7‰) is attributed to a significant magmatic fluid contribution to the evolved

seawater-dominated convective hydrothermal system. The two-stage filling of veins at increasing temperature from quartz-chlorite (275°C) to sulfides (350°C) may reflect the progressive maturation of volcanogenic hydrothermal systems. These results, together with field and geochemical data, suggest that formation of gold-rich volcanogenic systems require specific conditions that comprise a magmatic fluid contribution and gold from arc-related felsic rocks, coeval with the mineralizing events. This study shows that some auriferous quartz-vein orebodies in Archean terranes are formed in volcanogenic rather than mesothermal systems.

Résumé

La mine Géant Dormant correspond à un gisement aurifère filonien composé principalement de veines riches en sulfures. La minéralisation est encaissée par une séquence volcano-sédimentaires et par des roches felsiques formant un dôme subvolcanique et des essaims de dykes. Deux événements de minéralisation aurifère synvolcanique précèdent la formation des veines: un premier événement de sulfurisation d'origine volcanogène et un deuxième autométasomatique de pyrite disséminée dans le dôme dacitique. Ce gisement aurifère diffère des gîtes filoniens archéens classiques par la faible teneur en carbonates et le fort contenu en sulfures des veines aurifères et par leur formation précoce par rapport à la déformation ductile régionale.

La valeur moyenne $\delta^{18}O$ du quartz associé génétiquement avec la minéralisation volcanogène est de 11,9 ± 0,6‰ (n = 3). Les fluides minéralisateurs de cet événement ont une valeur $\delta^{18}O$ de 3,2‰ calculée à 250°C. Les compositions isotopiques moyennes de l'oxygène pour le quartz et la chlorite composant les veines aurifères sont respectivement de 12,5 ± 0,3‰ (n=20) et 5,9 ± 1,1‰ (n = 4). En supposant un équilibre isotopique entre le quartz et la chlorite, une température de formation de ~275°C est déterminée. Cette température est consistante avec celle de 269 ± 10°C, calculée à partir de la composition chimique des chlorites. À 275°C, la valeur $\delta^{18}O$ calculée des fluides à l'origine des veines est de 4,7‰. Les valeurs $\delta^{34}S$ des sulfures pour les trois événements de minéralisation sont comprises entre 0,6 et 2,8‰ (n = 32) et sont comparables avec la valeur magmatique du souffre. Les géothermomètres isotopiques du souffre indiquent une température de ~350°C pour la précipitation des sulfures dans les veines.

La similarité des données isotopiques, les valeurs calculées du $\delta^{18}O$ des fluides minéralisateurs et la source océanique probable des fluides suggèrent que les trois événements de minéralisation sont cogénétiques et résultent d'un système volcanogène évolutif. La nature évoluée des fluides ($\delta^{18}O$ = 4,7‰) est attribuée à l'apport de fluides magmatiques au système hydrothermal convectif dominé par l'eau de mer modifiée (~2‰). La séquence de remplissage des veines, qui montre une augmentation de la température de précipitation de 275°C (quartz-chlorite) à 350°C (sulfures), reflète la maturation progressive typique des systèmes volcanogènes. L'intégration de ces résultats avec les données de terrain et celles lithogéochimiques suggère que la formation des systèmes volcanogènes riches en or requiert des conditions particulières. Celles-ci incluent une contribution magmatique en fluides et en or, dérivée de magmas felsiques développés en contexte d'arc et de manière contemporaine à la formation de la minéralisation aurifère. Finalement, cette étude démontre que certains gisements aurifères de type veine de quartz dérivent de systèmes hydrothermaux volcanogènes plutôt que mésothermaux.

INTRODUCTION

Structurally-hosted auriferous vein systems (mesothermal) in metamorphic terranes of Archean to Phanerozoic ages constitute a coherent class of epigenetic deposits (Groves et al. 1998; McCuaig and Kerrich 1998), characterized by: (1) spatial distribution along transcrustal reverse faults; (2) structurally-controlled ore; (3) syn- to late-timing relative to the ductile deformation and metamorphism; and (4) CO_2-rich auriferous fluids. These features reflect the genetic association with accretionary tectonic regimes (Kerrich and Wyman 1990; Barley and Groves 1992). Typical vein-ore characteristics of Archean examples (e.g. Robert 1995) include: (1) low sulfide content (<5%); (2) quartz (<85%) and carbonate (10-15%) as the main gangue minerals, with variable amounts of tourmaline; and (3) Au/Ag ratios between 5 to 10.

The Géant Dormant gold mine is a quartz-sulfide vein-type deposit located within the central part of the Archean Abitibi greenstone belt in eastern Canada (Fig. 1). This deposit is of interest because it differs from typical lode gold deposits of the prolific Abitibi belt, by the high sulfide (5 to 80%) and low carbonate contents (~3%) of the gold-bearing veins, by their low Au/Ag ratios (<1), and by their formation prior to regional ductile deformation and greenschist metamorphism (Gaboury et al. 1996). In addition, the host sequence recorded two earlier gold-mineralizing events. The oldest is seafloor-related and the second is related to the endogenous dome emplacement (Gaboury and Daigneault 1999). The formation of the gold-bearing veins prior to ductile deformation implies that they can range in relative time from synvolcanic to early-orogenic, covering an absolute time span of more than 12 m.y. (see below). In the former case, veins probably result from

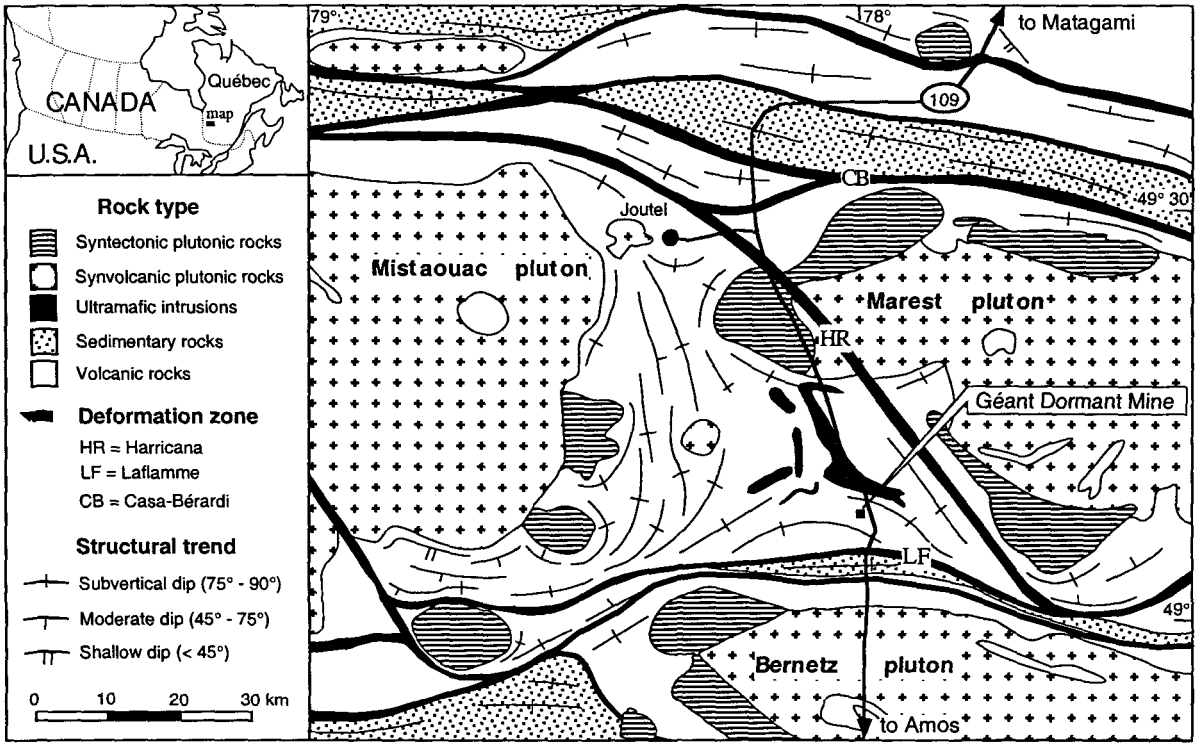

Figure 1. Simplified geological map of the mine district showing the location of the Géant Dormant gold deposit. Map modified from Chown et al. (1992).

an evolving hydrothermal system with volcanogenic roots. In the latter case, veins may be the product of a hydrothermal system unrelated to, and overprinting the two earlier volcanogenic mineralizing events.

A systematic stable isotope study (O, S) was undertaken on the three gold-bearing hydrothermal mineralizing events in order to: (1) determine the temperature of vein formation; (2) determine the source of mineralizing fluids and sulfur; (3) test the genetic relationships between the three auriferous events; and (4) compare the Géant Dormant hydrothermal system with typical Archean volcanogenic massive sulfides (VMS) and mesothermal lode gold deposits. In addition to isotope data, chlorite chemistry was used to independently estimate the vein formation temperature.

This study demonstrates that the three mineralizing events are genetically related and that isotopic signatures are consistent with a volcanogenic rather than an early-orogenic mesothermal origin for the auriferous sulfide-rich veins. This conclusion has significant implications for genetic models, especially for gold-rich volcanogenic systems, as well as for gold exploration in regionally metamorphosed greenstone belts.

GEOLOGICAL SETTING

The Géant Dormant deposit is hosted within the first volcanic cycle of the Northern Volcanic Zone of the Archean Abitibi Subprovince of the Superior craton in Canada (Chown et al. 1992). This volcanic cycle, formed between 2730 and 2720 Ma (Mortensen 1993), corresponds to an extensive subaqueous basalt plain with scattered felsic volcanic edifices, interstratified with or overlain by sedimentary assemblages. The volcano-

sedimentary sequence is intruded by voluminous synvolcanic diorite-tonalite-leucotonalite plutons (Chown et al. 1992). The Northern Volcanic Zone is interpreted as a diffuse arc passing laterally into a back-arc environment (Chown et al. 1992). Between 2708 and 2685 Ma, the Northern Volcanic Zone was affected by a N-S shortening, composed of a succession of several tectonic pulses (Chown et al. 1992). These generated in chronological order: (1) E-W-trending, subvertical, regional folds with axial planar, subvertical schistosity; (2) major E-W-trending, 1- to 4-km-wide reverse shear zones of regional extent; and (3) 1- to 5-km-wide, NW-SE-trending deformation zones. Sub- to greenschist facies regional metamorphism overprinted the rocks between 2677 and 2643 Ma (Powell et al. 1995).

Geology of the Géant Dormant deposit

The Géant Dormant mine is a gold-bearing quartz and sulfide vein type deposit with production of 1.4 million metric tons (MT) at 9.3 g/t Au and with reserves in all categories estimated at 0.6 MT at 10.7 g/t Au. Gold mineralization is hosted by a volcano-sedimentary succession which is intruded by a felsic complex (Fig. 2a). The volcano-sedimentary succession is composed of mafic sills, fine chemico-clastic sediments and flows of mafic pillowed and felsic lavas (Fig. 2). The felsic complex includes a dacitic dome and swarms of felsic plagioclase-porphyritic (FP) and quartz- and plagioclase-porphyritic (QFP) dikes. Two different generations of mafic dikes cut the gold-bearing veins: early aphanitic and late shoshonitic dikes.

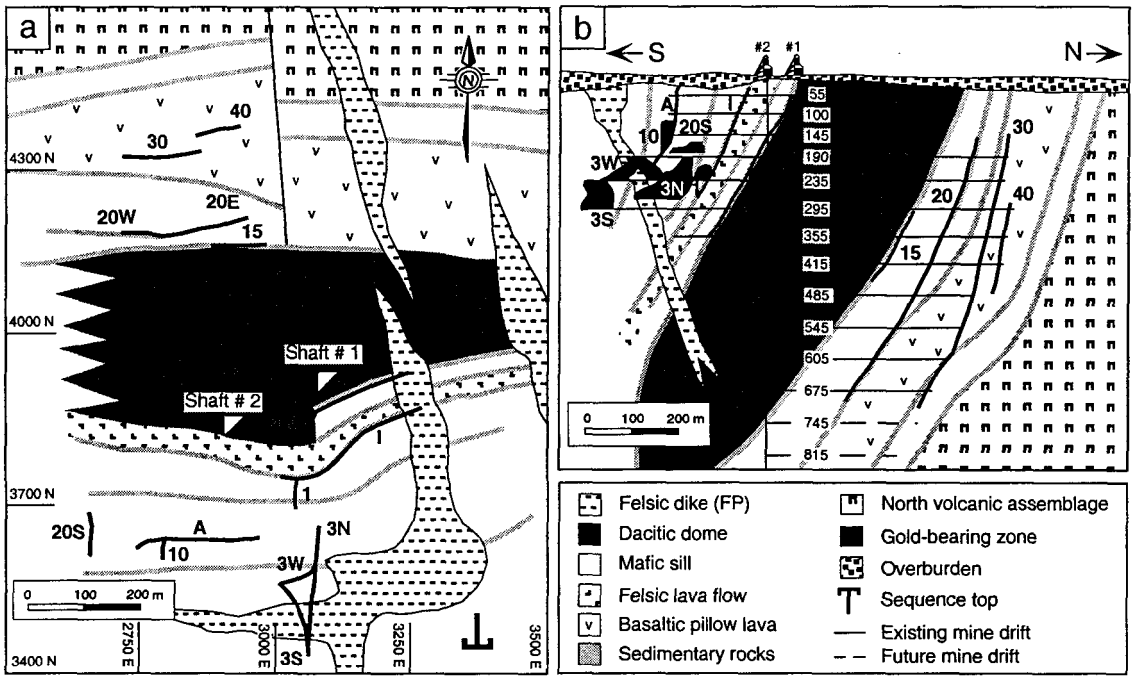

Figure 2. Characteristics of the mine sequence. (a) Simplified geological plan of the Géant Dormant mine area. (b) Idealized vertical N-S cross section. Various gold-bearing zones are labeled: A, 10, 40, etc.

The strata, the felsic complex and the gold-bearing vein network are altogether tilted (Fig. 2) along an E-W-trending subhorizontal regional fold axis and overprinted by the weakly penetrative, subvertical, E-W-trending, regional schistosity (Gaboury et al. 1996; Gaboury and Daigneault 1999). All rock types, including post-mineralization dikes, are metamorphosed to greenschist facies, as indicated by the chlorite, actinolite, albite, epidote and quartz mineral assemblages. As the internal deformation within the tilted sequence is weak and heterogeneous, primary geometrical relationships and vein textures are commonly well-preserved.

Volcanic pile construction and paleosetting

Physical, crosscutting, geochemical and age characteristics of rocks were used to define the sequential construction of the host pile (Fig. 3) and its submarine setting (Gaboury and Daigneault 1999). Basaltic followed by felsic lavas were extruded on the seafloor during continuous sedimentation. Later mafic sills cut the pillowed and felsic lava flows. The felsic complex formation is well-constrained by crosscutting relationships. These indicate formation of the dacitic endogenous dome followed by injections of FP dikes, and later intrusion of tabular QFP dikes along cross-stratal synvolcanic faults. Zircons from a QFP dike yield a U-Pb age of 2722 ± 2 Ma, consistent with the younger ages for the first volcanic cycle (Mortensen 1993). All felsic rocks are cogenetic and have calc-alkalic affinity ($Zr/Y \approx 12$), whereas all mafic rocks, including the early post-mineralization dikes, are cogenetic and tholeiitic ($Zr/Y \approx 2.5$). It is interpreted that the host pile was built from two different magma chambers: a distal mafic and a proximal felsic

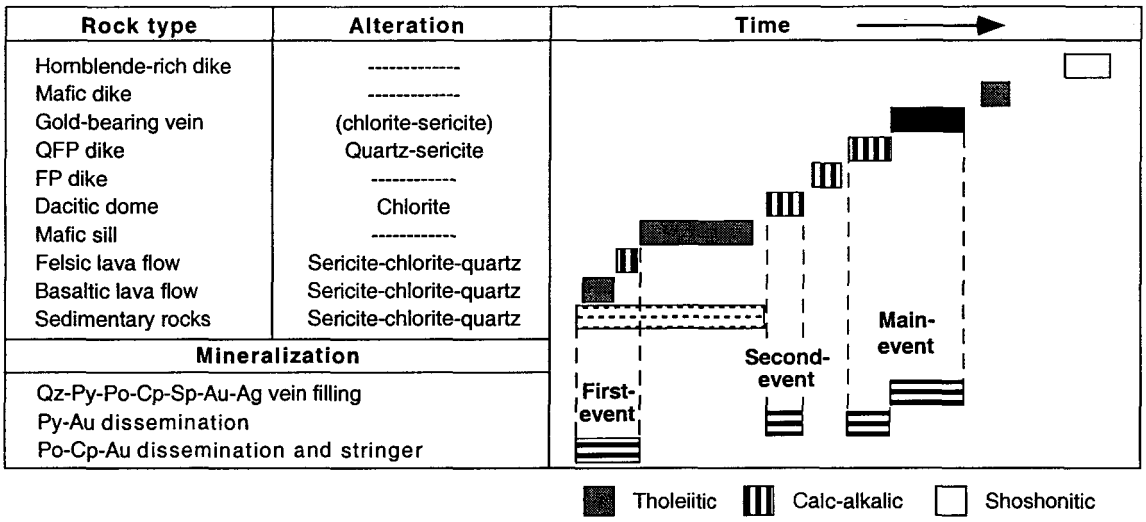

Figures 3. Chronological relationships between rock types, alterations and mineralizing events.

center. Hydrothermal activity is associated with the latter. A deep submarine setting (>3,150 m) is interpreted (Gaboury and Daigneault 1999) from the lack of explosive felsic volcanism, the low vesicle or amygdule content (<1%) of volcanic rocks, the pelitic nature of sedimentary rocks and the Algoma-type iron-formations, and the abundance of sill-like intrusive volcanic rocks.

Hydrothermal events

Three successive hydrothermal events (Fig. 3) are characterized by specific styles, sulfide assemblages, alteration, and gold grades, but only the last is economically significant (Gaboury and Daigneault 1999).

The first event is indicated by auriferous (<3 g/t Au) monoclinic-pyrrhotite (95%) and chalcopyrite (5%) hosted by seafloor-related rocks, such as mafic pillowed and felsic lava flows and sedimentary rocks (Fig. 3). Sulfides form up to 20% of the rocks and occur as: (1) stringers within pillow selvages (Fig. 4a); (2) partial replacements of magnetite-bearing iron-formation; and (3) disseminated in sedimentary rocks and felsic lava flow. Whitish quartz associated with the sulfides occurs locally as open space-filling within primary cavities in pillow selvages. Enclaves of sulfidized (pyrrhotite-chalcopyrite) sediments in some mafic sills (See Gaboury and Daigneault 1999, Fig. 11) constrain this mineralizing event to a period prior to the mafic sill injection, hence supporting a seafloor-related origin.

The second event is marked by disseminated gold-bearing pyrite within chloritized dacitic rock (Fig. 4b). Pyrite and chlorite are restricted to the inner dome (Fig. 3) and they

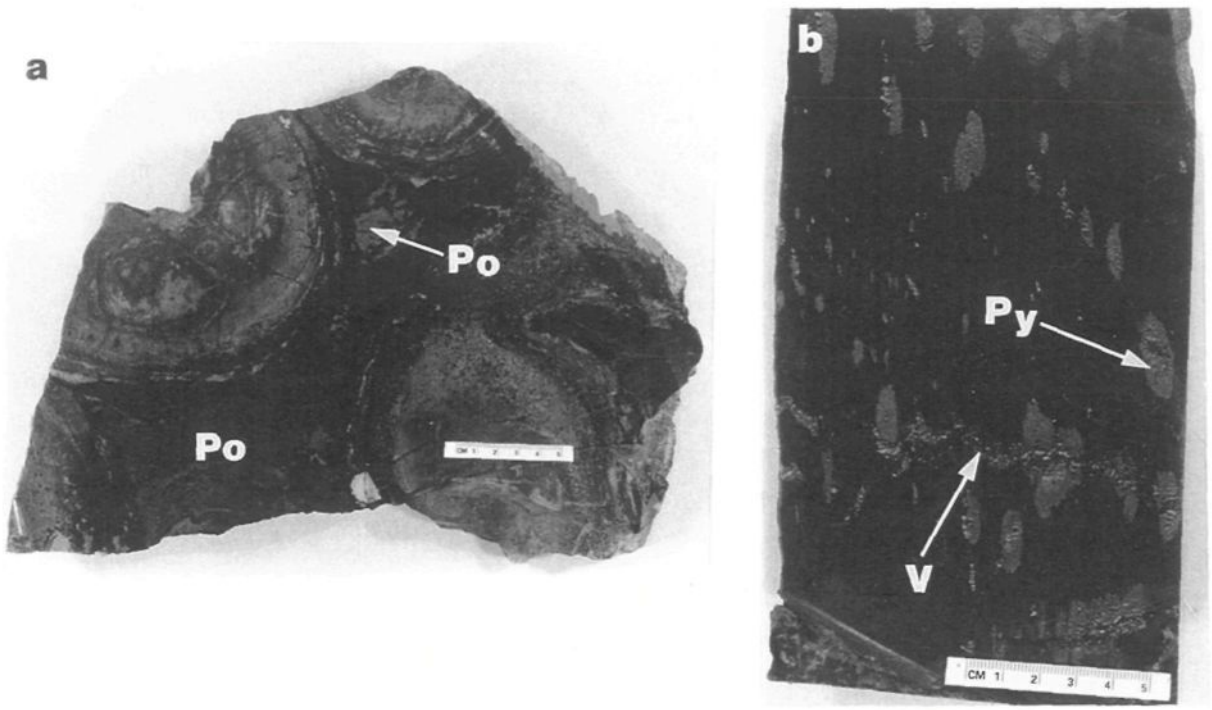

Figure 4. Slabs of typical styles of gold mineralization preceding vein formation. (a) Typical stringer of gold-bearing monoclinic pyrrhotite (Po) with trace of chalcopyrite occurring in the selvages of pillow lava related to the first mineralizing event. (d) Disseminated gold-bearing pyrite (Py) in pervasively chloritized dacite related to the second mineralizing event. Pyrite aggregates (Py) are crosscut by a younger quartz-sulfide veinlet (V) related to the main mineralizing event. Note that the veinlet and pyrite aggregates are overprinted by the ductile deformation.

are the product of hydrothermal activity during dome emplacement and cooling. Gold grade is low (<1 g/t Au) with erratic values up to 20 g/t Au. This mineralizing event is separated from the first event by a period of mafic sill injection. The syn-intrusion timing is constrained by the systematic crosscutting of the altered and mineralized dacite by fresh FP dikes.

The third and main event comprises mineralization in QFP dikes and the gold-bearing veins (Fig. 3). In QFP dikes, mineralization occurs as disseminated auriferous pyrite (<5%) associated with intense and pervasive sericite and quartz alteration. Altered QFP dikes are typically composed of about 50% sericite, 45% quartz and 5% quartz phenocrysts. Gold grade is similar to the disseminated pyrite in the dacite, but with erratic values reaching 100 g/t Au. Gold-bearing veins are generally massive, average 50 cm in thickness and are rich in gold (assays commonly >100 g/t Au). The gold-bearing vein network comprises four sets of planar fractures (Fig. 2), which in order of abundance and tonnage include: (1) E-W-striking steeply (70-85°) S-dipping; (2) N-S-striking moderately (45°) E-dipping; (3) SE-NW-striking moderately (50°) NE-dipping; and (4) SW-NE-striking moderately (40°) SE-dipping (Gaboury et al. 1996). Gold-bearing veins are composed of 5 to 80% (average of ~30%: Fig. 5) of sulfides, including mainly pyrite with lesser amounts of chalcopyrite, sphalerite and pyrrhotite, and a trace of arsenopyrite. Gangue minerals are dominated by quartz with minor amounts of chlorite, sericite, tourmaline, calcite and actinolite (Fig. 5). Altered and mineralized QFP dikes are spatially associated with gold-bearing veins and are interpreted as hydrothermal fluid feeder conduits for the veins. Chronologically, the main mineralizing event overprints the QFP dikes,

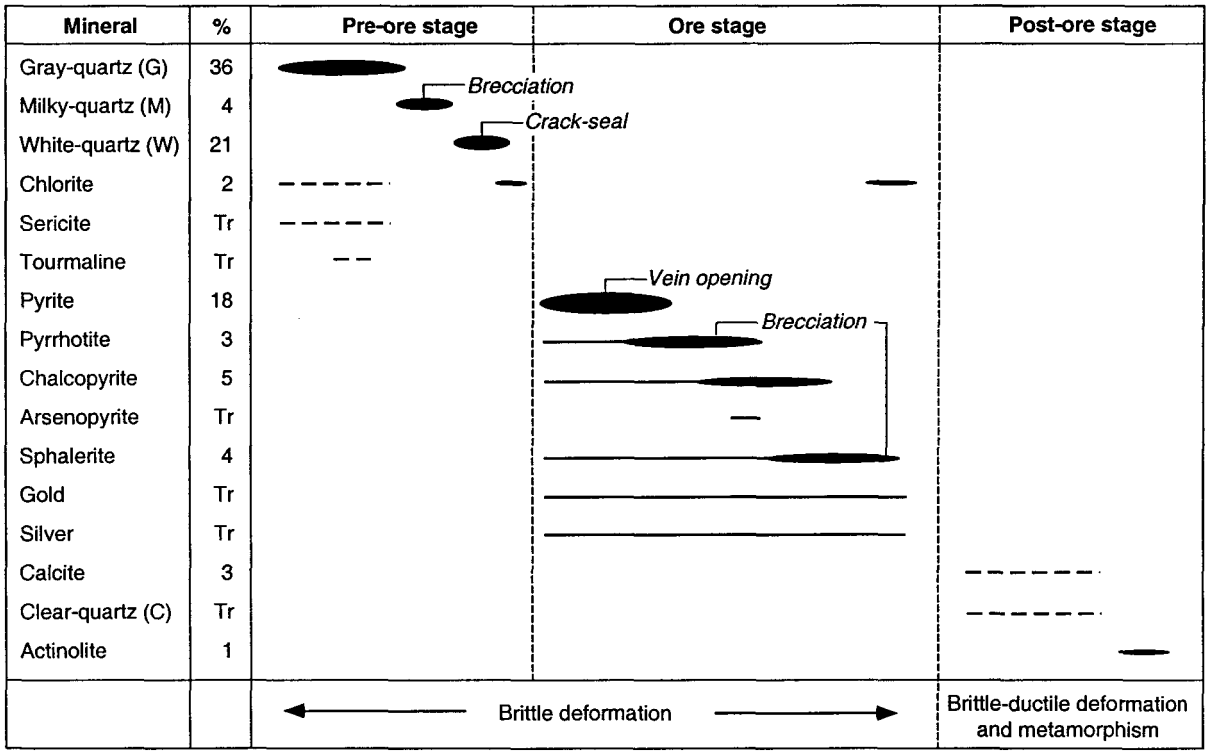

Figure 5. Detailed filling mineral paragenesis and average percentage composition for gold-bearing veins of the main mineralizing event. Data compiled from 66 slab samples (annexe 4).

whereas tholeiitic mafic dikes crosscut the gold-bearing veins. These features constrain the mineralizing event to post 2722 ± 2 Ma felsic calc-alkalic activity, but before the end of the mafic tholeiitic magmatism.

Gold-bearing vein paragenesis

Gold-bearing veins show various textures and proportions of minerals that are related to three successive stages of filling, which can be distinguished as pre-ore, ore and post-ore stages (Fig. 5). The pre-ore stage consists of quartz with minor chlorite, sericite and a trace of tourmaline. Three types of pre-ore quartz are recognized based on their color, grain size and habit (Fig. 5). Difference of color between the various quartz-types reflects their fluid inclusion content and grain size. The first type, which is the most volumetrically abundant, is a paragenetically early, grey to black quartz (referred to below as grey; Figs. 6a, 6b and 6c) that forms subhedral crystals up to 2-cm-long. This quartz forms massive (<50 cm) or locally composite veins comprised of a few narrow and subparallel veinlets which are separated by thin chloritic or sericitic layers of altered host rocks. The second type is milky and cherty (microcrystalline) and occurs as breccia cement of grey quartz (Figs. 6a and 6c). The third type is massive white quartz, which forms parallel crack-seal veinlets (<2 cm) cutting across the two earlier quartz generations (Figs. 6b and 6d). Stylolite-like layers of chlorite are associated with the white quartz (Fig. 6d).

The ore stage includes sulfides and minor chlorite and is devoid of quartz (Fig. 5). Massive aggregates and bands (<20 cm) of pyrite were deposited early in this stage in open-spaces (Figs. 6c and 6e). Pyrite crystals contain inclusions of pyrrhotite, chalcopyrite and

Figure 6. Slabs of gold-bearing veins showing textures and relationships between the various quartz types and sulfides. (a) Milky quartz (Qz-M) as cement in massive grey quartz (Qz-G) without significant sulfides. (b) White quartz (Qz-W) forming veinlets cutting across massive isogranular grey quartz (Qz-G) without significant sulfide mineralization. (c) Massive bands of brecciated pyrite cemented by pyrrhotite, chalcopyrite and sphalerite, bordered by marbled quartz (Qz) composed of brecciated grey quartz cemented by milky quartz. (d) Crack-seal texture defined by subpallel white quartz (Qz-W) veinlets separated by thin stylolitic layers of chlorite. Pyrite overprints the chlorite. (e) Massive lens of brecciated pyrite occurring as open space filling between wall rock coating of euhedral grey quartz crystals (Qz). The dashed lines highlight the vein contacts. (f) Veinlet of white quartz (Qz-W) crosscutting massive grey quartz (Qz-G). Sulfides overprint both generations of quartz. Pyrrhotite, chalcopyrite and sphalerite (Sul) occur as grey quartz cement filling breccia.

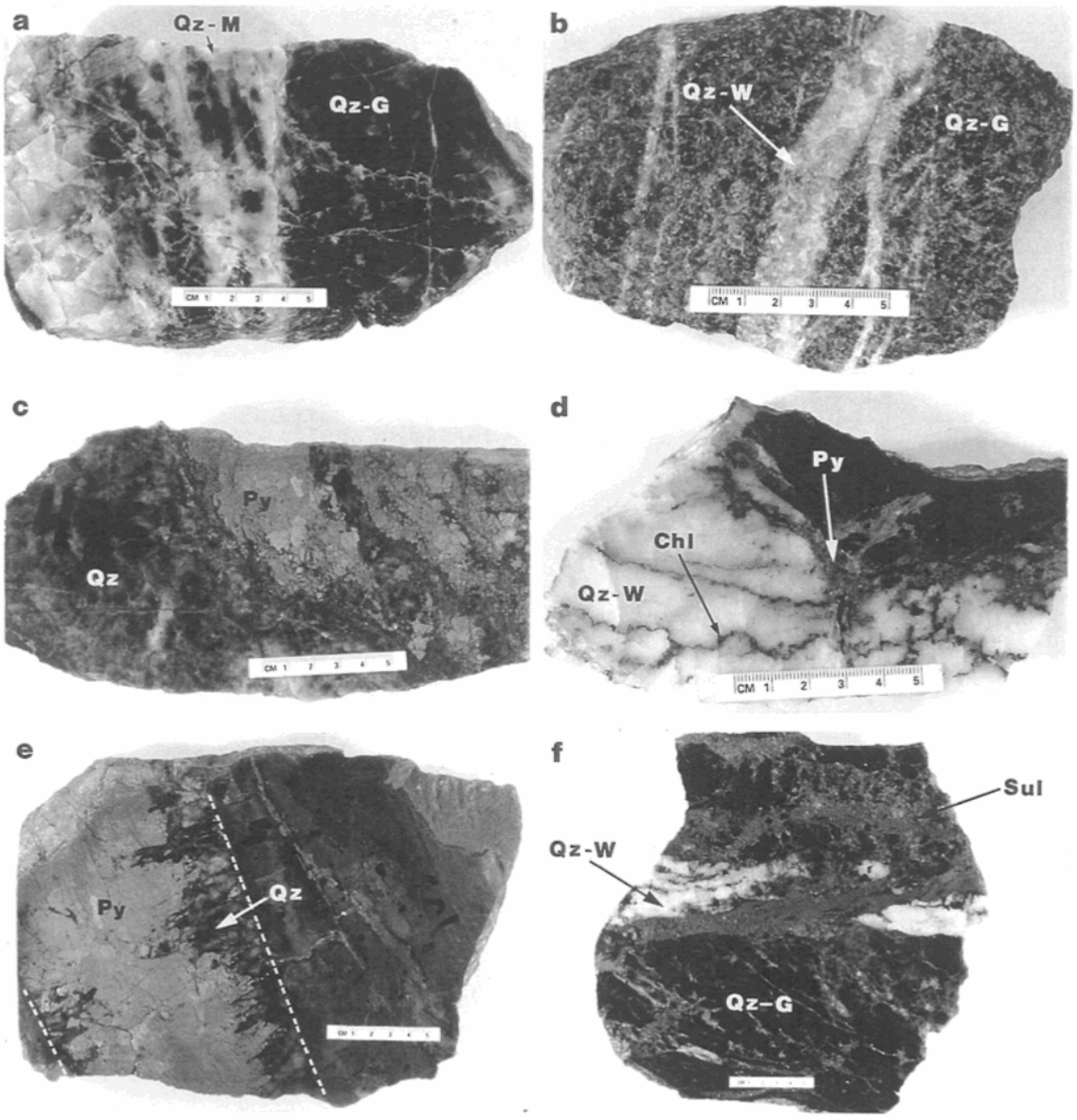
a
Qz-M
Qz-G
b
Qz-W
Qz-G
c
Py
Qz
d
Py
Chl
Qz-W
e
Py
Qz
f
Sul
Qz-W
Qz-G

sphalerite. Hexagonal-pyrrhotite followed by chalcopyrite and sphalerite (Fig. 5) cement fragments of grey, milky and white quartz (Fig. 6f) as well as fractured pyrite (Figs. 6c and 6e). Late chlorite flakes are intergrown with sphalerite (Fig. 7a). Native gold and silver, as well as electrum, occur as μm-scale inclusions in pyrite, pyrrhotite, chalcopyrite and sphalerite and as fine fracture fillings in pyrite associated with other sulfides (Fig. 5). There is an empirical relationship between the sulfide content (and gold grade) and the quartz texture of the veins. Segments of veins characterized by abundant milky quartz are commonly sulfide-rich (Fig. 6c), whereas those dominated by massive crack-seal white quartz are sulfide-poor (Fig. 6d). This can be related to the late introduction of sulfides in quartz veins during brecciation and dilatation events. Sulfide introduction was enhanced in vein segments having heterogeneous (anisotropic) quartz filling material such as the brecciated and cemented grey quartz, rather than the more homogeneous (isotropic) crack-seal white quartz.

The post-ore stage is related to ductile tectonism and greenschist metamorphism, which overprint the gold-bearing veins (Fig. 5) and comprises calcite, clear quartz and actinolite. Calcite occurs mainly as veinlets (<1-cm-thick) surrounding and cutting gold-bearing veins and as minor cement between all previously precipitated vein minerals (Fig. 7b). Clear quartz resulting from pressure-solution occurs locally in pressure shadows. The late overgrowth of radiating acicular actinolite in gold-bearing veins (Fig. 7b) is related to metamorphism.

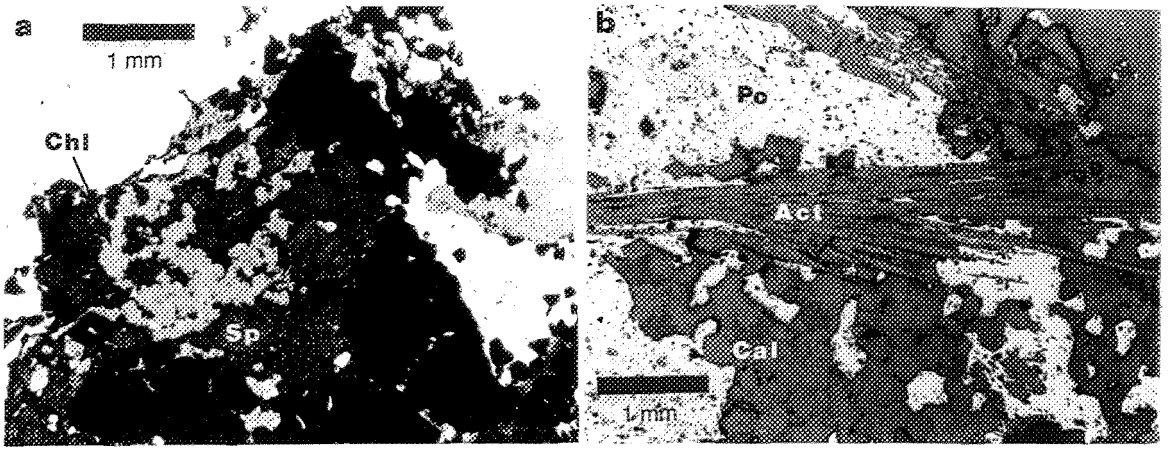

Figure 7. Photomicrographs showing mineralogical relationships. (a) Radiating flakes of late chlorite associated with sphalerite (natural transmitted light). (b) Metamorphic overgrown of acicular actinolite (Act) on pyrrhotite (Po) in gold-bearing veins (reflected natural light). Calcite (Cal) occurs as cement between other mineral except actinolite (Act).

ANALYTICAL METHODS

Studied samples from the three mineralizing events and their locations with respect to the mine grid are included in Tables 1 and 2. The two QFP dike samples come from dikes located about 700 m apart. Two gold-bearing veins were sampled in detail (Fig. 8) to test for isotopic zoning: the N-S-striking moderately E-dipping #3 vein in the southern part and the E-W-striking steeply S-dipping #20 vein in the northern part of the mine (Fig. 2). Only unstrained or weakly-deformed vein samples were selected for study.

Isotope analyses were performed on pure mineral concentrates that were hand-picked under a binocular microscope. Quartz grains were selected based on their megascopic types. Oxygen isotope ratios were determined for quartz, chlorite and whole-rocks from QFP dikes. Oxygen was extracted using BrF_5 and converted to CO_2 by reaction with hot graphite (Clayton and Mayeda 1963) at the Stable Isotope Laboratory of Université Laval. Sulfur isotope ratios were measured on pyrite, pyrrhotite, chalcopyrite and sphalerite at the G.G. Hatch Stable Isotope Laboratory of the University of Ottawa using SO_2 gas produced by sulfide oxidation using cuprous/cupric oxide. Isotopic data are expressed in δ values (‰) relative to VSMOW for oxygen and to VCDT for sulfur. Analytical precision is $\pm$ 0.2‰ for oxygen and sulfur at 1σ level of confidence.

Quantitative chemical analyses by energy-dispersive spectrometry (EDS) of pre-ore chlorite from gold-bearing veins were obtained using a SEMQ II electron microprobe at the Université du Québec à Chicoutimi. An acceleration voltage of 15kV with a beam current of 10nA and 5 μm of diameter and a counting time of 100 s were used for analysis. Analytical results were corrected using the Bence-Albee method. Analytical precision is ±

Table 1. Sample type, location (x, y, z) and oxygen isotopic results

Quartz in pillow selvage (First event)				$\delta^{18}O_{Quartz}$
Sample	X(E)	Y(N)	Z(level)	(‰)
97-014	2945	4080	605	11.9
95-999	2960	4180	545	12.4
94-444	2980	4237	355	11.3

Gold-bearing veins (Main event)				Quartz				
Sample	X(E)	Y(N)	Z(level)	$\delta^{18}O_{Grey}$ (‰)	$\delta^{18}O_{Milky}$ (‰)	$\delta^{18}O_{White}$ (‰)	$\delta^{18}O_{Clear}$ (‰)	$\delta^{18}O_{Chlorite}$ (‰)
93-055	3002	4210	338	14.6				6.7
93-077[1]	2824	4334	228	12.9				
93-080	2878	4196	245				12.8	
93-081	2932	4225	245	13.8				
93-086	3100	3600	235		13.7			
93-088	2910	4122	415	12.2	12.8		12.7	6.8
93-168	3130	3500	295	12.3				
94-464[2]	3075	3713	235			12.8		5.4
96-003	3075	3475	235				12.7	
96-005	3100	3448	255	12.6	12.4		12.1	
96-007	3045	3500	230		12.3			
96-009	3017	3572	190	12.3	12.4			
96-016	2945	4124	485	12.3				
96-017	3005	4155	470			12.6		4.5
96-018	3039	4147	605	12.5			12.4	
96-019	2930	4092	605	12.9				
96-021	3148	3588	295	12.1				

QFP dikes (Main event)				$\delta^{18}O_{Quartz\text{-}phenocryst}$	$\delta^{18}O_{Whole\text{-}rock}$
Sample	X(E)	Y(N)	Z(level)	(‰)	(‰)
93-138	2810	4337	235	9.6	11.0
94-542	2725	3602	190	9.9	10.9

[1] From gold-bearing vein # 30 [2] From gold-bearing vein # 1

Table 2. Sample type, location (x, y, z) and sulfur isotopic results.

Sample	X(E)	Y(N)	Z(level)	Habit	Event[1]	$\delta^{34}S_{Py}$ (‰)	$\delta^{34}S_{Po}$ (‰)	$\delta^{34}S_{Cp}$ (‰)	$\delta^{34}S_{Sp}$ (‰)
93-055	3002	4210	338	vein	3	2.3			1.9
93-080	2878	4196	245	vein	3	2.6			
93-081	2932	4225	245	vein	3	2.5			
93-086	3100	3600	235	vein	3	2.2			(2.6)
93-088	2910	4122	415	vein	3	2.6	1.8	1.7	1.9
93-168	3130	3500	295	vein	3	2.8		1.4	2.1
96-003	3075	3475	235	vein	3				2.2
96-007	3045	3500	230	vein	3	2.3	1.5	1.5	(2.4)
96-009	3017	3572	190	vein	3	2.7		(2.3)	2.3
96-016	2945	4124	485	vein	3	1.7	1.4	(1.6)	
96-999	2960	4180	545	Pillow selvages	1		1		
97-014	2945	4080	605	Pillow selvages	1		1.7	1.6	
94-552	2787	3755	190	Sediments	1		.6		
94-532	3082	3780	190	Dacite	2	1.5			
96-030	2940	3830	485	Dacite	2	1.3			
94-542	2725	3602	190	QFP dike	3	1.9			
93-138	2810	4337	235	QFP dike	3	1.9			

[1] numbers refer to mineralizing events: 1 = first, 2 = second, 3 = main

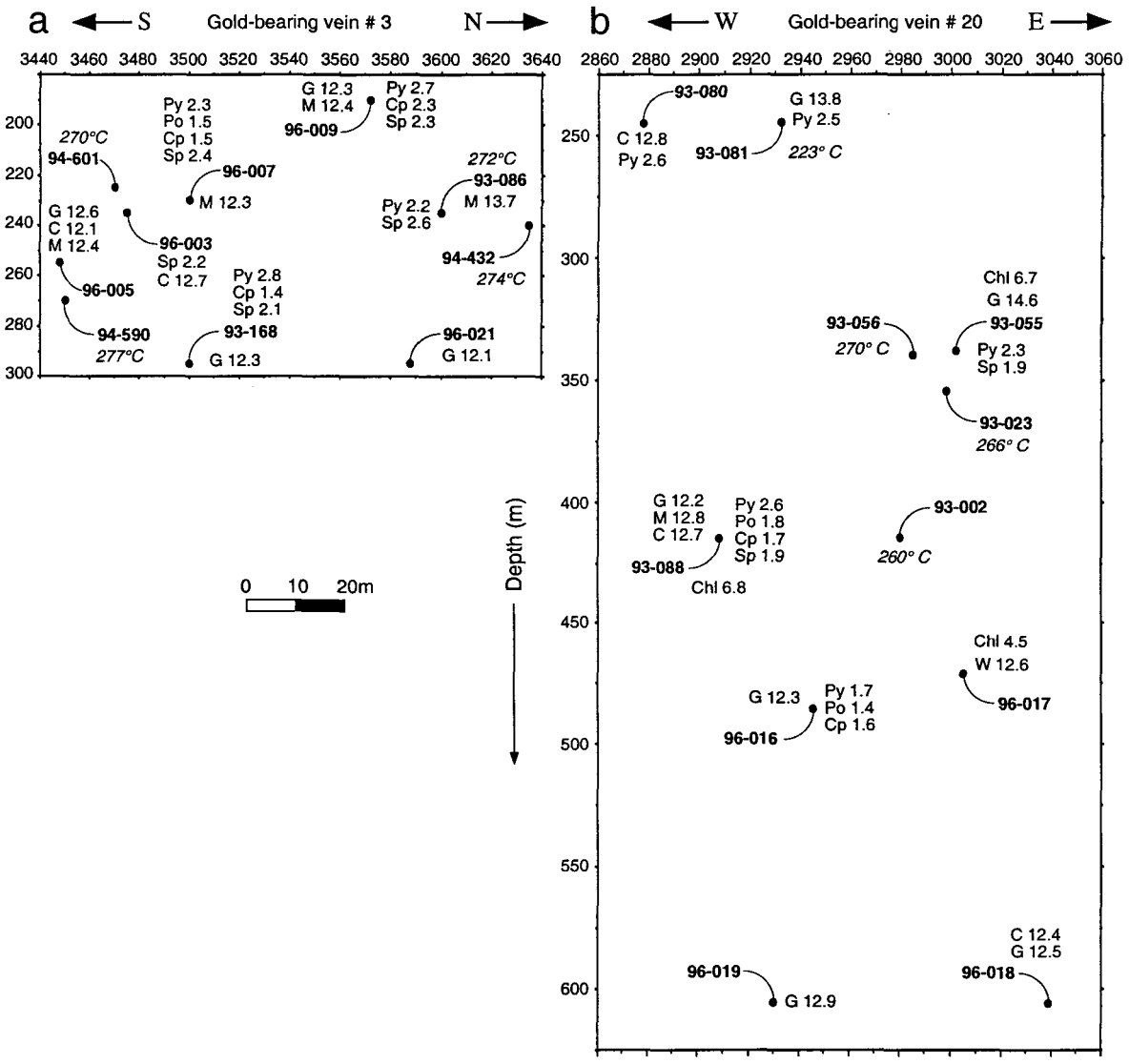

Figure 8. Sample locations and their related data projected in a vertical plane for (a) the #3 vein and (b) the #20 vein. Refer to Fig. 2 for vein locations. Oxygen isotopes are given in ‰ for quartz (G = grey; M = milky; W = white; C = clear) and chlorite (chl). Sulfur isotopes from sulfides are given in ‰ (Py = pyrite; Po = pyrrhotite; Cp = chalcopyrite; Sp = sphalerite). Temperatures refer to values determined by the chlorite geothermometer (Table 3).

0.5 % for concentration >20%; ± 0.2 % for concentration between 10-20% and ± 0.1 % for concentration <10%.

RESULTS

Oxygen isotopes

Oxygen isotope compositions for quartz, chlorite and whole-rocks are given in Table 1. Quartz from three pillow selvages associated with pyrrhotite-chalcopyrite mineralization yield $\delta^{18}O$ values ranging from 11.3 to 12.4‰ (Table 1; Fig. 9) with a mean of 11.9 ± 0.6‰. The $\delta^{18}O$ values of the various pre-ore quartz types from gold-bearing veins range from 12.1 to 14.6‰ (Table 1, Fig. 9) with a cluster of 20 values averaging 12.5 ± 0.3‰ and three values above 13.6‰ (Fig. 9). Although there are small oxygen isotope variations at sample-scale (Fig. 8), the four types of quartz display large overlaps such that they are isotopically indistinguishable at the deposit-scale (Fig. 9). Additionally, there are no obvious vertical or lateral variation trends in $\delta^{18}O$ values that are indicative of hydrothermal zoning at the vein- or deposit-scale (Fig. 8). This homogeneity implies either that the various quartz types were precipitated from hydrothermal fluids with similar $\delta^{18}O$ values and at similar temperatures at the deposit-scale, or that fluid compositions and temperatures temporally evolved in a manner such that the resulting $\delta^{18}O$ of quartz is homogeneous. The latter hypothesis, although possible from a theoretical point of view, is geologically unrealistic. Regarding the three values above 13.6‰, there is no obvious textural or spatial argument to explain their slightly different compositions. However, as the three quartz samples with relatively high $\delta^{18}O$ values belong to the earlier

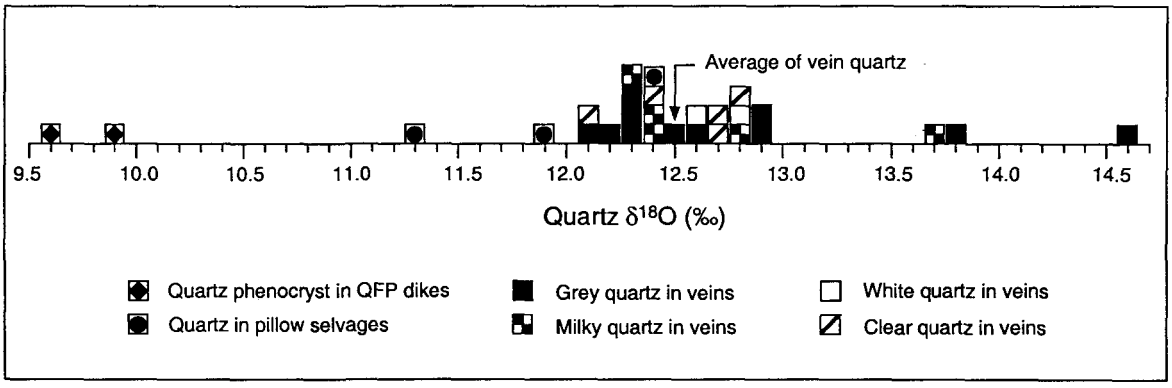

Figure 9. Histogram of $\delta^{18}O$ for quartz separates. Note the cluster of data for gold-bearing veins around 12.5‰ and the three values above 13.6‰.

stages of quartz deposition (Fig. 8), it is possible the earliest fluids were characterized by a slightly heavier oxygen isotope composition.

Pre-ore chlorite from gold-bearing veins yield values between 4.5 and 6.8‰ (Table 1) with an average of 5.9 ± 1.1‰ (n = 4). A graph of $\delta^{18}O$ values for coexisting (observed to occur in contact) chlorite and quartz (Fig. 10) shows their distribution in relation to equilibrium isotherms. Three pairs plot between isotherms at 250° and 275°C, which suggests isotope equilibrium for those samples, whereas the fourth sample plots close to the 350°C isotherm (Fig. 10). The sample close to the 350°C isotherm can be explained either by re-equilibration during a later fluid event associated with sulfide deposition at that temperature (see below) or by minor contamination of the analyzed chlorite by isotopically heavier quartz. A third interpretation is that three chlorite-quartz pairs plot along a temperature gradient between 250° and 350°C (Fig. 10). However, such a temperature gradient is not supported by chlorite geothermometry (Fig. 8).

Whole-rock analyses of altered and mineralized QFP dikes yield values of 10.9 and 11.0‰. Values of 9.6 and 9.9‰ were obtained for quartz phenocrysts from these two samples. (Table 1, Fig. 9). Considering a 1.5 to 2.5‰ enrichment in $\delta^{18}O$ of magmatic quartz relative to its source magma (Taylor 1968), the measured $\delta^{18}O$ values of quartz phenocrysts, if primary, suggest a prealteration $\delta^{18}O$ value of 8.0 ± 1‰ for the magma. This is consistent with most data from fresh rhyolites (Taylor 1968; Taylor and Sheppard 1986). Therefore, the hydrothermal alteration is estimated to account for a ~3‰ positive shift of the whole-rock oxygen isotope composition of the QFP dikes.

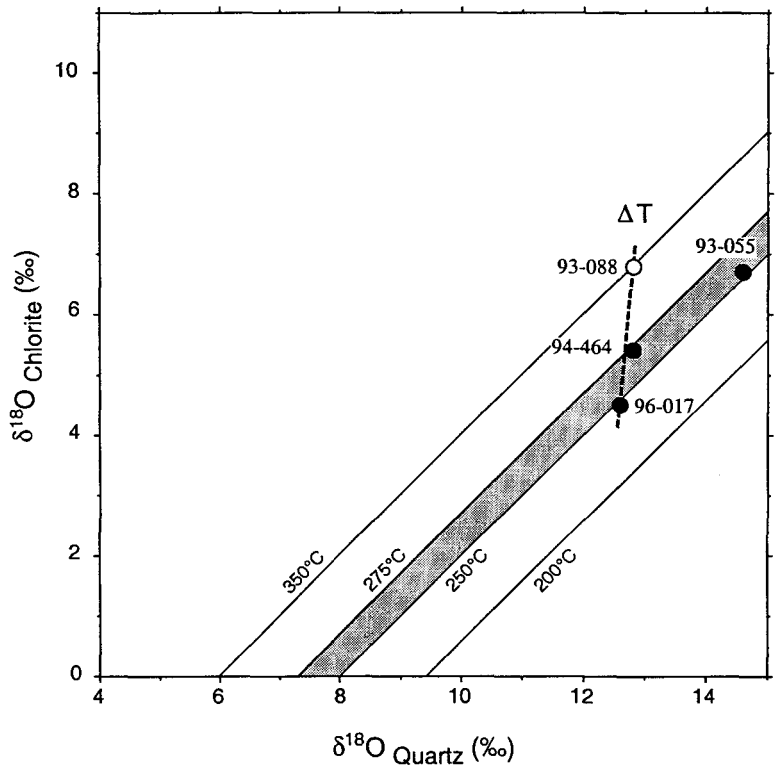

Figure 10. Plot of $\delta^{18}O_{Chlorite}$ versus $\delta^{18}O_{Quartz}$ for gold-bearing veins. Data plot along equilibrium isotherms between 250° to 275°C (filled circles), except for one sample close to 350°C (open circle). Dashed line illustrates the unsupported temperature gradient (ΔT) hypothesis. Isotherms were calculated using quartz-water fractionation factor of Clayton et al. (1972) and the chlorite-water fractionation factor of Wenner and Taylor (1971).

Sulfur isotopes

Sulfur isotope results are listed in Table 2 and graphically presented in Fig. 11. The $\delta^{34}S$ values of 32 sulfide samples range from 0.6 to 2.8‰. Pyrrhotite in pillow selvages and in sedimentary rocks has $\delta^{34}S$ values ranging from 0.6 to 1.7‰ (n = 3), whereas chalcopyrite associated with that pyrrhotite yields a $\delta^{34}S$ value of 1.6‰. Pyrite disseminated in chloritized dacite and sericitized QFP dikes has average $\delta^{34}S$ values of 1.4‰ (n = 2) and 1.9‰ (n = 2) respectively. Sulfides in veins (pyrite = 9; pyrrhotite = 3; chalcopyrite = 5; and sphalerite = 7) define a narrow range from 1.4 to 2.8‰ with an average of 2.1 ± 0.4‰ (n = 23). This very restricted range of $\delta^{34}S$ values suggests isothermal conditions and constant fluid $\delta^{34}S$ compositions during vein formation at the deposit-scale. In addition, sulfides in gold-bearing veins do not show any significant sulfur isotope zoning (Fig. 8), similar to results from the $\delta^{18}O$ data.

Graphs of $\delta^{34}S$ values for coexisting pyrrhotite, sphalerite and chalcopyrite with pyrite (Fig. 12) from gold-bearing veins show their distribution in relation to equilibrium isotherms, provided that they equilibrated together. Four pairs of pyrite-pyrrhotite and pyrite-sphalerite display isotope equilibrium at ~350°C (Fig. 12). Except for one pair of pyrite-chalcopyrite at ~300°C, most sulfide pairs plot above the 400°C isotherm. These geothermometers are not particularly temperature-sensitive (Ohmoto 1986). Consequently, the uncertainties of the fractionation factors (Ohmoto and Rye 1979) induce large temperature variations for the calculated equilibrium isotherms. Considering the uncertainties, most plotted pairs with their inherent ± 0.2‰ precision, except four which are clearly out of equilibrium, overlap the field defined by the uncertainty of the calculated

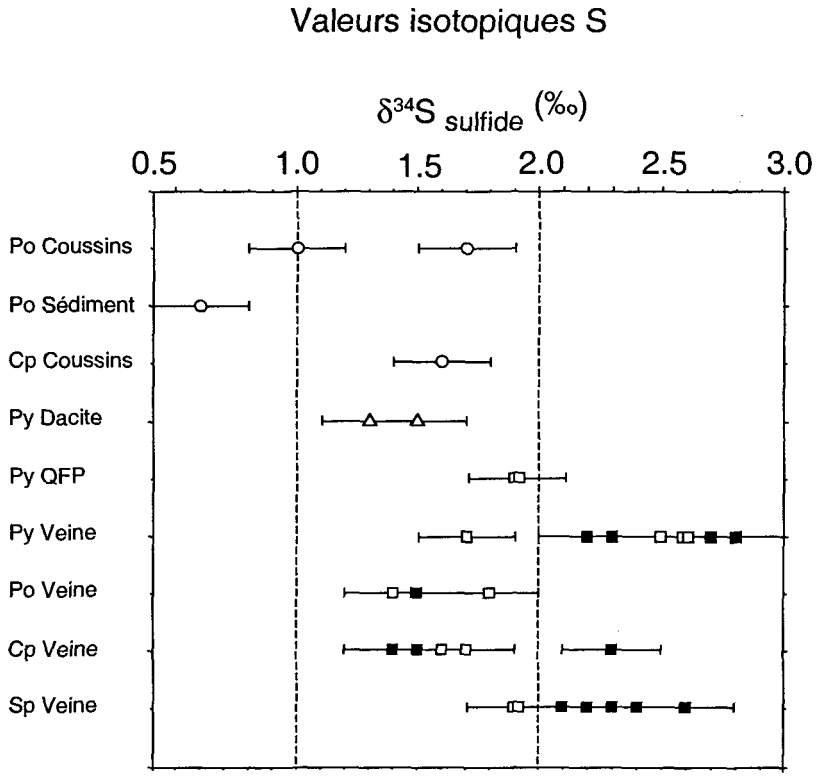

Figure 11. Hydrothermal events in relation to $\delta^{34}S$ values of sulfides. This diagram shows the clustering of $\delta^{34}S$ values. Sulfide abbreviations as in Fig. 8. Other capital letters indicate the habit of sulfides: P = pillow selvage; S = sediment; D = dacite; Q = QFP dike; V = vein. First, second and main mineralizing events are represented by circles, triangles and squares, respectively. For gold-bearing veins, filled squares are for samples from the #20 vein and open squares for the #3 vein.

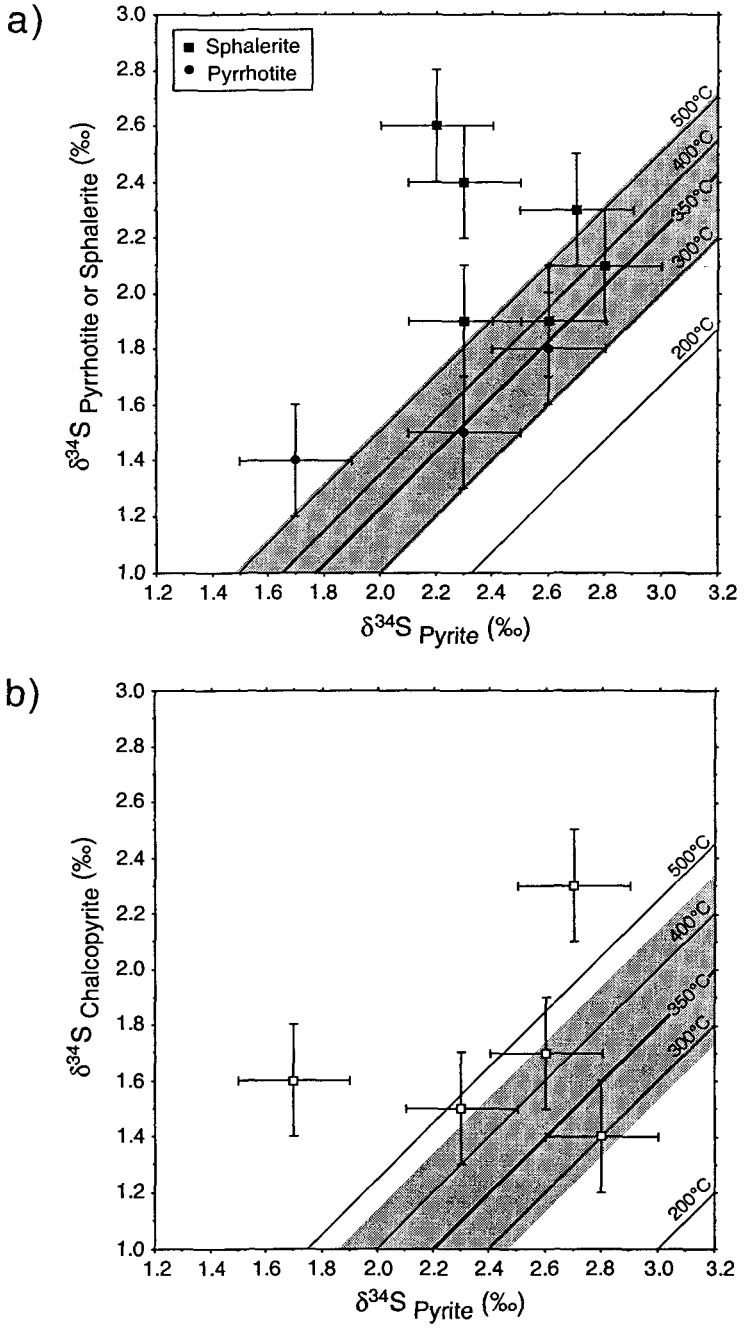

Figure 12. Plot of (a) $\delta^{34}S$ values of pyrrhotite and sphalerite versus pyrite and (b) chalcopyrite versus pyrite from gold-bearing veins. Considering the precision of the measured $\delta^{34}S$ and the uncertainty of the calculated isotherm illustrated by the grey field, the 350°C equilibrium isotherm accounts for the distribution of most plotted pairs. Equilibrium isotopic fractionation factors between sulfides and H_2S from Ohmoto and Rye (1979).

350°C isotherm (Fig. 12). Accordingly, ~350°C is considered as the best temperature estimate for sulfide deposition in the veins.

Chlorite chemistry

Analyses of pre-ore chlorite from the two selected gold-bearing veins are given in Table 3, together with their calculated cationic compositions. Chlorite compositions indicate a wide range of Si-Al(IV) and Mg-Fe solid solution, ranging from pycnochlorite to pseudothuringite although most are ripidolite (Fig. 13). Calculated temperatures of chlorite formation, using the Si-Al(IV) substitution geothermometer (Cathelineau and Nieva 1985; Kranidiotis and MacLean 1987) range from 223° to 277°C (Table 3; Fig. 8). Excluding the anomalously low 223°C value (Table 3), the average temperature is 269 ± 10°C. In addition, analysis of chlorite in other gold-bearing veins (Fig. 13) yields an average temperature of 269 ± 20°C (n = 10; annexe, Tableau 3b). Although, the uncertainty of the calculated values is unknown (Kranidiotis and MacLean 1987), the temperature estimate of 269 ± 10°C is quite consistent with the range of 250° to 275°C determined from chlorite-quartz isotopic geothermometry for the pre-ore stage veining event.

DISCUSSION

Preservation of Archean isotope and chemical signatures

Numerous studies of Archean VMS deposits, metamorphosed to greenschist facies, have demonstrated that the initial $^{18}O/^{16}O$ and $^{34}S/^{32}S$ ratios are commonly well-preserved (e.g. Beaty et al. 1988; Strauss 1989; MacLean and Hoy 1991). For oxygen, isotope

Table 3. Average composition of vein chlorite and calculated temperature of formation

Sample	93-081	94-590	94-601	93-002	93-023	93-056	93-086	94-432
#n	2	2	2	3	3	2	2	3
SiO_2 (wt %)	27.35	26.23	26.22	25.71	27.46	25.90	25.53	24.28
TiO_2	n.d.	.07	n.d.	.05	.05	n.d.	n.d.	n.d.
Al_2O_3	18.38	23.85	23.33	22.07	23.12	23.11	23.45	24.44
FeO	20.48	24.95	25.43	22.39	22.91	24.93	26.41	36.13
MgO	17.59	16.31	15.37	16.51	18.57	15.53	14.22	7.93
MnO	n.d.	.56	.67	n.d.	.30	n.d.	.58	n.d.
CaO	.59	n.d.	.33	n.d.	n.d.	n.d.	n.d.	n.d.
K_2O	n.d.	n.d.	n.d.	n.d.	n.d.	n.d.	n.d.	n.d.
SO_3	.55	n.d.	n.d.	.08	n.d.	.20	n.d.	n.d.
Total	84.93	91.95	91.42	86.82	92.41	89.65	90.18	92.79
	Number of ions on the basis of 28 oxygen atoms							
Si	5.783	5.232	5.286	5.371	5.377	5.290	5.244	5.080
AlIV	2.217	2.768	2.714	2.629	2.623	2.710	2.756	2.920
AlVI	2.364	2.840	2.832	2.806	2.716	2.854	2.925	3.109
Mg	5.544	4.848	4.618	5.140	5.421	4.726	4.353	2.474
Fe	3.622	4.162	4.288	3.911	3.753	4.258	4.537	6.322
Mn	0	.095	.114	0	.049	0	.101	0
Ti	0	.011	0	.008	.007	0	0	0
Ca	.134	0	.070	0	0	0	0	0
K	0	0	0	0	0	0	0	0
T cation	19.66	19.95	19.92	19.87	19.95	19.84	19.92	19.91
Fe/Fe+Mg	.40	.46	.48	.43	.41	.47	.51	.72
T°C	223	277	270	260	266	270	272	274

#n = number of analysis n.d. = not detected

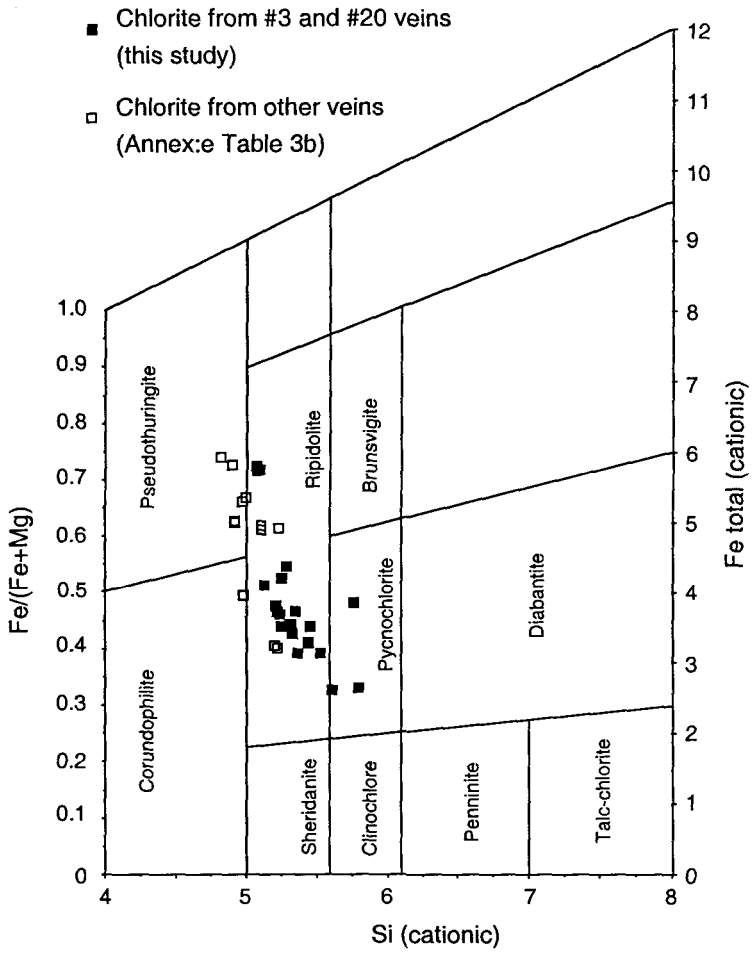

Figure 13. Chlorite chemistry plot according to Hey (1954). Note the solid solution defined by the range of chlorite compositions.

exchange rarely occurs in quartz below 400°C (Giletti and Yund 1984). For sulfur, isotope re-equilibration may occur if the coexisting sulfides are recrystallized during metamorphism at temperature above 350°C (Zheng 1990). Metamorphic recrystallization of sulfides commonly involves the loss of inclusions of gold and silver, and the remobilization of these metals along recrystallized sulfide boundaries (Larocque and Hodgson 1995). The inclusions of sulfides and gold and silver grains in the pyrite crystals suggest that the sulfides at the Géant Dormant mine were not recrystallized during post-ore stage metamorphism. The occurrence of low-temperature (<250°C) monoclinic-pyrrhotite in pillow lava, not recrystallized to the higher temperature (>300°C) hexagonal species (Vaughan and Craig 1978), also supports the interpretation that the sulfur isotopic system was not re-equilibrated. In addition, it has been demonstrated that the initial chlorite compositions are also commonly well-preserved in greenstone belts (McLeod and Stanton 1984; Eastoe et al. 1987; Doucet et al. 1998). This conclusion supports the validity of the pre-ore vein filling temperatures estimated from the chlorite compositions.

Temperature constraints

Two different formation temperatures of the gold-bearing veins are determined: a pre-ore quartz-chlorite stage at <275°C, reveled by chlorite-quartz equilibrium (250-275°C) and by chlorite geothermometry (269 ± 10°C); and a higher temperature of ~350°C for the later auriferous sulfide ore stage, as suggested by sulfur isotope geothermometry. The <275°C is consistent with the silica solubility relationships, as near-neutral, chloride-rich fluids typically precipitate large volumes of silica in the subsurface environment between

220° to 270°C (Fournier 1985). Data from active hydrothermal systems at the seafloor indicate that Cu-bearing sulfides form between 300° to 350°C, whereas Zn-bearing sulfides, with minor amounts of Cu-bearing sulfides, form at <300°C (Styrt et al. 1981; Paradis et al. 1988; Percival and Ames 1993; Ishibashi and Urable 1995). On this basis, the ~350°C probably represents a maximum temperature estimate for the ore stage.

Oxygen isotope composition of the mineralizing fluids

The fluid oxygen isotope composition for seafloor-related mineralization is estimated at 3.2‰ based on the fractionation factor between quartz and water (Clayton et al. 1972) calculated at 250°C from the average quartz $\delta^{18}O$ value of 11.9‰. A temperature of 250°C was selected on the basis of the paragenetic association of quartz and monoclinic-pyrrhotite, for which the documented maximum temperature of precipitation is 254°C (cf. Vaughan and Craig 1978). The restricted occurrence of this quartz to the sulfidized interpillow cavities supports its genetic association with the <254°C pyrrhotite species.

For the gold-bearing quartz veins, the $\delta^{18}O$ value of the fluids at 275°C is 4.7‰ as calculated from the average $\delta^{18}O$ value of 12.5‰ for quartz. Although the ore stage formed at greater temperatures (~350°C), 275°C is the best temperature estimate for pre-ore quartz precipitation, as discussed above. The calculated fluid isotope composition is *sensu stricto* for the pre-ore stage. Nevertheless, the $\delta^{18}O$ value of 4.7‰ is considered representative of the auriferous fluids, because the pre- and ore stages are intimately-related. Also, fluids with a similar $\delta^{18}O$ value can account for the alteration of the auriferous QFP dikes (see below).

For the altered and mineralized QFP dikes, two different approaches can be used to estimate the $\delta^{18}O$ value of the hydrothermal fluids ($\delta^{18}O_W$). The first is based on the alteration mineralogy and mineral isotopic composition calculated at equilibrium with the hydrothermal fluid, according to the following equation (MacLean and Hoy 1991):

$$\delta^{18}O_R{}^f = \Sigma_i \delta^{18}O_i * (X_i * Y_i) / \Sigma_i (X_i * Y_i) \quad (1)$$

where $\delta^{18}O_R{}^f$ is the $\delta^{18}O$ of altered rock, $\delta^{18}O_i$ is $\delta^{18}O$ composition of mineral i, X_i is the weight fraction of mineral i relative to all oxygen-bearing minerals, and Y_i is the weight fraction of oxygen in mineral i. The second approach is based on an equation using the $\delta^{18}O$ of fresh rock ($\delta^{18}O_R{}^i$) and altering fluids ($\delta^{18}O_W$), and the water/rock ratio (W/R). The equation is as follow (Green et al. 1983):

$$\delta^{18}O_R{}^f = (\delta^{18}O_R{}^i + (\delta^{18}O_W + \Delta^{18}O_{W\text{-}R})\ W/R) / (1+W/R) \quad (2)$$

where $\Delta^{18}O_{W\text{-}R}$ is the isotopic fractionation factor between rock and fluid.

The $\delta^{18}O_R{}^f$ was calculated as a function of the temperature and the $\delta^{18}O$ value of the hydrothermal water ($\delta^{18}O_w$) equilibrating with specific minerals. Calculations were performed for a temperature range of 200° to 400°C and for $\delta^{18}O_W$ values ranging from 0 to 8‰. Parameters used in equation 1 are: Xi = 45% quartz, 50% sericite and 5% quartz phenocrysts. The $\delta^{18}O$ compositions of quartz and sericite were computed using temperature dependent fractionation factors (Δ) between quartz and water (Clayton et al. 1972) and muscovite (for sericite) and water (O'Neil and Taylor 1969); Yi value of quartz = 0.533 and sericite = 0.482 (MacLean and Hoy 1991); and a value of 9.8‰ for quartz

phenocrysts (Table 1). Equation 2 was solved using W/R = 1, according to Green et al. (1983) and Taylor and South (1985); and an initial $\delta^{18}O$ composition of the QFP dikes of 8‰. The $\Delta^{18}O_{W\text{-}R}$ was estimated using the average of $\Delta_{quartz\text{-}water}$ (Clayton et al. 1972) and $\Delta_{muscovite\text{-}water}$ (O'Neil and Taylor 1969). This approximation is justified as the altered QFP dikes are composed of about equal proportion of quartz and sericite. By comparison, the use of $\Delta_{plagioclase\text{-}water}$ (O'Neil and Taylor 1967), as proposed by Taylor (1979) and Green et al. (1983), yields similar values of $\delta^{18}O_R{}^f$.

The alteration of the QFP dikes is paragenetically closely-related to the formation of the pre-ore assemblages in the auriferous quartz veins, suggesting that temperature of alteration should be in the range of 250° to 275°C. The calculations show that at equilibrium, the bulk oxygen isotope composition of the dikes (~11‰) can be the result of reaction with hydrothermal fluids having $\delta^{18}O$ values of 5 to 6‰ at temperatures ranging from 250° to 275°C (equation 1: Fig. 14a). This fluid composition is consistent with that calculated for quartz-sulfide veins. Calculations from equation 2, which is W/R ratio dependant, indicate that a whole-rock $\delta^{18}O$ value of ~11‰ for altered QFP dikes can be produced by reaction with a fluid having $\delta^{18}O$ values of 7 to 8‰ at temperatures ranging from 250° to 275°C for a W/R of 1 (Fig. 14b). Computation of W/R ratios for a variety of temperatures indicates that a W/R somewhere between about 5 and 100 would account for reaction of a fluid at $\delta^{18}O$ = 5‰ with a rock at $\delta^{18}O$ = 8‰, at temperatures of 250° to 275°C (Fig. 14c). Considering that W/R ratios for volcanogenic systems can reach 300 at the focused site of ore formation (MacLean and Hoy 1991), a W/R ratio somewhere

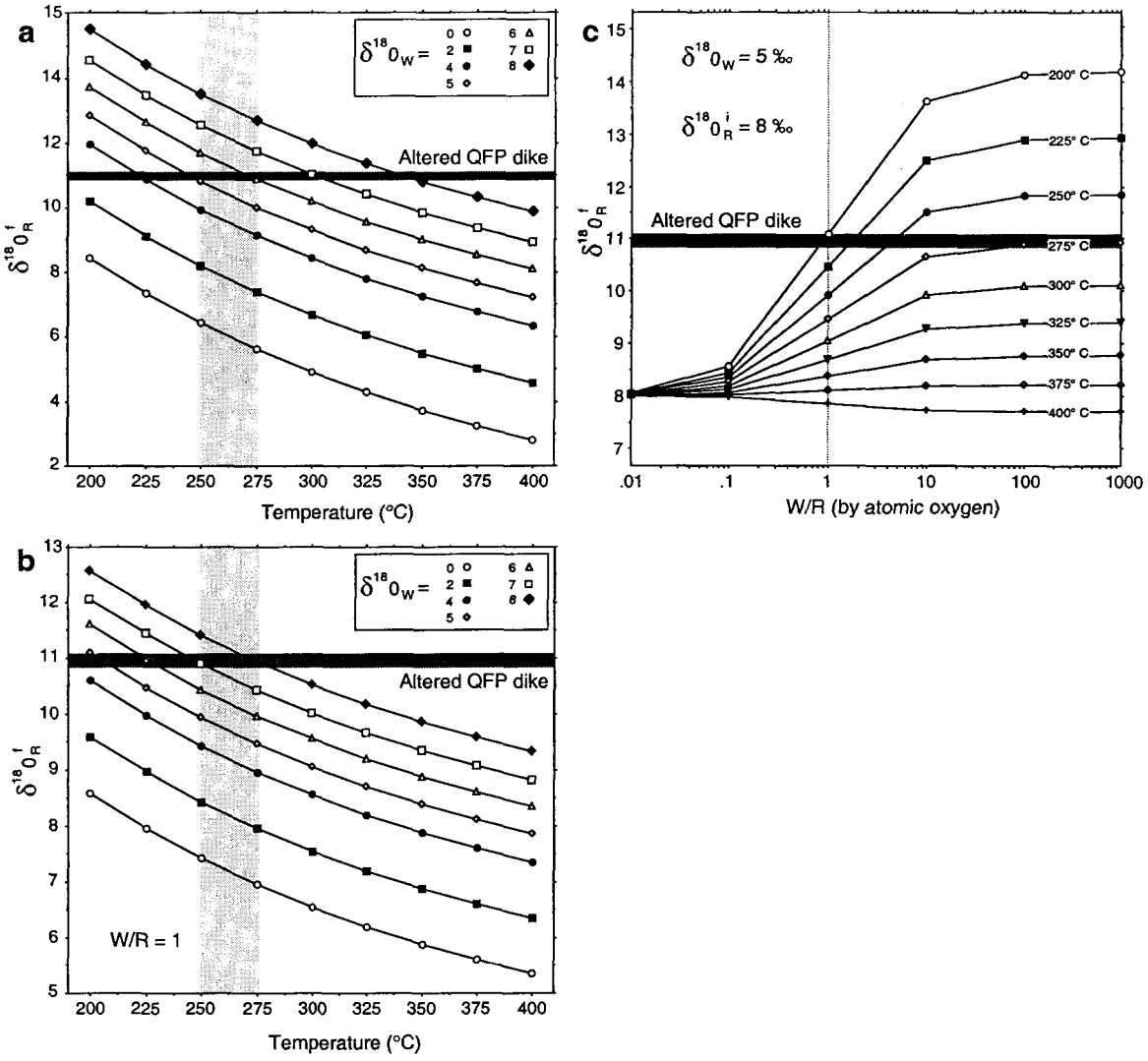

Figure 14. Calculated whole-rock $\delta^{18}O$ composition ($\delta^{18}O_R$) of the altered QFP dikes (dark grey line) as a function of temperature and initial $\delta^{18}O$ value of the altering fluid ($\delta^{18}O_W$) using equation from (a) MacLean and Hoy (1991) and (b) Green et al. (1983). (c) Calculated $\delta^{18}O$ composition of altered QFP dikes using the equation of Green et al. (1983) as a function of W/R ratios and temperatures for an initial $\delta^{18}O$ value of the altering fluid of 5‰. Light grey areas indicate the range of temperatures expected for the hydrothermal alteration.

between 5 and 100 appears realistic. These calculations indicate that an isotopically similar fluid can account for both the quartz vein formation and the quartz and sericite alteration of the QFP dikes.

Sources of the mineralizing fluids

The $\delta^{18}O$ value of the seafloor hydrothermal fluids (+3.2‰) is within the range (-4.0 to +4.5‰: see compilation by Huston 1997) calculated for fluids generating Archean VMS deposits. This oxygen isotope composition is also close to the range of 0.4 to 2.1‰ given for modern hydrothermal seafloor systems (Shanks et al. 1995). The $\delta^{18}O$ value of 4.7‰ for the gold-bearing vein mineralizing fluids falls within the 0 to 5‰ gap, which is bracketed by seawater at a value of 0 ± 1‰ (Gregory and Taylor 1981; de Ronde et al. 1997) and values of either magmatic at 5 to 10‰ or metamorphic waters at 5 to 25‰ (Taylor 1974). In addition, the 4.7‰ fluid value is close to overlapping the fluid fields for Archean VMS (-4.0 to +4.5‰) and mesothermal lode-gold deposits (4.5 to 12.0‰: see Kerrich 1987; Colvine et al. 1988; Roberts 1988; Hodgson 1993).

From the constraints imposed by field relationships, the hydrothermal system may record the contribution of three fluids: seawater, evolved seawater and magmatic. A major contribution of metamorphic fluids can be discarded based on the low carbonate and high sulfide contents of veins which are inconsistent with the CO_2-rich and low salinity chemistry of typical metamorphic fluids (e.g. Wood 1987; Kyser and Kerrich 1990). A meteoric fluid contribution is also unlikely considering the inferred deep water setting during vein formation (Gaboury and Daigneault 1999). In addition, meteoric fluid implies

the presence of a neighboring landmass, which is not easily reconcilable with the documented submarine origin of the first volcanic cycle (Chown et al. 1992).

Evolved, ^{18}O-enriched seawater can result from isotopic exchange under rock-dominated conditions (W/R <0.1) at high temperature (>400°C) in the deep reaction zones of seafloor hydrothermal systems (Munha et al. 1986). Under these conditions, the $\delta^{18}O$ value of the convective seawater can theoretically be shifted to values up to 4 to 6‰ (Munha et al. 1986). However, the $\delta^{18}O$ value of evolved seawater is more likely between 1 and 2‰ (Muehlenbachs 1998). If magmatic fluids are involved, they are likely related to the felsic magmatism. The oxygen isotope composition of quartz phenocrysts suggests that felsic magma has a $\delta^{18}O$ value of ~8‰. Fluids exsolved from that magma would have a $\delta^{18}O$ value of ~9‰ to account for ^{18}O fractionation between water and magma at high temperature (Ohmoto 1986).

Using the preceding estimated $\delta^{18}O$ values, fluid mixing calculations indicate than the contribution of magmatic fluids to the convective fluid system should be ~50% for seawater and ~40% for evolved seawater to account for the $\delta^{18}O$ vein-forming fluid composition of 4.7‰. For the earlier seafloor event, the mixing proportions of magmatic fluids into the convective fluid system are ~35% for seawater and <20% for evolved seawater (Fig. 15). These mixing calculations indicate that the sources of mineralizing fluids were likely comprised of evolved seawater with a possible magmatic fluid contribution up to 40% during vein formation (Fig. 15).

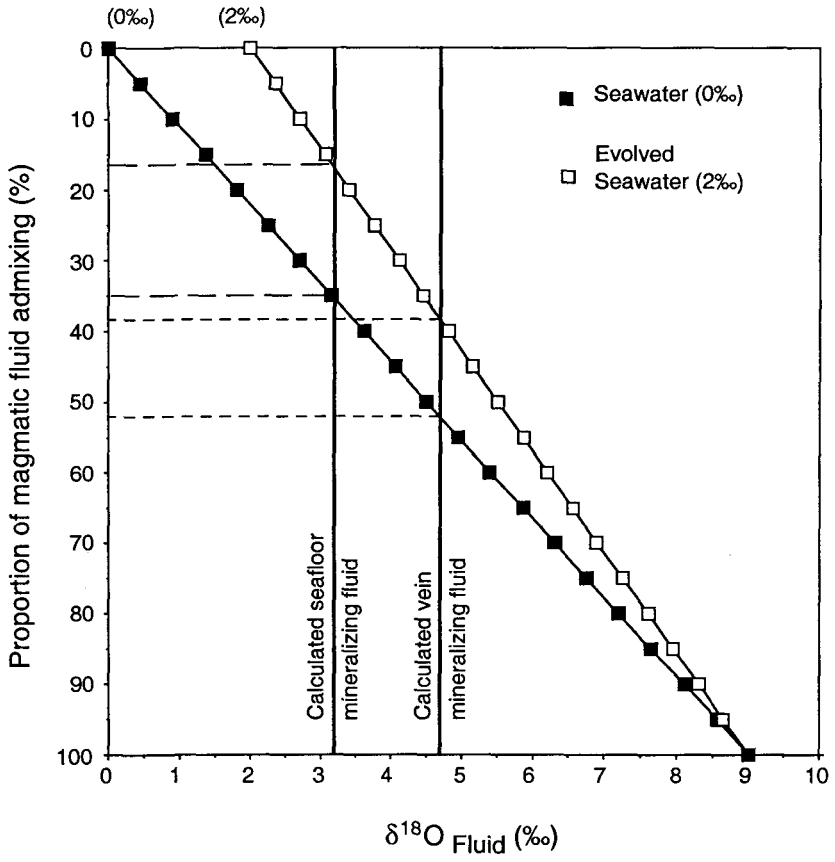

Figure 15. Diagram showing the proportion (%) of magmatic fluid ($\delta^{18}O$ = 9‰) admixing with seawater (0‰) and evolved seawater (2‰) to account for the calculated $\delta^{18}O$ fluid values for the gold-bearing veins and the seafloor mineralizing event.

Source of sulfur

The narrow range of $\delta^{34}S$ values (0.6 to 2.8‰: Fig. 11) suggests that the various hydrothermal events have the same sulfur source. This restricted range is also consistent with a genetic link for the three mineralizing events. The range of $\delta^{34}S$ values overlaps with magmatic values (0 ± 2‰: Ohmoto and Rye 1979) implying derivation of sulfur either directly from a magmatic source or from leaching of primary magmatic sulfides in volcanic rocks. From a comparative point of view, Archean VMS deposits are characterized by $\delta^{34}S$ values ranging from -1 to 5.3‰ with a mean around 1‰ (see compilation by Huston 1997). The $\delta^{34}S$ values for mesothermal-type Archean lode gold deposits range from -0.7 to +7.0‰ (see Kerrich 1987; Colvine et al. 1988; Roberts 1988). This overlap of $\delta^{34}S$ indicates that sulfur isotope data from the Géant Dormant are compatible with the VMS field, but cannot by themselves implicate a seafloor origin.

Evolution of the hydrothermal system

The interpreted sources of mineralizing fluids and the similarity of sulfur isotope compositions suggest a genetic link among the three mineralizing events, which together imply that gold-bearing veins are the product of a volcanogenic hydrothermal system. The transition in time from seafloor to vein-type mineralizations is manifested by the increase of fluid oxygen isotope compositions from 3.2‰ at 250°C to 4.7‰ at 275°C for the hydrothermal fluids. This increase of the fluid oxygen isotope compositions may be related to the mixing of an increasing amount of magmatic fluid to the convective evolved seawater (Fig. 15) as far as the underlying felsic magmatic chamber evolves through time.

Further evolution of the hydrothermal system is expressed by the transition from silicate deposition (mainly quartz) to subsequent sulfide mineral precipitation as vein filling material. This mineralogical transition coincides with a temperature increase of the hydrothermal system from 275° to about 350°C. The temperature increase probably reflects the thermal maturation of the hydrothermal system, as it has been documented for typical VMS deposits (e.g., Large 1992; Ohmoto 1996).

Considerations for gold-rich volcanogenic systems

Average gold grades of about 10 g/t in the gold-bearing veins at the Géant Dormant deposit are at least 10 times greater than typical gold grades of VMS deposits in the Abitibi belt (e.g. Chartrand and Cattalini 1990). Factors accounting for the relatively high gold concentrations in VMS-related ores include the boiling of mineralizing fluids and the contribution of gold-rich magmatic fluids (Hannington et al. 1997). It has been argued that boiling during vein formation at the Géant Dormant deposit favored the efficient precipitation of gold (Gaboury and Daigneault 1999). Nevertheless, fluids were also likely enriched in gold compared to typical VMS ore-forming fluids, because gold grades of the veins at the Géant Dormant deposit are commonly in the range of hundreds of g/t Au.

Magmatic gold contributions to arc-related ore deposits (porphyry Cu-Au, epithermal high-sulfidation Cu-Au and low-sulfidation Au-Ag) reflect specific petrogenetic processes that concentrated gold in the magma and released it in subvolcanic settings (Sillitoe 1997). Partial melting induced by a detached and immobile segment of subducted and metasomatized (H_2O-rich) lithospheric slab in an arc environment may promote the oxidation of gold-bearing sulfides in the mantle, the release of gold and its incorporation into the magma (McInnes and Cameron 1994). In subvolcanic settings, release of gold from a H_2O-rich and high fO_2 magma is governed by various parameters (cf. Thompson 1995).

Among these, fractional crystallization of plagioclase in the magma chamber is an important mechanism that enhances water oversaturation and the release of fluids and gold (Shinohara and Kazahaya 1995; Shinohara and Hedenquist 1997). The typical occurrence of plagioclase-porphyritic intermineral intrusions (e.g. Kirkham 1971) in Cu-Au ore settings may indicate that the underling magma chamber evolved by fractional crystallization. These petrogenetic processes are spatially and genetically related to calc-alkalic to alkalic arc magmatism in neutral to compressional tectonic regimes (Uyeda and Nishiwaki 1980). Conversely, in typical VMS settings, ore-associated rocks are commonly tholeiitic and derived from low H_2O and low fO_2 magmas (Lentz 1998). The tholeiitic composition, typical of extensional geodynamic regimes, is attributed to the rapid ascension and low crustal residence time of the magma, and to the consequent weak differentiation of the magma by fractional crystallization (Lentz 1998). According to these petrogenetic considerations, a significant magmatic contribution of fluids and gold into the ore-forming hydrothermal systems appears more likely in arc-settings rather than in typical VMS-settings. This interpretation is supported by the average content of gold in samples from modern seafloor VMS deposits (Lizasa et al. 1999), which is higher for deposits formed in arc-settings (>20 ppm Au) than in back-arc and midocean ridge settings (<5 ppm Au).

According to Gaboury and Daigneault (1999), felsic rocks coeval with the mineralizing events are calc-alkalic, porphyritic and belong to the group III of the Abitibi belt (Barrie et al. 1993). Rocks of this group are arc-related and typically recognized as unfavorable for classical VMS mineralization. The temporal and spatial link between the mineralizing and felsic magmatism events, the arc-related origin of felsic rocks, and the likely significant contribution of magmatic fluids into the volcanogenic system, are collectively compelling evidence to support a magmatic contribution of gold. Such a setting, involving the intercalation of the distal mafic tholeiitic rocks, typical of a rift

environment, and the proximal arc-related felsic rocks is atypical of Archean and Phanerozoic VMS deposits (Lentz 1998). The Géant Dormant deposit probably evolved in a geodynamic setting corresponding to the transitional zone between an opening basin of a back-arc spreading ridge and the arc environment.

CONCLUSIONS

The interpreted fluid and sulfur sources are consistent with a volcanogenic hydrothermal system. The genetic link among the three mineralizing events is supported by the similar $\delta^{34}S$ values of sulfides as well as by the similar $\delta^{18}O$ composition of the mineralizing fluids calculated from quartz. Such a link indicates that the gold-bearing veins are the product of a volcanogenic hydrothermal system. A significant magmatic contribution of fluids is inferred to account for the evolved $\delta^{18}O$ composition of the mineralizing fluids. A magmatic contribution of gold, to explain the anomalous gold content, is consistent with the fluid sources, field and geochemical characteristics of arc-related felsic rocks, to which the mineralization is temporally and spatially associated. A formation in transitional zone between back-arc and arc environment is envisaged to account for the particular characteristics of this deposit.

This study has important implications for genetic models and gold exploration. It emphasizes the gold potential of volcanogenic hydrothermal systems, a feature only recently recognized (Poulsen and Hannington 1996). However, the results suggest that special conditions should be involved, such as fluid and gold contributions from arc-related magmatism in particular geodynamic settings. Finally, it is shown that gold mineralization

is not only restricted temporally to the late accretion stage of Archean supracrustal belts, and thus some gold mineralizations are genetically unrelated to shear zones.

Acknowledgment

The authors express their sincere thanks to Cambior Inc., Aurizon Mine Ltd. and the Ministère des ressources naturelles du Québec for their scientific collaboration and financial support. Our thanks are extended to the mine staff for their generous assistance to the first author during four consecutive field seasons. R. Lechasseur and M. Lapointe are thanked for their advice with sample preparation. The manuscript has benefited from review at early stage by M.D. Higgins. Incisive and constructive comments by journal reviewers C.D. Taylor and B.E. Taylor, and editor R.J. Goldfarb greatly helped to improve the manuscript. The Natural Sciences and Engineering Research Council of Canada (NSERC) and the Fonds pour la Formation de Chercheurs et d'Aide à la Recherche (FCAR) also financed the project through Ph.D. postgraduate scholarships to the first author and NSERC grants to R.D. and G.B.

References

Beaty DW, Taylor HP Jr, Coads PR (1988) An oxygen isotope study of the Kidd Creek, Ontario, volcanogenic massive sulfide deposit: Evidence for high ^{18}O ore fluid. Econ Geol 83: 1-17

Barley ME, Groves DI (1992) Supercontinental cycles and the distribution of metal deposits through time. Geology 20: 291-294

Barrie CT, Ludden JN, Green TH (1993) Geochemistry of volcanic rocks associated with Cu-Zn and Ni-Cu deposits in the Abitibi Subprovince. Econ Geol 88: 1341-1358

Cathelineau M, Nieva D (1985) A chlorite solid solution geothermometer: The Los Azufres (Mexico) geothermal system. Contrib Mineral Petrol 91: 235-244

Chartrand F, Cattalani S (1990) Massive sulfide deposits in Northwestern Quebec. Can Inst Mines Metall, Spec Vol 43: 77-91

Chown EH, Daigneault R, Mueller W, Mortensen JK (1992) Tectonic evolution of the Northern Volcanic Zone, Abitibi belt, Quebec. Can J Earth Sci 29: 2211-2225

Clayton RN, Mayeda TK (1963) The use of bromine pentafluoride in the extraction of oxygen from oxides and silicates for isotope analysis. Geochim Cosmochim Acta 26: 43-52

Clayton RN, O'Neil JR, Mayeda T (1972) Oxygen exchange between quartz and water. J Geophys Res 77: 3057-3067

Colvine AC, Fyon KB, Heather KB, Marmont S, Smith PM, Troop DG (1988) Archean lode gold deposits in Ontario. Ontario Geol Surv, Miscellaneous Paper 139, 139 p

de Ronde CEJ, Channer DMD, Faure K, Bray CJ, Spooner ETC (1997) Fluids chemistry of Archean seawater hydrothermal vents: Implications for the composition of circa 3.2 Ga seawater. Geochim Cosmochim Acta 61: 4025-4042

Doucet P, Mueller W, Chartrand F (1998) Alteration and ore mineral characteristics of the Archean Coniagas massive sulfide deposit, Abitibi belt, Quebec. Can J Earth Sci 35: 620-636

Eastoe CJ, Solomon M, Walshe JL (1987) District-scale alteration associated with massive sulfide deposits in the Mount Read volcanics, Western Tasmania. Econ Geol 82: 1239-1258

Fournier RO (1985) Silica mineral as indicators of conditions during gold deposition. U.S Geol Surv Bull 1646: 15-26

Gaboury D, Daigneault R, Tourigny G, Gobeil C (1996) An Archean volcanic-related gold-sulfide-quartz vein orebody: the Géant Dormant mine, Abitibi Subprovince, Québec, Canada. Explor Mining Geol 5: 197-213

Gaboury D, Daigneault R (1999) Evolution from seafloor-related to sulfide-rich quartz vein-type gold mineralization during deep submarine volcanic construction: The Géant Dormant gold mine, Archean Abitibi belt, Canada. Econ Geol 94: 3-21

Giletti BJ, Yund RA (1984) Oxygen diffusion in quartz. J Geophys Res 89 (B6): 4039-4046.

Green GR, Ohmoto H, Date J, Takahashi T (1983) Whole-rock oxygen isotope distribution in the Fukazawa-Kosaka area, Hokuroku district, Japon, and its potential application to mineral exploration. Econ Geol Monogr 5: 395-411

Gregory RT, Taylor HP Jr (1981) An oxygen isotope profile in a section of Cretaceous oceanic crust, Samail ophiolite, Oman: Evidence for $\delta^{18}O$ buffering of the oceans by deep (>5 km) seawater-hydrothermal circulation at Mid-Oceanic Ridges. J Geophys Res 86: 2737-2755

Groves DI, Goldfarb RJ, Gebre-Mariam M, Hagemann SG, Robert F (1998) Orogenic gold deposits: A proposed classification in the context of their crustal distribution and relationship to other gold deposit types. Ore Geol Rev 13: 7-27

Hannington MD, Poulsen KH, Thompson JFH, Sillitoe RH (1997) Volcanogenic gold and epithermal-style mineralization in the VMS environment. In: Barrie CT, Hannington MD (eds) Volcanogenic-associated massive sulfide deposits: Processes and examples in modern and ancient setting. Geol Assoc Can, Short Course Handbook Vol 13: 183-214

Hey MH (1954) A new review of the chlorites. Mineral Mag 30: 277-292

Hodgson CJ (1993) Mesothermal gold deposits. In: Kirkham RV, Sinclair WD, Thorpe RI, Duke JM (eds) Mineral deposit modeling. Geol Assoc Can, Spec Vol 40: 635-678

Huston, DL (1997) Stable isotopes and their significance for understanding the genesis of volcanic-hosted massive sulfide deposits: A review. In: Barrie CT, Hannington MD (eds) Volcanogenic-associated massive sulfide deposits: Processes and examples in modern and ancient setting. Geol Assoc Can, Short Course Handbook Vol 13: 157-181

Ishibashi J-I, Urable T (1995) Hydrothermal activity related to arc-backarc magmatism in the western Pacific. In: B. Taylor (ed) Backarc basins: tectonics and magmatism. Plenum Press, New York, pp 451-495

Kerrich R (1987) The stable isotope geochemistry of Au-Ag vein deposits in metamorphic rocks. In: Kyser TK (ed) Stable isotope geochemistry of low temperature fluids. Mineral Assoc Can, Short Course Vol 13: 287-336

Kerrich R, Wyman D (1990) Geodynamic setting of mesothermal gold deposits: An association with accretionary tectonic regimes. Geology 18: 882-885

Kirkham RV (1971) Intermineral intrusions and their bearing on the origin of porphyry copper and molybdenum deposits. Econ Geol 66: 1244-1249

Kranidiotis P, MacLean WH (1987) Systematics of chlorite alteration at the Phelps Dodge massive sulfide deposit, Matagami, Quebec. Econ Geol 82: 1898-1911

Kyser TK, Kerrich R (1990) Geochemistry of fluids in tectonically active crustal regions. In: Nesbitt BE (ed) Fluids in tectonically active regimes of continental crust. Mineral Assoc Can, Short Course Vol 18: 133-230

Large RR (1992) Australian volcanic-hosted massive sulfide deposits: features, styles, and genetic models. Econ Geol 87: 571-500

Larocque ACL, Hodgson CJ (1995) Effects of greenschist-facies metamorphism and related deformation on the Mobrun massive sulfide deposits, Québec, Canada. Mineral Deposita 30: 439-448

Lentz DR (1998) Petrogenetic evolution of felsic volcanic sequences associated with Phanerozoic volcanic-hosted massive sulphide systems: the role of extensional geodynamics. Ore Geol Rev 12: 289-327

Lizasa K, Fiske, RS, Ishizuka O, Yuasa M, Hashimoto J, Ishibashi J, Naka J, Horii Y, Fujiwara Y, Imai A, Koyama S (1999) A Kuroko-type polymetallic sulfide deposit in a submarine silicic caldera. Science 283: 975-977

MacLean WH, Hoy LD (1991) Geochemistry of hydrothermally altered rocks at the Horne mine, Noranda, Quebec. Econ Geol 86: 506-528

McCuaig TC, Kerrich R (1998) P-T-t-deformation-fluid characteristics of lode gold deposits: evidence from alteration systematics. Ore Geol Rev 12: 381-453

McInnes BIA, Cameron EM (1994) Carbonated, alkaline hydridizing melts from a sub-arc environment: Mantle wedge samples from the Tabar-Lihir-Tanga-Feni arc, Papua New Guinea. Earth and Plan Sci Lett 122: 125-141

McLeod RL, Stanton RL (1984) Phyllosilicates and associated minerals in some Paleozoic stratiform sulfide deposits of south-eastern Australia. Econ Geol 79: 1-22

Mortensen JK (1993) U-Pb geochronology of the eastern Abitibi Subprovince. Part 1: Chibougamau-Matagami-Joutel region. Can J Earth Sci 30: 11-28

Muehlenbachs K (1998) The oxygen isotopic composition of the oceans, sediments and the seafloor. Chem Geol 145: 263-273

Munha J, Barriga, FJAS, Kerrich R (1986) High ^{18}O ore-forming fluids in volcanic-hosted base metal massive sulfide deposits: Geologic, $^{18}O/^{16}O$, and D/H evidence from the Iberian Pyrite Belt; Crandon, Wisconsin; and Blue Hill, Maine. Econ Geol 81: 530-552

Ohmoto H (1986) Stable isotope geochemistry of ore deposits. Rev Mineral 16: 491-559

Ohmoto H (1996) Formation of volcanogenic massive sulfide deposits: The Kuroko perspective. Ore Geol Rev 10: 135-177

Ohmoto H, Rye RO (1979) Isotopes of sulfur and carbon. In: Barnes HL (ed) Geochemistry of hydrothermal ore deposits. Wiley, New York, pp 509-567

O'Neil JR, Taylor HP Jr (1967) The oxygen isotope and cation exchange chemistry of feldspars. Am Mineral 52: 1414-1437

O'Neil JR, Taylor HP Jr (1969) Oxygen isotope fractionation between muscovite and water. J Geophys Res 74: 6012-6022

Paradis S, Jonasson IR, LeCheminant GM, Watkinson DH (1988) Two zinc-rich chimneys from Plume Site, southern Juan de Fuca Ridge. Can Mineral 26: 637-654

Percival JB, Ames DE (1993) Clay mineralogy of active hydrothermal chimneys and an associated mound, Middle Valley, northern Juan de Fuca Ridge. Can Mineral 31: 957-971

Poulsen KH, Hannington MD (1996) Volcanic-associated massive sulphide gold. In: Eckstrand OR, Sinclair WD, Thorpe RI (eds) Geology of the Canadian mineral deposits. Geol Surv Can, Geology of Canada no 8, pp 183-196

Powell WG, Carmichael DM, Hodgson CJ (1995) Conditions and timing of metamorphism in the southern Abitibi greenstone belt, Quebec. Can J Earth Sci 32: 787-805

Robert F (1995) Quartz-carbonate vein gold. In: Eckstrand OR, Sinclair WD, Thorpe RI (eds) Geology of the Canadian mineral deposits. Geol Surv Can, Geology of Canada no 8, pp 350-366

Roberts RG (1988) Archean lode gold deposits. In: Roberts RG, Sheahan PA (eds) Ore Deposit Models. Geol Assoc Can, pp 1-19

Shinohara H, Kazahaya K (1995) Degassing processes related to magma-chamber crystallization. In: Thompson JFH (ed) Magmas, fluids and ore deposits. Mineral Assoc Can, Short Course Handbook Vol 23: 47-70

Shinohara H, Hedenquist JW (1997) Constraints on magma degassing beneath the Far Southeast porphyry Cu-Au deposit, Philippines. J Petrol 38: 1741-1752

Sillitoe RH (1997) Characteristics and controls of the largest porphyry copper-gold and epithermal gold deposits in the circum-Pacific region. Aust J Earth Sci 44: 373-388

Shanks WC III, Bohlke JK, Seal, RR II (1995) Stable isotopes in mid-ocean ridge hydrothermal systems: interaction between fluids, minerals, and organisms. In: Humphris SE, Zierenberg RA, Mullineaux LS, Thompson RE (eds) Seafloor hydrothermal systems physical, chemical, biological, and geological interactions. Amer Geophys Union, Mono 91, 194-221

Strauss H (1989) Carbon and sulfur isotope data for the carbonaceous metasediments from the Kidd Creek massive sulfide deposit and vicinity, Timmins, Ontario. Econ Geol 84: 959-962

Styrt MM, Brackmann AJ, Holland HD, Clark BC, Pisutha-Arnond V, Eldridge CS, Ohmoto H (1981) The mineralogy and the isotopic composition of sulfur in the hydrothermal sulfide/sulfate deposits on the East Pacific Rise, 21°N latitude. Earth Plan Sci Let 53: 382-390

Taylor BE, South BC (1985) Regional stable isotope systematics of hydrothermal alteration and massive sulfide deposition in the West Shasta district, California. Econ Geol 80: 2149-2163

Taylor HP Jr (1968) The oxygen isotope geochemistry of igneous rocks. Contrib Mineral Petrol 19: 1-71

Taylor HP Jr (1974) The application of oxygen and hydrogene isotope studies to problems of hydrothermal alteration and ore deposition. Econ Geol 69: 843-883

Taylor HP Jr (1979) Oxygen and hydrogen isotope relationships in hydrothermal mineral deposits. In: Barnes HL (ed) Geochemistry of hydrothermal ore deposits, Wiley, New York, pp 236-277

Taylor HP Jr, Sheppard SMF (1986) Igneous rocks: I. Processes of isotopic fractionation and isotope systematics. Rev Mineral 16: 227-271

Thompson JFH (1995) Exploration and research related to porphyry deposits. In: Schroeter, TG (ed) Porphyry deposits of the Northwestern Cordillera of North America. Can Inst Mining Metall, Spec Vol 46: 857-870

Uyeda S, Nishiwaki C (1980) Stress field, metallogenesis and mode of subduction. In: Strangway, DW (ed) The continental crust and its mineral deposits. Geol Assoc Can, Spec paper 20: 323-339

Vaughan DJ, Craig JR (1978) Mineral chemistry of metal sulfides. Cambridge University Press, 493 p

Wenner DB, Taylor HP Jr (1971) Temperatures of serpentinization of ultramafic rocks based on O^{18}/O^{16} fractionation between coexisting serpentine and magnetite. Contrib Mineral Petrol 32: 165-185

Wood SA (1987) Application of a multiphase ore mineral solubility experiment to the separation of base metal and gold mineralization in Archean greenstone terrains. Econ Geol 82: 1044-1048

Zheng YF (1990) Sulfur isotopes in metamorphic rocks. Neues Jahrbuch Miner Abh 161: 303-325

CHAPITRE 6

Practical methods for correlating diamond-drill core intersections: Applications to complex vein-type orebodies

Ce chapitre représente la version intégrale d'un article publié en 1997 dans la revue *CIM Bulletin,* Volume 90, #1008, page 135-138 par Gaboury.

Abstract

Two practical methods for correlating two and more diamond-drill core intersections, using a stereographic projection software are presented. The first may be used to establish if two or more vein intersections are correlative, based on their core angles and diamond-drill hole attitudes. The second method allows prediction of main vein attitudes from numerous intersections, based on a spherical density contouring projection. The methods are suitable for : (1) correlating veins in complex orebodies; (2) ascertaining lateral continuity of ore for reserve estimations; (3) demonstrating the hidden complexity of an orebody; and (4) correlating and interpreting various planar elements.

Résumé

Deux méthodes pratiques de corrélation des intersections de veines en forages, utilisant un logiciel de projection stéréographique, sont présentées. La première méthode peut être utilisée pour déterminer si deux ou plusieurs intersections de veines sont corrélatives, sur la base de leur angle avec la carotte (core angle) et de l'attitude des forages. La seconde méthode permet de prédire l'attitude des veines principales à partir de plusieurs forages ayant des intersections de veines, en utilisant une projection sphérique de densité. Les deux méthodes sont applicables pour (1) corréler des veines dans un gisement filonien dont la géométrie est complexe; (2) augmenter le degré de certitude sur la continuité des veines minéralisées à des fins de calculs de réserves; (3) démontrer la complexité cachée d'un système filonien; et (4) corréler et interpréter d'autres éléments planaires.

INTRODUCTION

Modern exploration relies on diamond-drill core data and on the ability of geologists to interpret them. Drill core generally yields unoriented information, unless an expensive orientation device is used. As a consequence, strike and dip of planar elements such as lithological contacts or mineralized veins cannot be determined easily. This is particularly true for blind deposits (covered by thick overburden) and complex orebodies, where field data cannot support drilling interpretations. Such a problem has been addressed previously using two and three diamond-drillholes and several solutions were proposed based on trigonometry and geometric and stereographic projections (Mead, 1921; Wisser, 1932; Fischer, 1941; Stein, 1941; Bucher, 1943; Gilluly, 1944; Addie, 1962; Mills, 1963; Lyons, 1964). However, these solutions are time consuming and not relevant to present day computerized data plots.

This paper describes two practical methods for correlating two or more diamond-drill core intersections, using stereoplotting software. These methods are well suited to the mine environment where diamond-drillholes are abundant. The first method, a correlative method, verifies if the intersected planes are correlative, and it is based on using core angles, drillhole attitudes and their relative position on level maps. The second method, a statistical method, uses spherical density distribution to predict the main attitudes of planar elements from numerous drillhole intersections within a defined three-dimensional block. These methods were developed during diamond-drillhole compilation at the Géant Dormant mine and the examples presented below are from this case study. The Géant Dormant deposit is covered by thick (up to 50 m) overburden and is composed of a complex network of gold-bearing quartz veins (Gaboury et al., 1996). In this paper, the plane intersected in drillcore is referred to as a vein.

THEORETICAL CONSIDERATIONS

The following information is available from a diamond-drillhole: (1) the trend and plunge of the hole, (2) the distance along the hole to the intersected vein, and (3) the core angle, which is the acute angle of inclination between the vein and the core axis. This angle can yield the strike and dip of the vein directly if a reference plane of known attitude is included in the core segment. For example, a penetrative schistosity, with constant attitude, can be used to reorient the core and establish the real strike and dip of the intersected vein. Other special cases include the 90° core angle, that gives the strike and dip of the vein directly by calculating the plane perpendicular to the drillhole axis (pole to plane). However, these are specific cases and unoriented core generally yields a cone of infinite possible vein attitudes around the core axis (Fig. 1).

BASIS OF THE METHODS

Two unoriented vein intersections with their respective core angle, from two different diamond-drillholes with specific attitude and drilled across the same vein, yield two cones of infinite planar attitude. However, among the infinite possibilities, one plane is common to both cones and corresponds to the plane of the vein. The methods presented here are based on this statement and, therefore, aim to establish the common plane.

CORRELATIVE METHOD

In order to establish a common plane, representative cones must be generated. This can be achieved with several stereoplotting software, but in this case, Stereo for Macintosh™ was used. However, most stereoplotting softwares are not designed to generate small circles directly (i.e., the stereographic projection of planes tangent to the cone of possibilities). To plot a small circle, input data files were created for specific core

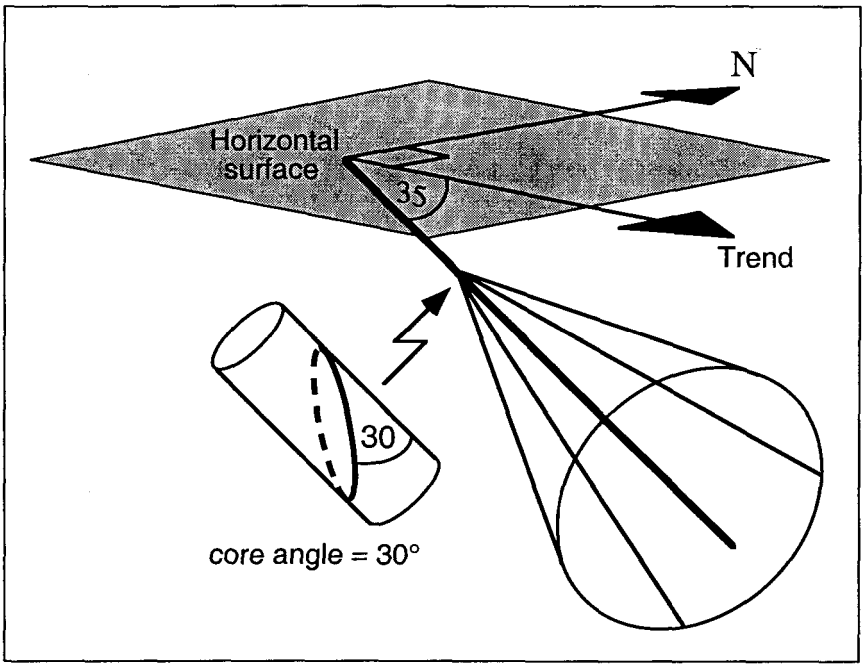

Figure 1. Schematic representation of the cone generated by a vein or planar element with a core angle of 30°. The illustrated diamond-drillhole strikes 090° and plunges 35° toward the east.

angles centered on a vertical drillhole axis (Fig. 2a). Hence, for an inclined drillhole, a rotation is applied to the input data file by the software in order to cente the representative planes around the line that corresponds to the drillhole axis (Fig. 2b). For simplicity, the poles are plotted rather than the planes. Finally, for determining the common plane, two small circles are plotted and if a pole is common to both small circles, then the corresponding plane yields the strike and dip of a possible continuous vein, intersected by both drillholes.

Three possible cases of plot results are as follows: (1) no common pole (Fig. 3a), which implies that the vein intersections may not share a common plane; (2) one to four common poles (Figs. 3b, 3c, 3d, 3e), indicating that both drill intersections share up to four common planes; and (3) superposition of both small circles (Fig. 3f). This later case is generated by parallel drill holes with the same or similar core angle, and implies that all the generated planes are possible.

The last stage involves testing the established common planes on mine level maps. Case 2, intersections are correlative (i.e., they can be interpreted as being a continuous vein), if the spatial position of both intersections can be linked by one of the planes established from the stereoplot. Case 3 is more subtle and involves trial and error testing of some of the planes defining the cones.

STATISTICAL METHOD

From a statistical point of view, poles which are common to both small circles represent a maximum in terms of frequency distribution of poles, because other poles only occur once in both rotated data files (Fig. 3). Therefore, the most frequent poles generated by small circles from numerous intersections are likely to represent common poles and, thus, the most probable attitudes of veins. From a geological point of view, this approach is

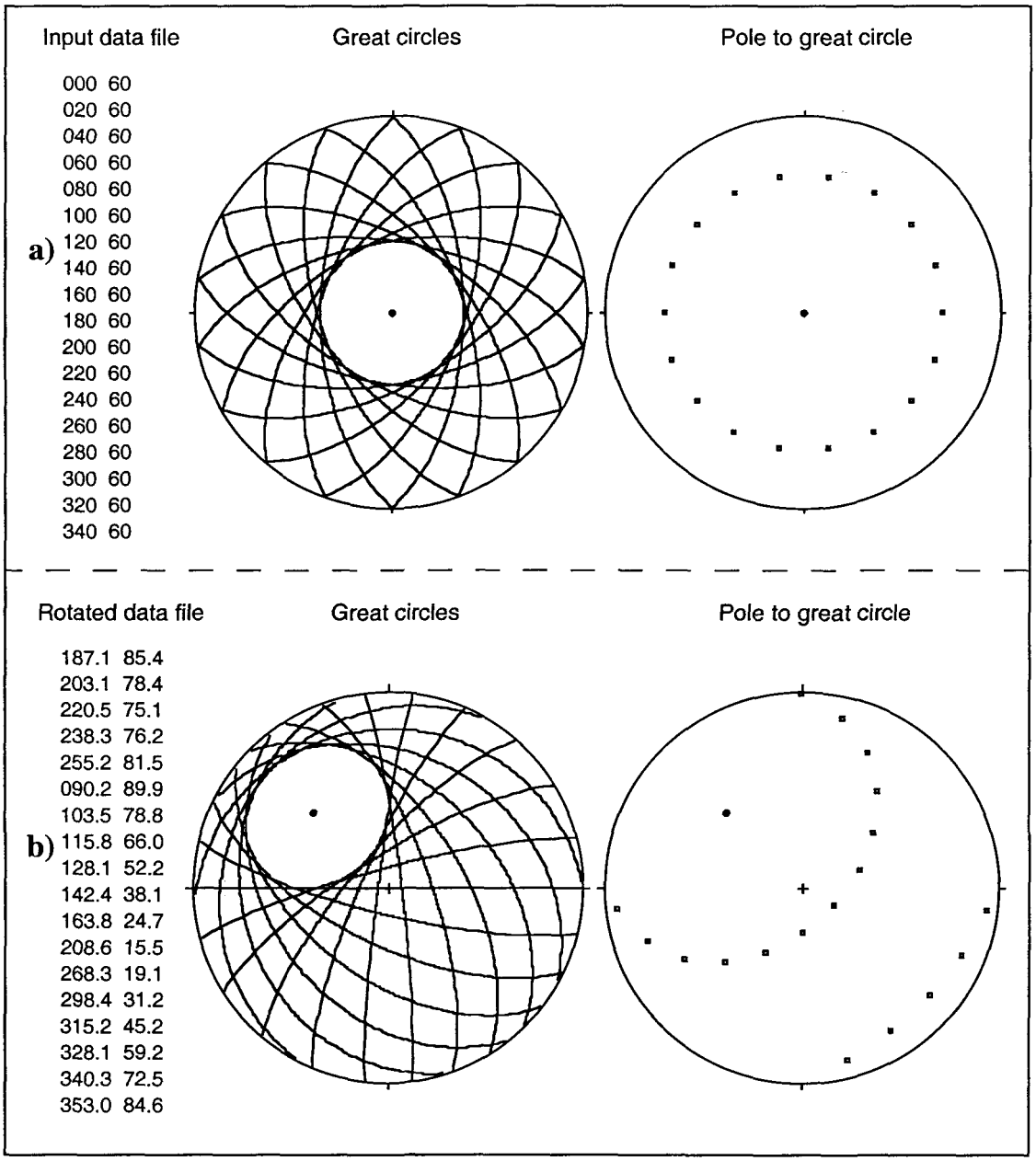

Figure 2. (a) Example of input data file, created for a core angle of 30°. The strike is incremented by 20° in order to generate a 360° small circle whereas the corresponding plunge is obtained by subtracting the core angle from 90° (pole to plane). Such a file has to be created for different core angles (5° increment). The stereplots show great circles and poles generated by the input data file. Note that the small circle is centered on a vertical axis and is defined by tangent great circles. (b) Example of a rotated file generated by the software for a diamond drillhole striking 315° with a 45° plunge and the corresponding plots of great circles and poles.

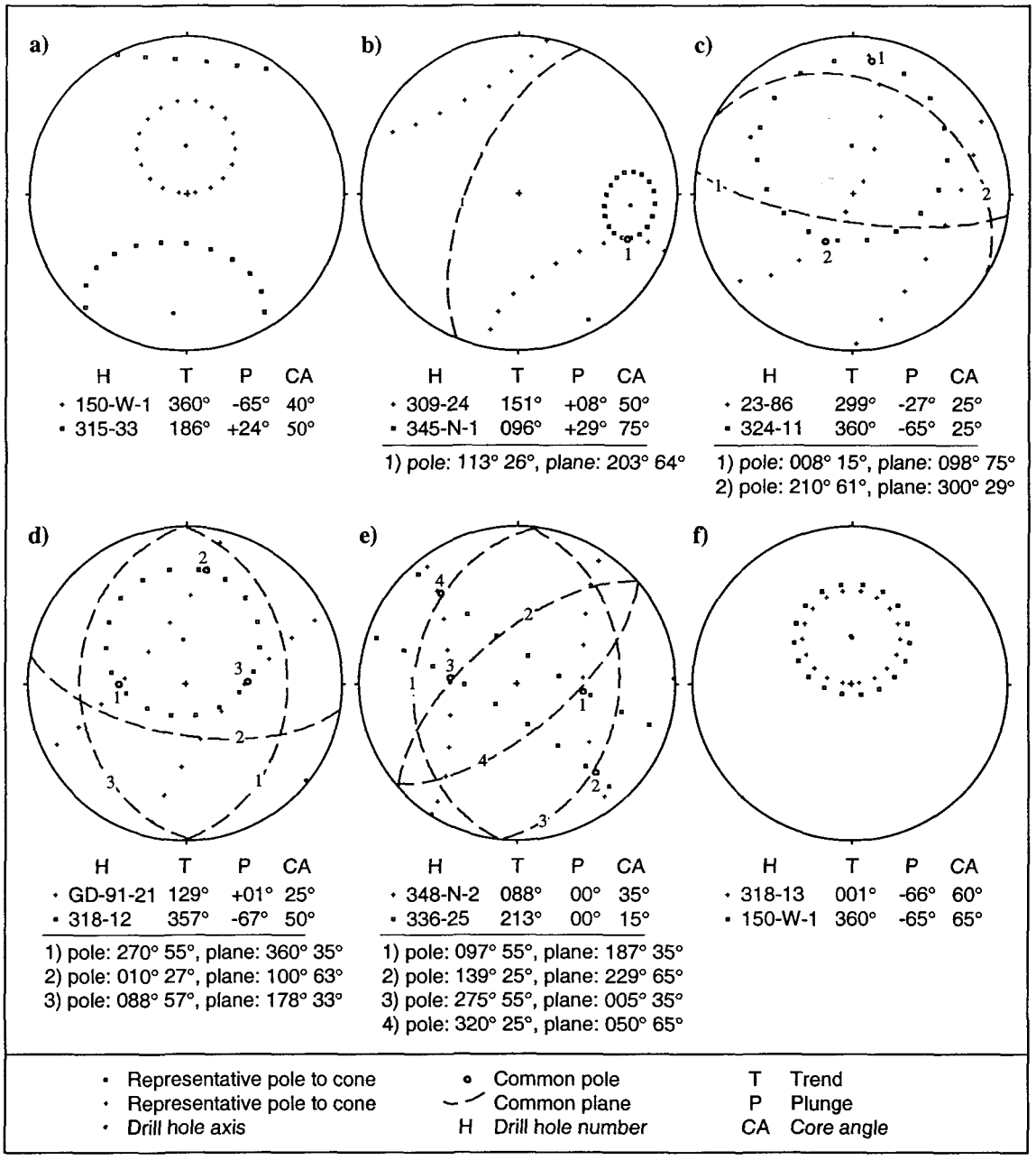

Figure 3. Stereographic projection of various small circles from different diamond-drillholes illustrating the possible cases of correlation from two drill holes. (a) No common pole. (b) One common pole. (c) Two common poles. (d) Three common poles. (e) Four common poles. (f) Superposition of both small circles.

valid because complex vein systems are commonly composed of subparallel vein arrays and, consequently, intersections come from the same or subparallel veins.

Technically, small circles are generated for each intersection considered, based on the previously described stereographic procedure, except that rotated files for each intersection are added in a single file, referred to as the sum file. The sum file contains 18 x n planes (pole) (Fig. 2a), where n is the number of intersections considered. Interpretation of the most frequently occurring poles is achieved with a contouring density plot, which is generated using the Stereo for Macintosh contouring option (Fig. 4).

Figure 4a shows the resulting plot for 114 intersections compiled within a 400 m x 400 m x 400 m block. The most frequent poles define a clear maximum on the density plot. Interpretation is done by grouping adjacent maxima (Fig. 4b), since the precision is limited by the 20° increment of the strike in the input data files (Fig. 2a). As a result, interpreted vein attitudes have uncertainties in the range of +/- 20° for the strike and +/- 10° for the dip, which are precise enough for correlating and testing purposes. Finally, it is important to note that the 320 80 and the 355 45 attitudes correspond to known vein arrays at the Géant Dormant mine (Gaboury et al., 1996), whereas the 080 45 attitude is a new and untested vein attitude.

DISCUSSION: VERACITY OF THE METHODS

Both methods are geometrically rigorous. Because they are applied to natural features that may not be strictly planar, some uncertainty is introduced. The validity of an established plane is clearly dependent on the representativeness of the core angle to the overall strike and dip of the vein. For example, folding of veins can induce perturbation of the core angles and lead to erroneous correlations. Additionally, subsequent faulting, implying relative displacement of vein intersections can also lead to false correlations.

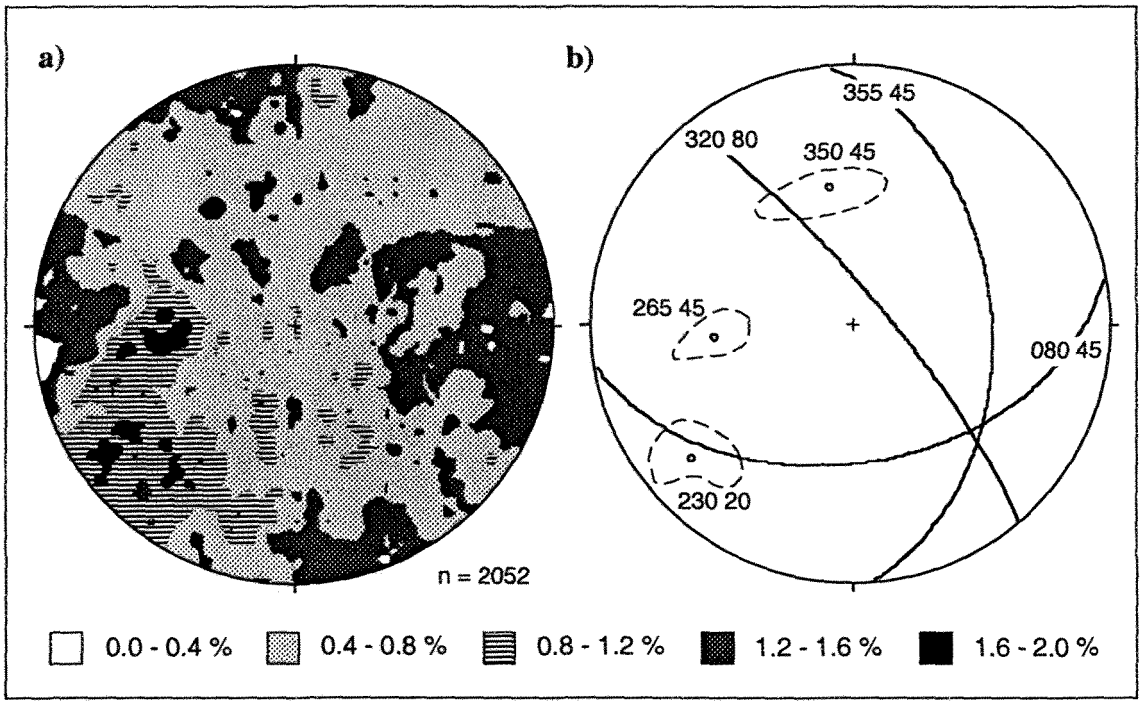

Figure 4. (a) Density contouring plot of small circles generated from 114 intersections compiled within a 400 m x 400 m x 400 m block. The sum file contains 2052 poles. (b) Interpretation of the maxima as illustrated by the dashed line contours. The projected great circles represent the most probable vein attitudes.

Therefore, results and interpretations generated by both methods have to be weighted using a knowledge of the geological setting. For the statistical method, the diversity of diamond-drillhole attitudes (trend and plunge) should also be considered. If there are too many parallel diamond-drillholes, the density contouring will be biased towards coincident small circles. To resolve this problem, only one intersection from parallel drillholes, with a specific core angle, should be included within the sum file.

CONCLUSION: APPLICABILITY

The methods presented above are suitable for correlating veins in a complex orebody, where vein attitudes cannot be easily predicted by geological features and where vein intersections and diamond-drillholes are abundant. They can also be used to gain confidence about continuity of the mineralized structure for reserve estimation. Such a continuity parameter is extremely important in assessing the accuracy of the mineral inventory (Sinclair and Vallée, 1994). Inversely, both methods can be applied to ascertain the hidden complexity of an orebody. This can be achieved by demonstrating that adjacent and intuitively correlative vein intersections do not share a common host plane, or using the statistical method, by demonstrating that the most frequent planes do not correspond to those expected. Finally, these methods can be used to correlate various planar elements such as dykes, bedding and faults.

Acknowledgments

The author acknowledges C. Gobeil and N. Vachon from Cambior (Géant Dormant Mine) for their enthusiastic collaboration during the compilation work. The manuscript has benefited from constructive criticism by M.I. Legault, J.-F. Couture, G. Tourigny, E.H. Chown and by two CIM Bulletin reviewers.

References

ADDIE, G., 1962. A simplified stereographic projection solution of the two drillhole problem. Economic Geology, Vol. 57, p. 1122-1126.

BUCHER, W.H., 1943. Dip and strike from three not parallel drill cores lacking key beds. Economic Geology, Vol. 38, p. 648-657.

FISCHER, D.J., 1941. Drillhole problem in the stereographic projection. Economic Geology, Vol. 36, p. 551-560.

GABOURY, D., DAIGNEAULT, R., TOURIGNY, G. and GOBEIL, C., 1996. An Archean volcanic-related gold-sulfide-quartz vein orebody: the Géant Dormant mine, Abitibi Subprovince, Québec, Canada. Exploration and Mining Geology, Vol 5, p. 197-213.

GILLULY, J., 1944. Dip and strike from three not parallel drill cores lacking key beds. Economic Geology, Vol. 39, p. 359-363.

LYONS, M.S., 1964. Interpretation of planar structure in drill-hole cores. Geological Society of America, Special Paper 78, 66 p.

MEAD, W.J., 1921. Determination of attitude of concealed bedded formations by diamond drilling. Economic Geology, Vol. 16, p. 37-47.

MILLS, J. W., 1963. A simplified stereographic projection solution of the two drillhole problem. Economic Geology, Vol. 58, p. 618-621.

SINCLAIR, A. J. and VALLÉE, M., 1994. Reviewing continuity: an essential element of quality control for deposit and reserve estimation. Exploration and Mining Geology, Vol. 3, p. 95-108.

STEIN, H.A., 1941. A trigonometric solution of the two-drillhole problem. Economic Geology, Vol. 36, p. 84-94.

WISSER, E., 1932. An aid in the interpretation of diamond drill cores. Economic Geology, Vol. 27, p. 437-449.

CHAPITRE 7

Discussion

INTRODUCTION

Les chapitres précédents (2, 3, 4 et 5) ont permis de démontrer que les veines aurifères sont antérieures au développement de la fabrique ductile pénétrante et du métamorphisme régional et que leur origine est reliée à l'évolution particulière d'un système hydrothermal de type volcanogène. Par comparaison avec ces mêmes systèmes hydrothermaux, deux éléments particularisent le Géant Dormant, soit la présence de veines et leur fort contenu aurifère. Il apparaît donc impératif de discuter du mécanisme de formation de telles veines en contexte sous-marin et des facteurs probables d'enrichissement en or et ce, dans la mesure où ces deux points n'ont été que brièvement abordés au chapitre 3. Dans le but d'asseoir sur des bases factuelles la discussion concernant la formation des veines et la forte teneur en or, les principaux arguments appuyant le modèle volcanogène sont résumés ci-dessous et orchestrés de manière à préciser le schème interprétatif. La prochaine section se veut donc essentiellement une synthèse pour servir de tremplin à la discussion d'éléments spécifiques, étant donné que la validité des différents éléments appuyant le model proposé a été discutée dans les chapitres précédents.

MODÈLE GÉNÉTIQUE POUR LE GÉANT DORMANT

Les caractéristiques temporelles, de profondeur de formation et géochimiques, définissant les différents types génétiques (Chap. 1), peuvent être utilisées ensemble dans le but de diagnostiquer l'affinité génétique d'un gisement particulier. La chronologie relative de formation peut être considérée en fonction des relations de recoupement entre la minéralisation et l'empreinte des différents événements géologiques (magmatisme, déformation, métamorphisme) ainsi que sur la base de la datation d'événements particuliers. La profondeur crustale de formation peut être estimée en utilisant les

caractéristiques géométriques de la minéralisation, sa composition minéralogique et sa relation avec le métamorphisme régional. La composition géochimique d'un système hydrothermal peut être caractérisée en utilisant les signatures métalliques de la minéralisation, les types d'altération hydrothermale et la signature isotopique des minéralisations et des altérations hydrothermales. Ces différents éléments ont été considérés pour déterminer l'affiliation génétique des veines aurifères à la mine Géant Dormant et sont résumés ci-dessous.

Chronologie relative de formation de la minéralisation

La chronologie relative de formation des veines a été initialement centrée sur la détermination de la relation entre la schistosité régionale et les veines aurifères, telle que présentée au chapitre 2. Les relations de recoupement qui indiquent que la déformation ductile régionale est superposée aux veines minéralisées sont les suivantes. Les dykes mafiques à hornblende, qui recoupent les veines, sont eux-mêmes schistosés. Le système de veines est caractérisé par un manque de compatibilité structurale avec les caractéristiques de la déformation ductile, dominée par une extension verticale. De plus, tel que démontré au chapitre 3, le système de veines est géométriquement plus cohérent lorsqu'il est considéré comme étant basculé avec les couches hôtes. Ceci suggère que la mise en place des veines s'est faite lorsque les couches étaient dans leur position sub-horizontale initiale. D'autre part, la présence dans les veines des rosettes d'actinote (Chap. 4), se superposant aux sulfures, suggère que les veines ont été imprégnées par le métamorphisme régional. Ces différents arguments géométriques et minéralogiques démontrent que la formation des veines est antérieure au développement de la schistosité et du métamorphisme régional, ainsi qu'au plissement régional qui, selon la chronologie

connue (Chown et al., 1992), correspond à un stade précoce de la déformation progressive régionale.

La chronologie relative entre les différents événements de minéralisation et ceux volcaniques et magmatiques, présentée au chapitre 3, illustre bien le parallélisme entre l'activité hydrothermale et la construction de la séquence volcanique hôte. Ainsi, la formation des veines est précédée par deux événements de minéralisation aurifère. Le plus ancien est d'origine volcanogène. Le second est associé à un processus d'autométasomatisme induit par la disponibilité de fluides hydrothermaux volcanogènes durant la mise en place et le refroidissement du dôme dacitique. Pour les veines, la chronologie établie indique que leur formation suit dans le temps la mise en place des dykes felsiques de QFP, mais précède l'injection des dykes mafiques tholéiitiques post-minéralisation.

Sur une base comparative, l'âge des dykes de QFP de 2722 ± 2 Ma, déterminé par une datation U-Pb sur des zircons (Chap. 3), est cohérent avec l'âge connu (2730-2720 Ma) du premier cycle volcanique (Chown et al., 1992). Cet âge implique premièrement que les dykes de QFP font partie intégrante de la période de construction volcanique, un point également supporté par la similarité des signatures géochimiques entre les dykes de QFP et les roches felsiques antérieures, que sont l'unité de lave felsique, le dôme dacitique et les dykes de FP. Deuxièmement, il indique que les deux événements de minéralisation, qui précèdent la formation des veines, sont syn-volcaniques parce qu'ils sont recoupés par les dykes de QFP. Pour les veines, cet âge indique que leur formation peut être aussi vieille que la fin de la période de la construction volcanique. En outre, le recoupement des veines par les dykes mafiques tholéiitiques, dont la signature géochimique est comparable à celle des filons-couches hôtes et dont la texture et les structures internes indiquent une mise en

place crustale sub-volcanique, suggère que la formation des veines correspond à un événement hydrothermal développé à la fin de l'activité volcanique.

Profondeur crustale de formation

La profondeur crustale de formation des veines est un paramètre relativement difficile à déterminer étant donné qu'elle s'étend de 0 à >25 km (Gebre-Mariam et al., 1995). Dans le cas présent, étant donné que le métamorphisme est superposé sur les veines aurifères, leur profondeur crustale de formation ne peut pas être estimée à partir du grade de métamorphisme des roches encaissantes, comme dans le cas des gisements filoniens orogéniques (p. ex. Groves et al., 1995). L'estimation de la profondeur crustale de formation des veines repose donc sur la considération de paramètres empiriques.

Une profondeur crustale de formation, correspondant à l'équivalent de la pression lithostatique d'une charge de 2 à 3 km de roches, est suggérée sur la base des arguments suivants. (1) Les veines sont distribuées au sein d'une séquence de roches de 1 000 m d'épaisseur, correspondant à la distance en plan entre la veine #40 et la terminaison méridionale de la veine #3 (Chap. 3: Fig. 2). (2) Une épaisseur de 500 m de roches, géochimiquement cohérentes avec la séquence hôte, surmonte stratigraphiquement l'extrémité sud de la veine #3 (Chap. 3: Fig. 3). (3) Enfin, l'environnement sous-marin profond (> 3 150 m) lors de la formation des veines ajoute une pression significative correspondant à environ 1 500 m de roches, considérant que la densité de l'eau de mer est deux fois moindre que celle des roches. Cette profondeur crustale inférée s'accorde avec l'augmentation de la complexité du système de veines vers le sommet de l'empilement volcanique (Chap. 2) et la position verticale interprétée de la composante $\sigma 1$ lors de la formation des veines (Chap. 3). Ensemble, ces deux caractéristiques sont typiques des systèmes filoniens formés en milieux superficiels et associés à un régime tectonique en

extension. Une profondeur crustale superficielle est également compatible avec le style cassant de la fracturation qui contrôle la formation des veines (Chap. 2). D'autre part, les dykes mafiques tholéiitiques, qui recoupent les veines aurifères, sont caractérisés par une texture aphanitique et par la présence de joints columnaires indiquant une cristallisation rapide, compatible avec un environnement volcanique superficiel (Chap. 3).

Caractéristiques chimiques du système hydrothermal

Les différentes caractéristiques minéralogiques, géochimiques et isotopiques appuient d'une part la spécificité des trois événements hydrothermaux et suggèrent d'autre part leur lien génétique et leur origine volcanogène.

La spécificité des événements hydrothermaux est démontrée, outre par les relations de recoupement et les styles particuliers de la minéralisation, par: (1) la minéralogie des altérations hydrothermales et leur signature géochimique, caractérisée par la méthode de calcul de bilan de masses (Chap. 3); (2) la composition en sulfures; (3) la signature en ÉTR des sulfures et en éléments traces (Au, Ag, As, Sb, Ni et Co: Chap. 4). Cette spécificité atteste premièrement qu'il s'agit réellement d'événements distincts de minéralisation et non pas de styles différents reliés à un événement hydrothermal unique et deuxièmement, que des conditions physico-chimiques relativement particulières caractérisent chacun de ces événements.

Le lien génétique entre les trois événements de minéralisation est appuyé par: (1) la similarité des signatures isotopiques $\delta^{34}S$ du souffre provenant des différents sulfures (Chap. 5); (2) la similarité des valeurs du $\delta^{18}O$ pour le fluide minéralisateur à l'origine des veines et du premier événement de minéralisation (Chap. 5); et (3) la cohérence du contenu en éléments traces des différents sulfures (Au, Ag, As, Sb, Ni et Co) qui définit une tendance évolutive du premier au troisième événement minéralisateur (Chap. 4).

D'un point de vue génétique, l'origine volcanogène du premier événement de minéralisation, qui est indiquée par le style, l'habitus et la chronologie précoce de la minéralisation, est également supportée par: (1) la signature en ÉTR de la pyrrhotite, où l'anomalie négative en Ce peut être attribuable au mélange entre le fluide minéralisateur et l'eau de mer au site de précipitation des sulfures (Chap. 4); (2) la composition isotopique du souffre de la pyrrhotite et de la chalcopyrite qui se compare à celle des systèmes volcanogènes archéens (Chap. 5); et (3) la valeur du $\delta^{18}O$ de 3,2‰ calculée à 250°C pour le fluide minéralisateur qui est également cohérente avec la signature isotopique des fluides volcanogènes (Chap. 5).

Quant aux veines, une origine volcanogène est supportée par: (1) l'assemblage de sulfures des veines qui est composé essentiellement de pyrite, pyrrhotite, chalcopyrite, sphalérite et arsénopyrite; (2) la composition isotopique du souffre des sulfures (Chap. 5) qui, quoique non discriminante d'une manière absolue, se compare aux minéralisations volcanogènes archénnes; et (3) la signature fractionnée en ÉTR avec une anomalie positive en Eu des sulfures, qui est typique des systèmes volcanogènes matures et présentement actifs (Chap. 4).

Certaines caractéristiques suggèrent également une origine volcanogène du système hydrothermal dans son ensemble. Ainsi, les différentes altérations hydrothermales, quoique relativement spécifiques pour chaque événement hydrothermal, se comparent à celles des systèmes volcanogènes, étant composées essentiellement de chlorite, de séricite et de quartz (Chap. 3). Parallèlement, la tendance évolutive enregistrée par les éléments traces dans les sulfures (augmentation progressive du contenu en Au, Ag, As, Sb et diminution du Ni et Co) est également cohérente avec la maturation progressive d'un système hydrothermal volcanogène, telle que proposée au chapitre 4. Quant aux fluides minéralisateurs, la valeur relativement élevée du $\delta^{18}O$ calculée pour les veines (4,7‰ à

275°C) suggère une contribution de fluides magmatiques au système volcanogène (Chap. 5), une hypothèse compatible avec le lien entre l'activité hydrothermale et le magmatisme felsique (Chap. 3). D'autre part, la valeur du $\delta^{18}O$ pour le premier événement minéralisateur (3,2‰ à 250°C) peut s'expliquer par la dilution du ^{18}O avec l'eau de mer (~0‰) au site de précipitation des sulfures. Cette hypothèse de dilution d'un fluide initialement évolué et de composition uniforme tout au long de l'activité hydrothermale (~5‰) est supportée par le contenu constant en Se des sulfures provenant des différents événements minéralisateurs (Chap. 4).

Intégration des paramètres

Les relations chronologiques indiquent que les veines sont précoces à la déformation régionale ductile (Fig. 1). L'âge maximum des veines aurifères est de 2722 ± 2 Ma, correspondant à l'âge des dykes de QFP recoupés par les veines, alors que l'âge minimum absolu demeure inconnu en raison de l'absence de roches facilement datables par la méthode U-Pb sur zircons (Fig. 1). Toutefois, le recoupement des veines par les dykes mafiques tholéiitiques indique un âge relatif précoce à la terminaison du magmatisme mafique, suggérant une formation des veines tardi-volcaniques (Fig. 1).

Les différentes caractéristiques géochimiques de la minéralisation appuient le lien génétique entre les trois événements. L'origine des veines aurifères s'explique donc mieux lorsque leur formation est intégrée dans l'évolution temporelle d'un système hydrothermal unique (Fig. 1). Parallèlement, les caractéristiques des différents événements de minéralisation et de leur altération hydrothermale s'intègrent particulièrement bien au sein d'un système hydrothermal de type volcanogène. Le faible niveau crustal de formation des veines et le régime tectonique en extension sont également compatibles avec un tel système hydrothermal.

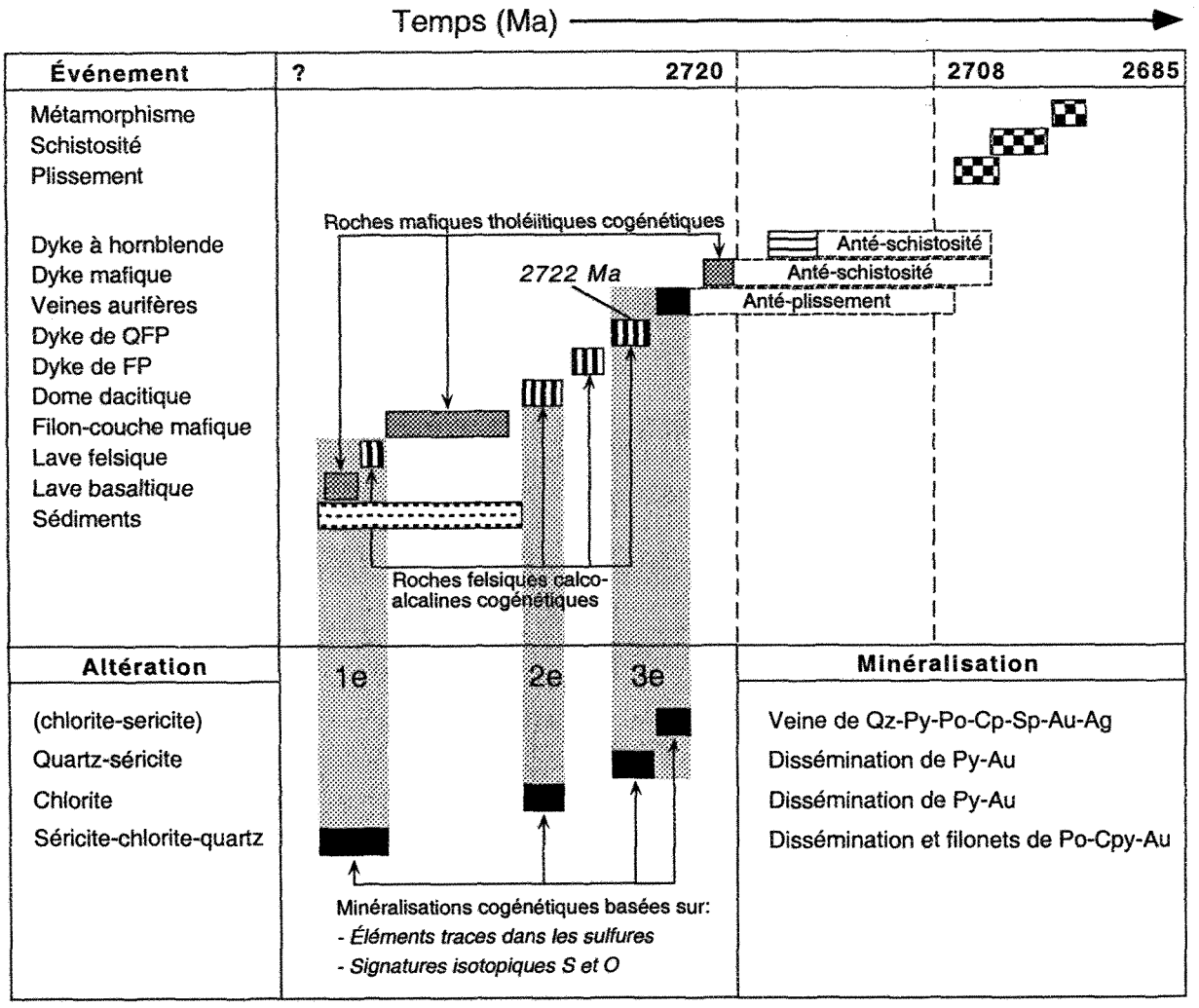

Figure 1. Résumé des différents arguments composant le schème interprétatif. Les événements de minéralisation sont indiqués par: 1e, 2e et 3e. Les rectangles en pointillés indiquent l'âge relatif maximum déterminé sur la base de recoupement avec les éléments de la déformation ductile régionale. Les âges sur l'échelle de temps proviennent de Chown et al. (1992). À noter que l'âge maximum des roches hôtes est indéterminé.

Par conséquent, même si l'âge minimum absolu des veines aurifères demeure inconnu, le lien génétique proposé entre les veines aurifères et les deux autres événements minéralisateurs indiquent qu'elles sont d'affiliation volcanique et génétiquement associées à l'évolution temporelle d'un système volcanogène (Fig. 1).

Modèle génétique

En mettant en parallèle l'histoire de l'édification volcanique et de l'activité hydrothermale, et sur la base des caractéristiques géochimiques des différents événements de minéralisation, il est proposé que la minéralisation filonienne est d'origine volcanogène et qu'elle représente l'épisode final de l'évolution du système hydrothermal. Le modèle d'évolution de ce système, qui est détaillé au chapitre 3, comporte quatre stades. Le stade 1 implique l'altération (chlorite, séricite, quartz) et la minéralisation (pyrrhotite et chalcopyrite faiblement aurifère et argentifère) des roches du paléofond océanique à la suite du développement d'un système hydrothermal volcanogène diffus. Au stade 2, l'injection des filons-couches mafiques entraîne le colmatage du système hydrothermal à la base de l'empilement nouvellement formé, qui fut préalablement altéré et minéralisé. Le stade 3 est relié à l'introduction du dôme dacitique et à la réactivation du système hydrothermal et se manifeste par la minéralisation disséminée en pyrite faiblement argentifère et aurifère et la chloritisation interne du dôme dacitique. Le stade 4 marque la fin du système hydrothermal avec la mise en place des dykes de QFP qui, subséquemment, ont servi de conduits hydrothermaux lors de la formation des veines aurifères. Ces dernières résultent du remplissage hydrothermal de fractures développées à proximité des dykes de QFP.

MÉCANISME EMPIRIQUE DE FORMATION DES VEINES

Le Géant Dormant représente un des premiers, sinon le seul cas documenté, où il est proposé que des veines de quartz aurifères dérivent d'un système volcanogène. Une telle origine des veines implique *de facto* des conditions de formation spécifiques et conséquemment un mécanisme de formation potentiellement différent de ceux documentés pour la formation des veines aurifères dans des contextes plus classiques. L'approche utilisée ci-dessous repose essentiellement sur l'estimation, à partir d'une base comparative, des paramètres essentiels qui contrôlent la formation des veines. Par conséquent, le mécanisme proposé pour la formation des veines au Géant Dormant en est un empirique. Enfin, si le modèle proposé a le mérite d'intégrer la majeure partie des caractéristiques particulières du système filonien, il doit néanmoins être considéré comme une première ébauche pour résoudre un problème complexe. Au risque de se répéter, le lecteur est prié de se référer au manuscrit en annexe 1 pour une version plus complète et plus robuste du modèle.

État des connaissances

Deux principaux mécanismes de formation de veines ont été documentés, soit celui des failles-valves (Sibson et al., 1988; Sibson, 1990a, 1990b; Cox et al., 1990) et celui des pompes sismiques (Sibson, 1987; 1990b). Ces deux modèles s'appliquent pour la formation de veines à des profondeurs crustales différentes, dans des régimes tectoniques particuliers et impliquent des pressions de fluides spécifiques. Les concepts de base de chacun des deux modèles sont résumés ci-dessous parce qu'ils serviront de référence pour le modèle proposé.

Le modèle des failles-valves est basé sur la surpressurisation des fluides hydrothermaux à un niveau supralithostatique au sein d'un environnement crustal relativement profond (zone sismologique: 5-15 km), imperméable et soumis à un régime de raccourcissement horizontal (Fig. 2a, b). La surpressurisation des fluides sous des couches imperméables engendre des ruptures sismiques le long de zones de failles modérément à fortement inclinées constituant les conduits hydrothermaux de décharge (Fig. 2c). Les veines subhorizontales, qui accompagnent généralement les veines formées au sein des zones de failles, se développent durant la période de surpressurisation avant la rupture sismique (Fig. 2c). Leur formation est favorisée conjointement par la surpressurisation des fluides et le régime tectonique (Fig. 2a, b). La répétition de ce processus est invoquée pour expliquer les multiples événements d'ouvertures et de remplissages des veines de quartz (Fig. 2d). Spécifiquement, ce modèle implique des variations considérables de la pression des fluides qui sont démontrées par la présence de brèches hydrothermales à fragments d'encaissants (Robert et Brown, 1986).

Le modèle des pompes sismiques est applicable pour les environnements crustaux superficiels (< 2 km), soumis à un régime tectonique en décrochement et où la pression des fluides est en régime hydrostatique (Fig. 3a, b). Dans de telles conditions, il est invoqué que le coulissage relatif le long de failles subverticales induit des zones d'ouverture en relais (dilatational jog) (Fig. 3c). Ces zones d'extension exercent alors une force d'aspiration qui draine les fluides environnants (Fig. 3c). La réduction instantanée de la pression des fluides dans les zones de dilatation provoque la bréchification hydrothermale, l'ébullition des fluides et la précipitation des minéraux formant les veines. La répétition temporelle de ce processus est également invoquée pour expliquer les multiples événements d'ouverture et de bréchification qui caractérisent les veines (Fig. 3d).

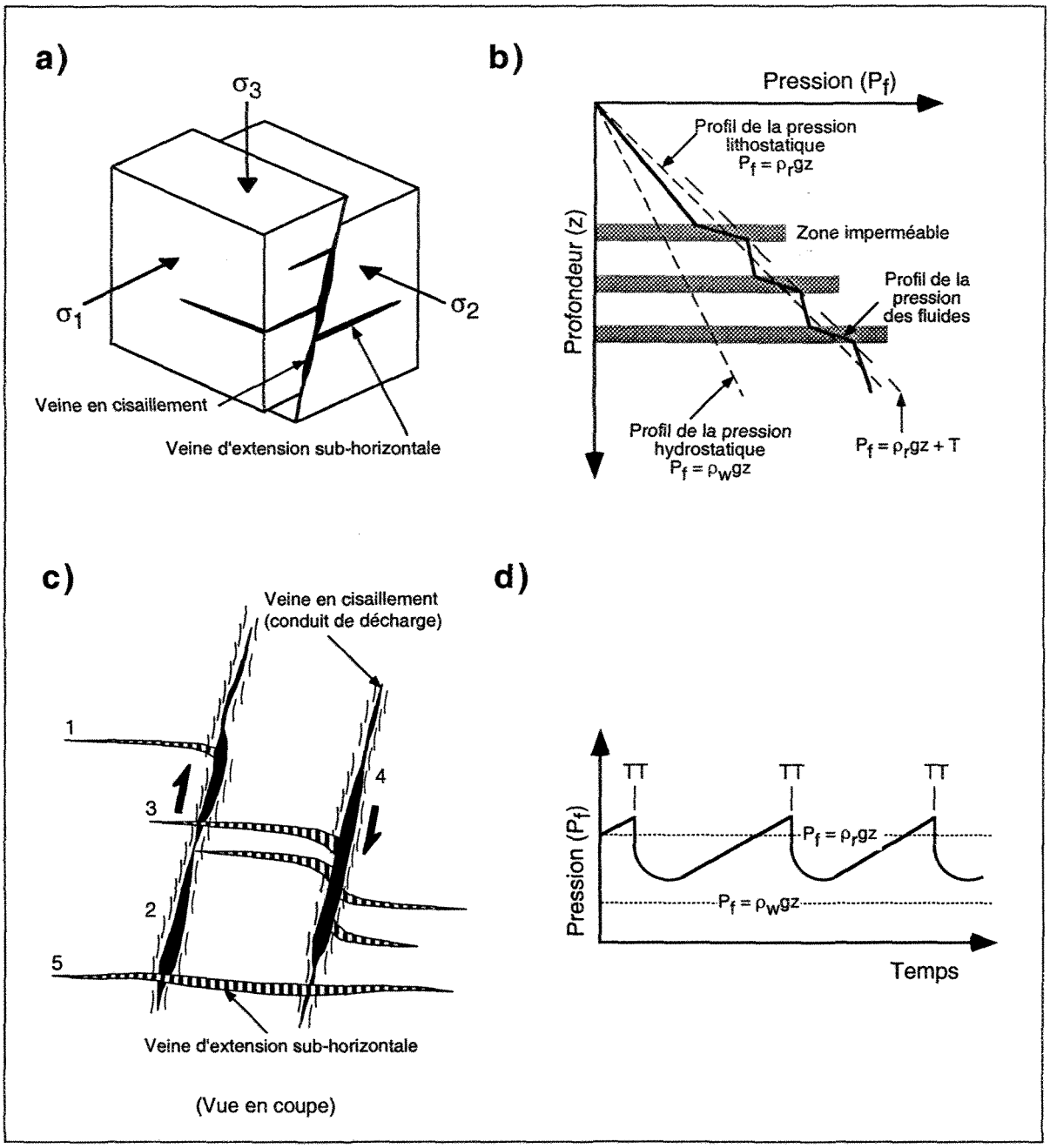

Figure 2. Résumé des caractéristiques s'appliquant au modèle des failles-valves. (a) Régime tectonique chevauchant et champ de contraintes associé. (b) Diagramme de la pression des fluides en fonction de la profondeur, illustrant la présence de couches imperméables qui favorisent la pressurisation des fluides et les événements de rupture hydraulique conséquents. Figure modifiée de Cox et al. (1990). (c) Représentation schématique de la géométrie classique des différentes veines résultant du mécanisme des failles-valves, modifiée de Sibson (1990b). Les numéros indiquent la chronologie relative de formation des différentes veines. (d) Diagramme de la pression en fonction du temps, illustrant la fluctuation de la pression des fluides et la cyclicité du mécanisme des failles-valves. TT signifie tremblement de terre. Figure modifiée de Sibson et al., (1988).

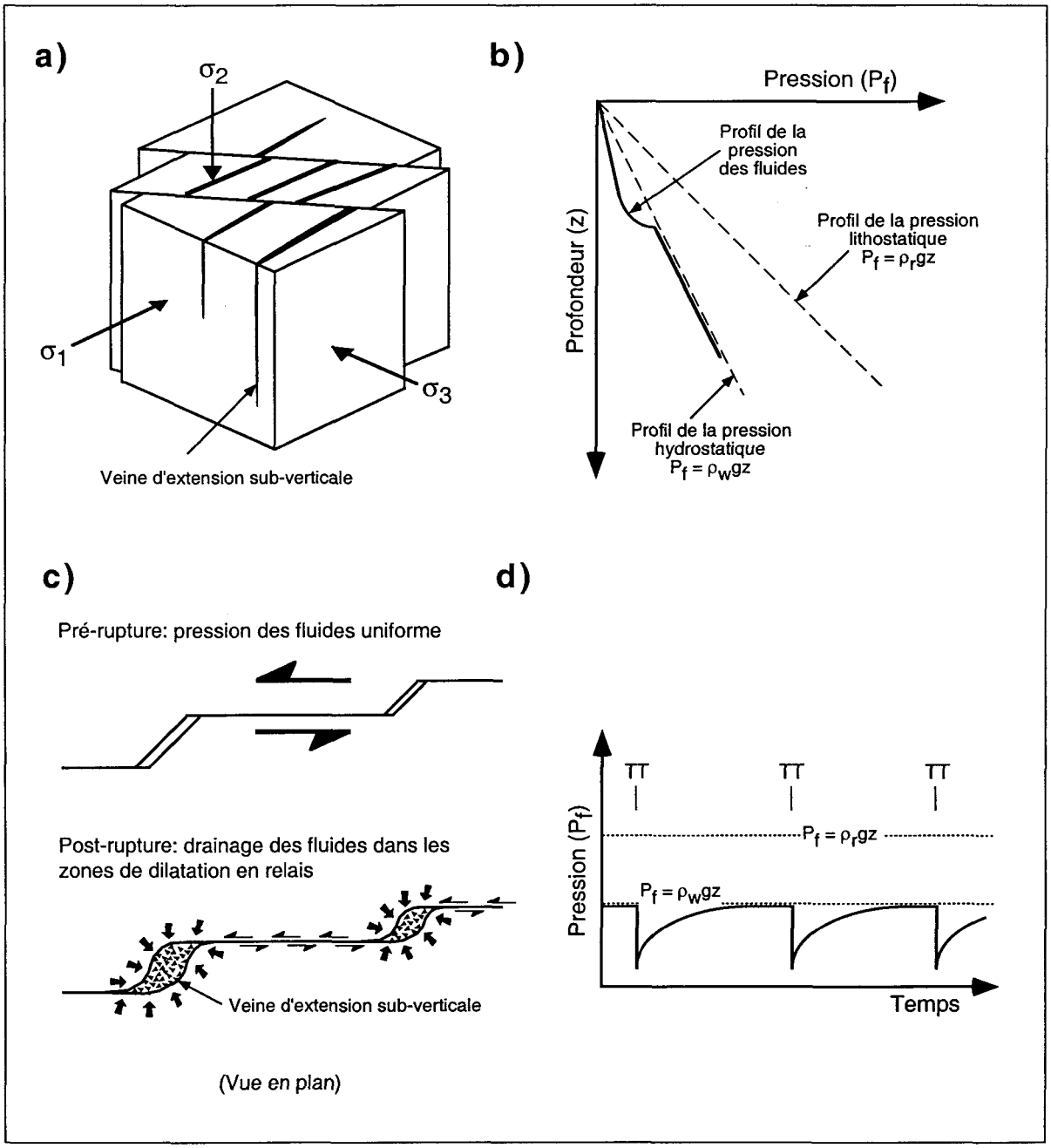

Figure 3. Résumé des caractéristiques s'appliquant au modèle des pompes sismiques. (a) Régime tectonique décrochant et champ de contraintes associé. (b) Diagramme de la pression des fluides en fonction de la profondeur, illustrant la pression des fluides à un niveau hydrostatique et le niveau infra-hydrostatique généré par le pompage sismique. (c) Représentation schématique de la géométrie classique des veines en extension sub-verticales résultant du mécanisme de la pompe sismique, modifiée de Sibson (1987). (d) Diagramme de la pression en fonction du temps, illustrant la fluctuation de la pression des fluides et la cyclicité du mécanisme de la pompe sismique. TT signifie tremblement de terre. Figure modifiée de Sibson et al., (1990b).

Détermination des conditions de formation des veines

La formation d'une veine implique la circulation de fluides hydrothermaux dans une fracture et des conditions favorables pour la précipitation des minéraux (Jébrak, 1992; Peters, 1993). Les veines correspondent à un système hydrothermal fossilisé. Les caractéristiques des veines et leurs relations avec l'environnement hôte peuvent donc être utilisées pour estimer leurs conditions de formation. Ces conditions, discutées à travers les thèmes suivants: (1) le régime tectonique; (2) le vecteur d'écoulement des fluides; (3) la profondeur crustale; (4) la perméabilité de l'environnement hôte; (5) la pression des fluides; (6) les conditions de précipitation des minéraux de remplissage; et (7) l'échelle des processus de remplissage des veines, serviront de base, en combinaison avec les modèles présentés précédemment, pour l'élaboration d'un mécanisme empirique de formation des veines.

Régime tectonique

Un régime tectonique en extension a été proposé pour la formation des veines au Chapitre 3. Ce régime tectonique est cohérent avec le fait que l'ensemble des veines aurifères montre des caractéristiques indiquant une ouverture des fractures en extension (Chap. 3). Ces caractéristiques, également typiques aux veines d'extension subhorizontales des gîtes filoniens orogéniques, correspondent à des contacts planaires, à une continuité latérale étendue, et à la présence de ponts (bridge stud) et de sauts en échelon des veines. Enfin, le système de veines en position initiale partage une direction commune avec les dykes syn-volcaniques de QFP (Chap. 3) qui eux, de par leur abondance impliquent un régime volcanique en extension (Gudmundsson, 1983). Ce parallélisme s'accorde avec un lien structural entre les deux générations d'éléments planaires et conséquemment avec un régime en extension pour la formation des fractures qui sont devenues des veines.

Vecteur d'écoulement des fluides

La géométrie du système de veines est révélatrice dans une certaine mesure des vecteurs d'écoulement. Les veines principales au Géant Dormant sont essentiellement parallèles aux couches (15, 20, 30, 40, A, H et I). Celles à angle, comme les veines 1, 3, 10 et 20s, constituent des structures minéralisées dont l'extension latérale et verticale est plus restreinte en comparaison avec les autres veines (Chap. 2: Tableau 2). Considérant que le système de veines est basculé avec les couches hôtes (Chap. 3: Fig. 18), les veines peuvent donc être considérées essentiellement comme des conduits subhorizontaux. Elles étaient donc perpendiculaires à subperpendiculaires par rapport à la direction d'écoulement des fluides vers la paléosurface. Puisque la décharge des fluides à la surface est fondamentale pour entretenir la circulation hydrothermale, les dykes de QFP constituent donc des conduits privilégiés vers la paléosurface (Chap. 3) en raison de: (1) leur direction subperpendiculaire à l'empilement volcanique; (2) leur grande continuité latérale et verticale; (3) leur lien spatial et chronologique avec les veines minéralisées; et (4) leur minéralisation et altération internes spécifiques. De plus, la modélisation a démontré que la signature $\delta^{18}O$ des dykes de QFP altérés et minéralisés est cohérente avec celle du quartz composant les veines (Chap. 5), démontrant ainsi le lien génétique entre les deux types de structures minéralisées. Par comparaison, les dykes de FP, qui précèdent les QFP et qui ne sont pas altérés, ni minéralisés (Chap. 2-3), sont des intrusions irrégulières et sans grande continuité apparente. Le rôle de conduit joué par les dykes de QFP et non par les dyke de FP repose probablement sur cette différence de continuité latérale, mais aussi sur la forte probabilité que les dykes de QFP constituaient lors de la formation des veines, les seules structures planaires qui atteignaient la surface du fond océanique (Annexe 1). Ces considérations géométriques indiquent que les veines correspondent essentiellement à des structures subparallèles aux couches, empilées dans la séquence volcanique le long des

dykes de QFP qui eux, constituent les conduits principaux de décharge des fluides hydrothermaux vers la paléosurface.

Profondeur crustale

La profondeur crustale est superficielle et estimée à environ 2-3 km sur la base de critères empiriques (voir ci-dessus). Cette profondeur crustale inclut la pression bathymétrique (> 3 150 m) exercée par la colonne d'eau de mer lors de la formation des veines (Chap. 3).

Perméabilité de l'environnement hôte

La perméabilité de l'empilement volcanique est considérée comme étant relativement faible (Chap. 3), en raison de l'homogénéité texturale des filons-couches et de leur nature intrinsèque imperméable (p. ex. Brace, 1984). De plus, ces filons-couches ont été initialement injectés au sein de sédiments fins, préalablement durcis et imperméabilisés par l'activité hydrothermale (Chap. 3).

Pression des fluides

Certains critères empiriques peuvent être utilisés pour estimer la pression limite et ses variations potentielles. Ainsi, le fait que les veines soient essentiellement subhorizontales lors de leur formation implique que la pression des fluides était suffisante pour maintenir ouverte des fractures perpendiculaires à la charge lithostatique ($\sigma 1$). Cette considération s'accorde avec la nature imperméable de l'environnement hôte. Ainsi, la pression des fluides peut être caractérisée de lithostatique. Considérant le cadre tectonique en extension, la pression des fluides (P_f) peut être définie mathématiquement par: $P_f = \rho_r g z = \sigma 1$, où ρ_r est la densité des roches, g la force gravitationnelle et z la profondeur.

Les variations de pression d'un système hydrothermal sont révélées par la présence de brèches hydrothermales. En milieu imperméable et suprahydrostatique, la bréchification hydrothermale des épontes se produit par explosion et par implosion (Jébrak, 1998), suite à la pressurisation des fluides à des niveaux excédants les conditions lithostatiques et la résistance à la tension du matériel (T). La bréchification par explosion, correspond à une fracturation hydraulique induite par une forte pression des fluides, où $P_f > \rho_r gz + T$ (Phillips, 1972). La bréchification par implosion se produit lorsqu'un conduit, pressurisé à un niveau supralithostatique $P_f \geq \rho_r gz + T$, subi un relâchement brusque de la pression des fluides. Ceci a pour effet d'engendrer l'expansion instantanée des fluides pressurisés se trouvant dans les épontes de la veine (Fig. 4). La bréchification par implosion se produit si la différence entre la pression dans la roche et celle dans l'ouverture est supérieure à la résistance à la tension du matériel (T) (Philips, 1972; Sibson, 1987; Craw et McKeag, 1995). Dans le cas du Géant Dormant, l'absence caractéristique de bréchification des épontes en bordures des veines est donc un élément diagnostique des conditions de formation des veines. Ainsi, la pression maximale des fluides correspond à une valeur égale ou faiblement supérieure à celle de la pression lithostatique, mais inférieure à celle combinant la pression lithostatique et la résistance à la tension du matériel. Ainsi, la pression maximale des fluides correspond à: $\sigma 1 \leq P_f < \sigma 1 + T$. Dans ces conditions, des variations de la pression des fluides sont possibles sans pour autant engendrer la bréchification hydrothermale des épontes.

Condition de précipitation des minéraux de remplissage

Plusieurs études ont démontré que les textures de remplissage du quartz caractérisent les conditions de formation des veines (Dowling et Morrison, 1989; Vearncombe, 1993; Dong et al., 1995). Au Géant Dormant, les veines résultent de la

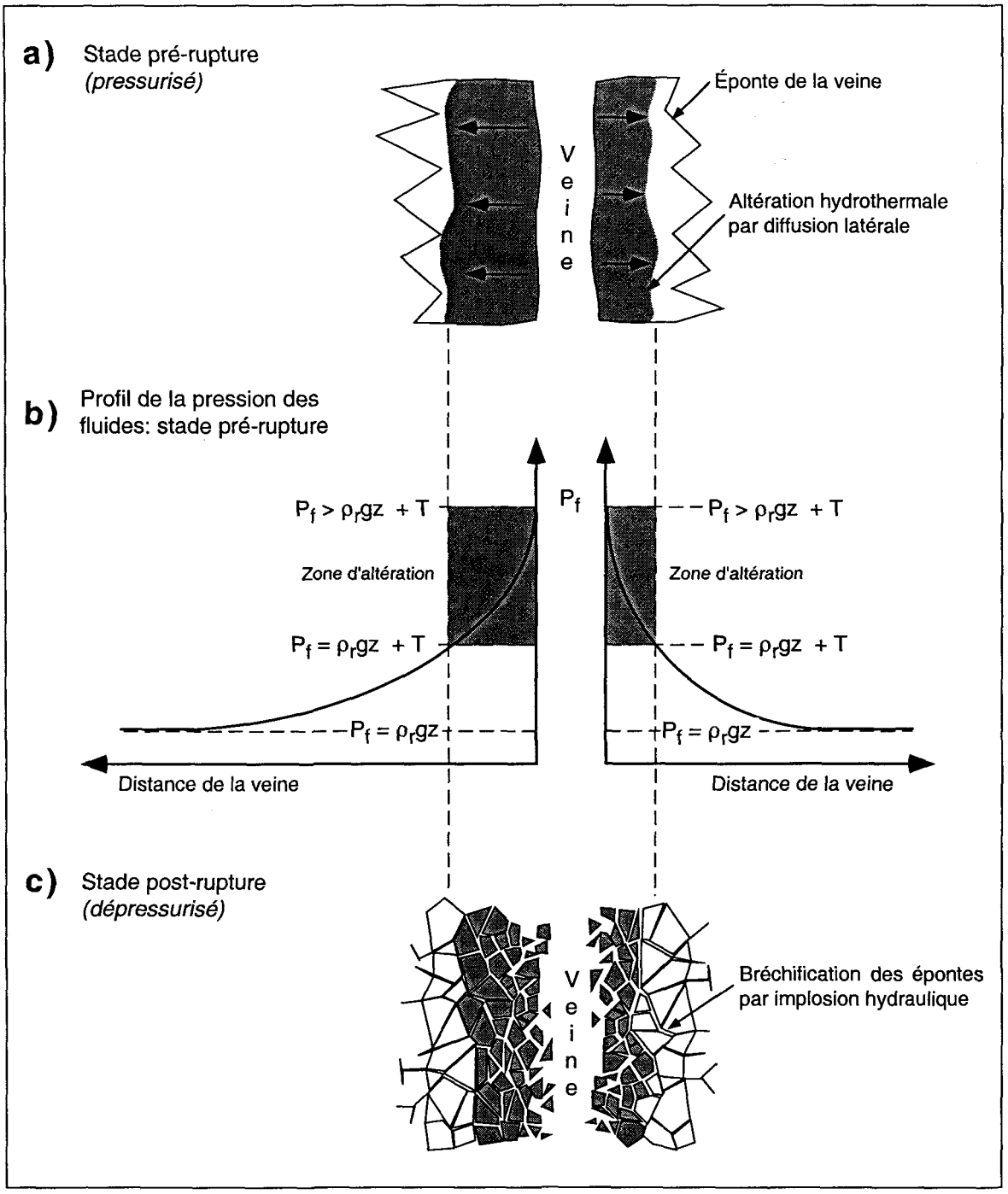

Figure 4. Mécanisme de formation des brèches hydrothermales à fragments d'épontes pour un système hydrothermal surpressurisé, adapté à partir des concepts développés par Craw et McKeag (1995). (a) Représentation schématique de l'altération hydrothermale des épontes d'une veine surpressurisée. (b) Profil schématique de la pression des fluides hydrothermaux dans les épontes. (c) Bréchification des épontes par implosion hydraulique suite au relâchement de la pression effective et à l'expansion des fluides se trouvant dans les épontes.

superposition complète ou partielle des différentes phases de remplissage successif, qui composent les trois stades paragénétiques (Chap. 5: Fig. 5). La séquence paragénétique du stade pré-minéralisation se compose de 3 phases successives de remplissage de quartz (Chap. 5), caractérisées par des teintes et des textures distinctes. La première phase correspond au quartz gris à noirâtre (référé ci-dessous comme gris) qui constitue communément la majeure partie du quartz dans les veines (Fig. 5a). Ce quartz forme des veines d'aspect massif composées de cristaux grossiers, de taille uniforme (< 2 cm) et dont l'axe C est communément aléatoire ou localement orienté perpendiculairement aux épontes (texture dendritique). La seconde phase correspond à un quartz laiteux et microcristallin qui forme un mince ciment entre les cristaux de quartz gris (Fig. 5b). Enfin, la dernière phase correspond à un quartz blanc qui forme des veinules planaires et subparallèles (< 5 cm) de type *crack-seal* (Fig. 5c).

Le développement de veines de quartz massif, composées de gros cristaux uniformes, implique un remplissage homogène de la fracture hôte, qui suppose des conditions de précipitation stables (Vearncombe, 1993) et une ouverture relativement constante de la fracture (Jébrak, 1992). À l'inverse, le quartz microcristallin en ciment implique une cristallisation rapide, conséquente à une déstabilisation des conditions de précipitation du quartz (Vearncombe, 1993). Les attributs texturaux du quartz laiteux sont compatibles avec une bréchification par implosion des veines due à la dépressurisation des conduits (Jébrak, 1992). Quant aux veinules de type *crack-seal*, leur formation indique des conditions relativement stables et une cristallisation constante pendant l'ouverture (Ramsay, 1980). La différence de texture entre les veines de quartz gris et celle de type *crack-seal* est probablement dépendante du taux d'ouverture et de remplissage des fractures qui est vraisemblablement plus rapide pour les veines de type *crack-seal* en raison de la taille réduite des cristaux.

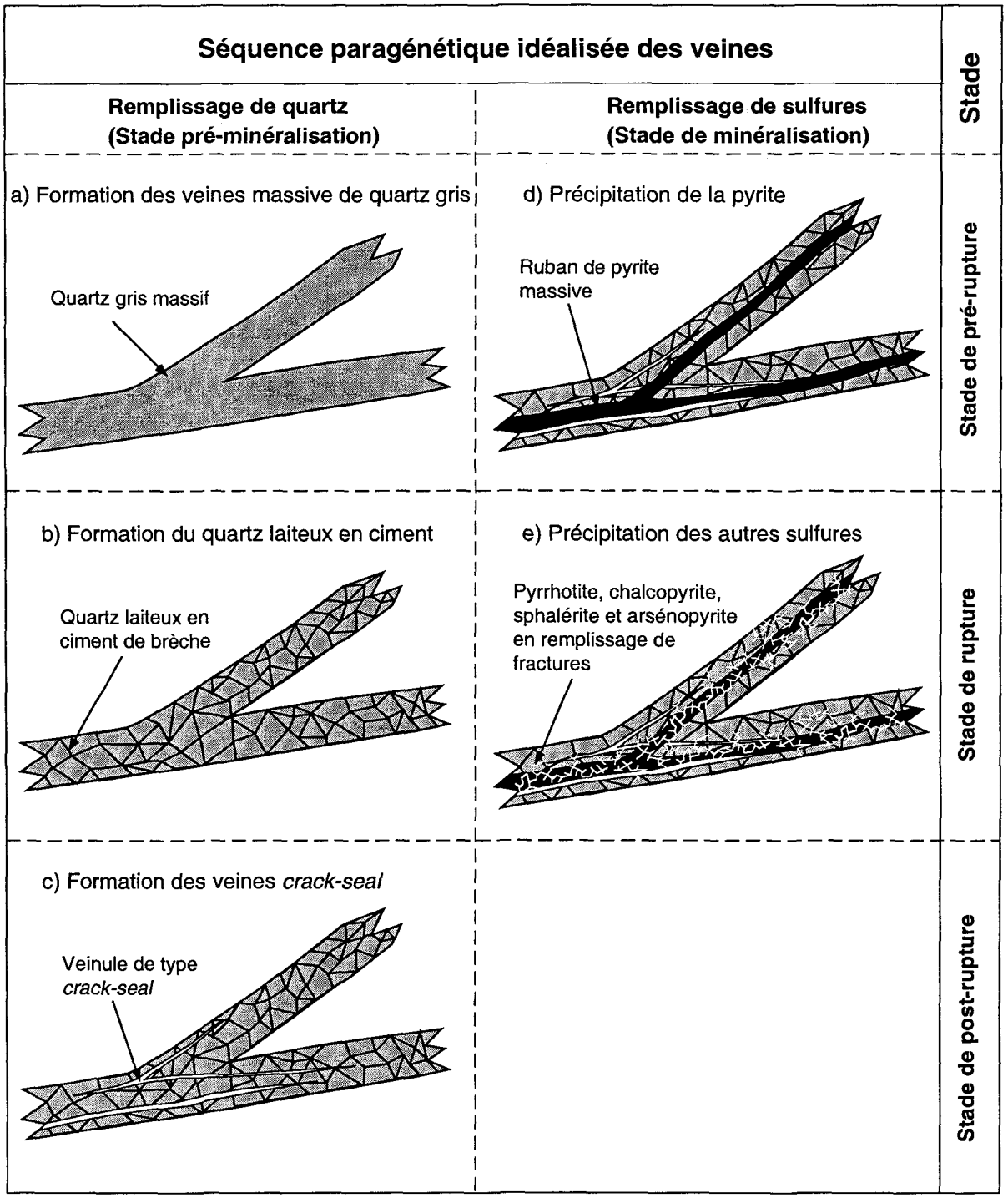

Figure 5. Séquence de remplissage en quartz et en sulfures des veines aurifères. Les différents stades font référence au modèle proposé pour la formation des veines, schématisé aux figures 6 et 7.

En combinant les contraintes fixées par la pression des fluides et celles indiquées par la texture de remplissage du quartz, les implications suivantes peuvent être dégagées. Le stade de remplissage de quartz gris témoigne d'une période de conditions relativement stables, où la pression des fluides est constante et légèrement supérieure à celle lithostatique ($\sigma 1 \leq P_f < \sigma 1 + T$) pour tenir compte de l'ouverture lente et constante des fractures. Le quartz laiteux en ciment implique un événement de relâchement de la pression de fluide ($P_f < \sigma 1$) qui engendre la précipitation instantanée du quartz. À ce moment, aucune bréchification des épontes n'est induite en raison de la pression des fluides avant rupture qui était inférieure à la résistance en tension des roches ($\sigma 1 \leq P_f < \sigma 1 + T$). Quant aux veinules de type *crack-seal*, leur distribution aléatoire au sein des veines existantes et leurs relations mutuelles de recoupement (Chap. 5: Fig. 6b) suggèrent qu'elles sont reliées à des événements locaux et répétitifs de pressurisation des fluides.

Pour les sulfures (Chap. 5), la paragénèse séquentielle est également suggestive d'une évolution temporelle analogue à celle qui caractérise la séquence de remplissage du quartz. Ainsi, une période de conditions stables, dominée par $\sigma 1 \leq P_f < \sigma 1 + T$ durant laquelle s'est produit la réouverture des veines de quartz existantes et la précipitation de la pyrite en remplissage de cavités, est suggérée par les amas et les rubans massifs de pyrite (Fig. 5d). Des événements subséquents de bréchification hydrothermale intra-veines, reliées probablement à la variation de la pression des fluides, ont engendré la précipitation en remplissage de fractures des autres sulfures (Fig. 5e).

Échelle des processus de remplissage des veines

Dans les systèmes de veines épithermales, la zonalité verticale typique se manifeste par une variation de la composition métallique et minéralogique et de la texture des veines (White et al., 1995; Panteleyev, 1996). Cette zonalité témoigne de l'évolution chimique

progressive des fluides lors de leur ascension et des conditions physico-chimiques variables en fonction de la profondeur crustale de formation des veines. En comparaison, le système de veines au Géant Dormant est caractérisé par une homogénéité chimique et texturale. L'homogénéité chimique est exprimée par l'assemblage minéralogique relativement uniforme des veines (Annexe 4) et par la composition en éléments traces (Chap. 4) et isotopique (Chap. 5) des minéraux de remplissage. Quant aux textures de remplissage, les différentes veines sont caractérisées par les mêmes relations chronologiques et texturales (Annexe 4). L'homogénéité chimique des veines implique qu'elles ont été formées par un ou des fluides de même composition chimique. Parallèlement, l'homogénéité texturale implique que la précipitation des minéraux de remplissage résulte d'une série de processus communs à l'échelle du dépôt.

D'autre part, la jonction entre les veines de différentes attitudes, sans relation de recoupement, démontre que leur formation résulte de processus contemporains (Chap. 2). Cette relation est pertinente à la compréhension de l'homogénéité des veines dans la mesure où leur formation résulte d'un processus de remplissage polyphasé (Fig. 5). Ainsi, quoique les différents stades de remplissage se superposent les uns sur les autres dans une veine, il y a pas de relation de recoupement entre les différents stades de remplissage à la jonction de deux veines (Fig. 5). En d'autres termes, les veines interconnectées partagent les mêmes phases de remplissage. Cette relation indique que le remplissage n'est pas un processus propre à une veine spécifique, mais que chaque stade de remplissage correspond à un événement unique, enregistré par les veines en formation. Cette particularité s'accorde bien avec les implications dégagées précédemment concernant l'homogénéité des fluides et des processus de dépôt.

Mécanisme empirique de formation des veines

Sur la base des contraintes déterminées précédemment et en considérant les fondements des deux modèles documentés, un mécanisme de formation en 3 stades est proposé. Il est dénommé mécanisme de la *pression régularisée*. Le terme *régularisé* est ici utilisé pour qualifier le régime constant de la pression des fluides, régularisé par les dykes de QFP. Ceux-ci agissent essentiellement comme des tampons ou des amortisseurs contrôlant les variations de la pression des fluides.

Stade pré-rupture

Le stade pré-rupture correspond à un état stable du système hydrothermal (t0-t1; Fig. 6) où la pression des fluides est à un niveau lithostatique ($\sigma 1 \leq P_f < \sigma 1 + T$). La pression constante des fluides est contrôlée par les dykes de QFP, qui agissent comme des régulateurs sur le débit des fluides se déchargeant à la paléosurface (Fig. 7a). C'est durant cette période que se forment le remplissage de quartz gris des veines. La formation des veines est essentiellement contrôlée par la présence de fractures préexistantes (Chap. 2), une caractéristique qui s'accorde avec une pression des fluides inférieures à la limite critique de la fracturation hydraulique (Phillip, 1972). Au niveau des veines en formation, les conditions stables de la pression des fluides favorisent ainsi l'ouverture lente et progressive des fractures et la croissance des cristaux de quartz. La précipitation du quartz est favorisée par la pression ambiante au sein des fractures ouvertes qui est légèrement plus faible que celle des roches hôtes (milieu de base pression). Par comparaison, les dykes de QFP constituent des conduits de plus forte pression, peu favorables à la précipitation de la minéralisation (Ridley, 1993). La circulation des fluides au sein des veines en formation est maintenue active par la décharge vers la paléosurface d'une partie des fluides via les dykes de QFP (Fig. 7a). Cet apport de fluides juvéniles constant est en accord avec l'homogénéité

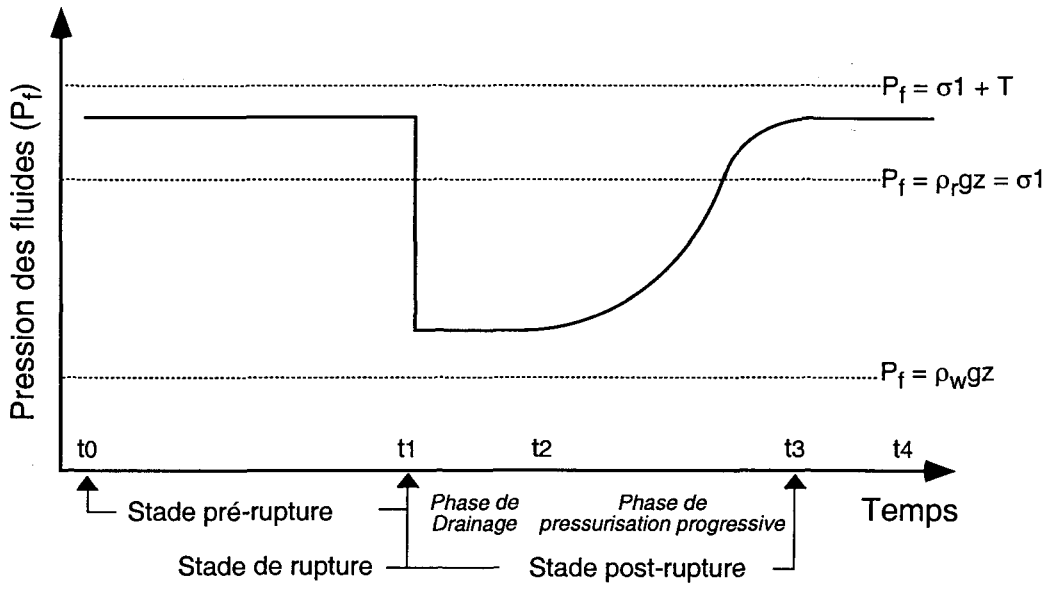

t0-t1: Conditions de stabilité, pression lithostatique des fluides et formation des veines de quartz gris. Décharge faible des fluides hydrothermaux à la surface du fond océanique via les dykes de QFP.

t1: Rupture de la pression des fluides, précipitation instantanée du quartz laiteux en ciment. Décharge des fluides à la surface.

t1-t2: Condition de drainage du réservoir hydrothermal. Écoulement des fluides à la surface du fond océanique en conditions presque hydrostatiques. Pas de formation de veine durant cet épisode.

t2-t3: Repressurisation progressive du système hydrothermal. Conditions locales de haute pression des fluides qui engendrent la formation des veinules de type *crack-seal*.

t3-t4: Retour aux conditions de stabilité initiales. Le cycle recommence avec la précipitation des sulfures.

Figure 6. Diagramme de la pression des fluides en fonction du temps, illustrant la variation de la pression invoquée pour la formation des veines à la mine Géant Dormant.

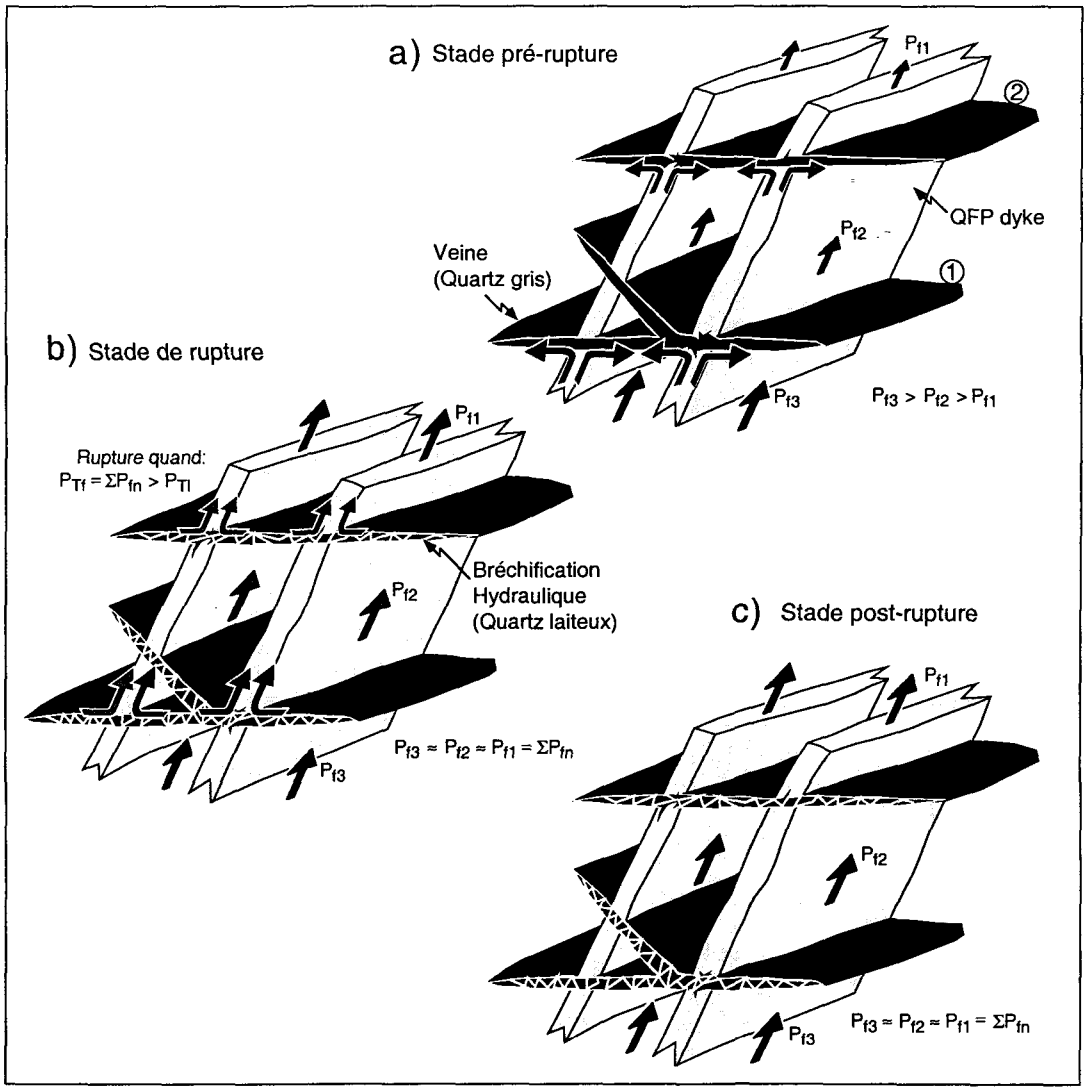

Figure 7. Croquis illustrant les relations géométriques entre les veines et les dykes de QFP, ainsi que les vecteurs d'écoulement des fluides (flèches) et la pression relative des fluides (taille des flèches) pour chacun des trois stades du mécanisme de la pression régularisée. (a) Stade pré-rupture. Les fluides sont maintenus à une pression lithostatique constante grâce au contrôle exercé par les dykes de QFP sur le débit des fluides vers la paléosurface. La pression des fluides permet l'ouverture lente et progressive de fractures orientées à angles forts par rapport à la charge lithostatique, et la formation des veines par la croissance de cristaux de quartz idiomorphes (quartz gris) dans un milieu rempli de fluides. Les numéros indiquent la chronologie relative. (b) Stade de rupture. La rupture survient à un état critique du système pressurisé, lorsque la pression totale des fluides dans l'ensemble de la pile volcanique excède celle de la charge lithostatique totale. La précipitation du quartz microcristallin est induite instantanément en raison du drainage des fluides se trouvant dans les veines en formation. (c) Stade post-rupture illustrant le drainage des fluides vers la paléosurface, sans contribution à la formation des veines car la pression des fluides est insuffisante pour les garder ouvertes.

du système de veines. Le volume de fluides déchargé correspond à la différence entre le volume d'afflux de fluides juvéniles et celui nécessaire pour maintenir une pression dans la ou les veines en formation à une profondeur spécifique. Il est proposé que l'état de pressurisation se développe progressivement à différents niveaux, de la partie inférieure vers la partie sommitale de l'empilement volcanique imperméable (Fig. 7a) et que, à un stade avancé, la majeure partie de l'empilement volcanique devient pressurisée par les fluides.

Stade de rupture

Le stade de rupture correspond au relâchement de la pression des fluides (t1; Fig. 6). Ce stade se manifeste par l'omniprésence du quartz laiteux en ciment dans les veines de quartz gris (Fig. 7b). Suite à la rupture, les fluides emmagasinés dans les veines en croissance sont drainés vers la paléosurface (Fig. 7b). Une telle rupture indique que la pression des fluides est passée d'un régime lithostatique ($P_f \approx \sigma 1 \approx \rho_r gz$) à un régime suprahydrostatique ($\rho_w gz < P_f < \sigma 1$; où ρ_w est la densité des fluides). Cette dépressurisation des fluides est attribuable à l'augmentation soudaine de la perméabilité au sein des dykes de QFP qui résulte de facteurs extrinsèques ou intrinsèques au système hydrothermal. Dans le premier cas, il s'agit par exemple d'une perméabilité fissurale induite par des mouvements normaux le long des dykes de QFP, dus à la subsidence de l'édifice volcanique. Dans le second cas, la dépressurisation peut correspondre à un état critique du système qui se manifeste à une phase avancée du stade pré-rupture, et où l'ensemble du système est pressurisé. À un état où la pression totale des fluides excède la pression lithostatique totale ($P_{fT} > P_{lT}$), c'est-à-dire quand l'ensemble de la pile volcanique est pressurisé par les fluides hydrothermaux, il s'ensuit une rupture hydraulique de la partie sommitale de l'empilement qui provoque la dépressurisation instantanée et intégrale du

système hydrothermal. Cette dernière hypothèse est préférée puisqu'elle explique mieux le caractère relativement homogène du système de veines. Toutefois, les évidences d'une telle bréchification de la partie sommitale demeure spéculatives.

Stade post-rupture

Le stade post-rupture correspond à un état transitoire et métastable du système hydrothermal. Il se subdivise en deux phases distinctes que sont le drainage (t1-t2; Fig. 6) et la repressurisation progressive (t2-t3; Fig. 6). Suite à la rupture (t1; Fig. 6), le réservoir hydrothermal sous-jacent est drainé et la décharge à la paléosurface se produit à un régime suprahydrostatique ($\rho_w gz < P_f < \sigma 1$). Durant la phase de drainage, il n'y a pas de contribution à la formation des veines (Fig. 7c). Les veines sont alors des structures fermées, isolées de la circulation hydrothermale, en raison de la pression insuffisante des fluides pour les maintenir ouvertes. Cette phase permet de réduire la pression effective du réservoir hydrothermal sous-jacent. Après un certain temps (t2; Fig. 6) le débit des fluides hydrothermaux, déchargés à la paléosurface, diminue proportionnelement avec la pression effective du réservoir. Il s'ensuit un colmatage progressif des conduits hydrothermaux (dykes de QFP), induit par la précipitation de minéraux hydrothermaux comme le quartz (p. ex. Sibson et al., 1988). Une telle précipitation de quartz s'accorde avec le gain considérable en SiO_2 enregistré par ces dykes (Chap. 3). Progressivement, le système hydrothermal se pressurise à nouveau (t2-t3; Fig. 6). Il est probable que les veinules de type *crack-seal* se forment durant cette phase, étant le résultat de la pressurisation locale des fluides. Finalement, le système retrouve l'état de stabilité à une pression lithostatique ($\sigma 1 \leq P_f < \sigma 1 + T$) caractérisant le stade pré-rupture (t3-t4; Fig. 6).

La répétition complète des stades du mécanisme (t0-t4; Fig. 6) se résume, selon les données actuelles, à deux épisodes. Comme mentionné précédemment, la séquence

paragénétique des sulfures est également compatible avec un cycle complet. Ainsi, la précipitation de la pyrite en remplissage de cavités correspond au stade pré-rupture alors que le stade de rupture est manifesté par les autres sulfures en remplissage de fractures. Avec le drainage subséquent des fluides vers la paléosurface du fond océanique, le système hydrothermal prend fin progressivement. Toutefois, il est possible que le système hydrothermal a continué à se décharger sur le fond océanique, donnant ainsi naissance à un amas de sulfures massifs volcanogènes, et que la fin réelle du système hydrothermal n'a pas été enregistrée par les veines elles-mêmes.

Comparaison entre les mécanismes de formation des veines

La figure 8 résume les attributs du mécanisme de la *pression régularisée*. Le tableau 1 expose les caractéristiques spécifiques de chacun des trois mécanismes de formation des veines. La figure 8 et le tableau 1 font ressortir l'aspect transitionnel entre les trois mécanismes aux niveaux de la profondeur crustale, du régime tectonique, de la pression des fluides et de leur rôle intrinsèque sur la formation des veines. Le mécanisme de la *pression régularisée* apparaît comme transitionnel au niveau crustal (2-5 km) entre le mécanisme des failles-valves (5-15 km) et celui des pompes sismiques (0-2 km). En termes tectoniques, le mécanisme de la *pression régularisée* est également associé à un régime tectonique spécifique en extension alors que les failles-valves et les pompes sismiques sont associés respectivement aux régimes chevauchant et décrochant. Pour la pression des fluides, le mécanisme de la *pression régularisée*, avec une pression lithostatique ($\rho_r gz \leq P_f < \rho_r gz + T$), s'intercale entre la pression supralithostatique ($P_f > \rho_r gz + T$) des failles-valves et la pression hydrostatique ($P_f \approx \rho_w gz$) des pompes sismiques. Quant au rôle des fluides, il peut être considéré comme: actif pour les failles-valves, puisque la pression des fluides engendre la fracturation hydraulique et la sismicité; passif pour les pompes sismiques, en

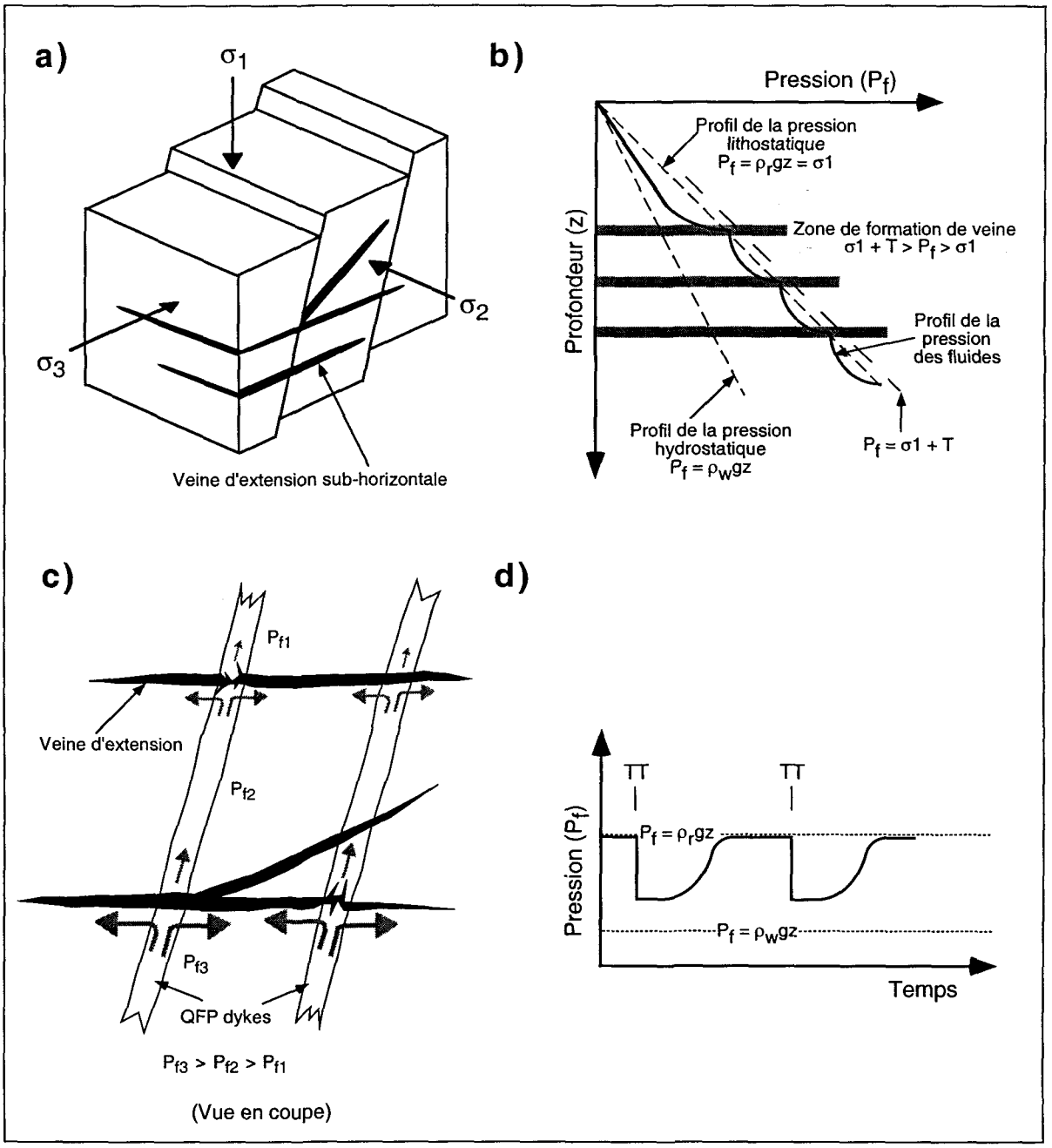

Figure 8. Résumé des caractéristiques s'appliquant au modèle de la pression régularisée. (a) Régime tectonique en extension et champ de contraintes associé. (b) Diagramme de la pression des fluides en fonction de la profondeur. Le profil illustré correspond à un état avancé du stade de pré-rupture. (c) Représentation schématique des relations géométriques entre les veines et les dykes de QFP. Les flèches montrent la direction de l'écoulement des fluides et leur grosseur est représentative de l'afflux de fluides. (d) Diagramme de la pression en fonction du temps, illustrant la fluctuation de la pression des fluides et la bi-cyclicité proposée du mécanisme dans le cas présent. TT signifie tremblement de terre.

Tableau 1. Comparaison des caractéristiques entre les trois mécanismes

Élément	Failles-valves	Pression régularisée	Pompe sismique
Profondeur crustale	5-15 km	2-5 km	0-2 km
Régime tectonique	Chevauchant	Extension	Décrochant
Pression des fluides	Supralithostatique $P_f > \rho_r gz + T$	Lithostatique $P_f = \rho_r gz = \sigma 1$	Hydrostatique $P_f = \rho_w gz$
Rôle des fluides	Actif: provoque la rupture tectonique	Semi-actif: provoque la rupture lorsque la $P_{fT} > P_{lT}$	Passif: ne provoquent pas de rupture tectonique
Texture des veines (Brèche)	Présence de brèche hydrothermale	Absence de brèche hydrothermale	Présence de brèche hydrothermale
Altération hydrothermale	Altération des épontes sur quelques mètres	Pas ou peu d'altération des épontes des veines	Halo d'altération à l'échelle du système de veines
Répétition du cycle	Multiple	Unitaire	Multiple

raison du fait que la pression des fluides est indépendante de la sismicité et du tectonisme; et semi-actif pour le mécanisme de la *pression régularisée*, étant donné que les fluides jouent un rôle partiel sur la fracturation et la sismicité induite.

D'autre part, trois éléments caractérisant le mécanisme de la *pression régularisée* sont distincts comparativement aux deux autres, soit: (1) l'absence de brèche hydrothermale à fragments d'épontes dans les veines; (2) la faible altération hydrothermale associée aux veines; et (3) le caractère peu répétitif du mécanisme. L'absence de brèche hydrothermale a été discutée précédemment et résulte de la pressurisation des fluides à un niveau lithostatique inférieur à celui nécessaire pour engendrer la bréchification (Fig. 4). L'étendue et la distribution spatiale des altérations hydrothermales caractérisent les conditions de circulation et de pression des fluides. Pour les minéralisations développées par le mécanisme de pompe sismique, le large halo d'altération ceinturant les veines est attribuable aux conditions de forte perméabilité et de pression hydrostatique, qui permettent une percolation étendue des fluides (p. ex. Bogie et Lawless, 1987; White et Hedenquist, 1990). Pour les veines reliées génétiquement au mécanisme de faille-valve, l'altération hydrothermale des épontes résulte de la percolation des fluides sous la forte pression ($P_f \geq \sigma 1 + T$) des fluides (Cox et al., 1990) durant la période d'ouverture des fractures (Fig. 4b). Dans le cas spécifique du Géant Dormant, il est proposé que (1) l'imperméabilité de la séquence a inhibé le développement d'un large halo d'altération; et que (2) les épontes des veines ont été essentiellement préservées de l'altération par percolation en raison de la pression des fluides inférieure à celle nécessaire pour pénétrer les parois de la roche encaissante ($P_f < \sigma 1 + T$; Fig. 4b). En outre, l'imperméabilisation des parois des veines par la précipitation précoce du quartz (encroûtement) peut également contribuer à limiter l'interaction fluide-roche et donc limiter le développement de l'altération hydrothermale dans les épontes. La répétition temporelle des mécanismes de

faille-valve et de pompe sismique est une caractéristique propre à la formation de veines volumineuses. Pour ces mécanismes, la contribution majeure à la formation des veines se produit dans les phases instables de la pressurisation et de la dépressurisation du système. Pour le mécanisme de la *pression régularisée*, la formation des veines résulte essentiellement de l'état pressurisé stable. La répétition temporelle du cycle, si ce n'est que pour engendrer la maturation du système hydrothermal, ne constitue donc pas un facteur essentiel à la formation de veines volumineuses.

Applicabilité du mécanisme de la pression régularisée

Les conditions d'application du modèle de la *pression régularisée* reposent sur la coexistence de trois caractéristiques que sont: (1) un environnement hôte imperméable pour favoriser la pressurisation des fluides; (2) des zones tabulaires de faible perméabilité recoupant à angle fort l'empilement volcanique imperméable, pour assurer la décharge des fluides et régulariser la pression des fluides; et (3) des anisotropies planaires subhorizontales pour favoriser la formation de veines dans des fractures non connectées avec la surface.

Ces trois conditions, à la lumière de la faible profondeur crustale et du régime en extension inférés, peuvent être considérées comme relativement particulières, un point supporté par la rareté de gîtes aurifères analogues au Géant Dormant. Toutefois, le gisement filonien de type épithermal *low-sulfidation* de la mine Emperor (Chap. 2), localisé dans les îles Fidji, peut être considéré comme un analogue récent sur la base des caractéristiques suivantes:

1) L'abondance de veines volumineuses de quartz aurifères subhorizontales (< 45°) développées principalement le long des couches volcaniques (Anderson et Eaton, 1990).

2) La faible altération hydrothermale en bordure des veines qui varie de 0 à 5 cm d'épaisseur (Ahmad et Walshe, 1990; Anderson et Eaton, 1990).
3) Le halo d'altération faible à inexistant, indiquant la faible perméabilité des roches encaissantes (Ahmad et Walshe, 1990; Eaton et Setterfield, 1993).
4) L'abondance de dykes subverticaux fortement altérés mais faiblement minéralisés recoupant les couches strates volcaniques (Anderson et Eaton, 1990).
5) L'homogénéité métallique et minéralogique du système de veine à l'échelle du dépôt, qui s'étend latéralement et verticalement sur plus de 2 500 et 800 m respectivement (Ahmad et al., 1987; Anderson et Eaton, 1990).
6) La profondeur crustale superficielle de formation comprise entre 2 et 3 km considérant le niveau d'érosion actuel (Anderson et Eaton, 1990; Richards, 1990).
7) Le régime tectonique en extension, inféré à partir de la localisation du gisement en bordure de la caldeira Tavua (Richards, 1995).

À l'exception de la paragénèse plus complexe des veines (Ahmad et al., 1987), les caractéristiques énumérées ci-dessus se comparent à celles du Géant Dormant mais sont atypiques en comparaison avec les gîtes épithermaux de type *low-sulfidation* (White et al., 1995; Panteleyev, 1996). De plus, ces caractéristiques s'accordent également avec celles considérées comme fondamentales pour la formation de veines par le mécanisme de la *pression régularisée*. Sur la base de ces arguments, le mécanisme de la *pression régularisée* semble applicable à ce gisement filonien. Il est donc raisonnable de suggérer que ce mécanisme puisse être appliqué à d'autres gisements filoniens pour expliquer la formation de veines subhorizontales en contexte superficiel et en régime d'extension.

Paragénèse des veines versus les systèmes volcanogènes

Le passage des silicates aux sulfures comme minéraux de remplissage peut être attribuable à la maturation du système hydrothermal, telle que documentée pour les systèmes volcanogènes (Large, 1992; Ohmoto, 1996). Le passage des silicates aux sulfures se traduit également par l'augmentation de la température des fluides de 275 à 350°C (Chap. 5). Dans le cas présent, la maturation est probablement conséquente à la phase de drainage des fluides lors du stade post-rupture. Une hypothèse qui peut être envisagée est que l'augmentation du débit des fluides vers la paléosurface a induit l'élargissement et l'abaissement vers la source de chaleur des cellules de convection, engendrant ainsi le réchauffement du système hydrothermal (Galley, 1992; Brauhart et Groves, 1998).

D'autre part, l'assemblage paragénétique des veines au Géant Dormant et son évolution au niveau de la température apparaît problématique en comparaison avec les caractéristiques minéralogiques des amas de sulfures massifs volcanogènes. Toutefois, les comparaisons doivent être dosées en fonction du fait que les veines représentent un environnement de formation distinct par rapport aux amas de sulfures massifs formés par des exhalations sur le fond océanique ou par remplacement près de la surface. Le modèle proposé pour la formation des veines implique également que les fluides sont continuellement déchargés sur le fond océanique. Les veines n'ont donc enregistré qu'une partie des caractéristiques du système hydrothermal. Les mécanismes de précipitation sont aussi passablement différents pour les deux environnements. Pour la formation des amas exhalatifs de sulfures, la précipitation des sulfures résulte communément du mélange avec l'eau de mer froide, qui induit une baisse de température instantanée (p. ex. Herzing et

Hannington, 1995; Ohmoto, 1996). Pour la formation des veines, une baisse de la pression des fluides est invoquée comme le facteur prépondérant pour la précipitation des minéraux hydrothermaux.

Le fait que le quartz soit précipité à 275°C dans les veines sans association avec des métaux de basse température (Zn, As), comme on devrait s'attendre pour les systèmes volcanogènes exhalatifs, peut refléter simplement la sursaturation de la silice dans le fluide par rapport à la concentration sous-saturée des métaux en solution. La précipitation du quartz est d'ailleurs documentée dans certaines zones de filonets sous-jacentes à des amas de sulfures massifs exhalatifs, où la précipitation du quartz est favorisée par la nucléation le long des parois des fractures et par la température de refroidissement qui est très faible (Ohmoto, 1996). Par ailleurs, l'utilisation des diagrammes de stabilité des sulfures versus la température, développés pour les systèmes volcanogènes aurifères (Hannington et al., 1997), est problématique pour le cas du Géant Dormant. À 350°C, il est difficile d'expliquer la coexistence de la pyrite, de la pyrrhotite, de la chalcopyrite et de la sphalérite, de même que la forte teneur en or et en argent de ces sulfures (Chap. 4). La difficulté d'utilisation de ces diagrammes réside probablement dans le fait que les sulfures ont précipité par dépressurisation dans les veines au Géant Dormant. En bref, une comparaison en détail des caractéristiques des veines du Géant Dormant avec celles des amas sulfurés volcanogènes peut être hasardeuse, même si dans les faits plusieurs caractéristiques décrites précédemment appuient l'origine volcanogènes des veines.

FACTEURS CONTROLANT L'ENRICHISSEMENT EN OR

Des travaux récents ont permis de démontrer que les fluides volcanogènes possèdent une grande capacité pour transporter l'or (Poulsen et Hannington, 1995; Hannington et al., 1997). Toutefois, les causes exactes de l'enrichissement primaire de certains gisements volcanogènes demeurent un sujet de discussion. Selon Hannington et al. (1997), l'enrichissement en or est attribuable essentiellement à deux facteurs, soit à des fluides enrichis en or, soit à un mécanisme de précipitation efficace, ou encore à une combinaison des deux facteurs.

L'enrichissement primaire des fluides est principalement attribué à une contribution magmatique en or due à la séparation d'une solution riche en or à la fin de la cristallisation des magmas felsiques (Sillitoe, 1989; 1995; de Ronde, 1995). D'autre part, une chimie favorable des fluides pour le transport de l'or, due à leur interaction avec des roches volcaniques felsiques calco-alcalines, a également été proposée pour expliquer les valeurs atypiques (3-30 ppm Au) des systèmes volcanogènes actifs dans les environnements modernes de bassins arrières-arcs (Herzing et al., 1993).

L'ébullition est considérée comme le mécanisme prédominant pour la précipitation de l'or (Hannington et al., 1997). Pour les systèmes ouverts, où les fluides hydrothermaux s'échappent librement sur le fond océanique, l'ébullition est limitée par la pression de confinement hydrostatique, restreignant ainsi l'action de ce mécanisme à des environnements marins peu profonds (Hannington et al., 1997). Le gisement de la mine Eskay Creek est considéré comme le cas type de minéralisation volcanogène développée en milieu sous-marin peu profond et où l'ébullition des fluides a induit l'enrichissement en or des veines et lentilles de sulfures (p. ex. Roth et al., 1997).

Teneur en or des différents événements de minéralisation

La teneur en or des veines au Géant Dormant (Fig. 9) est au moins 10 fois supérieures, et même jusqu'à 1000 fois supérieures à la concentration typique des amas sulfurés volcanogènes archéens (p. ex. Chartrand et Cattalani, 1990). Par contre, le premier événement de minéralisation, qui est typique de l'activité hydrothermale de fond océanique, est caractérisé par une teneur aurifère (Fig. 9) comparable à celle des systèmes volcanogènes classiques (Chap. 3). Les analyses en éléments traces des sulfures (Chap. 4) démontrent que la teneur en or est faible pour l'ensemble des minéralisations disséminées (Fig. 9), et ce indépendamment de leur chronologie de formation, incluant la pyrrhotite et la chalcopyrite dans les coussins, ainsi que la pyrite dans la dacite et les dykes de QFP. Les fortes teneurs aurifères sont donc associées exclusivement au style de minéralisation en veines. Cette particularité implique que la forte teneur en or des veines résulte d'un enrichissement spécifique lors de la terminaison de l'activité hydrothermale (Fig. 1) et/ou que le mécanisme de précipitation de l'or dans les veines est plus efficace. Ces deux points sont discutés ci-dessous à la lumière des données présentées dans les chapitres précédents.

Enrichissement primaire des fluides minéralisateurs

Une contribution magmatique est appuyée par la valeur élevée du $\delta^{18}O$ de 4,7‰ calculée à 275°C pour le fluide minéralisateur (Chap. 5) à l'origine des veines. Toutefois, une contribution magmatique de fluides, uniquement lors de la formation des veines est incohérente avec les valeurs constantes du Se dans les sulfures des différents événements de minéralisation (Chap. 4). Parallèlement, la valeur du $\delta^{18}O$ de 3,2‰ calculée à 250°C pour le fluide minéralisateur du premier événement de minéralisation peut s'expliquer par la dilution d'un fluide initialement lourd ($\delta^{18}O \approx 5$ ‰) par l'eau de mer (Chap. 5). Ainsi, il est fort probable que la contribution magmatique en fluides a été constante tout au long de

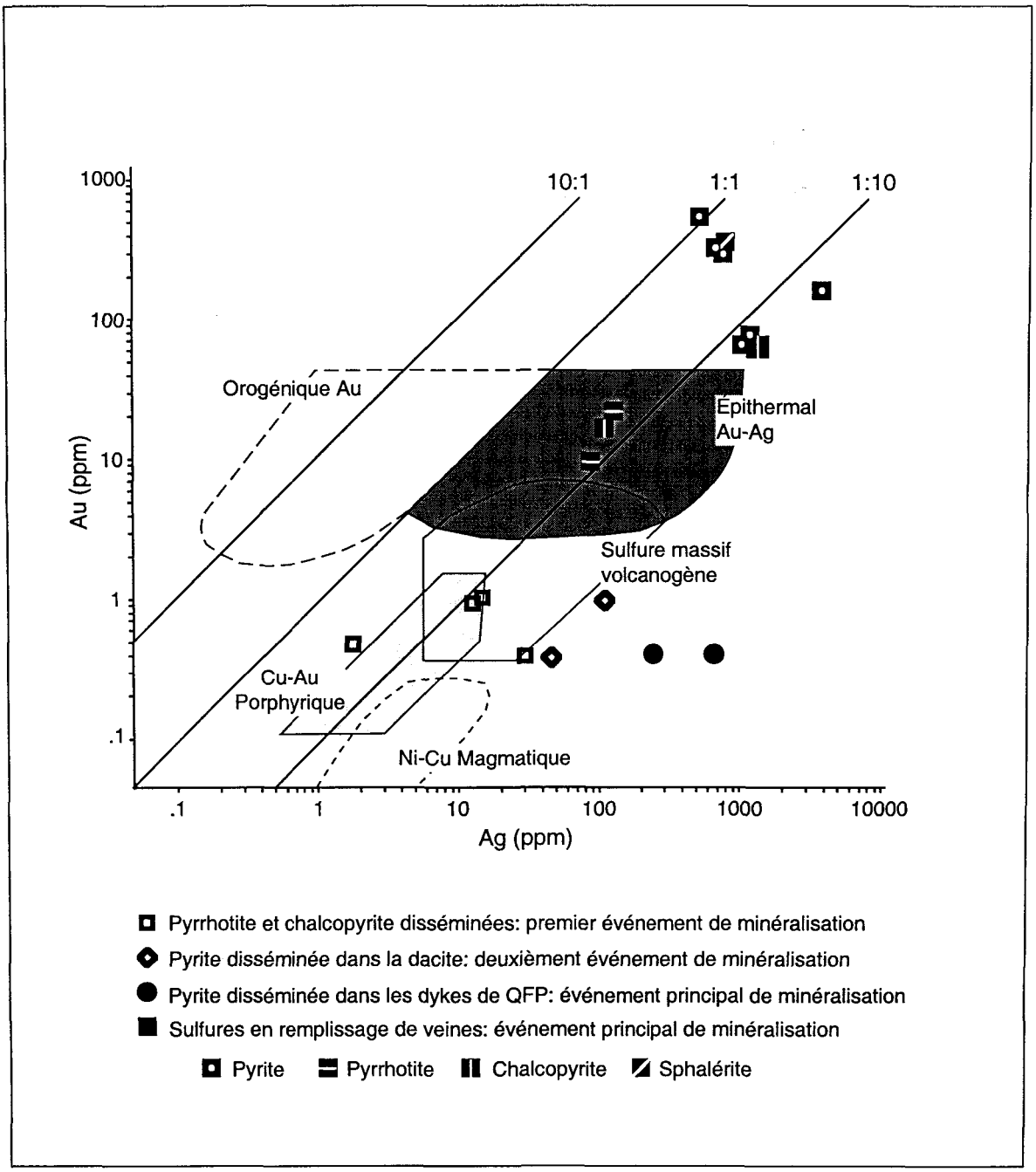

Figure 9. Diagramme Au versus Ag illustrant la composition des différents sulfures analysés par l'activation neutronique (Chap. 4) pour chacun des trois événements de minéralisation. Les différents champs sont tirés de Hodgson (1993)

l'évolution du système hydrothermal, un point compatible avec le lien temporel et spatial entre les événements de minéralisation et de magmatisme felsique (Chap. 3). D'autre part, une contribution en fluides magmatiques n'implique pas nécessairement une contribution en métaux. En outre, une contribution magmatique en or, spécifique à la formation des veines, s'accorde difficilement avec la faible teneur en or des dykes de QFP (Fig. 9) qui eux, représentent les conduits hydrothermaux pour la formation des veines. En ce sens, le lien hydrothermal entre les dykes de QFP et les veines est démontré par la modélisation de la signature isotopique ^{18}O des dykes (Chap. 5).

Quant à l'interaction entre les fluides minéralisateurs et les roches felsiques, cette hypothèse est plausible en raison de l'association entre la minéralisation et les roches felsiques calco-alcalines. Toutefois, considérant que la pyrite des dykes de QFP est peu aurifère (Fig. 9), cette hypothèse apparaît faible pour expliquer l'enrichissement considérable en or lors de la formation des veines. En bref, indépendamment du contenu initial en or des fluides, un enrichissement spécifique lors de la formation des veines peut être écartée comme facteur déterminant pour expliquer la forte teneur en or des veines aurifères.

Mécanisme efficace de précipitation

La morphologie de la minéralisation en veines implique des conditions physico-chimiques de précipitation des sulfures différentes de celles à l'origine des minéralisations de type disséminé (Chap. 4). À la lumière des caractéristiques des veines et de leur mécanisme de formation, il a été proposé que la précipitation de certaines phases minérales, comme le quartz microcristallin et les sulfures en remplissage de fractures (pyrrhotite, chalcopyrite, sphalérite, ± arsénopyrite) est induite par des baisses de la pression des fluides. Dans des systèmes filoniens, l'ébullition peut être engendrée par des

variations de la pression des fluides (Sibson et al., 1988) et ce, même à des pressions lithostatiques (Helgeson et Lichtner, 1987). Ainsi, dans un contexte sous-marin, où la profondeur bathymétrique excède la limite de l'ébullition dans un système ouvert, l'ébullition des fluides est quand même possible au sein d'un système filonien fermé. Un système fermé implique ici que la pression des fluides minéralisateurs peut être indépendante momentanément de celle exercée par la colonne d'eau. Quoique aucune des données de l'étude n'appuie directement l'hypothèse de l'ébullition, elle est néanmoins compatible avec certaines textures de remplissage des veines. En ce sens, les sulfures en remplissage de fractures, qui coexistent avec l'or et l'argent (Chap. 4: Fig. 5c), définissent une texture compatible avec la dépressurisation des veines et la précipitation des métaux précieux due à l'ébullition instantanée.

D'autre part, la prépondérance du mode de précipitation des sulfures sur leur contenu aurifère est également appuyée par la faible teneur en or des dykes de QFP. La teneur en or de la pyrite disséminée dans ces dykes se compare à celle des autres sulfures disséminés (Fig. 9), et ce indépendamment du fait que cette pyrite est reliée à la formation des veines aurifères. Cette pyrite résulte vraisemblablement d'un mécanisme de précipitation par sulfurisation, tel que suggéré par le remplacement de la magnétite. Un tel mécanisme n'est probablement pas favorable à la déstabilisation des complexes aurifères (Chap. 4). Il est aussi fort probable que le mécanisme de sulfurisation est commun aux autres sulfures disséminés composant le premier et le deuxième événements de minéralisation. Ainsi, la spécificité de l'enrichissement en or en fonction du style (veine versus disséminé: Fig. 9), et non pas en fonction des événements de minéralisation, supporte l'hypothèse que le mécanisme de précipitation de l'or est un facteur fondamental. Enfin, considérant que la majeure partie de l'or dans les systèmes exhalatifs modernes demeure en solution au sein d'un panache diffus (Hannington et Scott, 1988), il est donc

plausible qu'un mécanisme de précipitation efficace peut, à lui seul, expliquer l'enrichissement en or des veines.

Conclusion

L'enrichissement en or des veines apparaît comme une caractéristique intrinsèque de leur formation plutôt que le résultat d'un enrichissement extrinsèque en or des fluides au cours de l'évolution du système hydrothermal. L'ébullition des fluides minéralisateurs, engendrée par une dépressurisation des veines, est considérée comme la meilleure hypothèse pour expliquer la précipitation efficace de l'or et son enrichissement relatif. Toutefois, même si l'enrichissement relatif en or des veines est attribuable essentiellement au mécanisme de précipitation, la possibilité que les fluides minéralisateurs soient exceptionnellement riches ne peut pas être définitivement écartée. La contribution magmatique interprétée et le lien génétique entre le magmatisme felsique et les événements de minéralisation sont des évidences, circonstancielles certes, qui appuient l'hypothèse de fluides particulièrement riches en or. Quoiqu'il en soit, la forte teneur en or du système filonien peut donc être considérée comme la conséquence logique de l'évolution proposée du système hydrothermal (Chap. 3).

Références

Ahmad, M. et Walshe, J.L. 1990. Wall-rock alteration at the Emperor gold-silver telluride deposit, Fiji. Australian Journal of Earth Sciences, 37:189-199.

Ahmad, M., Solomon, M. et Walshe, J.L. 1987. Mineralogical and geochemical studies of the Emperor gold-telluride deposit, Fiji. Economic Geology, 82: 345-370.

Anderson, W. A. et Eaton, P.C. 1990. Gold mineralisation at the Emperor Mine, Vatakoula, Fiji. Journal of Geochemical Exploration, 36: 267-296.

Bogie, I. et Lawless, J.V. 1987. Controls on the hydrology of large volcanically hosted geothermal systems: Implications for exploration for epithermal mineral deposits. Dans: Proceedings Pacific Rim Congress 87. Australasian Institute of Mining and Metallurgy, Parkville, p. 57-60.

Brace, W.F. 1984. Permeability of crystalline rocks: New in situ measurements. Journal of Geophysical Research, 89: 4327-4330.

Brauhart, C.W. et Groves, D.I. 1998. Regional alteration systems associated with volcanogenic massive sulfide mineralization at Panorama, Pilbara, Western Australia. Economic Geology, 93: 292-302.

Chartrand, F. et Cattalani, S., 1990. Massive sulfide deposits in Northwestern Quebec. Dans: La ceinture polymtallique du Nord-Ouest Québécois: Synthèse de 60 ans d'exploration minière. Édité par: M. Rive, P. Verpaelst, Y. Gagnon, J. M. Lulin, G. Riverin et A. Simard. L'institut canadien des mines et de la métallurgie, Volume spécial 43, p. 77-91.

Chown, E.H., Daigneault, R., Mueller, W. et Mortensen, J.K. 1992. Tectonic evolution of the Northern Volcanic Zone, Abitibi belt, Quebec. Journal Canadien des Sciences de la Terre, 29: 2211-2225.

Cox, S.F., Etheridge, M.A. et Wall, V.J. 1990. Fluid pressure regimes and fluid dynamics during deformation of low-grade terranes, implications for the genesis of mesothermal gold deposits. Dans: Greenstone gold and crustal evolution. Édité par: F. Robert, P.A. Sheahan et S.B. Green. Nuna conference volume, Association Géologique du Canada, p. 46-53.

Craw, D. et McKeag, S.A. 1995. Structural control of tertiary Au-Ag-bearing breccias in an extensional environment, Nelson area, Southern Nevada, USA. Mineralium Deposita, 30: 1-10.

de Ronde, C.E.J. 1995. Fluid chemistry and isotopic characteristics of seafloor hydrothermal systems and associated VMS deposits: Potential for magmatic contributions. Dans: Magmas, fluids and ore deposits. Édité par: J.F.H. Thompson. Association Minéralogique du Canada, Short Course Series 23, p. 479-509.

Dong, G., Morrison, G. et Jaireth, S. 1995. Quartz textures in epithermal veins, Queensland - Classification, origin, and implication. Economic Geology, 90: 1841-1856.

Dowling, K. et Morrison, G. 1989. Application of quartz textures to the classification of gold deposits using North Queensland examples. Dans: The Geology of Gold Deposits: The Perspective in 1988. Édité par: R.R. Keays, W.R.H. Ramsay et D.I. Groves. Economic Geology, Monograph 6, p. 342-355.

Eaton, P.C. et Setterfield, T.N. 1993. The relationship between epithermal and porphyry hydrothermal systems within the Tavua caldera, Fiji. Economic Geology, 88: 1053-1083.

Galley, A.C. 1993. Characteristics of semi-conformable alteration zones associated with volcanogenic massive sulphide districts. Journal of Geochemical Exploration, 48: 175-200.

Gebre-Mariam, M., Hagemann, S.G. et Groves, D.I. 1995. A classification scheme for epigenetic Archaean lode-gold deposits. Mineralium Deposita, 30: 408-410.

Gudmundsson, A. 1983. Form and dimensions of dykes, feeder-dykes in eastern Iceland. Tectonophysics, 95: 295-307.

Hannington, M.D. et Scott, S.D. 1988. Gold and silver potential of polymetallic sulfide deposits on the sea floor. Marine Mining, 7: 271-285.

Hannington, M.D., Poulsen, K.H., Thompson, J.F.H. et Sillitoe, R.H. 1997. Volcanogenic gold and epithermal-style mineralization in the VMS environment. Dans: Volcanogenic-associated massive sulfide deposits: Processes and examples in modern and ancient settings. Édité par: C.T. Barrie et M.D. Hannington. Association Géologique du Canada, Short Course Handbook, 13, p. 183-214.

Helgeson, H.C. et Lichtner, P.C. 1987. Fluid flow and mineral reactions at high temperatures and pressures. Geological Society of London Journal, 144: 313-326.

Herzing, P.M. et Hannington, M.D. 1995. Polymetallic massive sulfides at modern seafloor: a review. Ore Geology Reviews, 10: 95-115.

Herzing, P.M., Hannington, M.D., Fouquet, Y., Von Stackelberg, U. et Peterson, S. 1993. Gold-rich polymetallic sulfides from the Lau back arc and implications for the geochemistry of gold in sea-floor hydrothermal system of the southwest Pacific. Economic Geology, 88: 2182-2209.

Hodgson C.J. 1993. Mesothermal gold deposits. Dans: Mineral deposit modeling. Édité par: R.V. Kirkham, W.D. Sinclair, R.I. Thorpe, J.M. Duke. Association Géologique du Canada, Volume Spécial 40: 635-678

Jébrak, M. 1992. Les textures intra-filoniennes, marqueurs des conditions hydrauliques et tectoniques. Chroniques de la Recherche Minière, 506: 25-36.

Jébrak, M. 1998. Hydrothermal breccias in vein-type ore deposits: A review of mechanisms, morphology and sized distribution. Ore Geology Review, 12, 111-134.

Large, R.R. 1992. Australian volcanic-hosted massive sulfide deposits: features, styles, and genetic models. Economic Geology, 87: 571-500.

Ohmoto, H. 1996. Formation of volcanogenic massive sulfide deposits : The Kuroko perspective. Ore Geology Reviews, 10: 135-177.

Panteleyev, A. 1996. Epithermal Au-Ag: Low sulfidation. The Gangue. Association Géologique du Canada, issue 53: 3-5.

Peters, S.G. 1993. Nomenclature, concepts and classification of oreshoots in vein deposits. Ore Geology Reviews, 8: 3-22.

Phillip, W.J. 1972. Hydraulic fracturing and mineralization. Journal of the Geological society of London, 12: 337-359.

Poulsen, K.H. et Hannington, M.D. 1995. Volcanic-associated massive sulphide gold. Dans: Geology of the Canadian mineral deposits. Édité par: O.R. Eckstrand, W.D. Sinclair et R.I. Thorpe. Geological Survey of Canada, Geology of Canada no 8, p. 183-196.

Ramsay, J.G. 1980. The crack-seal mechanism of rock deformation. Nature, 244: 135-139.

Richards, J.P. 1995. Alkalic-type epithermal gold deposits – A review. Dans: Magmas, fluids, and ore deposits. Édité par: J.F.H. Thompson. Association Minéralogique du Canada, Short Course Volume 23, p. 367-400.

Ridley, J. 1993. The relations between mean rock stress and fluid flow in the crust : With inference to vein- and lode-style gold deposits. Ore Geology Review, 8: 23-37.

Robert, F. 1990. An overview of gold deposits in the Eastern Abitibi Subprovince. Dans: La ceinture polymétallique du Nord-Ouest Québécois: Synthèse de 60 ans d'exploration minière. Édité par: M. Rive, P. Verpaelst, Y. Gagnon, J. M. Lulin, G. Riverin et A. Simard. L'institut canadien des mines et de la métallurgie, Volume spécial 43, p. 93-105.

Robert, F. et Brown, A.C. 1986. Archean gold-bearing quartz veins at the Sigma Mine, Abitibi greenstone belt, Québec: Part I. Geologic relations and formation of the vein system. Economic Geology, 81: 578-592.

Roth, T., Thompson, J.F.H. et Barrett, T.J. 1997. The precious metal-rich Eskay Creek deposit, northwestern British Colombia. Dans: Volcanogenic-associated massive sulfide deposits: Processes and examples in modern and ancient settings. Édité par: C.T. Barrie

et M.D. Hannington. Association Géologique du Canada, Short Course Handbook, 13, p. 367-385.

Sibson, R.H. 1987. Earthquake rupturing as a mineralizing agent in hydrothermal systems. Geology, 15: 701-704.

Sibson, R.H. 1990a. Fault structure and mechanics in relation to greenstone gold deposits. Dans: Greenstone gold and crustal evolution. Édité par: F. Robert, P.A. Sheahan et S.B. Green. Nuna conference volume, Association Géologique du Canada, p. 64-60.

Sibson, R.H. 1990b. Faulting and fluid flow. Dans: Fluids in tectonically active regimes of continental crust. Édité par: B.E. Nesbitt. Association Minéralogique du Canada, Short Course Volume 18, p. 93-132.

Sibson, R.H., Robert, F. et Poulsen, K.H. 1988. High-angle reverse faults, fluid-pressure cycling and mesothermal gold-quartz deposits. Geology, 16: 551-555.

Sillitoe, R.H. 1989. Gold deposits in western Pacific island arcs: The magmatic connection. Dans: The Geology of Gold Deposits: The Perspective in 1988. Édité par: R.R. Keays, W.R.H. Ramsay et D.I. Groves. Economic Geology Monograph 6, p. 274-291.

Sillitoe, R.H. 1995. The influence of magmatic-hydrothermal models on exploration strategies for volcano-plutonic arcs. Dans: Magmas, Fluids, and Ore Deposits. Édité par: J.F.H. Thompson. Association Minéralogique du Canada, Short Course Handbook, 23, p. 511-525.

Vearncombe, J.R. 1993. Quartz vein morphology and implications for formation depth and classification of Archaean gold-vein deposits. Ore Geology Review, 8, p. 407-424.

White, N.C. et Hedenquist, J.W. 1990. Epithermal environments and styles of mineralization: variations and their causes, and guidelines for exploration. Journal of Geochemical Exploration, 36: 445-474.

White, N.C., Leake, M.J., McCaughey, S.N. et Parris, B.W. 1995. Epithermal gold deposits of the southwest Pacific. Journal of Geochemical Exploration, 54: 87-136.

CHAPITRE 8

Sommaire et conclusions

INTRODUCTION

Les objectifs principaux du projet de recherche étaient d'établir l'origine de la minéralisation aurifère filonienne à la mine Géant Dormant, de proposer un modèle génétique et des guides pour l'exploration. Quatre thématiques secondaires avaient été ciblées pour atteindre ces trois objectifs principaux, à savoir:

1) Caractériser la minéralisation aurifère et établir les facteurs contrôlant sa mise en place.
2) Caractériser la nature de l'altération hydrothermale et déterminer sa distribution spatiale.
3) Caractériser l'environnement hôte de la minéralisation.
4) Placer les événements de minéralisation dans un cadre évolutif qui intègre les différents événements de magmatisme, de déformation et de métamorphisme.

Les résultats de l'étude sont concluants par rapport aux objectifs initiaux secondaires et principaux. Un sommaire des éléments pertinents est présenté ci-dessous en fonction des différentes thématiques. Enfin, les grandes conclusions de cette étude sont résumées en fonction des trois objectifs principaux.

MINÉRALISATIONS ET ALTÉRATIONS HYDROTHERMALES

Trois événements de minéralisation et d'altération hydrothermale ont été reconnus sur la base de relations chronologiques relatives.

Premier événement

Le premier événement correspond à la sulfurisation volcanogène des roches du paléo-fond océanique. La minéralisation, composée de pyrrhotite (monoclinique) et de traces de chalcopyrite, se présente sous la forme de filonnets dans les bordures de coussins associés avec du quartz et de la chlorite, et sous la forme de disséminations dans les horizons sédimentaires et l'unité de lave felsique. L'altération hydrothermale se manifeste par la

chloritisation, la séricitisation et la silicification. Une séricitisation intense, caractérisée par un lessivage en Fe_2O_3 et MgO, affecte le sommet de la coulée de lave coussinée. Cet événement hydrothermal précoce est omniprésent dans la mine, quoique d'intensité variable. La valeur moyenne $\delta^{18}O$ du quartz dans les coussins est de 11,9 ± 0,6‰ et les fluides ont une valeur $\delta^{18}O$ de 3,2‰ calculée à 250°C. Les valeurs $\delta^{34}S$ de la pyrrhotite et de la chalcopyrite sont comprises entre 0,6 et 1,7‰; comparables avec les valeurs typiquement volcanogènes (archéen). La pyrrhotite est caractérisée par des spectres en ÉTR (normalisés aux chondrites) faiblement fractionnés avec des anomalies négatives en Ce et par des concentrations fortes en Ni et Co et faibles en Au et Ag.

Deuxième événement

Le deuxième événement correspond à la pyritisation et à la chloritisation interne du dôme dacitique résultant d'un processus autométasomatique. La chloritisation, qui correspond à un gain en Fe_2O_3 et MgO, (± K_2O) et une perte en Na_2O, se manifeste par des taches millimétriques de chlorite et par une chloritisation intense des parties sommitale et basale du dôme. La pyrite disséminée (< 10 %) se caractérise par des spectres en ÉTR fortement fractionnés, représentatifs de la composition de la roche encaissante, et par des concentrations faibles en Au et Ag. La valeur moyenne du $\delta^{34}S$ de la pyrite est de 1,4‰.

Événement principal

Les veines aurifères, le style stratoïde et la minéralisation interne des dykes de QFP composent l'événement principal. Les veines aurifères sont massives, d'épaisseur moyenne de 50 cm et renferment communément des teneurs supérieures à 100 g/t Au. La séquence paragénétique se subdivise en trois stades. Le quartz et en moindre proportion la chlorite, la séricite et des traces de tourmaline composent le Stade pré-minéralisation. Le Stade de

minéralisation est associé à l'introduction des sulfures (pyrite, pyrrhotite (hexagonale), chalcopyrite, sphalérite et arsénopyrite) qui constituent entre 5 et 80% (moyenne de 25%) des veines. Le Stade post-minéralisation résulte de la déformation ductile et du métamorphisme. Il regroupe la calcite et l'actinote. L'altération des épontes est nulle à faible (chlorite-séricite). Le système filonien se compose de 4 familles de veines qui sont par endroits interconnectées. La géométrie du système filonien devient plus complexe vers la paléosurface. Les facteurs de contrôle correspondent à des anisotropies primaires que sont: les contacts stratigraphiques, les failles synvolcaniques, et les joints préexistants. Les compositions isotopiques moyennes de l'oxygène pour le quartz et la chlorite sont respectivement de 12,5 ± 0,3‰ et 5,9 ± 1,1‰. En supposant un équilibre isotopique entre le quartz et la chlorite, une température de formation des veines de 250 à 275°C est déterminée. La température de formation des chlorites hydrothermales, calculée sur la base de leur composition chimique, est de 269 ± 10°C; cohérente avec la température isotopique. À 275°C, la valeur $\delta^{18}O$ calculée des fluides à l'origine des veines est de 4,7‰. Les valeurs $\delta^{34}S$ des différents sulfures sont comprises entre 1,4 et 2,8‰. Une température de précipitation des sulfures de ~350°C est estimée en assumant un équilibre isotopique. Les sulfures sont également caractérisés par des contenus faibles en Ni et Co mais élevés en Au et Ag, ainsi que par des spectres montrant un fractionnement prononcé en ÉTR légères et une anomalie positive en Eu.

Le style stratoïde correspond à des segments d'horizons sédimentaires où la minéralisation prend l'aspect d'une dissémination et de rubans concordants de pyrite ou encore de veinules de quartz et sulfures subconcordantes. Ce style est communément développé dans la continuité latérale et verticale de veines aurifères recoupant des horizons sédimentaires.

Les dykes de QFP, qui sont spatialement associés avec les veines aurifères et le style stratoïde, constituent les conduits hydrothermaux pour leur formation. Ceux-ci sont caractérisés par une intense séricitisation, correspondant à un gain en SiO_2 et en K_2O, et par une pyritisation. La composition isotopique moyenne de l'oxygène des dykes de QFP est de 11‰, attribuable à la réaction entre les dykes et les fluides hydrothermaux de composition $\delta^{18}O \approx 5‰$ à des températures comprises entre 250 et 275°C. Ces valeurs sont cohérentes avec celles calculées pour les veines, appuyant ainsi leur rôle de conduits hydrothermaux. La valeur moyenne du $\delta^{34}S$ de la pyrite est de 1,9‰. La pyrite disséminée est caractérisée par des spectres en ETR fortement fractionnés, similaires à ceux de la pyrite disséminée dans la dacite, et par des concentrations faibles en Au et Ag.

ENVIRONNEMENT HÔTE DE LA MINÉRALISATION

Les caractéristiques lithologiques, géochimiques et structurales ont été utilisées pour reconstruire l'histoire de la construction de l'empilement volcanique.

Caractéristiques lithologiques

La minéralisation aurifère est centrée sur un complexe felsique recoupant une séquence volcano-sédimentaire. La séquence volcano-sédimentaire se compose essentiellement de filons-couches mafiques injectés au sein d'un empilement de roches formé sur le fond océanique, incluant des sédiments fins et des unités de laves mafique coussinée et felsique. Un dôme dacitique subvolcanique et un essaim de dykes felsiques porphyriques composent le complexe felsique intrusif. La dacite définit un corps lenticulaire injecté de manière subconcordante dans la séquence de filons-couches mafiques. L'essaim de dykes felsiques recoupe à angle fort la séquence volcano-sédimentaire et l'intrusion dacitique. Il se compose de deux générations, soit les dykes à

plagioclase (FP) et les dykes à quartz et plagioclase (QFP). Les dykes de QFP recoupent les FP et définissent des injections tabulaires et continues à l'échelle du dépôt, injectés le long de failles syn-volcaniques préexistantes. Deux générations de dykes mafiques recoupent la minéralisation filonienne. La première correspond à des dykes subvolcaniques. La seconde génération correspond à des dykes riches en hornblende. L'empilement volcanique a été construit en milieu sous-marin profond (> 3 150 m).

Caractéristiques géochimiques primaires

Les roches mafiques, indépendamment de leur mode de mise en place (filon-couche ou lave) sont de composition basaltique et d'affinité tholéiitique (Zr/Y≈2,5), caractérisées par un spectre en ÉTR-HFSE relativement plat et exprimé par un rapport $[La/Yb]_N$ variant de 0,6 à 1,9. Les unités felsiques (dôme, lave et dykes) regroupent des roches de composition dacitique à rhyolitique et d'affinité calco-alcaline (Zr/Y≈12). Elles sont caractérisées par un fractionnement prononcé des ÉTR légères, exprimé par un rapport moyen $[La/Yb]_N$ de 11,6. Des compositions spécifiques distinguent les deux générations de dykes mafiques. La première génération a une signature géochimique comparable à celle des roches mafiques tholéiitiques. Ces dykes sont d'affinité tholéiitique et caractérisés par un spectre des ÉTR-HFSE relativement plat ($[La/Yb]_N$ de 0,8 à 1,3). Les dykes à hornblende sont d'affinité shoshonitique et sont caractérisés par un spectre des ÉTR-HFSE montrant un fractionnement intense des ÉTR légères ($[La/Yb]_N$=26,8), analogue à celle des lamprophyres syn- à post-tectoniques de l'Abitibi.

L'homogénéité des signatures géochimiques indique que les roches felsiques calco-alcalines sont cogénétiques alors que celles mafiques tholéiitiques, incluant la première génération de dykes post-minéralisation sont également cogénétiques entre elles. Ces données, en combinaison avec les caractéristiques morphologiques des roches, indiquent

que l'empilement volcanique a été construit d'une manière séquentielle à partir de deux sources magmatiques: une source felsique proximale et une source mafique distale.

Caractéristiques structurales

Les couches (S0), à polarité sud, s'orientent E-O et sont fortement inclinées vers le sud, formant une séquence homoclinale normale. La schistosité régionale E-O et subverticale (Sp), renfermant une linéation d'étirement subverticale, se superpose sur toutes les roches, incluant les dykes post-minéralisation. L'intensité de la déformation est faible et hétérogène. En section verticale, la relation angulaire entre les surface planaires S0 et Sp indique que la mine est située sur le flanc nord d'un pli synclinal régional de direction E-O et d'axe subhorizontal.

CHRONOLOGIE RELATIVE

Le premier événement de minéralisation affecte uniquement les roches du fond océanique, qui ont été les premières formées. Les filons-couches mafiques, injectés au sein des roches du fond océanique, recoupent cet événement précoce de minéralisation. Le deuxième événement de minéralisation est associé à l'introduction subséquente du dôme dacitique. Le synchronisme entre l'activité magmatisme et hydrothermale est indiqué par le recoupement systématique de la minéralisation disséminée et de l'altération (chlorite) par les dykes de FP frais, qui suivent chronologiquement la formation du dôme. L'injection des dykes de QFP succède dans le temps. L'âge de 2722 ±2 Ma indique que les dykes de QFP font partie intégrante du premier cycle volcanique (2730-2720 Ma). L'événement principal de minéralisation recoupe les dykes de QFP mais est antérieur aux dykes mafiques tholéiitiques. Cette relation indique que les veines ont été formées avant la terminaison complète de la construction volcanique.

Une origine pré-déformation ductile des veines est indiquée par: (1) l'absence de compatibilité structurale entre le corps minéralisé et la déformation ductile; (2) la superposition systématique de la déformation sur la minéralisation; et (3) le recoupement systématique de la minéralisation par les dykes shoshonitique schistosés. La superposition du métamorphisme sur les veines est indiquée par la présence de rosettes d'actinote aciculaire se superposant sur les phases sulfurées. Enfin, la cohérence du système filonien en posture re-basculée, pour éliminer l'effet du plissement, suggère que les veines ont été formées lorsque les couches étaient en position initiale subhorizontale.

ORIGINE DE LA MINÉRALISATION

La similarité des données isotopiques du souffre et des valeurs calculées du $\delta^{18}O$ des fluides minéralisateurs suggère que les trois événements de minéralisation sont cogénétiques. Cette interprétation est également appuyée par la tendance évolutive de la concentration en éléments traces des sulfures. Une origine volcanogène des veines est compatible avec les valeurs $\delta^{34}S$ des sulfures et la source océanique probable des fluides minéralisateurs, telle que suggérée par la valeur calculée du $\delta^{18}O$. Elle est également appuyée par la signature en ÉTR des sulfures qui se compare à celle typique des systèmes volcanogènes matures et actifs. Un modèle volcanogène s'accorde également avec l'évolution dans le temps de la concentration des éléments traces dans les sulfures. Celle-ci manifeste la transition temporelle entre les sources minérales des éléments lessivés dans les basaltes sous-jacents (ferro-magnésiens à plagioclase). Enfin, une origine volcanogène des veines s'accorde avec les relations chronologiques relatives.

MODÈLE GÉNÉTIQUE

Évolution du système hydrothermal

Un modèle volcanogène évolutif, comprenant quatre stades a été proposé. Le Stade 1 est associé à un système hydrothermal volcanogène diffus qui se manifeste par la minéralisation et l'altération enregistrées par les roches du fond océanique. Le site de précipitation des sulfures sur ou près du fond océanique est supporté par les anomalies négatives en Ce de la pyrrhotite. Celles-ci sont attribuables au mélange entre les fluides hydrothermaux et l'eau de mer oxydante au site de minéralisation. Le stade 2 correspond à l'injection des filons-couches mafiques au sein de la séquence de roches développées sur le fond océanique. Cet événement a eu pour effet de gonfler l'empilement volcanique et de colmater le système hydrothermal diffus, inhibant ainsi les possibilités pour les fluides hydrothermaux d'atteindre la surface du fond océanique. Le stade 3 est relié à la mise en place du dôme subvolcanique de dacite. Cet événement magmatique s'accompagne d'une réactivation de l'activité hydrothermale volcanogène qui se manifeste par la minéralisation et l'altération internes et autométasomatiques du dôme de dacite. Le stade 4 marque la fin du système hydrothermal avec la formation des veines aurifères et de la minéralisation de style stratoïde. Durant ce stade, les dykes de FP et de QFP sont successivement injectés. Les fluides hydrothermaux ont été canalisés par les dykes de QFP, qui constituent les seules injections tabulaires et continues à l'échelle du dépôt. Le matériel minéralogique des veines a été précipité dans les fractures ouvertes développées à proximité des dykes de QFP.

La formation des veines est la conséquence directe de la construction séquentielle de l'empilement volcanique à partir des deux sources magmatiques. L'injection des filons-couches, qui est un événement extrinsecte, a perturbé l'activité hydrothermale associée au centre felsique proximal en construction. La reprise du magmatisme felsique, au quel est

associé génétiquement le système hydrothermal, a généré des fractures pour la formation des veines au sein d'une environnement imperméable.

La nature évoluée des fluides ($\delta^{18}O \approx 5‰$) est attribuée à l'apport constant de fluides magmatiques au système hydrothermal convectif dominé par l'eau de mer modifiée (~2‰). La plus faible valeur initiale ($\delta^{18}O = 3,2‰$) des fluides associés à l'activité hydrothermale du fond océanique est expliquée par la dilution des fluides hydrothermaux ($\delta^{18}O \approx 5‰$) avec l'eau de mer au site de précipitation des sulfures.

Mécanisme de formation des veines

Un mécanisme empirique de formation des veines à été proposé sur la base des caractéristiques texturales et géométriques du système filonien. Ce mécanisme comporte trois stades. Le premier (Stade de pré-rupture) implique des conditions stables, où la pression des fluides est maintenue à un niveau lithostatique, favorisant ainsi la formation progressive et lente des veines. Les dykes de QFP constituent les conduits nourriciers pour la formation des veines et pour la décharge des fluides sur le fond océanique. La pression des fluides est régularisée à un niveau lithostatique constant grâce au contrôle exercé par les dykes de QFP sur le débit des fluides hydrothermaux se déchargeant à la surface. Le deuxième stade (Stade de rupture) correspond au relâchement instantané de la pression des fluides. Cette dépressurisation est conséquente à l'augmentation subite de la perméabilité au sein des dykes de QFP, induite probablement par la rupture hydraulique de la partie sommitale de la séquence volcanique initialement imperméable. Il est proposé que la rupture correspond à un état critique du système dans son ensemble, où la pression totale des fluides dans la tuyauterie hydrothermale excède celle de confinement de l'empilement volcanique. Le dernier stade (Stade de post-rupture) correspond à un état transitoire et métastable. Durant ce stade, le réservoir hydrothermal sous-jacent est drainé. Les fluides

hydrothermaux s'écoulent alors le long des dykes de QFP pour se décharger à la surface du fond océanique. Il n'y a pas de contribution à la formation des veines durant ce stade, les veines étant alors des structures fermées dues à la faible pression des fluides. Après une diminution du débit des fluides et le colmatage hydrothermal, il s'ensuit une phase de repressurisation progressive des fluides au sein de l'empilement, dont la finalité est l'atteinte des conditions stables du Stade de pré-rupture.

La répétition complète du cycle est double dans le cas du Géant Dormant: un cycle pour la précipitation des silicates (Stade pré-minéralisation) et un second pour les sulfures (Stade de minéralisation). La transition des silicates aux sulfures, correspondant à une augmentation de la température de précipitation de 275 à 350°C, est attribuée à la phase de drainage du réservoir hydrothermale. Cette dernière a probablement contribué à la maturation du système hydrothermal. La meilleure hypothèse pour expliquer la précipitation efficace de l'or est une ébullition des fluides due à la dépressurisation des veines en formation lors du stade de rupture.

IMPLICATIONS POUR l'EXPLORATION

L'exploration minérale moderne repose essentiellement sur l'utilisation de concepts et sur l'application de techniques spécifiques. Les concepts regroupent tout les critères empiriques utilisés pour sélectionner des secteurs favorables. Les techniques correspondent à des outils pour optimiser l'exploration. Les résultats de cette étude ont permis de dégager des implications pour l'exploration à ces deux niveaux.

Techniques d'exploration

La complexité apparente du système de veines aurifères au Géant Dormant, combinée à l'absence de surface planaire de référence, représente un défi considérable pour

l'interprétation de l'attitude des veines en forages. Dans le but d'augmenter le niveau de certitude de l'interprétation, deux méthodes pratiques de corrélation des intersections de veines en forages, utilisant un logiciel de projection stéréographique, ont été développées. La première peut être utilisée pour déterminer si deux ou plusieurs intersections de veines sont corrélatives. La seconde méthode permet de prédire l'attitude des veines principales à partir de plusieurs forages, en utilisant une projection sphérique de densité. Ces deux méthodes sont applicables à des systèmes filoniens complexes où une certaine quantité de forages sont disponibles.

Pour la recherche de gisements de sulfures massifs, la maturation progressive des systèmes hydrothermaux volcanogènes, enregistrée par le contenu en éléments des sulfures, représente un outil potentiel pour optimiser l'exploration. Par exemple, la signature en éléments traces des sulfures disséminés, communément développés au sein des laves coussinées dans les environnements volcanogènes, peut être utilisée pour déterminer la maturité du système hydrothermal. Dans le cas d'une signature immature, l'exploration doit être dirigée dans les niveaux stratigraphiques supérieurs de l'empilement volcanique, dans l'espoir que le système ait atteint une certaine maturité. Dans le cas contraire, l'exploration doit être orientée dans les niveaux inférieurs, puisse que les sulfures disséminés correspondent peut-être à des percolations à travers une pile volcanique perméable qui recouvre un amas mature et économique.

Concepts d'exploration

Les résultats de cette étude démontrent que la formation des veines aurifères résulte de l'évolution particulière d'un système volcanogène. Cette conclusion a plusieurs implications conceptuelles pour l'exploration aurifère. Premièrement, elle démontre le potentiel aurifère des systèmes volcanogènes, une caractéristique reconnue seulement

depuis quelques années. Deuxièmement, cette étude démontre que les minéralisations volcanogènes aurifères ne sont pas restreintes uniquement aux environnements sous-marins peu profond, où la faible pression hydrostatique ne limite pas l'ébullition des fluides. Troisièmement, elle démontre également que les minéralisations aurifères filoniennes ne sont pas uniquement restreintes chronologiquement à la phase d'accrétion tectonique, et spatialement aux zones majeures de déformation. Enfin, considérant le modèle génétique proposé, les complexes de filons-couches mafiques, en association avec du magmatique felsique et de l'activité hydrothermale synchrone, peuvent être considérés comme fertiles pour la formation des veines aurifères volcanogènes.

ANNEXE

Liste des abréviations utilisées dans les tableaux en annexe

BC	Basalte coussiné tholéiitique
FCM	Filon-couche mafique tholéiitique
DM1	Dyke mafique tholéiitique post-minéralisation
LF	Lave felsique calco-alcaline
DAC	Dacite calco-alcaline
FP	Dyke felsique calco-alcalin à phénocristaux de plagioclase
QFP	Dyke felsique calco-alcalin à phénocristaux de plagioclase et quartz
DM2	Dyke à hornblende shoshonitique post-minéralisation
PAF	Perte au feu

X(E)	Localisation par rapport système de la mine selon un axe E-O
Y(N)	Localisation par rapport système de la mine selon un axe N-S
Z	Profondeur en m par rapport à la surface

Cata	Cataclasé
Rx	Roche
Sédi	Sédiment

Act	Actinote
Amp	Amphibole
Cal	Calcite
Chl	Chlorite
Leu	Leucoxène
Qz	Quartz
Qz-B	Quartz blanc
Qz-L	Quartz laiteux
Qz-G	Quartz gris à noir
Ser	Séricite
Tm	Tourmaline
Cp	Chalcopyrite
Po	Pyrrhotite
Py	Pyrite
Sp	Sphalérite

ANNEXE 1

The "self-equilibrating" mechanism: a model for flat vein formation in a transitional crustal depth (2-5 km), example from the Géant Dormant gold mine, Canada.

Ce chapitre représente la version intégrale d'un article soumis pour publication au Journal *Ore Geology Reviews* par Gaboury et Daigneault.

Abstract

Gold-bearing veins form in the wide range of crustal depths and tectonic regimes. However, only two mechanisms, covering specific crustal segments in particular tectonic regimes, are widely accepted: the suction pump model for epithermal (0 to 2 km) and the fault-valve model for mesothermal (5 to > 25 km) veins. Characteristics of the Géant Dormant gold-bearing vein network are atypical comparing to both types of vein systems. In this paper, vein, alteration, and host rock characteristics are used to constraint the following empirical parameters: the tectonic regime, the fluid flow vectors, the crustal depth, the host rock permeability, the fluid pressure, the mineral precipitating conditions and the scale of filling processes (zoning). Based on these parameters, a three-stage mechanism for vein formation is envisaged. The self-equilibrating mechanism involves the formation of mostly flat veins stacked along cross-stratal dikes within an impermeable volcanic pile. The dikes served as flow-restricted fluid feeders and as conduits for fluid discharge at the paleosurface. During the stable prefailure stage, the dike conduits act as dampers for controlling the fluid discharge rate and for keeping fluid pressure at a constant level needed for the opening of preexisting fracture for vein formation ($P_f \approx \sigma_1 + 0.5T$) at specific depths. The formation of veins corresponds to an equilibrating process to release differential fluid pressure (ΔP) that builds up vertically in the flow-restricted conduits. The ΔP is induced by the decrease of the lithostatic pressure as far as the hydrothermal fluids move upward at a low velocity. At a critical state, when the total fluid pressure accumulated by the veins exceeds the total lithostatic load, hydraulic rupturing of the sommital part of the volcanic pile induces instantaneous fluid depressurization (failure stage) at the vein

network-scale. The postfailure stage involves draining at the paleosurface of the underlying pressurized hydrothermal reservoir. At an advanced state, hydrothermal self-sealing leads progressively to the restoration of the initial and prefailure, flow-restricted conditions of the dike conduits. A crustal depth of 2 to 5 km and an extensional regime (neutral external stress) are critical features for vein formation. The specificity of the tectonic regime and the crustal depth for the proposed and the previously documented models has significant genetic and exploration implications. This specificity suggests that for each tectonic regime corresponds an optimal crustal depth for the formation of gold-bearing veins.

INTRODUCTION

Hydrothermal veins are one of the most common styles of gold-bearing mineralization, known and mined since ancestral times (Haynes, 1993). However, the understanding of vein formation mechanisms is far from complete mainly because gold-bearing quartz veins form in a wide range of tectonic regimes and crustal depths (0 to > 25 km), thus involving different physical conditions and specific mechanisms. Studies aimed to decipher conditions of vein formation focused mainly on hydrothermal mineral filling textures (e.g., Robert and Brown, 1986a; Dowling and Morrison, 1989; Vearncombe, 1993; Dong et al., 1995; Dong and Morrison, 1995) or on the geometrical relationships between vein networks and tectonic settings at mine- and camp-scale (e.g., Robert and Brown, 1986b; Moritz and Crocket, 1990; Foxford et al., 1995; Miller et al., 1995; Reid et al., 1995) or on both (e.g., Boullier and Robert, 1992; Harley and Charlesworth, 1996; Callan and Spooner, 1998).

Two different mechanisms of vein formation have been documented for specific geotectonic environments and crustal depths: the fault-valve and the suction pump models. The fault-valve mechanism was inferred from characteristics of typical "mesothermal" vein deposits (Sibson et al., 1988; Cox et al., 1990; Sibson, 1990a, 1990b). It is invoked as the prominent mechanism for vein formation in crustal depth ranging from about 5 to >25 km (Groves et al., 1995; McCuaig and Kerrich, 1998). The suction pump model (Sibson, 1987; 1990b) accounts for vein formation in epithermal settings (0 to 2 km).

This paper documents the self-equilibrating mechanism for vein formation, which was elaborated to account for the particular characteristics of the gold-bearing vein network

at the Géant Dormant gold mine. The proposed mechanism is based on the basic concepts supporting both documented mechanisms of vein formation and on various parameters, including: the tectonic regime, the fluid flow vectors, the crustal depth, the host rock permeability, the fluid pressure, the mineral precipitating conditions and the scale of filling processes (zoning). These parameters were estimated using the characteristics of the veins, the hydrothermal alterations and the host rocks at the Géant Dormant mine. The comparison with a recent gold-bearing vein system (Emperer mine, Fiji), suggests that the proposed mechanism may be applicable for vein systems formed in a transitional (2 to 5 km) crustal depth, between epithermal and mesothermal environments. The proposed model has significant implications for gold-bearing vein formation and exploration.

SUMMARY OF THE GÉANT DORMANT CHARACTERISTICS

The geological setting and gold-mineralization characteristics are described by Gaboury et al. (1996a) and Gaboury and Daigneault (1999a). Only important features are summarized below.

Mine geology

The Géant Dormant mine is a sulfide-rich quartz vein-type gold deposit hosted within the first volcanic cycle (2730 to 2720 Ma) of the Northern Volcanic Zone (Chown et al., 1992) of the Archean Abitibi greenstone belt (Fig. 1). As of January 1999, production had attained 1.4 million metric tons (MT) at 9.3 g/t Au with reserves in all categories estimated at 0.6 MT at 10.7 g/t Au. The gold mineralization is centered about a calc-alkalic

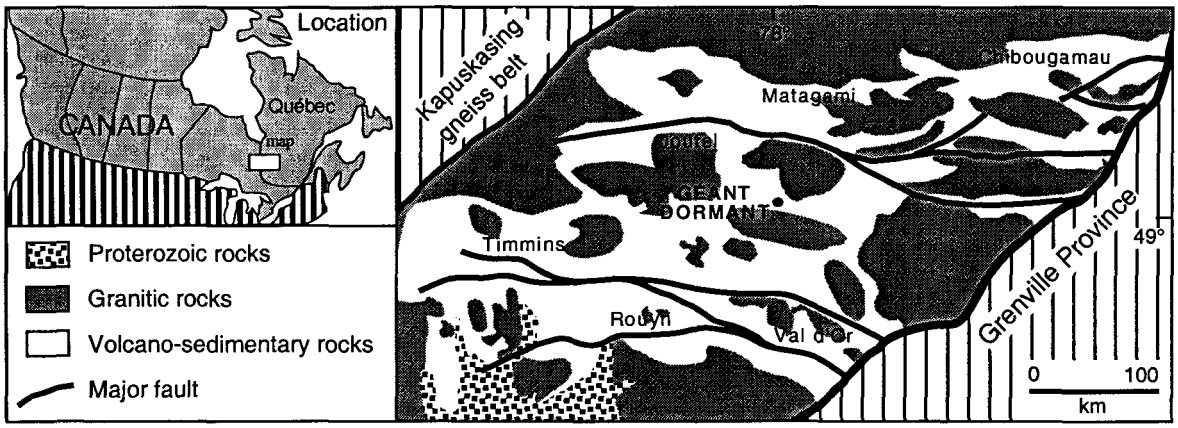

Figure 1. Simplified geological map showing the location of the Géant Dormant gold deposit at the Abibibi belt scale. Modified from MERQ-OSG (1983).

felsic complex which intrudes a volcano-sedimentary succession composed of mafic tholeiitic sills and lesser interbedded pelagic sediments (fine-grained volcaniclastic rocks, cherts and magnetite-rich iron-formations) and units of mafic tholeiitic pillowed and felsic calc-alkalic lavas (Figs. 2 and 3). The felsic complex comprises a dacitic subvolcanic dome and a swarm of polyphazed plagioclase-phyric (FP) and quartz and plagioclase-phyric (QFP) felsic dikes (2722 ± 2 Ma). Synvolcanic mafic tholeiitic and early-tectonic shoshonitic dikes crosscut the gold-bearing veins. The 1.5-km-thick host volcano-sedimentary sequence lies conformably on the North volcanic assemblage and it is structurally overlain by the South volcanic assemblage (Fig. 2a). A strongly altered (sericite, Fe-carbonate, pyrite with traces of gold) QFP unit defines the top of the host sequence (Fig. 2a). The host volcanic pile formed in a deep (> 3,150 m) submarine setting by sequential pulses from two different and spatially isolated magmatic sources: a proximal felsic calc-alkalic source and a distal mafic tholeiitic source.

The volcanic strata strike predominantly E-W and dip steeply to the south (Fig. 2), forming a normal homoclinal stratigraphic succession lying on the northern limb of an east-trending regional syncline with a subhorizontal axis. The weakly penetrative subvertical E-W trending regional schistosity overprints locally all rock types. As the internal deformation within the tilted sequence is weak and heterogeneous, primary geometrical relationships and vein textures are commonly well-preserved. All rock types, including gold-bearing veins, have been metamorphosed to the greenschist facies.

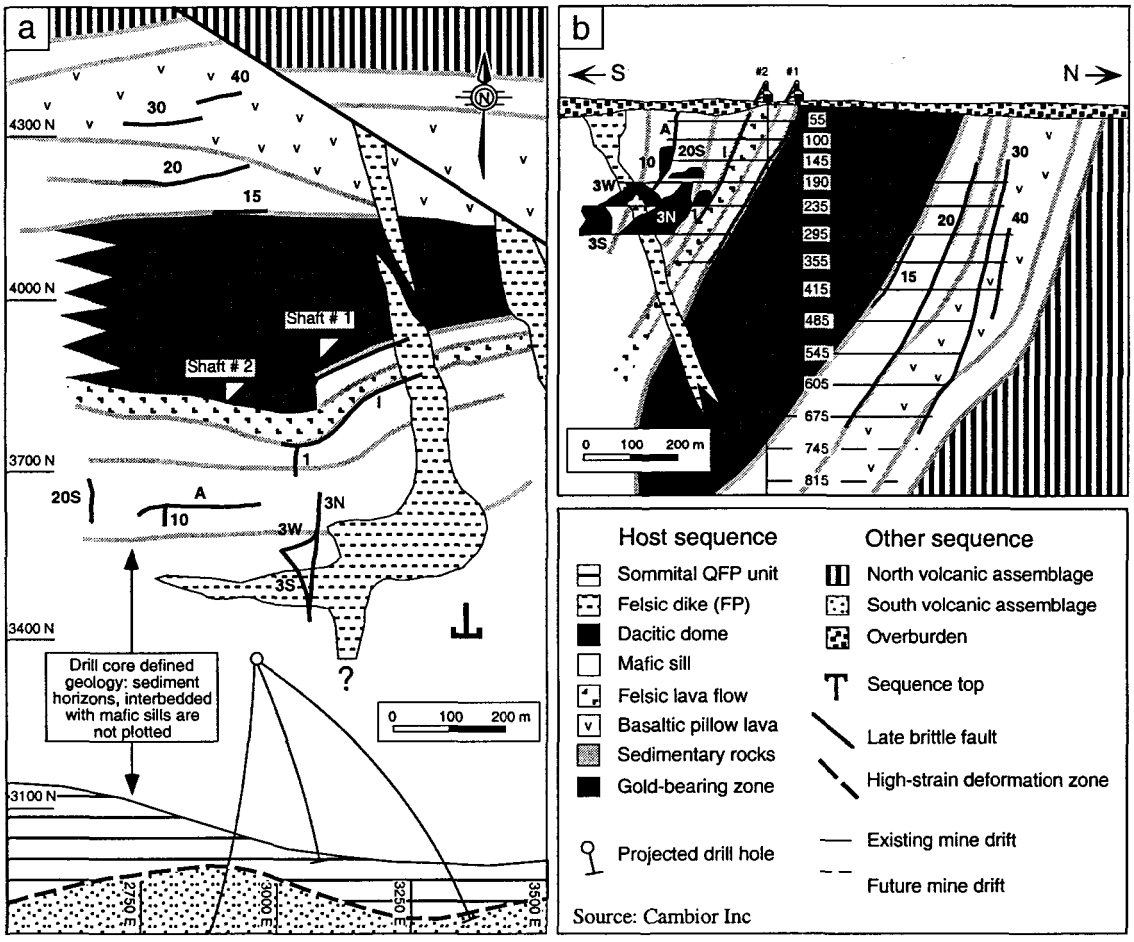

Figure 2. Characteristics of the mine sequence. (a) Simplified geological plan of the Géant Dormant mine area. (b) Idealized vertical N-S cross section. Various gold-bearing zones are labeled: A, 10, 40, etc.

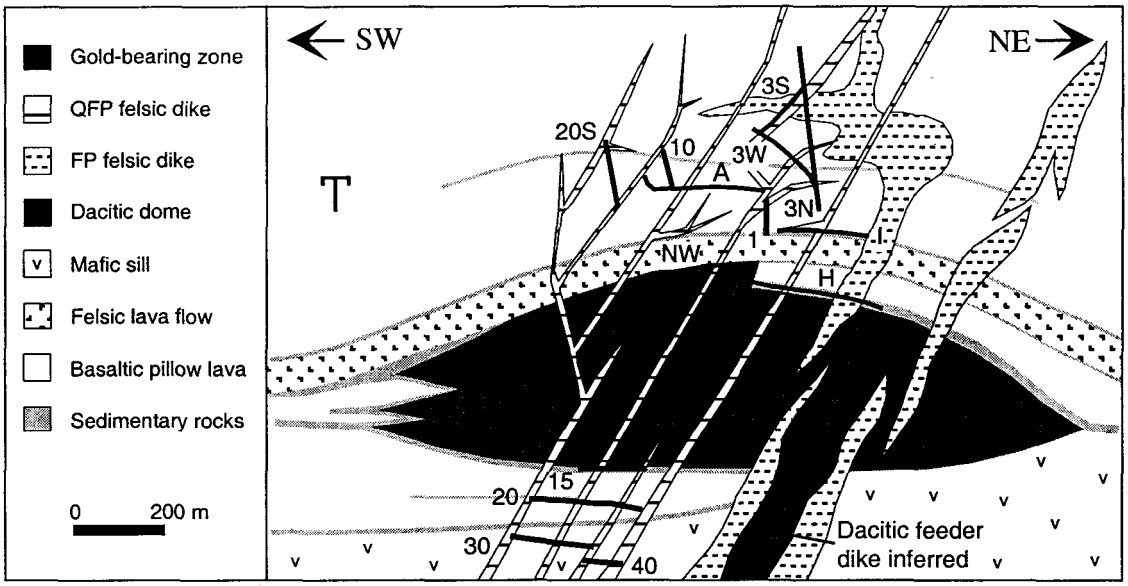

Figure 3. Reconstructed SW-NE cross-section of the volcanic sequence before tilting related to the ductile regional shortening, showing the spatial association between veins and QFP dikes at the deposit-scale. Figure modified from Gaboury and Daigneault (1999a) to account for the representation of the true dips of QFP dikes and veins (See Fig. 5b).

Hydrothermal events

Hydrothermal activity comprises three successive mineralizing events related to specific stages of the volcanic pile construction: (1) a seafloor-related gold-poor event; characterized by sericite, chlorite, and quartz alteration with disseminations and stringers of gold-bearing pyrrhotite and chalcopyrite affecting rocks formed on the paleo-seafloor; (2) an autometasomatic event affecting only the dacitic dome, expressed by chloritization and dissemination of auriferous pyrite; and (3) quartz-sulfide vein-style gold mineralization and associated altered and mineralized QFP dikes.

Gold-bearing veins are composed of 5 to 80% (average ≈ 30%) of sulfides including pyrite, pyrrhotite, chalcopyrite, sphalerite and traces of arsenopyrite. Quartz is the dominant gangue mineral with lesser amounts (< 1%) of chlorite, sericite, tourmaline, calcite and actinolite. Mass balance calculations demonstrated that selvage alteration along vein margins is commonly lacking or only weakly developed (chlorite-sericite), and that the mafic sills are devoid of significant alteration at the deposit-scale (Gaboury and Daigneault, 1999a). QFP dikes, characterized by strong internal sericitization (gains of SiO_2, K_2O; loss of Na_2O) and disseminated auriferous pyrite (~ 5%), are spatially associated with the veins (Fig. 3) and are interpreted as fluid conduits for vein formation at the deposit-scale (Gaboury and Daigneault, 1999a).

Geometrical features of gold-bearing veins

Gold-bearing veins are massive (cf. Dong et al., 1995) and tabular structures ranging in thickness from 5 to 100 cm, averaging 50 cm. Vein contacts, preserved of the

overprinting deformation, are sharp, planar and free of surrounding breccia and schistosity (Figs. 4a, 4b and 4c). The lack of hydrothermal breccia is a ubiquitous characteristic of the veins (Fig. 4). The orebody comprises four main sets of veins and displays an increasing complexity toward the paleosurface (Figs. 2a and 3). The sets include in order of tonnage (Gaboury et al., 1996): (1) E-W-striking steeply (70-85°) S-dipping; (2) N-S-striking moderately (45°) SE-dipping; (3) SE-NW-striking moderately (50°) NE-dipping and; (4) SW-NE-striking moderately (40°) SE-dipping (Fig. 5a). Interbranching of the main vein sets, without any crosscutting relationships, is a common phenomenon (Fig. 4d). There is an empirical ~100 m distance ("magic" distance: see Peters, 1993) that characterize the spacing between most E-W-trending veins (Fig. 2). Factors controlling vein formation correspond to primary permeable features such as stratigraphic contacts, synvolcanic faults, and preexisting joints (Gaboury et al., 1996). Veins, regardless of their attitude, display the same characteristics: (1) open-space filling textures (below); (2) planar contacts; (3) extensive continuity (> 800 m); (4) bridge stud occurrences; (5) absence of slip lineation, slickenside and hydrothermal mineral elongation along the veinwall surface indicating any component of movement during vein formation. Collectively, these characteristics indicate that veins were formed by extensional fracture opening.

Crosscutting, structural and geometric relationships indicate that veins formed in original subhorizontal strata closely after the injection of calc-alkalic QFP dikes, but before the end of synvolcanic mafic tholeiitic magmatism (Gaboury and Daigneault, 1999a). The actual geometry of the vein network results from the strata folding related to regional horizontal shortening (Fig. 5).

Figure 4. Field photographs of the main vein characteristics. (a) Massive NW-SE-trending vein of grey quartz (black material) and sulfides showing typical planar and sharp contacts, as indicated by white arrows. Note the crosscutting of a pyrite aggregate (Py) by pyrrhotite (Po). Pocket knife (8-cm-long) as scale. Face stope view of the vein #3S, level 235. (b) Massive, E-W-trending vein of grey quartz (black material) and sulfides showing typical planar and sharp contacts (white arrows). Sulfides occur as stringers cementing brecciated quartz fragments. Rockbolt (10 cm) as scale. Face stope view of the vein #30, level 235. (c) Vein showing mottled quartz composed of grey quartz (Qz-G) cemented by milky quartz (Qz-M), and later sulfides occurring as cement of both quartz. Note the sharp and planar contact of the vein with the mafic sill host rock, and the lack of significant visual hydrothermal alteration and breccia along the vein margin (white arrow). Pocket knife as scale, located close to the white arrow. Face stope view of the vein #A, level 235. (d) Typical interbranching of gold bearing-veins showing the merging of early grey quartz (Qz-G) and the merging of later pyrite bands (Py). Hammer (33-cm-long) as scale. Wall stope view of the vein #A, level 190. (e) Vein showing a massive lens of prismatic pyrite (Py) occurring as open space filling between wallrock coating of comb-textured grey quartz crystals (black material) up to 2-cm-long. The grey quartz crystals are cemented by later, pre-pyrite, milky quartz (white material). Vein contacts are indicated by the white arrows. Pocket knife as scale. Floor stope view of the vein #3W, level 235. (f) Close-up view showing typical brecciated textures of veins: grey quartz (Qz-G) cemented by milky quartz (Qz-M). Sulfides (chalcopyrite and pyrrhotite) occur as cement of both generations of quartz. Pocket knife as scale. Roof stope view of the vein #20, level 355.

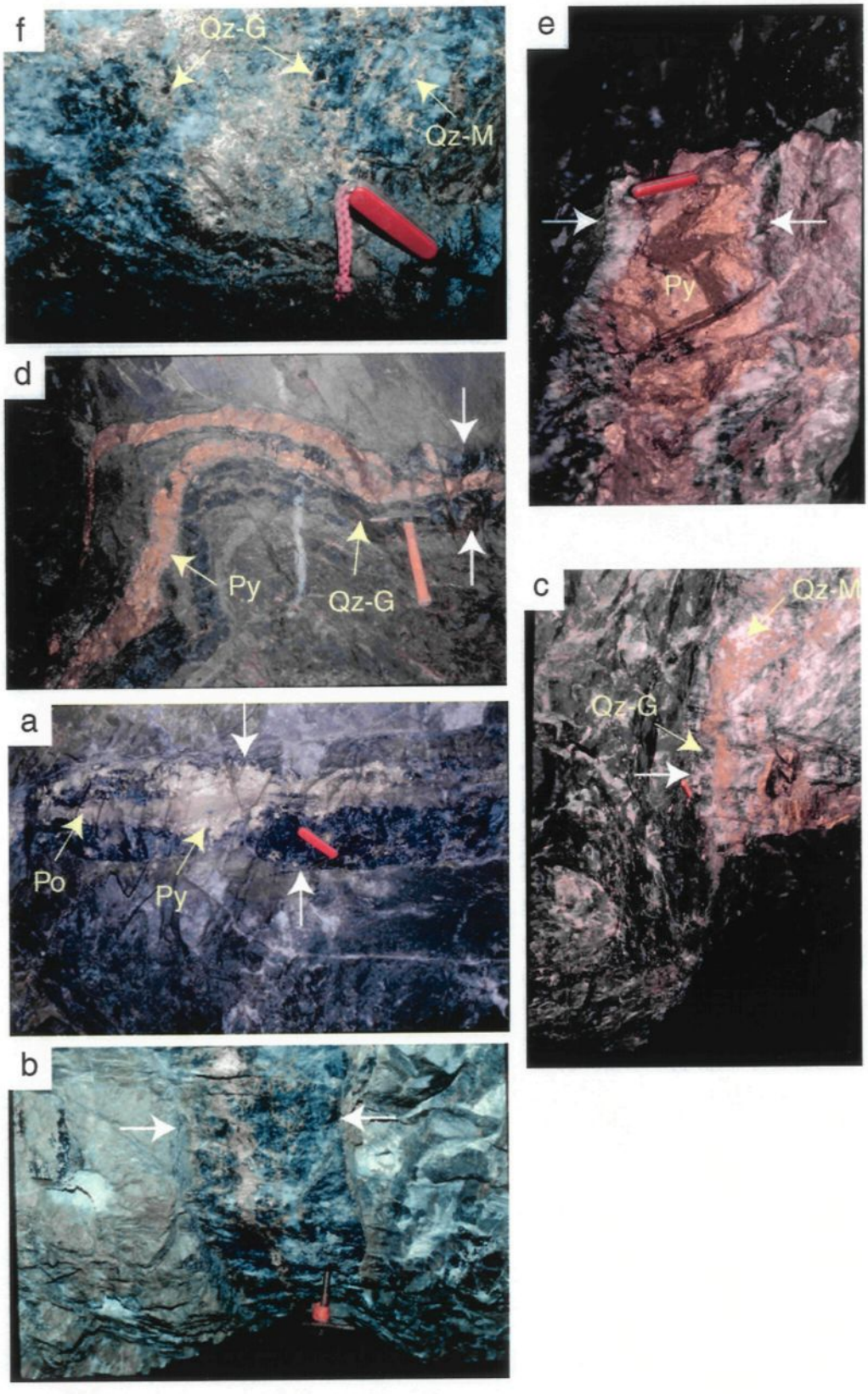
f
Qz-G
Qz-M
e
Py
d
Py
Qz-G
c
Qz-M
Qz-G
a
Po
Py
b

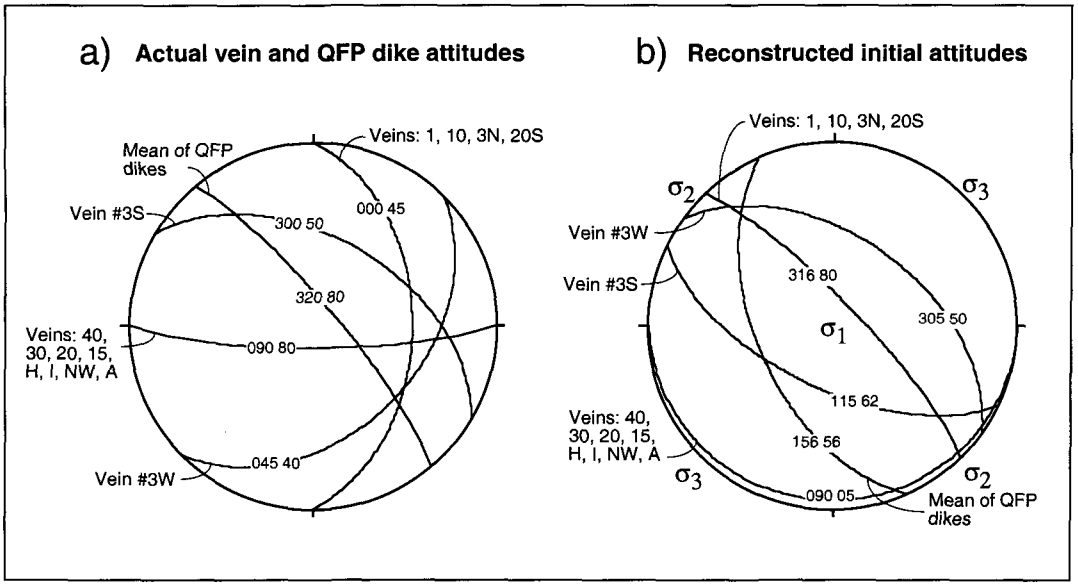

Figure 5. Structural features of veins and QFP dikes. Equal area projections (lower hemisphere) of (a) actual and (b) reconstructed (untilted) main vein and QFP dike attitudes (vein data from Gaboury et al., 1996a; QFP dike data from Gaboury and Daigneault, 1999a). The reconstructed attitude results from a 75° northward rotation along an E-W subhorizontal axis, corresponding to the strata dip and fold axis (Gaboury et al., 1996a). The projection of reconstructed cross-stratal structures (1, 3N, 3S, 3W, 10, 20S) yields a geometry coherent with the Anderson's (1951) conjugated normal fault pattern, where s1 is vertical and s2 and s3 are horizontal.

Vein paragenesis and texture

Gold-bearing veins show various textures and proportions of hydrothermal minerals that are related to three successive stages of filling: pre-ore, ore and post-ore stages (Fig. 6). The pre-ore stage consists of quartz with minor (< 1%) chlorite, sericite and a trace of tourmaline. Three types of quartz are recognized based on their color, grain size and habit (Fig. 6). The first type, which is the most volumetrically abundant, is a paragenetically early grey to black quartz (referred to below as grey; Fig. 4) that forms subhedral crystals up to 2 cm long. This quartz forms essentially massive veins (< 50 cm) defined by interlocking of variously oriented isogranular quartz crystals (Figs. 4a and 4b). In some cases, this quartz also forms comb-textured veins (Fig. 4e). The second type is milky and cherty (microcrystalline) and occurs as breccia cement of grey quartz (Figs. 4c, 4f, 6, and 7). The third type is massive white quartz and forms parallel crack-seal veinlets (< 2 cm) cutting across the two earlier quartz generations. Stylolite-like layers of chlorite are associated with the white quartz.

The ore stage includes sulfides and minor chlorite and is devoid of quartz (Fig. 6). Massive aggregates (Fig. 4d) and bands (< 20 cm) of prismatic pyrite (Figs. 4d and 4e) were deposited early in this stage in open-spaces (Fig. 7). Pyrite crystals contain inclusions of pyrrhotite, chalcopyrite and sphalerite. Pyrrhotite followed by chalcopyrite and sphalerite (Fig. 6) cement fragments of grey and milky quartz (Figs. 4c and 4f) and fractured pyrite. Late chlorite flakes are intergrown with sphalerite. Native gold and silver, as well as electrum occur as μm-scale inclusions in pyrite, pyrrhotite, chalcopyrite and sphalerite and as fine fracture fillings in pyrite associated with other sulfides (Fig. 6).

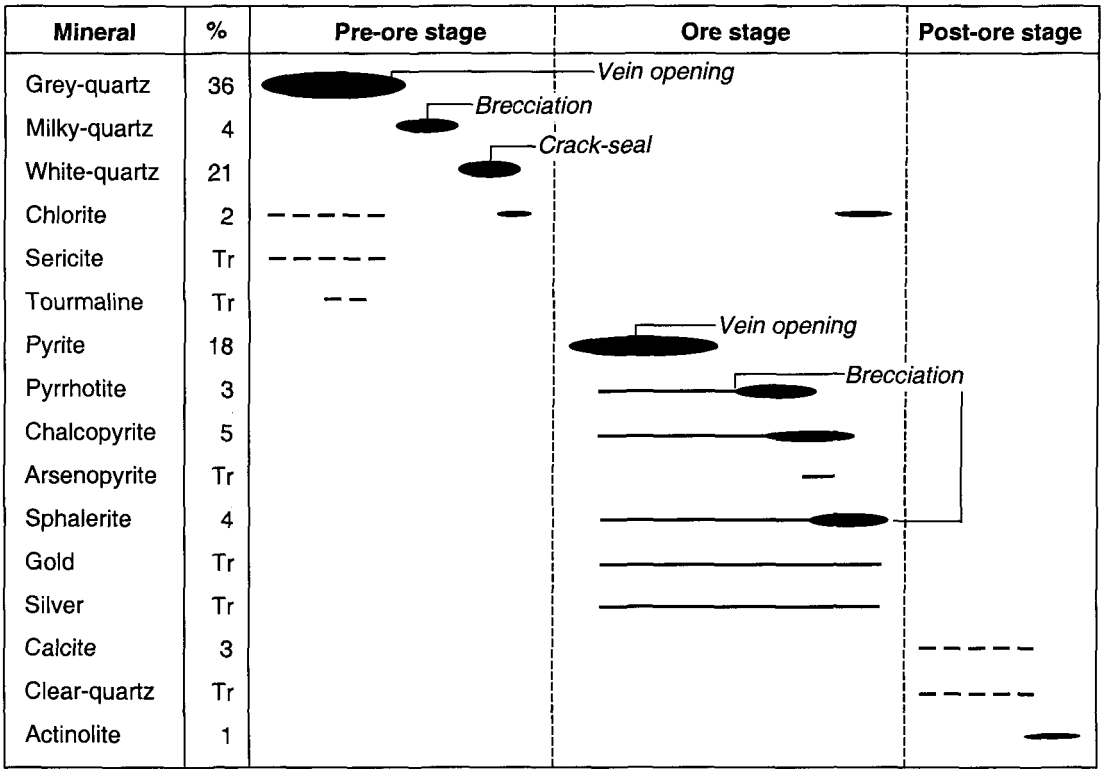

Figure 6. Detailed filling mineral paragenesis and average percentage composition for gold-bearing veins. Data compiled from 66 slab samples (Annexe 4). Figure modified from Gaboury et al. (1999).

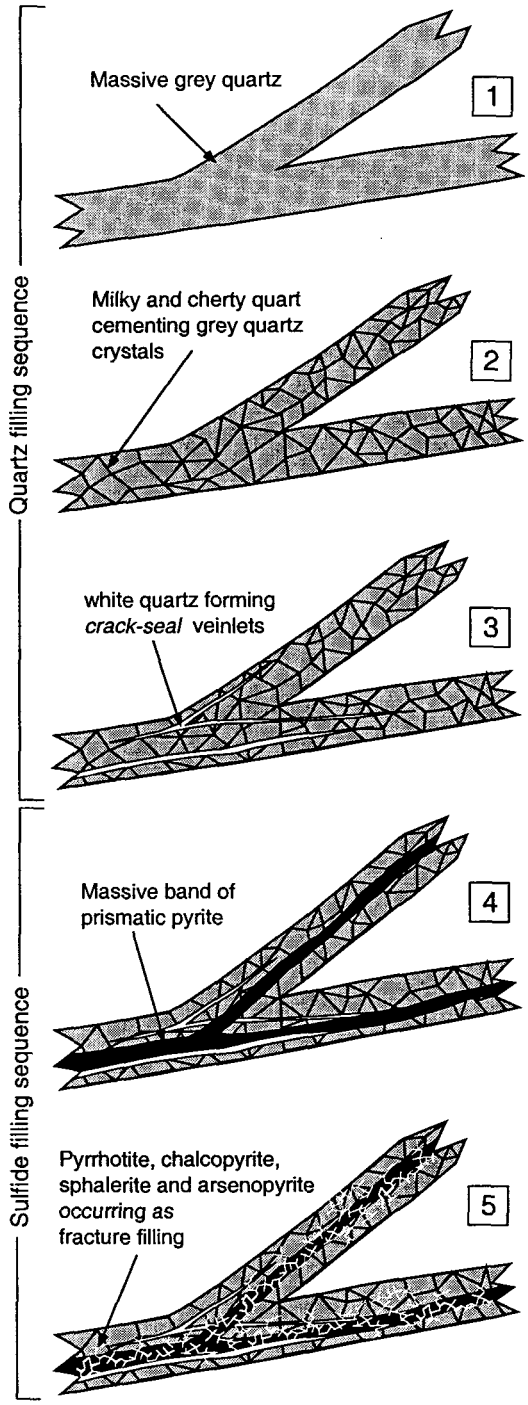

Figure 7. Schematic representation of the sequential filling stage of the gold-bearing, quartz-sulfide veins at the Géant Dormant deposit.

The post-ore stage is related to the overprinting ductile deformation and greenschist metamorphism (Fig. 6) and comprises calcite, clear quartz and actinolite. Calcite occurs mainly as veinlets (< 1 cm thick) surrounding and cutting gold-bearing veins and as minor cement between all previously precipitated hydrothermal minerals. Clear quartz resulting from pressure-solution occurs in pressure shadows. The late overgrowth of radiating acicular actinolite in gold-bearing veins is related to metamorphism.

Genetic Model

The gold-bearing veins were formed during the last stage of a volcanogenic hydrothermal system, which evolved from gold-poor seafloor-related to gold-rich vein-type mineralization during deep-water volcanic construction (Gaboury and Daigneault, 1999a). This volcanogenic affiliation of the veins, interpreted from field relationships, is also supported by trace element contents in sulfides of the various hydrothermal events (Gaboury and Daigneault, 1999b) as well as by oxygen and sulfur isotope data (Gaboury et al., 1999).

REVIEW OF VEIN FORMATION MODELS

Fault-valve mechanism

The fault-valve mechanism involves supralithostatic fluid pressurization within an impermeable and moderate to deep (5 to >25 km) crustal environment stressed by a horizontal shortening regime (Sibson et al., 1988; Cox et al., 1990; Sibson, 1990a, 1990b). Fluid overpressurizations below impermeable barriers (Fig. 8a) induce hydraulic

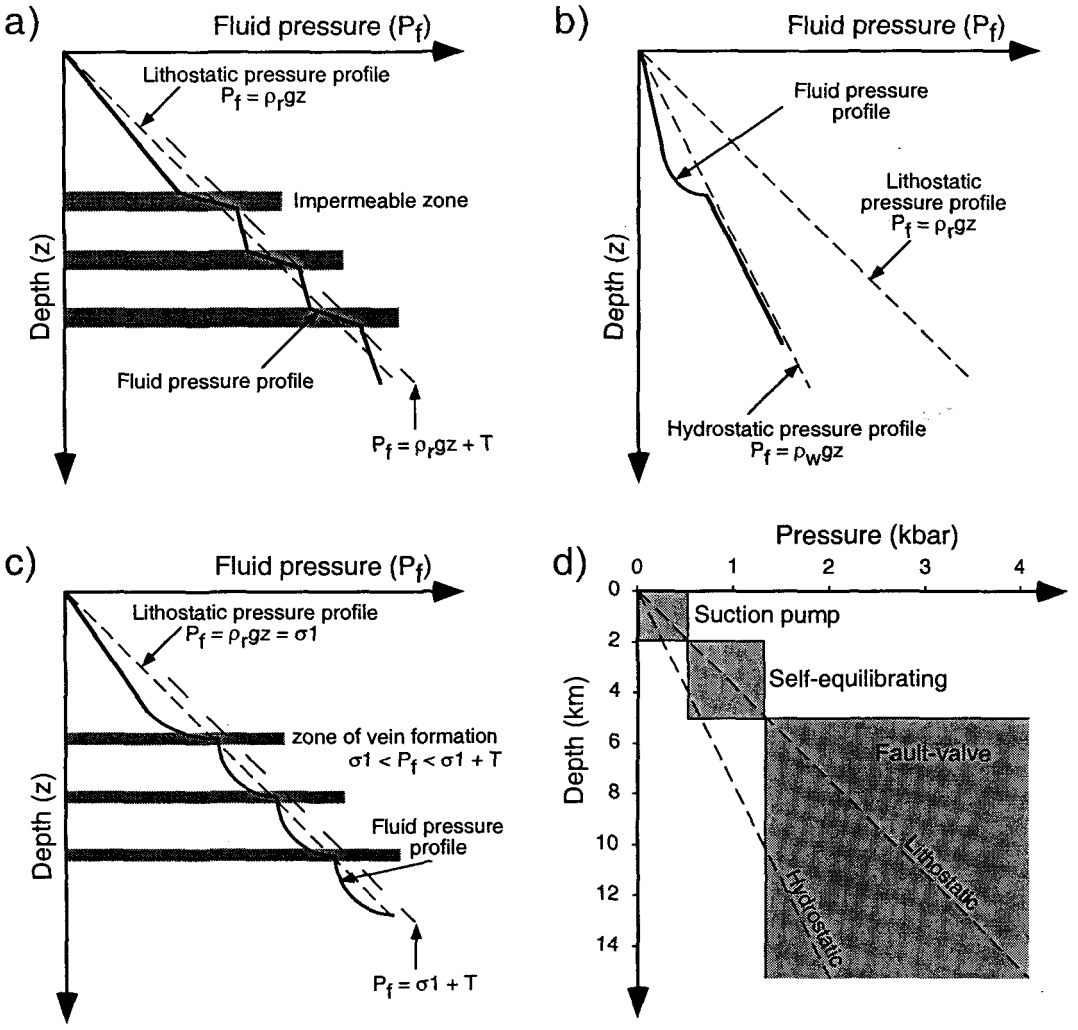

Figure 8. Inferred pressure versus depth for (a) the fault-valve (Sibson et al., 1988; Cox, 1990), (b) the suction pump and (c) the self-equilibrating mechanisms. The illustrated fluid profile for the self-equilibrating mechanism corresponds to an advanced state of the prefailure stage, when a major part of the impermeable pile is fluid pressurized. (d) Diagram showing the relative inferred depth and pressure of action of the three mechanism. Pressure data from Thompson and Connolly (1992).

reactivation along subvertical inverse faults and shear zones acting as hydrothermal discharge conduits. The resulting fault failures create fracture permeability for fluid draining and fault-fill vein formation. Subhorizontal extension veins (flats), commonly associated with the fault-fill veins, are formed during the pressurization period and before fault rupturing. Flat formation is favored by the high fluid pressure and by the subhorizontal maximum stress vector (σ_1). Repetition of pressurization and rupturing cycle (Fig. 9) is invoked to account for the multiple events of vein opening and filling. This model implies considerable fluid pressure variations from supralithostatic to hydrostatic (Fig. 9), which are manifested by hydrothermal breccias (Robert and Brown, 1986a; Groves et al., 1995).

Suction pump mechanism

The suction pump model applies to superficial crustal environments (0-2 km) affected by a wrench tectonic regime and where the fluid regime is hydrostatic (Sibson, 1987; 1990b). In such a context, it is invoked that relative strike-slip movements along *en échelon* fault systems are accommodated by extensional zones named dilatational jogs. The extensional zones act as suction pumps, draining the surrounding fluids in the dilatational jogs. The resulting fluid inflow induces instantaneous drops of fluid pressure (Fig. 8b) leading to hydrothermal brecciation, boiling of hydrothermal fluids and mineral precipitation within the jogs. The repetition of this mechanism (Fig. 9), triggered by tectonic activities, accounts for the episodic events of opening, brecciation, and mineral filling recorded in the jogs.

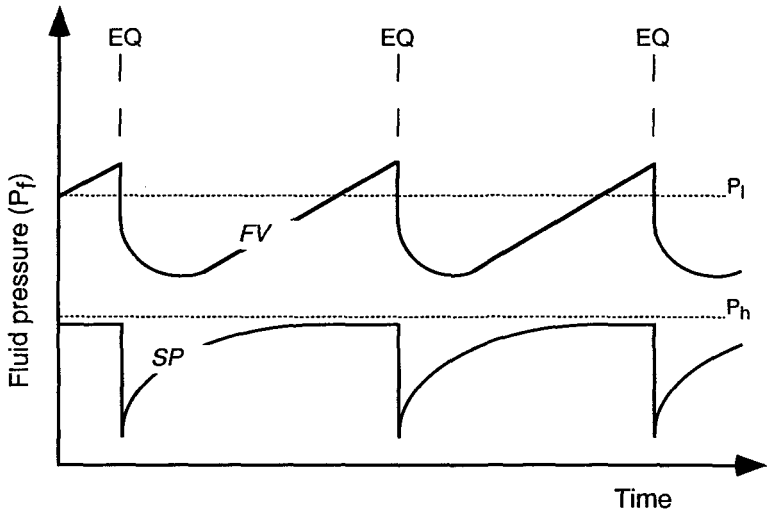

Figure 9. Inferred fluid pressure fluctuations for the fault-valve (FV) and the suction pump (SP) mechanisms in relation with earthquake (EQ) rupturing episodes. Pl and Ph correspond to lithostatic and hydrostatic pressures respectively. Figure modified from (Sibson et al., 1988; Cox, 1990).

VEIN FORMATION CONDITIONS AT THE GÉANT DORMANT DEPOSIT

Vein formation implies fluid circulation into fractures and favorable conditions for mineral precipitation (Jébrak, 1992; Peters, 1993). As vein networks represent fossil hydrothermal systems, their characteristics as well as their relations with the host environment can be used to ascertain the conditions governing vein formation. These conditions are addressed below.

Tectonic regime

Examination of the Fig. 5b reveals that the reconstructed, pre-folding network of veins and QFP dikes shares a common NW-SE-trending. Such a trending-parallelism between QFP dikes and veins suggests a structural link between both generations of planar elements. In addition, the geometry of the reconstructed mineralized structures, except for veins formed along the strata-parallel anisotropies, is reminiscent of the Anderson's (1951) conjugated normal fault pattern (Fig. 4b). These geometrical observations suggest that the cross-stratal veins (1, 3N, 3W, 3S, 10 and 20S), which occur in the upper part of the host sequence (Fig. 3), were formed by the opening of preexisting fractures developed during an extensional regime. Such a tectonic regime is also coherent with the abundance of the QFP dikes, because dikes forming parallel-trending swarms are commonly injected during synvolcanic extensional regime (Gudmundsson, 1983). These structural evidences coupled to the mode of vein formation by extensional opening of preexisting fractures, indicate that the gold-bearing veins were likely formed during an extensional regime.

Crustal depth

Absolute crustal depth of vein formation is not constrained but inferred to be equivalent to a charge of 2-3 km of rocks. First, veins are distributed within a 1 km-thick rock pile (Figs 2 and 3). Second, there is at least 500 m of rocks, geochemically coherent with the hosts (Gaboury and Daigneault, 1999a), that lie up-section the most southern mined vein (Fig. 2a). Third, the inferred deep submarine setting (> 3,150 m) during vein formation (Gaboury and Daigneault, 1999a) adds a significant pressure load. Since seawater is less than one half the density of the rocks, this implies an additional load corresponding to about 1.5 km of rock. This 2-3 km inferred crustal level is consistent with the vein characteristics indicating formation in shallow structural levels, such as: (1) the interpreted vertical σ_1 attitude during vein formation (Fig. 5b); (2) the increasingly complex geometry of the vein network toward the paleosurface (Fig. 3); and (3) the brittle but cohesive nature of the mineralized fractures (Gaboury et al., 1996a).

Fluid flow vectors

Vein network geometry can be used to interpret initial fluid flow vectors. In the present case, the parallelism between the stata and most veins (40, 30, 20, 15, A, I, H, NW: Figs. 2 and 3) implies that these veins were formed initially as subhorizontal conduits without hydraulic connectivity with the paleosurface. Other veins (1, 3S, 3W, 3N, 10, 20S), which are smaller gold-bearing structures (Gaboury et al., 1996), have an initial (reconstructed) dip ranging from 45° to 80° (Figs. 3 and 5b). These cross-stratal structures share the same mineralogical composition and textures with the subhorizontal veins

(Annexe 4). Therefore, these latter veins are also interpreted as structures that have been formed without connectivity with the paleosurface.

Since hydrothermal systems are analogous to plumbing networks, fluid discharge toward the surface is fundamental in maintaining hydrothermal activity. As such, QFP dikes constitute preferential conduits for fluid discharge at the seafloor because of: (1) their initial steep attitude (dip $\approx 56°$: Fig. 5b), perpendicular to the strata; (2) their lateral and vertical continuity at the deposit-scale (Fig. 3); (3) their temporal and spatial association with the gold-bearing veins (Fig. 3); (4) their strong internal alteration and mineralization (Gaboury and Daigneault, 1999a); and (5) their alteration oxygen isotopic signature attesting of the hydrothermal link with the gold-bearing veins (Gaboury et al., 1999). Based on REE patterns (Gaboury and Daigneault, 1999a; Gaboury, Unpub. data), some of these cross-stratal QFP dikes are interpreted as magma feeders of the strongly altered QFP unit lying at the top of the host sequence (Fig. 2a). Hence, some QFP dikes were likely continuous conduits to the seafloor surface during vein formation. Finally, these geometrical considerations indicate that veins represent mostly flat structures staked along QFP dikes, and that the latter constitute subvertical channelways for feeding the veins and for fluid discharge at seafloor.

Host rock permeability

The permeability of a volcanic pile can be ascertained by considering the documented permeability of the rocks and their geometrical relationships, as well as the nature and extent of hydrothermal alteration. Mafic massive igneous rocks, as the mafic

sills which are the dominant host of the gold-bearing veins, have a very low permeability (e.g., Brace, 1984). Furthermore, mafic sills promote the impermeability of the volcanic pile because the sill stack acts as a subhorizontal barrier. The lack of significant alteration in the mafic sills (Gaboury and Daigneault, 1999a), even along vein margins, is consistent with the invoked impermeable nature of the mafic sills. Finally, as the sedimentary rocks were endured by the seafloor-related hydrothermal event before mafic sill injection (Gaboury and Daigneault, 1999a), the whole volcanic host pile can be considered impermeable during vein formation.

Fluid pressure

Some empirical criteria can be used to estimate the fluid pressure limits and their variations in time. The initial subhorizontal attitude of gold-bearing veins implies that fluid pressure was at a sufficient level to maintain open fractures oriented perpendicular to the lithostatic charge. This consideration corroborates the impermeable nature of the host sequence and implies that fluid pressure was at a lithostatic level. Considering the stress field of an extensional tectonic regime (Fig. 5b), the fluid pressure (P_f) can be expressed as: $P_f = \rho_r g z = \sigma_1$, where ρ_r is the density of rock overburden, g is the gravitational acceleration, and z is the depth.

Hydrothermal breccias express fluid pressure variations in time (Jébrak, 1998). In impermeable settings, pressurized at lithostatic levels, breccias form by explosion and by implosion (Jébrak, 1998). In both cases, breccia development involves fluid pressure exceeding the tensile strength of the pressurized rock (T). Explosion breccia or hydraulic

fracturing is related to fluid pressure increase to a level of $P_f > \rho_r gz + T$ (Phillips, 1972). Implosion breccia occurs when pressurized conduits at supralithostatic levels ($P_f > \rho_r gz + T$) are subjected to a sudden fluid pressure drop (Fig. 10). Brecciation occurs if the difference in pressure between the rock and the fluid-pressurized fracture is greater than the tensile strength of the rock (Jébrak, 1992). In such case, fluids having penetrated the wall rock under the high fluid pressure then expand instantaneously and brecciate the wallrock (Craw and McKeag, 1995). For the Géant Dormant vein network, the lack of hydrothermal breccia along vein margins implies that fluid pressure was equal to or weakly greater than the lithostatic pressure, but lower than the critical pressure limit for brecciation. The maximum fluid pressure can thus by expressed as: $\sigma_1 < P_f < \sigma_1 + T$. In such conditions, fluid pressure variations can occur without creating wallrock brecciation along the pressurized hydrothermal conduits.

The spatial distribution of hydrothermal alteration reflects the fluid pressure regimes and the fluid flow patterns. The large alteration halo surrounding epithermal deposits manifests the permeability of the rocks and the hydrostatic fluid regime (e.g., Bogie and Lawless, 1987; White and Hedenquist, 1990). Conversely, the wallrock alteration associated with mesothermal veins (Fig. 10) is attributed to lateral fluid infiltration within the impermeable enclosing rocks (Jébrak, 1992), due to the fluid pressure at supralithostatic level (Cox et al., 1990). In such a view, the impermeable nature of the host sequence at the Géant Dormant, combined with a fluid pressure lower that the critical value for penetrating the enclosing rocks ($P_f < \sigma_1 + T$), inhibited both the development of an alteration halo and the formation of wallrock alteration respectively.

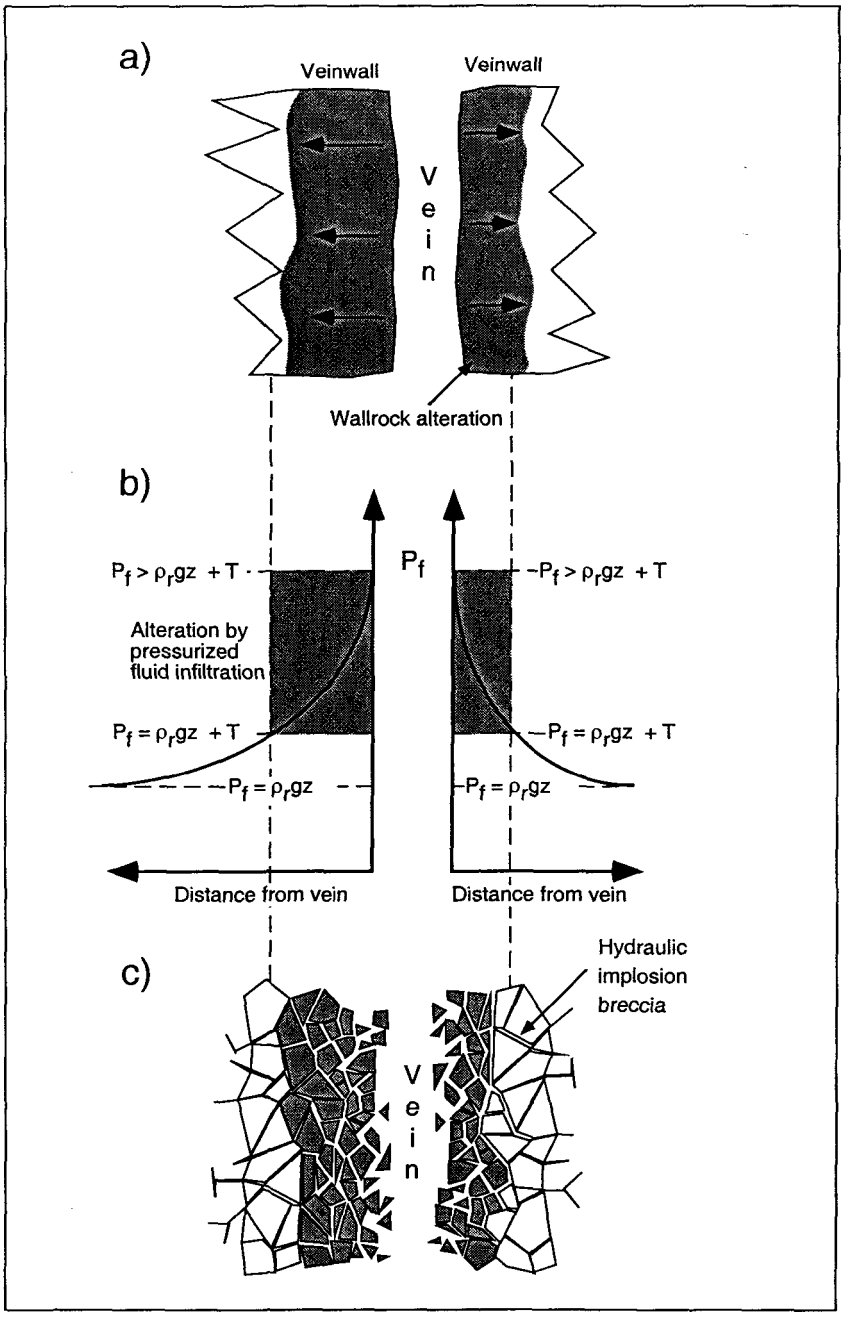

Figure 10. Role of fluid pressure for alteration development and hydraulic brecciation associated with vein formed at high fluid pressure. (a) Initial state of supralithostatic fluid pressure (Pf) and hydrothermal alteration by lateral fluid infiltration within the wallrock. (b) Fluid profile across the pressurized conduit (vein), showing the link between the fluid pressure and the lateral extent of wallrock alteration. (c) Hydraulic breccia resulting of fluid pressure drop and fluid expansion within the wallrock.

Hence, a maximum pressure limit of $\sigma_1 < P_f < \sigma_1 + T$ is supported by both the lack of hydrothermal breccia and the alteration characteristics.

Mineral precipitating conditions

Various studies have demonstrated that filling quartz textures reflect the conditions of vein formation (Dowling and Morrison, 1989; Vearncombe, 1993; Dong et al., 1995). Veins comprise three successive phases of pre-ore quartz deposition, which are characterized by specific textures and grain sizes (Figs. 6 and 7). Early paragenetic grey quartz forming isogranular and massive textures of attests to the homogenous filling conditions (Vearncombe, 1993). This implies a constant rate of fracture opening and a homogeneous fluid pressure to maintain the stable conditions needed for the growth of euhedral quartz crystals in fluid-filled spaces. Inversely, the microcrystalline milky quartz, cementing the grey quartz crystals, indicates a rapid precipitation due to a destabilization of the quartz precipitation conditions (Vearncombe, 1993). The cement texture and the cherty aspect are features compatible with an instantaneous precipitation of silica following fluid depressurization of the veins (Jébrak, 1992). The formation of the crack-seal veinlets implies crack opening and quartz filling at a subdued rate compared to cavity-fill textures (Ramsay, 1980; Foxford et al., 1995) during fluid pressurized regime.

Combining fluid pressure constraints with the quartz textures, the following implications can be drawn. The first stage of quartz filling requests stable conditions in which fluid pressure was constant and at a certain lithostatic level ($\sigma_1 < P_f < \sigma_1 + T$) in order to maintain a progressive and slow opening rate of pre-existing fractures. Milky

quartz implies a release of fluid pressure to induce instantaneous quartz precipitation ($P_f < \sigma_1$). Wallrock brecciation during this event would be prevented due to the fluid being at a pressure lower than $\sigma_1 + T$. For the crack-seal veinlets, their mutual crosscutting and their scattered distribution within grey quartz veins suggest that their formation is related to isolated and repetitive events of fluid pressurization.

For the sulfides, similar textural relationships regarding the fluid pressure conditions can be drawn from the sequential paragenesis (Figs. 6 and 7). First, stable conditions, dominated by fluid pressure at a certain lithostatic level ($\sigma_1 < P_f < \sigma_1 + T$), account for the re-opening of the quartz vein and the early precipitation in this stage of the prismatic pyrite as massive aggregates and bands. Second, the cement-breccia texture of the other sulfides indicates that they precipitated during a brecciation event. Such a brecciation is compatible with a fluid pressure release, analogous to that involved for the precipitation of the milky quartz.

Scale of filling processes

Vein network zonings, as those expressed by textural, mineral and metallic variations of epithermal veins, reflect the evolution of hydrothermal fluids as they flow upward and equilibrate at various depths during vein filling events (Buchanan, 1981; White and Hedenquist, 1990). By comparison, veins at the Géant Dormant are characterized by homogeneous chemical and textural compositions. The chemical homogeneity is supported by the uniform mineralogical composition (Annexe 4), and by the lack of $\delta^{18}O$ and $\delta^{34}S$ data zoning (Gaboury et al., 1999) and trace element data zoning (Gaboury and Daigneault,

1999b) of the filling minerals at the deposit-scale. The textural homogeneity was reveled by vein mapping (Gaboury et al., 1996a) and by the systematic recording of textures from 66 samples (Annexe 4). These features imply that veins at the deposit-scale were formed by common processes and by similar fluids to account respectively for the textural and chemical characteristics.

The interbranching of the main veins (Fig. 7) corroborates their coeval formation. Furthermore, as veins result from polyphazed filling stages (Fig. 6), mineral relationships at the junctions of veins are of particular interest to ascertain the scale of filling processes. At the junction segments, the interbranching veins record systematically the same particular filling stages, in the same paragenetic sequence (Figs. 4d and 7). Therefore, each stage of vein filling should be a common and specific event recorded at the same time by all forming veins at specific crustal levels (interbranching veins) and probably at the deposit-scale. These large-scale vein filling processes are in good agreement with the lack of textural and chemical zoning, as the hydrothermal fluids equilibrated at the deposit- rather than at the vein-scale.

EMPIRICAL MODEL FOR VEIN FORMATION

Considering the preceding constraints and the bases of the two reviewed models, the following three-stage self-equilibrating mechanism for vein formation is envisaged. The "self-equilibrating" term is used to qualify first the constant pressure of the hydrothermal fluids at the locus of vein formation. Second, the term accounts for the invoked process by

which fluid pressure is equilibrated along cross-stratal conduits, by vein formation at specific crustal levels (see below).

Prefailure stage

The prefailure stage corresponds to a stable state of the hydrothermal system (t0-t1: Fig. 11), where the fluid pressure is at a lithostatic level ($\sigma_1 < P_f < \sigma_1 + T$). At the vein formation locus, fluids are maintained at a constant pressure by the weak permeability of the QFP dikes, which act as fluid discharge dampers (Fig. 12a). Grey quartz precipitates in open fractures during this stage. Open fractures represent lower pressure channelways than the surrounding rocks, hence favoring hydrothermal precipitation (Ridley, 1993). Inversely, QFP dikes, which are not free-flowing (open fracture) but rather flow-restricted conduits, constitute higher-pressure channelways, where hydrothermal precipitation is weak during this stage. Vein formation is essentially controlled by the opening of preexisting fractures (Gaboury et al., 1996a). This feature is compatible with the inferred fluid pressure level, which is close to, but lower than, the critical limit for fracture development by hydraulic fracturing (Phillip, 1972). The stable conditions of the fluid pressure favor the low and constant rate of fracture opening necessary for the growth of the massive-textured grey quartz. The constant discharge at the seafloor of ascending hydrothermal fluids through the QFP dikes maintains the fluid circulation within the growing veins (Fig. 12a). At the deposit-scale, the pressurization state builds up progressively from deeper to lower levels (Fig. 12a) and ultimately, the whole impermeable portion of the volcanic pile becomes fluid pressurized (Fig. 8c).

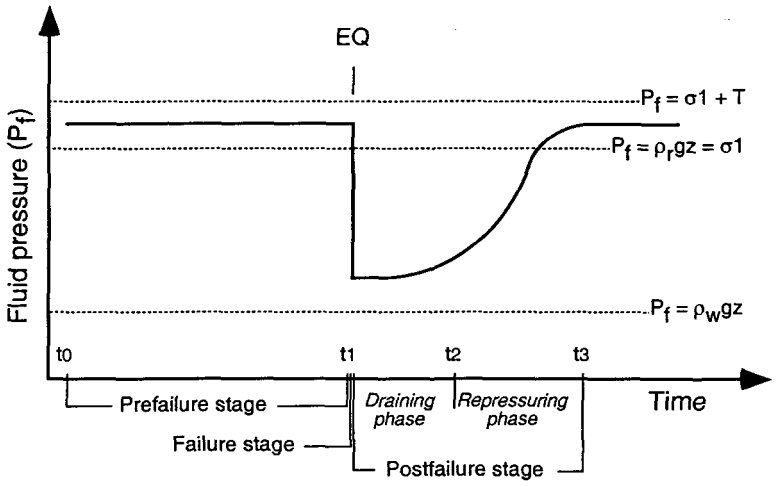

Figure 11. Inferred fluid pressure fluctuations over the time at the locus of a forming vein for the Géant Dormant deposit.

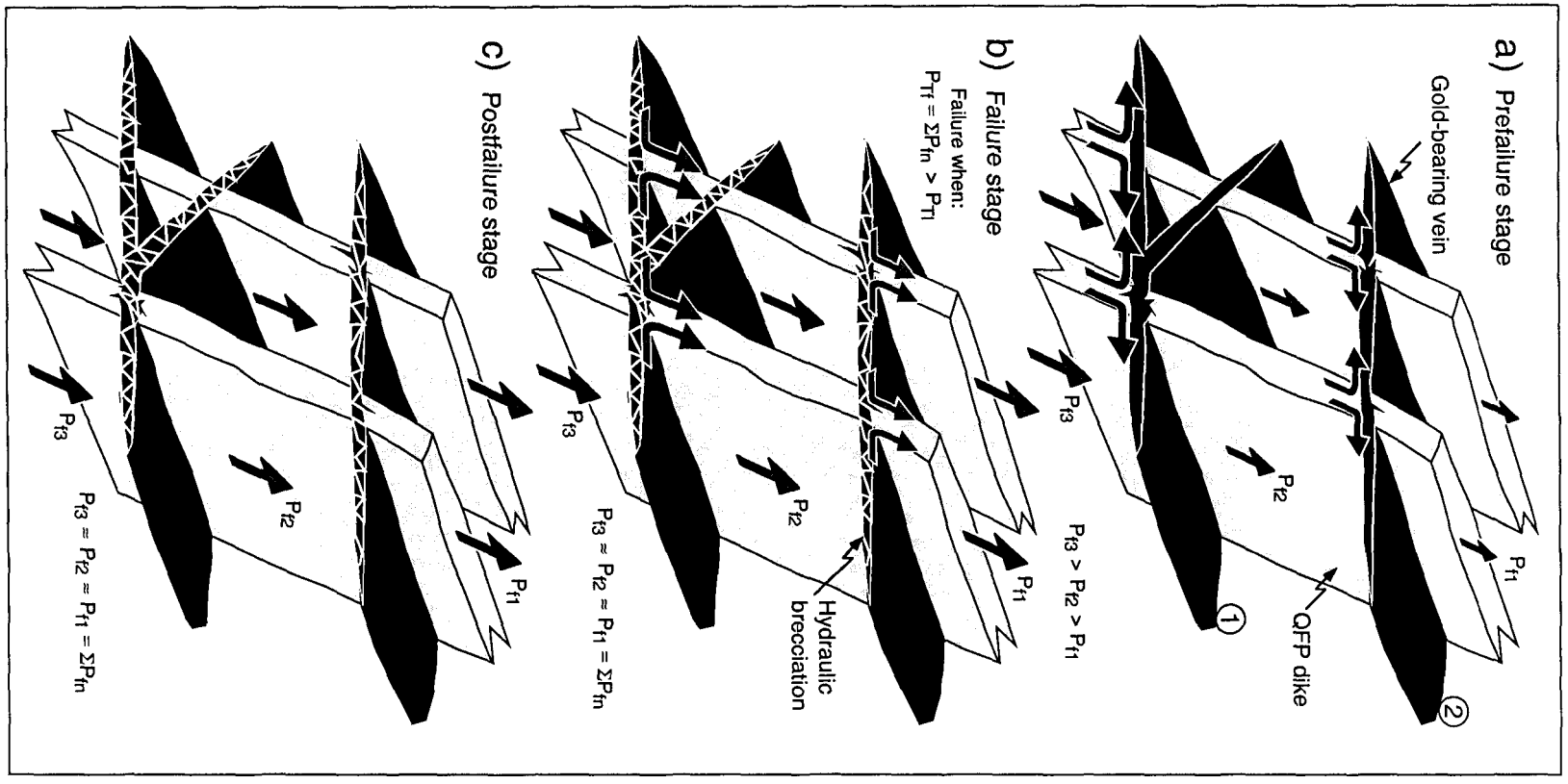

Figure 12. Geometrical relationship between veins and fluid feeder QFP dikes, and inferred fluid flows (arrows) and relative pressures (arrow size) for each stage of the self-equilibrating mechanism. (a) Prefailure stage: fluid at lithostatic pressure, regularized by the QFP dike, keeps open fractures perpendicular to the rock load, inducing vein formation. The numbers refer to the order of vein formation, from the deeper to the lower levels. (b) Failure stage occurring when the total fluid pressure exceeds the total lithostatic load. Hydraulic implosion breccias are induced within the fluid-filled space of the forming veins due to the instantaneous draining of fluid within the forming veins. (c) Postfailure stage showing fluid flow toward the paleosurface, without contribution to vein formation.

Failure stage

The failure stage involves fluid depressurization (t1; Fig. 11). This stage is manifested by the ubiquitous milky quartz cementing grey quartz crystals. The sharp transition from grey euhedral crystalline to microcristalline milky quartz implies quick, if not instantaneous, change of precipitating conditions reflecting a fluid depressurization (Fig. 12b). This pressure release implies that fluid dynamics changed from a lithostatic to a suprahydrostatic regime within the impermeable volcanic pile. Such a pressure drop is likely related to the breakdown of the damper action of the QFP dikes due to a permeability increase of these channelways. Extrinsic and intrinsic factors to the hydrothermal system can account for permeability development throughout the QFP dikes. Extrinsic factors, such as tectonic events, are a plausible feature to generate fracture permeability along fluid pressurized QFP dikes. Inversely, intrinsic depressurization may correspond to a critical state of the hydrothermal system, occurring at the end of the prefailure stage, when the total fluid pressure, accumulated over the time in the volcanic pile by the forming veins, exceeds the total lithostatic load ($P_{Tf} > P_{Tl}$). In such a scenario, hydraulic fracturing of the sommital portion of the volcanic pile (QFP unit) would lead to instantaneous permeability increases within the QFP dikes. This latter hypothesis is preferred because it self-accounts for the homogeneity of the vein system at the deposit-scale.

Postfailure stage

This stage corresponds to a transient and metastable state of the evolving hydrothermal system. Two distinct phases compose this stage: the draining phase (t1-t2:

Fig. 11) and the repressurization phase (t2-t3: Fig. 11). Following the failure stage, hydrothermal fluids from the underlying pressurized reservoir are drained to the seafloor along QFP dikes (Fig. 12c). Since the QFP dike conduits at this phase are more permeable (free-flowing conduits), fluid pressures at level $\sigma_1 < P_f < \sigma_1 + T$ cannot built up within the dikes. Therefore, there is no contribution to vein formation during the draining phase. As far as the hydrothermal fluids are discharged at the seafloor surface, the fluid pressure of the reservoir decreases progressively. As a consequence, the volume of fluid discharged along the QFP dikes also decreases proportionally. Following fluid flow decrease, hydrothermal deposition of quartz starts to progressively restore the flow-restricted conditions of the QFP dikes. Silica precipitation is indicated by the mass balance calculation (Gaboury and Daigneault, 1999a). Fluid pressure progressively builds up again (repressurization phase) and it is envisaged that crack-seal veinlets were formed during this phase due to local fluid pressurization within the vein network. Finally, as fluid pressure reaches lithostatic level, the damper action of the QFP dikes is restored. Stable conditions of the prefailure stage are re-established.

The paragenetic sequence of sulfides is also compatible with the described mechanism. The early pyrite precipitated in open spaces during the prefailure stage, whereas the failure stage is manifested by the other sulfides occurring as fracture filling. Following the failure stage, the hydrothermal system collapses progressively as the fluids are drained onto the seafloor.

The transition from silicates to sulfides as filling minerals coincides with a temperature increase of the fluids from 275° to about 350°C (Gaboury et al., 1999), and

confirms the maturation of the hydrothermal system. In the present case, because the mineralogical change is coincident with the end of a cycle, it is likely that the increase of fluid flow during the draining phase induced an enlargement and a lowering of the hydrothermal convection cells, leading to the warming of the volcanogenic hydrothermal system (cf. Galley, 1993; Brauhart and Groves, 1998).

DISCUSSION

Initiation and locus of veins

The formation of epithermal and mesothermal gold-bearing veins is triggered by pressure fluctuations related to seismic activity. The locus of vein formation corresponds to the sites of the highest fluid pressure variations. For the self-equilibrating mechanism, most of the vein minerals are instead precipitated during stable and aseismic conditions. As the QFP dikes are flow-restricted conduits, it is likely that hydrothermal fluids moved upwardly at a very low rate. Hence, the fluid pressure within QFP dikes should become progressively overpressurized relative to the surrounding lithostatic pressure, as far as the fluids move upward. Based on these considerations, it is likely that veins formed by differential pressure ($\Delta P = P_f - P_l$, where P_l: lithostatic pressure), i.e. when the fluid pressure in the flow-restricted conduits was higher than the surrounding lithostatic load by a specific ΔP value. Calculations using the inferred depth of vein formation, 100 m-spacing between veins, and published pressure data indicate that the ΔP value is about 25 bar for the Géant Dormant vein network (Fig. 13). This value corresponds about to the half of the tensile strength of mafic sills (~50 bar for unfractured diorite: Lama and Vutukuri, 1978). A ΔP value of ~25

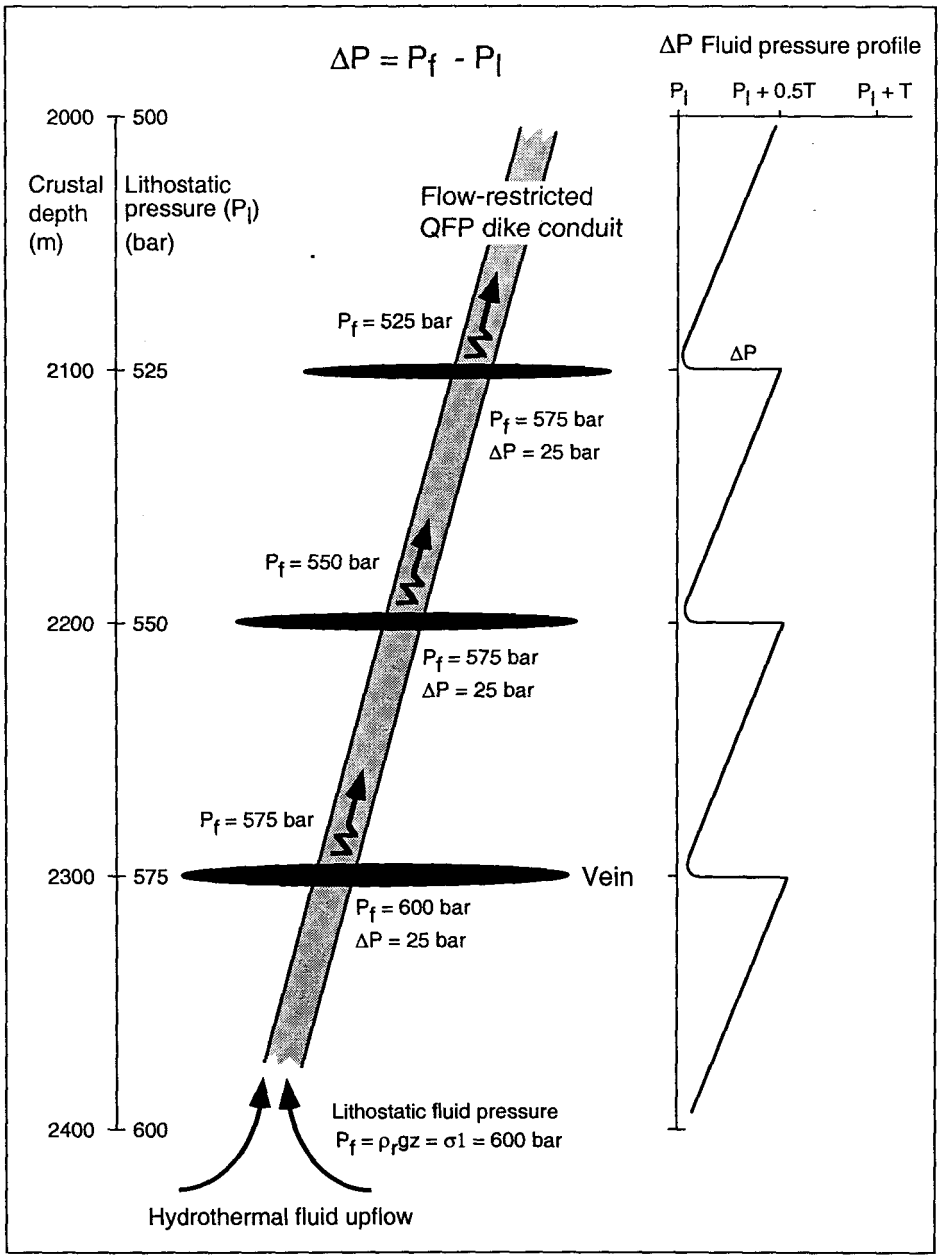

Figure 13. Schematic cross-section showing the development of differential pressure (ΔP) along a flow-restricted QFP dike conduit during the stable prefailure stage. As far as hydrothermal fluids move upward at a low velocity, differential pressure (ΔP) increases to a maximum value of about 25 bar. This critical ΔP value is sufficient to induce the opening of preexisting fracture and vein formation. Vein formation at specific depths restores the fluid pressure in the flow-restricted conduits to a level close to the lithostatic pressure just above the forming vein. This process of vein opening occurs along the QFP dike conduits at specific intervals. Pressure data from Thompson and Connolly (1992).

bar is also consistent with the fluid pressure level invoked previously to open preexisting fractures for vein formation, that is above the lithostatic pressure ($P_f \approx \sigma_1 + 0.5T$), but below the critical level for hydraulic fracturing ($P_f > \sigma_1 + T$). Therefore, veins stacked vertically along the cross-stratal dike conduits correspond to the locus of fluid pressurization at a value of $P_f \approx \sigma_1 + 0.5T$ relative to specific crustal levels. Fracture opening and vein formation may be viewed as an equilibrating process to restore, just above the forming veins, the fluid pressure in the QFP dike conduits at about a lithostatic value (Fig. 13).

The build up of ΔP pressure within the QFP dike conduits should occur first in the deepest levels of the impermeable volcanic pile. Therefore, veins formed in the deepest levels should be the first opened structures, and thus the most volumetrically important. This is consistent with the tonnage of the mined veins at the Géant Dormant (Gaboury et al., 1996a). Furthermore, the differential pressurization also suggests a quite constant vertical spacing for vein formation, because the lithostatic pressure decreases linearly toward the surface (Fig. 13). Such a predicated constant spacing accounts for the 100 m "magic" distance between strata-parallel gold-bearing veins.

Comparison between mechanisms

The typical characteristics of the three mechanisms for vein formation are summarized in Table 1. This table highlights the transitional aspect of the characteristics for the three mechanisms relative to their operating crustal depth, such as: the fluid pressure levels, the role of the fluid pressure for vein formation, the geometry of the vein network

Table 1. Typical characteristics associated with each documented mechanism for gold-bearing vein formation.

Feature	Fault-valve	Self-equilibrating	Suction pump
Crustal depth	5 to >25 km	2 to 5 km	0 to 2 km
Fluid pressure	Supralithostatic $P_f > \rho_r gz + T$	~ Lithostatic $\rho_r gz < P_f < \rho_r gz + T$	Hydrostatic $P_f = \rho_w gz$
Role of Fluid	Active: induces tectonic rupturing and hydraulic fracturing	Semi-active: induces Preexisting fracture opening at: $P_f \approx \sigma_1 + 0.5T$	Passive: tectonic events induce fluid flows
Vein geometry	Flats and subverticals	Mainly flats (strata-parallel)	Mainly subverticals
Tectonic regime	Shortening	Extensional (near-neutral)	Wrench
Breccia occurrence	Hydraulic implosion and explosion breccias: common	Lack of hydrothermal breccia	Hydraulic implosion breccia: typical
Hydrothermal alteration	Wallrock alteration penetrating a few meters away from veins	Weak to undeveloped wallrock alteration and lack of alteration halo	Well-developed alteration halo exceeding the deposit scale
Cycle repetition	Multiple	Single	Multiple

and the specificity of tectonic regime for each mechanism. On the other hand, three characteristics of the self-equilibrating mechanism are clearly distinct, such as: the lack of hydrothermal breccia, the weak wallrock hydrothermal alteration associated with the veins; and the very limited repetition of the vein forming cycles. As discussed previously, the lack of hydrothermal breccia and the weak wallrock alteration, is related to the specific fluid pressure level (Fig. 10). The multiple repetition of the fault-valve and suction pump actions is an intrinsic feature to generate voluminous veins. For these mechanisms, pressurization and depressurization are transient and unstable stages of the cycle. Conversely, vein formation by the self-equilibrating mechanism occurs mainly during the pressurized and stable stage. Thus, the repetition of the cycle is not, except maybe for inducing the maturation of the hydrothermal systems, an essential feature to generate voluminous veins.

The self-equilibrating mechanism shares some characteristics with the fault-valve model, especially those needed for the formation of flat veins, such as an impermeable environment and a lithostatic fluid regime. However, the crustal level as well as the tectonic regime should be considered as critical parameters for vein formation by the self-equilibrating mechanism. Crustal depth is clearly limited downwardly as well as upwardly. The connectivity of the fractures with the surface and the permeability of the rocks delimit the upper limit. The lower limit is constrained by the pressure load which controls the fluid pore permeability of the host rocks (cf. Thompson and Connolly, 1990). Hence, the inferred 2-5 km depth range appears to be realistic.

Vein formation by the fault-valve and the suction pump mechanisms results from the interactions between the tectonic stress field, fluid pressure and characteristics of the

host rocks. An extensional regime, as inferred for the self-equilibrating mechanism, implies that the external stress field is low, in such a manner that the rock load becomes the main principal stress vector (σ_1). Vein formation by the self-equilibrating mechanism can be attributed to the simple interactions between the fluid pressures and the characteristics of the host rocks. Such a two-component system, preserved of external tectonic constraints, is consistent with the model basis, that supposes a self-induced and a self-sustained equilibrium between fluid pressures (ΔP) at different levels of the impermeable pile. In short, the extensional regime appears to be a critical but passive feature in favoring the simple interaction between fluids and rocks rather than an active feature enhancing vein formation.

The preceding characteristics highlighted the transitional aspect of the self-equilibrating mechanism relative to the two other mechanisms for gold-bearing vein formation. This transitional aspect may indicate that for each tectonic regime corresponds an optimal crustal depth for gold-bearing vein formation.

Applicability of the self-equilibrating mechanism

The self-equilibrating mechanism requires four specific conditions: (1) an impermeable volcanic pile to promote the fluid pressurization; (2) the occurrence of cross-stratal tabular and continuous dikes of greater permeability than the surrounding rocks, to serve as fluid feeders for the veins and as conduits for fluid discharge to the paleosurface, and to act as dampers to maintain high fluid pressure in the volcanic pile; (3) the presence

of strata-parallel fractures without hydraulic connectivity with the paleosurface; and (4) an extensional (near-neutral) regime to promote the self-induced fluid pressure equilibrium.

The well-documented Emperor mine (Fiji), a vein-type gold deposit of Tertiary age, shares the following characteristics with the Géant Dormant: (1) the abundance of subhorizontal (< 45°) and laterally extensive auriferous quartz veins (flatmakes) hosted along stratal contacts (Anderson and Eaton, 1990); (2) the narrow (0-5 cm) wallrock alteration associated with the flatmakes (Ahmad and Walshe, 1990; Anderson and Eaton, 1990); (3) the weakly developed deposit-scale alteration halo indicating a low permeability of the host strata (Ahmad and Walshe, 1990; Eaton and Setterfield, 1993); (4) the abundance of weakly mineralized and strongly altered cross-stratal dikes (Anderson and Eaton, 1990); (5) the lack of metallic and mineralogical zoning at the deposit-scale, which extends vertically and laterally over 800 m and 2,500 m respectively (Ahmad and al., 1987; Anderson and Eaton, 1990); (6) the shallow crustal level of vein formation ranging from 2-3 km considering the pre-erosion level (Anderson and Eaton, 1990; Richards, 1995); and (7) the extensional tectonic regime setting inferred from the location of the deposit along the margin of a caldera (Richards, 1995).

The emperor mine is considered as a low-sulfidation epithermal deposit. However, the preceding characteristics are quite contrasting with typical epithermal deposits (cf. White et al., 1995; Panteleyev, 1996). Conversely, these atypical characteristics rather express a setting in which the conditions of vein formation by the self-equilibrating mechanism may have been developed. Therefore, the application of the self-equilibrating mechanism does not appears to be restricted to the Géant Dormant. The proposed

mechanism for vein formation should not be considered unusual or unique. Other vein-type ore deposits inferred to be deeper epithermal examples (Silitoe, 1988) may also constitute good candidates for direct application or adaptation of the proposed mechanism.

Cause of gold precipitation

Depressurization is invoked as a prominent mechanism for precipitating gold in both epithermal (Buchanan, 1981) and mesothermal (Sibson et al, 1988; Herrington and Wilkinson, 1993; Wilkinson and Johnston, 1996) veins. The specific association of gold with sulfides, occurring as fracture fillings and interpreted to be precipitated during the failure stage, suggests that gold was mostly precipitated during instantaneous fluid pressure drops and possibly during consequent fluid boiling.

Implications for exploration

Efficient exploration for vein-type gold deposit requires knowledge of the factors controlling the geometry of the gold mineralization at the regional- and deposit-scale (e.g., Poulsen and Robert, 1989; Gaboury et al., 1996a; 1996b). Models for vein formation can be used as an exploration tool for predicting the geometry of an orebody (Table 1) relative to its tectonic setting. In such a view, the self-equilibrating model implies that gold-bearing veins should be stacked within the strata along cross-stratal dike swarms rather than formed along strata-parallel trends for mesothermal shear veins or along subvertical fault arrays for epithermal veins. Furthermore, the proposed optimal crustal depth of gold-bearing vein formation for each tectonic regime (Fig. 8d) can also be used as a discriminating criterion to

appreciate the gold potential of a specific area relative to its structural level of exposure and its tectonic history.

CONCLUDING REMARKS

The self-equilibrating mechanism for vein formation represents an attempt to integrate field, megascopic and microscopic characteristics of the veins and their host rocks. The proposed model is particular with respect to other documented mechanisms because it involves aseismic conditions, near-neutral horizontal stress, and flow-restricted cross-stratal conduits. The formation of mostly flat veins, staked vertically along dike conduits, corresponds to an equilibrating process to release the differential fluid pressure that builds up vertically in the flow-restricted conduits. The differential pressure built up is induced by the decrease of the lithostatic load as far as the hydrothermal fluids move upward at a low velocity. Although the conditions requested may seem very specific, the general application of this mechanism for deposits having strata-parallel veins formed at shallow crustal levels is suggested by the case of the Tertiary gold deposit of the Emperor mine. Furthermore, this mechanism also appears to be a viable complement to account for vein formation in transitional crustal depths between the fault-valve and the suction pump models. Such a transitional feature suggests that for each tectonic regime corresponds an optimal crustal depth for gold-bearing vein formation.

One of the main aspects of the self-equilibrating model is the role of dike swarms as subvertical conduits for hydrothermal fluids. Cross-stratal dikes, and especially the felsic one, represent privileged hydrothermal conduits because of their physical connections with

subvolcanic magma chambers. These chambers, for the volcanic-related mineralization (volcanogenic and epithermal), commonly act as the thermal source for convective hydrothermal activity (Franklin et al., 1981; Cathles, 1983; Sillitoe and Bonham, 1984). Furthermore, these subvolcanic magmas can also be a direct source of mineralizing fluids and metals (Sillitoe, 1989; 1995; Hedenquist and Lowenstern, 1994; de Ronde, 1995). However, even if the spatial association between ore deposits and dike swarms is well known, this study demonstrates for one of the first time that dikes can play an active role as fluid conduits without be the main economic mineralized structures.

Acknowledgment

The model presented in this paper results from an incessant reflection about vein formation during the course of the first author's Ph.D. work. Cambior Inc., Aurizon Mine Ltd. and the Ministère des Ressources naturelles du Québec are thanked for their scientific collaboration and financial support. Our thanks are extended to the mine staff for their generous assistance to the first author during four consecutive field seasons. The manuscript has benefited from early reviews by M. Jébrak and M.I. Legault. The Natural Sciences and Engineering Research Council of Canada (NSERC) and the Fonds pour la Formation de Chercheurs et d'Aide à la Recherche (FCAR) also financed the project through Ph.D. postgraduate scholarships to the first author.

References

Ahmad, M., Walshe, J.L., 1990. Wall-rock alteration at the Emperor gold-silver telluride deposit, Fiji. Aust. J. Earth Sci. 37, 189-199.

Ahmad, M., Solomon, M., Walshe, J.L., 1987. Mineralogical and geochemical studies of the Emperor gold-telluride deposit, Fiji. Econ. Geol. 82, 345-370.

Anderson, E.M., 1951. The dynamic of faulting. Edingburgh, Oliver and Boyd, 241 p.

Anderson, W.A., Eaton, P.C., 1990. Gold mineralisation at the Emperor Mine, Vatakoula, Fiji. J. Geochem. Explor. 36, 267-296.

Bogie, I., Lawless, J.V., 1987. Controls on the hydrology of large volcanically hosted geothermal systems: Implications for exploration for epithermal mineral deposits. In: Proceedings Pacific Rim Congress 87, Australasian Inst. Mining and Metall. Parkville, pp. 57-60.

Boullier, A-M., Robert, F., 1992. Paleoseismic events recorded in Archaean gold-quartz vein networks, Val d'Or, Abitibi, Quebec, Canada. J. Struct. Geol. 14, 161-179.

Brace, W.F., 1984. Permeability of crystalline rocks: New in situ measurements. J. Geophys. Res. 89, 4327-4330.

Brauhart, C.W., Groves, D.I., 1998. Regional alteration systems associated with volcanogenic massive sulfide mineralization at Panorama, Pilbara, Western Australia. Econ. Geol. 93, 292-302.

Buchanan, L.J., 1981. Precious metal deposits associated with volcanic environments in the Southwest. Arizona Geol. Soc. Digest 14, 237-262.

Callan, N.J., Spooner, E.T.C., 1998. Repetitive hydraulic fracturing and shear zone inflation in an Archean granitoid-hosted, ribbon banded, Au-quartz vein system, Renabie area, Ontario, Canada. Ore Geol. Rev. 12, 237-266.

Cathles, L.M., 1983. An analysis of the hydrothermal system responsable for massive sulfide deposition in the Hokuroku basin of Japan. Econ. Geol. Monogr. 5, 439-487.

Chown, E.H., Daigneault, R., Mueller, W., Mortensen, J.K., 1992. Tectonic evolution of the Northern Volcanic Zone, Abitibi belt, Quebec. Can. J. Earth Sci. 29, 2211-2225.

Cox, S.F., Etheridge, M.A., Wall, V.J., 1990. Fluid pressure regimes and fluid dynamics during deformation of low-grade terranes, implications for the genesis of mesothermal gold deposits. In: Robert, F., Sheahan, P.A., Green, S.B. (Eds.), Greenstone gold and crustal evolution. NUNA conference volume, Geol. Ass. Can., pp. 46-53.

Craw, D., McKeag, S.A., 1995. Structural control of Tertiary Au-Ag-bearing breccias in an extensional environment, Nelson area, Southern Nevada, USA. Mineral Deposita 30, 1-10.

de Ronde, C.E.J., 1995. Fluid chemistry and isotopic characteristics of seafloor hydrothermal systems and associated VMS deposits: Potential for magmatic contributions. In: Thompson, J.F.H. (Ed.), Magmas, fluids and ore deposits. Mineral. Ass. Can., Short Course Series 23, pp. 479-509.

Dong, G., Morrison, G., 1995. Adularia in epithermal veins, Queensland: morphology, structural state and origin. Mineral Deposita 30, 11-19.

Dong, G., Morrison, G., Jaireth, S., 1995. Quartz textures in epithermal veins, Queensland - Classification, origin, and implication. Econ. Geol. 90, 1841-1856.

Dowling, K., Morrison, G., 1989. Application of quartz textures to the classification of gold deposits using North Queensland examples. Econ. Geol. Monogr. 6, 342-355.

Eaton, P.C., Setterfield, T.N., 1993. The relationship between epithermal and porphyry hydrothermal systems within the Tavua caldera, Fiji. Econ. Geol. 88, 1053-1083.

Foxford, K.A., Nicholson, R., Hebblethwaite, R.P.B., Polya, D.A., 1995. Conceptual methods for modelling systems of mineralized echelon veins: Examples from Southern England and Portugal. Explor. Mining Geol. 4, 285-296.

Franklin, J.M., Lydon, J.W., Sangster, D.F., 1981. Volcanic-associated massive sulfide deposits. Econ. Geol. 75th Anniversary Vol., 485-627.

Gaboury, D., Daigneault, R., 1999a. Evolution from seafloor-related to sulfide-rich quartz vein-type gold mineralization during deep submarine volcanic construction: The Géant Dormant gold mine, Archean Abitibi belt, Canada. Econ. Geol. 94, 1-19.

Gaboury, D. and Daigneault, R., (1999b). Constraints on the evolution of a hydrothermal system from REE and trace-elements of sulfides: Example from the Géant Dormant gold mine, Archean Abitibi Belt, Canada. Submitted to Can. Mineral.

Gaboury, D., Daigneault, R., Beaudoin, G., 1999. Volcanogenic-related origin of sulfide-rich quartz veins: evidence from O and S isotopes at the Géant Dormant gold mine, Abitibi belt, Canada. Mineral Deposita, In press.

Gaboury, D., Daigneault, R., Tourigny, G., Gobeil, C., 1996a. An Archean volcanic-related gold-sulfide-quartz vein orebody: the Géant Dormant mine, Abitibi Subprovince, Québec, Canada. Explor. Mining Geol. 5, 197-213.

Gaboury, D., Dubé, B., Laflèche, M., Lauzière, K., 1996b. Geology of the Hammer Down mesothermal lode gold deposit, Newfoundland Appalachians, Canada. Can. J. Earth Sci. 33, 335-350.

Galley, A.C., 1993. Characteristics of semi-conformable alteration zones associated with volcanogenic massive sulphide districts. J. Geochem. Explor. 48, 175-200.

Groves, D.I., Ridley, J.R., Bloem, E.M.J., Gebre-Mariam, M., Hagemann, S.G., Hronsky, J.M.A., Knight, J.T., McNaughton, N.J., Ojala, J., Vielreicher, R.M., McCuaig, T.C., Holyland, P.W., 1995. Lode-gold deposits of the Yilgarn block: products of Late Archaean crustal-scale overpressured hydrothermal systems. In: Coward, M.P., Ries, A.C. (Eds), Early Precambrian Processes. Geol. Soc. Special Publ. No 95, pp. 155-172.

Gudmundsson, A., 1983. Form and dimensions of dikes, feeder-dikes in eastern Iceland. Tectonophysics 95, 295-307.

Harley, M., Charlesworth, E.G., 1996. The role of fluid pressure in the formation of the bedding-parallel, thrust-hosted gold deposits, Sabie-Pilgrim's Rest goldfield, eastern Transvaal. Precambrian Res. 79, 125-140.

Haynes, S.J., 1993. Vein-type ore deposits: Introduction. Ore Geol. Rev. 8, 205-211.

Hedenquist, J.W., Lowenstern, J.B., 1994. The role of magmas in the formation of hydrothermal ore deposits. Nature 370, 519-526.

Herrington, R.J., Wilkinson, J.J., 1993. Colloidal gold and silica in mesothermal vein systems. Geology 21, 539-542.

Jébrak, M., 1992. Les textures intra-filoniennes, marqueurs des conditions hydrauliques et tectoniques. Chron. Rech. Min. 506, 25-36.

Jébrak, M., 1998. Hydrothermal breccias in vein-type ore deposits: A review of mechanisms, morphology and sized distribution. Ore Geol. Rev. 12, 111-134.

Lama, R.D., Vutukuri, V.S. 1978. Handbook on mechanical properties of rocks, Vol. 2. Clausthal (W. Germany), Trans. Tech. Publ., 481 p.

McCuaig, T.C., Kerrich, R., 1998. P-T-t-deformation-fluid characteristics of lode gold deposits: evidence from alteration systematics. Ore Geol. Rev. 12, 381-453.

MERQ-OGS, 1983. Lithostratigraphic map of the Abitibi Subprovince. Ontario Geological Survey - Ministère de l'Energie et des Ressource du Québec, Map 2484, DV 83-16, scale 1: 50 000.

Miller, L.D., Goldfarb, R.J., Snee, L.W., Gent, C.A., Kirkham, R.A., 1995. Structural geology, age and mechanisms of gold vein formation at the Kensigton and Jualin deposits, Berners Bay District, Southeast Alaska. Econ. Geol. 90, 343-368.

Moritz, R.P., Crocket, J.M., 1990. Mechanics of formation of the gold-bearing quartz-fuschsite vein at the Dome mine, Timmins area, Ontario. Can. J. Earth Sci. 27, 1609-1620.

Panteleyev, A., 1996. Epithermal Au-Ag: Low sulfidation. The Gangue. Geol. Ass. Can., issue 53, 3-5.

Peters, S.G., 1993. Nomenclature, concepts and classification of oreshoots in vein deposits. Ore Geol. Rev. 8, 3-22.

Phillip, W.J., 1972. Hydraulic fracturing and mineralization. J. Geol. Soc. London 12, 337-359.

Poulsen, K.H., Robert, F., 1989. Shear zones and gold: Practical examples from the Southern Canadian Shield. In: Bursnall, J.T. (Ed), Mineralization and shear zones. Geol. Ass. Can., Short Course Note Volume 6, pp. 239-266.

Ramsay, J.G., 1980. The crack-seal mechanism of rock deformation. Nature 244, 135-139.

Reid, R.R., Craig. S.W., Bond, W.D., 1995. Constriction fracture flow: A mechanism for fault and vein formation in the Cœur d'Arlene District, Idaho. Econ. Geol. 90, 81-87.

Richards, J.P., 1995. Alkalic-type epithermal gold deposits – A review. In: Thompson, J.F.H. (Ed.), Magmas, fluids and ore deposits. Mineral. Ass. Can., Short Course Series 23, pp. 367-400.

Ridley, J., 1993. The relations between mean rock stress and fluid flow in the crust: With inference to vein- and lode-style gold deposits. Ore Geol. Rev. 8, 23-37.

Robert, F., Brown, A.C., 1986a. Archean gold-bearing quartz veins at the Sigma Mine, Abitibi greenstone belt, Québec: Part II. Vein paragenesis and hydrothermal alteration. Econ. Geol. 81, 593-619.

Robert, F., Brown, A.C., 1986b. Archean gold-bearing quartz veins at the Sigma Mine, Abitibi greenstone belt, Québec: Part I. Geologic relations and formation of the vein system. Econ. Geol. 81, 578-592.

Sibson, R.H., 1987. Earthquake rupturing as a mineralizing agent in hydrothermal systems. Geology 15, 701-704.

Sibson, R.H., 1990a. Fault structure and mechanics in relation to greenstone gold deposits. In: Robert, F., Sheahan, P.A., Green, S.B. (Eds.), Greenstone gold and crustal evolution. NUNA conference volume, Geol. Ass. Can., 64-60.

Sibson, R.H., 1990b. Faulting and fluid flow. In: Nesbitt, B.E. (Ed.), Fluids in tectonically active regimes of continental crust. Mineral. Ass. Can., Short Course Volume 18, pp. 93-132.

Sibson, R.H., Robert, F., Poulsen, K.H., 1988. High-angle reverse faults, fluid-pressure cycling and mesothermal gold-quartz deposits. Geology 16, 551-555.

Sillitoe, R.H., 1988. Environments, styles and origins of gold deposits in western Pacific island arcs. In: Bicentennial Gold 88, Geol. Soc. Aust., Abstracts No. 22, pp. 127-138.

Sillitoe, R.H., 1989. Gold deposits in western Pacific island arcs: The magmatic connection. Econ. Geol. Monogr. 6, 274-291.

Sillitoe, R.H., 1995. The influence of magmatic-hydrothermal models on exploration strategies for volcano-plutonic arcs. In: Thompson, J.F.H. (Ed.), Magmas, fluids and ore deposits. Mineral. Ass. Can., Short Course Series 23, pp. 511-525.

Sillitoe, R.H., Bonham, H.F., 1984. Volcanic landforms and ore deposits. Econ. Geol. 70, 1286-1298.

Thompson, A.B., Connolly, J.A.D., 1992. Migration of metamorphic fluid: some aspects of mass and heat transfer. Earth Sci. Rev. 32, 107-121.

Vearncombe, J.R., 1993. Quartz vein morphology and implications for formation depth and classification of Archaean gold-vein deposits. Ore Geol. Rev. 8, 407-424.

White, N.C., Hedenquist, J.W., 1990. Epithermal environments and styles of mineralization: variations and their causes, and guidelines for exploration. J. Geochem. Explor. 36, 445-474.

White, N.C., Leake, M.J., McCaughey, S.N., Parris, B.W., 1995. Epithermal gold deposits of the southwest Pacific. J. Geochem. Explor. 54, 87-136.

Whilkinson, J.J. Johnston, J.D. 1996. Pressure fluctuations, phase separation, and gold precipitation during seismic fracture propagation. Geology 24, 395-398.

ANNEXE 2: Analyses géochimiques

Les échantillons représentatifs des différentes unités lithologiques et des différents faciès d'altération ont été sélectionnés pour fin d'analyse par le Centre de recherches minérales du Ministère des Ressources naturelles du Québec. L'analyse des éléments majeurs, mineurs et de certains éléments en traces (Ga, Nb, Rb, Sr, Y, et Zr) fut réalisée par fluorescence-X. Des échantillons sélectionnés (~60) ont été analysés pour les éléments des terres rares (ÉTR: La, Ce, Sm, Eu, Tb, Yb, Lu), ainsi que pour Hf, Ta et Th, par la technique d'activation neutronique instrumentale. La précision sur les valeurs obtenues est de 1% pour les éléments majeurs, 5% pour les éléments mineurs, en traces et les ÉTR, à l'exception du Tb et du Lu (5-10%) et du Nb (15%).

Annexe 2. Données géochimiques brutes

#	61	62	63	64	65	66	75	7	22	28	31	33	90
Roche	BC	BC	BC	BC	BC	BC	BC	FCM	FCM	FCM	FCM	FCM	FCM
SiO2 (%)	46.42	45.78	48.78	46.00	46.64	44.07	48.99	47.71	46.64	48.78	48.35	47.49	47.92
TiO2	0.82	0.78	0.83	0.78	0.78	0.77	0.85	0.72	0.73	0.90	0.83	0.92	0.87
Al2O3	14.36	14.17	14.55	13.98	14.17	13.42	15.12	15.68	15.49	14.17	14.36	14.17	13.23
Fe2O3	10.15	11.87	10.01	12.87	11.87	13.15	11.15	12.30	11.87	11.72	12.44	12.44	12.01
MnO	0.15	0.19	0.18	0.22	0.23	0.23	0.22	0.19	0.17	0.15	0.19	0.18	0.14
MgO	4.38	5.31	4.00	6.02	7.01	5.21	4.43	8.92	8.12	6.57	8.11	7.56	6.93
CaO	9.16	10.91	12.73	11.33	11.33	10.35	13.43	9.23	10.35	10.21	9.64	9.12	7.35
Na2O3	1.64	0.90	1.16	0.09	0.88	1.40	1.23	1.13	1.16	1.56	1.78	1.70	0.36
K2O	1.20	0.01	0.01	0.01	0.01	0.37	0.01	0.34	0.33	0.48	0.05	0.02	1.43
P2O5				0.02		0.02		0.01	0.01	0.02	0.02	0.01	0.02
PAF	11.10	9.28	8.11	8.90	6.60	11.10	5.20	4.31	5.62	5.29	4.63	5.06	10.70
Total	99.38	99.20	100.36	100.22	99.52	100.09	100.63	100.53	100.48	99.85	100.40	98.66	100.96
Ga (ppm)	21	23	20	19	20	19	22	19	21	22	17	20	22
Nb	4	4	4	3	4	4		3		4	4	3	4
Rb	42					16	3	16	15	21	3	3	59
Sr	74	140	170	130	160	81	260	120	120	100	150	150	49
Y	19	18	20	19	20	20	21	17	18	25	22	18	21
Zr	56	61	63	58	60	56	56	50	50	62	59	54	57
La (ppm)	2.4						2.2						
Lu	0.24						0.32						
Sm	1.9						1.9						
Yb	1.7						2						
Ce	6						7						
Cs	1.6						0.6						
Eu	0.7						0.6						
Hf	1						1.3						
Nd	7						5						
Sc	38						40						
Ta	0.4						0.4						
Tb	0.4						0.3						
Th	0.07						0.16						

Annexe 2. Données géochimiques brutes

# Roche	91 FCM	92 FCM	93 FCM	95 FCM	96 FCM	98 FCM	99 FCM	100 FCM	101 FCM	102 FCM	103 FCM	104 FCM	105 FCM
SiO2 (%)	47.06	47.71	47.49	43.86	47.06	46.85	47.28	48.35	47.92	47.49	43.64	46.21	45.57
TiO2	0.87	0.92	0.92	0.78	0.92	0.85	0.82	0.92	0.88	0.87	0.82	0.82	0.82
Al2O3	13.79	14.36	14.93	13.23	13.79	13.42	13.79	13.98	14.55	14.17	13.79	13.98	13.98
Fe2O3	12.72	13.87	13.73	10.15	12.58	12.01	12.30	12.87	12.87	12.58	10.72	11.72	11.87
MnO	0.17	0.17	0.18	0.19	0.23	0.17	0.21	0.18	0.17	0.19	0.19	0.18	0.19
MgO	7.79	7.89	7.96	5.87	8.31	6.72	6.09	7.25	7.31	6.90	5.46	6.96	6.65
CaO	9.39	6.90	7.63	10.63	9.26	10.63	9.28	9.37	9.93	9.43	9.35	11.05	8.65
Na2O3	1.20	1.58	2.12	0.85	0.96	1.56	2.49	2.52	1.36	2.28	1.71	1.33	1.33
K2O	1.08	0.02	0.35	1.36	0.06	0.02	0.07	0.06	0.01	0.02	1.19	0.17	0.77
P2O5	0.02	0.02	0.01	0.02	0.02	0.02	0.02	0.02	0.02	0.02	0.01	0.02	0.02
PAF	5.76	6.31	4.95	12.00	7.75	6.19	8.53	4.40	4.72	5.69	11.20	7.64	10.50
Total	99.85	99.75	100.26	98.94	100.94	98.44	100.88	99.92	99.74	99.64	98.07	100.08	100.35
Ga (ppm)	24	20	22	20	22	19	17	23	22	21	21	17	19
Nb	4	3	3	3	5	4	3	4	3				3
Rb	59		17	49	4		3	4			38	8	27
Sr	78	78	110	49	97	120	110	100	96	100	30	110	49
Y	22	23	22	22	21	22	21	24	21	19	21	19	20
Zr	58	58	63	55	64	62	51	60	55	55	50	51	51
La (ppm)					2.4	2.3	1.8	2.4	2.1	2.1			
Lu					0.3	0.29	0.26	0.33	0.28	0.31			
Sm					2	2	1.7	2.1	1.9	1.9			
Yb					2	1.8	2	2.2	2.1	2			
Ce					6	6	5	7	5	5			
Cs						0.4		0.3	0.2	0.4			
Eu					0.8	0.7	0.7	0.7	0.7	0.7			
Hf					1.4	1.3	1.1	1.3	1.4	1.2			
Nd					2	5	4	4		4			
Sc					40	40	41	42	41	41			
Ta					0.4	0.3	0.3	0.2	0.5	0.3			
Tb					0.4	0.4	0.4	0.4	0.4	0.4			
Th					0.12	0.15	0.16	0.15	0.15	0.16			

Annexe 2. Données géochimiques brutes

# Roche	108 FCM	110 FCM	112 FCM	117 FCM	118 FCM	121 FCM	122 FCM	123 FCM	124 FCM	125 FCM	126 FCM	127 FCM	128 FCM
SiO2 (%)	47.71	47.49	48.13	43.00	43.21	47.06	48.13	44.50	47.49	43.43	45.78	44.07	48.56
TiO2	0.82	0.77	0.77	0.82	0.77	0.88	0.88	0.82	0.82	0.82	0.88	0.78	0.93
Al2O3	14.93	14.93	15.12	13.60	12.28	13.60	14.74	13.23	14.17	13.23	14.17	12.85	13.98
Fe2O3	12.01	12.01	12.44	12.44	13.30	12.15	12.87	10.44	13.01	12.87	12.44	12.87	11.87
MnO	0.21	0.19	0.25	0.18	0.23	0.15	0.22	0.19	0.21	0.25	0.19	0.18	0.19
MgO	7.89	7.79	8.19	7.16	6.04	6.81	7.56	5.64	6.95	5.39	6.95	5.72	7.36
CaO	9.85	11.33	9.98	9.16	10.35	7.29	8.21	12.03	10.35	11.75	9.09	9.09	9.77
Na2O3	1.48	1.39	1.58	0.31	0.09	1.56	1.25	1.44	0.15	0.92	1.15	0.89	1.13
K2O	0.02	0.04	0.02	1.43	1.31	0.66	0.02	0.08	0.01	0.45	0.02	1.19	0.02
P2O5	0.02	0.01	0.02	0.01	0.02	0.02	0.02	0.02	0.01	0.02	0.02	0.01	0.02
PAF	5.12	4.64	4.30	12.00	13.10	9.81	6.87	11.00	7.49	11.20	9.15	11.40	6.20
Total	100.06	100.58	100.80	100.10	100.70	99.99	100.77	99.39	100.65	100.33	99.84	99.04	100.03
Ga (ppm)	15	16	24	19	19	24	18	20	23	22	21	19	22
Nb			3	4	4	3				5	3	4	4
Rb				64	38	25	3	5		19		45	3
Sr	120	150	170	47	59	43	180	150	150	80	110	38	130
Y	19	22	18	23	22	19	19	20	18	23	23	22	22
Zr	49	50	50	50	51	53	54	52	50	51	54	49	62
La (ppm)		2.2											
Lu		0.29											
Sm		1.9											
Yb		1.9											
Ce		6											
Cs		0.5											
Eu		0.7											
Hf		1.2											
Nd		4											
Sc		36											
Ta		0.3											
Tb		0.4											
Th		0.13											

Annexe 2. Données géochimiques brutes

# Roche	140 FCM	141 FCM	142 FCM	143 FCM	144 FCM	147 FCM	148 FCM	152 FCM	153 FCM	158 FCM	159 FCM	160 FCM	161 FCM
SiO2 (%)	48.56	47.28	48.78	48.13	48.13	47.49	46.21	47.49	45.78	47.28	48.78	47.06	46.85
TiO2	0.82	0.88	0.83	0.82	0.87	0.82	0.87	0.75	0.73	0.83	0.88	0.83	0.90
Al2O3	14.55	13.79	14.17	14.55	14.55	13.79	13.98	13.98	13.60	14.36	14.74	14.17	14.36
Fe2O3	12.01	13.01	12.01	12.58	12.72	10.58	12.58	10.44	10.15	12.30	11.87	11.72	11.58
MnO	0.19	0.19	0.17	0.18	0.17	0.17	0.17	0.13	0.15	0.25	0.19	0.22	0.23
MgO	7.06	7.83	7.53	7.26	7.38	6.85	5.94	6.90	6.67	7.15	7.13	6.68	5.74
CaO	11.33	10.49	11.47	9.74	11.19	11.47	10.91	8.31	9.72	9.82	9.85	10.91	12.03
Na2O3	0.67	1.56	0.78	1.51	1.19	1.02	0.54	1.90	2.17	1.51	2.04	0.27	0.35
K2O	0.01	0.07	0.28	0.42	0.18	0.04	0.04	0.66	0.42	0.06	0.02	0.05	0.01
P2O5	0.01	0.02	0.01	0.02	0.01	0.01	0.01	0.01	0.01	0.02	0.02	0.01	0.02
PAF	5.08	5.72	4.41	4.99	4.43	7.67	8.96	10.40	11.20	5.22	4.75	8.95	8.34
Total	100.28	100.84	100.43	100.20	100.81	99.90	100.20	100.96	100.59	98.80	100.27	100.86	100.41
Ga (ppm)	25	21	16	17	23	24	19	20	18	21	23	20	21
Nb	4						4			3		3	3
Rb			14	17	6	3	3	28	17			4	
Sr	170	110	110	82	130	120	120	66	59	110	110	150	220
Y	22	22	22	24	22	20	24	17	16	17	18	23	22
Zr	52	55	53	53	52	52	54	47	45	49	52	52	58
La (ppm)													
Lu													
Sm													
Yb													
Ce													
Cs													
Eu													
Hf													
Nd													
Sc													
Ta													
Tb													
Th													

Annexe 2. Données géochimiques brutes

# Roche	162 FCM	170 FCM	410 FCM	414 FCM	417 FCM	421 FCM	422 FCM	438 FCM	440 FCM	445 FCM	455 FCM	468 FCM	469 FCM
SiO2 (%)	45.35	48.35	45.20	46.60	46.60	47.10	48.20	47.30	46.10	47.80	46.30	46.90	43.30
TiO2	0.82	1.08	0.78	0.99	0.89	0.84	1.03	0.65	0.68	0.83	0.62	1.08	0.82
Al2O3	13.23	14.17	14.60	15.20	15.40	15.00	14.40	14.60	14.40	14.20	16.30	13.20	13.90
Fe2O3	11.44	14.15	12.00	12.60	11.90	11.00	11.80	12.50	13.30	12.20	11.70	12.60	12.60
MnO	0.23	0.21	0.22	0.20	0.21	0.19	0.18	0.20	0.20	0.19	0.20	0.19	0.17
MgO	6.58	6.38	9.88	8.43	9.66	8.69	8.14	8.46	8.69	6.88	9.23	5.35	8.05
CaO	10.77	9.96	8.99	9.02	9.39	10.50	9.26	10.10	10.60	11.80	10.40	8.94	7.60
Na2O3	0.84	1.62	1.37	1.76	1.38	1.90	1.22	0.96	1.22	1.04	1.41	1.78	1.64
K2O	0.01	0.40	0.32	0.50	0.65	0.98	0.49	0.46	0.52	0.15	0.53	0.15	0.48
P2O5	0.02	0.05	0.04	0.07	0.07	0.05	0.06	0.04	0.04	0.03	0.02	0.10	0.05
PAF	9.54	3.96	5.69	3.94	3.63	3.35	4.83	3.97	3.91	4.71	3.81	8.44	10.30
Total	98.83	100.33	99.09	99.31	99.78	99.60	99.61	99.24	99.66	99.83	100.52	98.73	98.91
Ga (ppm)	24	23	12	18	17	13	20	14	16	17	12	18	13
Nb	4	3	3	3	3	3	3	4		3	3	5	
Rb		12	12	23	26	41	20	19	24	5	24	8	23
Sr	120	180	90	210	110	100	87	110	170	120	120	150	110
Y	23	27	20	24	21	21	26	18	17	23	16	31	21
Zr	53	67	50	65	56	56	61	49	44	55	42	81	53
La (ppm)										2.5	1.7	3.5	
Lu										0.31	0.24	0.45	
Sm										2	1.3	3	
Yb										2	1.7	3	
Ce										6	4	10	
Cs										0.4	1.1	0.5	
Eu										0.8	0.5	1.1	
Hf										1.2	1	1.9	
Nd										6		8	
Sc										40	34	42	
Ta										0.1	0.1	0.2	
Tb										0.4	0.3	0.7	
Th										0.15	0.097	0.16	

Annexe 2. Données géochimiques brutes

# Roche	470 FCM	473 FCM	474 FCM	475 FCM	476 FCM	477 FCM	478 FCM	479 FCM	480 FCM	481 FCM	482 FCM	483 FCM	484 FCM
SiO2 (%)	46.50	46.50	47.70	46.80	45.80	45.80	47.50	46.90	47.90	46.90	45.60	46.40	47.70
TiO2	1.02	0.95	0.92	0.98	0.91	0.91	0.94	0.87	0.93	0.81	0.85	0.89	1.09
Al2O3	15.40	14.60	15.10	14.70	14.20	14.70	14.70	14.70	15.30	14.80	15.00	16.00	13.60
Fe2O3	13.20	10.90	11.60	12.10	11.20	10.80	12.00	10.90	12.40	11.70	12.10	12.10	13.80
MnO	0.16	0.17	0.17	0.18	0.17	0.18	0.19	0.17	0.19	0.18	0.17	0.17	0.18
MgO	9.07	6.48	7.88	7.97	6.87	6.89	7.19	7.03	7.71	9.18	9.46	8.89	5.84
CaO	7.33	9.52	8.90	9.04	10.30	9.04	10.70	10.90	9.93	9.78	10.40	9.39	8.48
Na2O3	1.65	1.40	1.40	1.85	1.84	1.84	1.66	1.42	1.11	1.23	1.01	1.51	1.20
K2O	0.62	1.11	0.99	1.18	0.76	0.87	0.19	0.65	0.65	0.32	0.26	0.18	0.08
P2O5	0.07	0.05	0.06	0.05	0.05	0.05	0.04	0.05	0.06	0.05	0.05	0.06	0.09
PAF	4.99	7.34	5.00	4.80	7.17	8.22	4.38	5.52	4.34	4.69	4.09	4.65	7.06
Total	100.01	99.02	99.72	99.65	99.27	99.30	99.49	99.11	100.52	99.64	98.99	100.24	99.12
Ga (ppm)	18	16	18	17	15	15	15	15	17	14	15	12	15
Nb	3			3	3				3		4		3
Rb	31	47	47	50	34	36	10	27	31	14	5	10	4
Sr	350	150	150	180	130	120	170	120	140	89	97	95	200
Y	24	22	22	22	20	20	23	20	24	20	21	20	29
Zr	70	62	59	65	58	58	63	57	63	53	55	51	84
La (ppm)	6	2.9		3.2	2.9		2.3		3.1				
Lu	0.36	0.35		0.38	0.33		0.35		0.35				
Sm	3	2.2		2.3	2.1		2.2		2.2				
Yb	2.1	2.1		1.9	1.9		1.9		2.1				
Ce	14	7		8	7		6		7				
Cs	1.5	1.6		2	1.2		0.5		1				
Eu	1.2	0.8		0.8	0.7		0.7		0.7				
Hf	1.4	1.3		1.5	1.2		1.4		1.4				
Nd	10	3		6	3		6		5				
Sc	40	38		40	37		39		38				
Ta	0.2	0.2		0.1	0.2		0.4		0.2				
Tb	0.6	0.5		0.5	0.4		0.5		0.5				
Th	0.12	0.24		0.18			0.17		0.21				

Annexe 2. Données géochimiques brutes

# Roche	485 FCM	486 FCM	487 FCM	488 FCM	489 FCM	490 FCM	506 FCM	507 FCM	522 FCM	525 FCM	527 FCM	528 FCM	538 FCM
SiO2 (%)	46.90	46.30	47.40	47.20	47.20	46.10	46.90	46.80	46.00	46.20	45.20	46.40	46.60
TiO2	0.95	0.96	0.95	0.83	0.81	0.88	0.64	0.66	1.09	1.08	0.94	0.88	0.99
Al2O3	13.50	15.00	15.40	16.00	16.90	15.20	15.60	14.80	13.80	12.90	14.20	14.70	14.50
Fe2O3	12.80	13.90	12.20	11.20	10.20	11.70	11.70	12.50	14.70	14.30	12.70	12.50	13.30
MnO	0.21	0.23	0.18	0.19	0.17	0.18	0.19	0.21	0.24	0.24	0.19	0.21	0.24
MgO	7.96	9.15	7.39	8.04	7.88	8.08	8.25	8.91	6.60	6.79	7.04	8.60	8.06
CaO	9.22	8.93	8.54	10.30	10.50	10.30	10.90	10.60	9.06	10.80	12.80	9.71	11.40
Na2O3	1.61	1.38	1.79	1.70	1.87	1.48	0.73	1.08	1.65	1.55	1.29	1.45	1.25
K2O	0.26	0.21	0.33	0.23	0.22	0.19	0.68	0.27	0.45	0.07	0.22	0.80	0.35
P2O5	0.06	0.05	0.05	0.06	0.04	0.05	0.04	0.03	0.06	0.07	0.07	0.06	0.05
PAF	5.24	4.61	4.95	3.59	4.04	4.96	4.09	4.89	5.82	6.23	4.76	4.37	3.82
Total	98.71	100.72	99.18	99.34	99.83	99.12	99.72	100.75	99.47	100.23	99.41	99.68	100.56
Ga (ppm)	15	14	14	12	13	16	14	14	17	20	17	15	20
Nb	3	3	3	4	4		3	3	5	3		3	
Rb	12	6	11	8	9	8	34	13	20	5	9	34	15
Sr	67	78	100	120	110	130	160	130	130	150	180	130	150
Y	26	23	23	19	19	21	20	18	29	29	23	21	24
Zr	66	60	60	56	54	60	44	44	70	71	61	54	57
La (ppm)	3		5			2.7	1.7		2.9				
Lu	0.37		0.35			0.3	0.24		0.41				
Sm	2.5		2.6			2	1.4		2.4				
Yb	2.3		2			2.2	1.4		2.4				
Ce	8		12			7	4		7				
Cs	0.4		0.6			0.4	0.9		0.6				
Eu	0.8		0.9			0.7	0.6		0.8				
Hf	1.6		1.4			1.5	0.9		1.5				
Nd	7		7						4				
Sc	40		40			38	37		39				
Ta			0.1			0.3	0.1		0.2				
Tb	0.5		0.5			0.4	0.3		0.6				
Th	0.14		0.17			0.09	0.05		0.095				

Annexe 2. Données géochimiques brutes

#	539	540	546	556	569	578	580	583	584	106	446	471	606
Roche	FCM	FCM	FCM	FCM	FCM	FCM	FCM	FCM	FCM	DM1	DM1	DM1	DM1
SiO2 (%)	45.50	46.40	44.90	45.00	45.90	46.20	45.90	46.70	44.40	48.78	47.80	42.40	46.80
TiO2	0.92	0.92	0.68	0.68	0.96	0.86	0.92	0.94	0.90	0.98	1.05	1.27	1.02
Al2O3	14.40	14.70	15.70	16.00	14.70	14.70	14.80	14.20	13.90	15.30	14.50	15.60	14.40
Fe2O3	12.00	11.90	12.30	12.50	13.50	13.80	12.00	12.00	10.60	12.87	13.60	17.80	13.20
MnO	0.20	0.21	0.23	0.21	0.22	0.21	0.20	0.20	0.17	0.19	0.20	0.16	0.18
MgO	7.94	8.30	9.25	8.99	7.72	9.03	7.59	7.77	5.97	7.18	6.87	6.96	6.92
CaO	11.40	10.70	10.10	10.00	11.60	11.00	10.50	10.20	9.28	8.56	8.82	4.33	7.11
Na2O3	1.52	1.50	1.02	1.95	1.02	1.47	2.26	1.33	0.65	1.56	1.32	0.65	2.28
K2O	0.04	0.16	1.08	0.49	0.09	0.76	0.17	0.58	1.72	0.01	0.02	1.73	0.00
P2O5	0.05	0.06	0.05	0.03	0.06	0.06	0.06	0.06	0.07	0.02	0.06	0.08	0.06
PAF	5.14	4.80	3.79	3.85	4.09	2.89	4.99	5.31	11.50	4.44	5.01	8.93	7.89
Total	99.11	99.65	99.10	99.70	99.86	100.98	99.39	99.29	99.16	99.89	99.25	99.91	99.86
Ga (ppm)	18	21	16	15	19	13	13	17	16	23	20	23	20
Nb		3			4	3	3	4	3			3	4
Rb		6	44	24	4	27	7	30	64	3		90	
Sr	150	130	89	230	150	160	120	110	64	240	200	47	140
Y	20	23	16	16	25	22	23	23	20	18	20	38	19
Zr	56	59	44	45	60	53	58	61	54	52	60	78	68
La (ppm)					2.7							4.3	4.1
Lu					0.34							0.52	0.3
Sm					2.3							2.4	2.6
Yb					2.2							3.8	2.2
Ce					7							9	10
Cs					0.2							1.9	0.3
Eu					0.8							0.8	1
Hf					1.5							1.8	1.3
Nd					3							5	7
Sc					38							49	27
Ta					0.2								0.1
Tb					0.5							0.8	0.5
Th					0.098							0.19	0.23

Annexe 2. Données géochimiques brutes

#	515	516	517	518	519	520	521	631	137	139	436	505	560
Roche	LF	LF	LF	LF	LF	LF	LF	LF	DAC	DAC	DAC	DAC	DAC
SiO2 (%)	62.50	74.20	60.60	61.00	68.10	71.00	72.20	54.70	63.32	62.90	72.70	66.40	73.80
TiO2	0.56	0.21	0.54	0.74	0.36	0.23	0.19	0.92	0.52	0.32	0.23	0.45	0.11
Al2O3	14.40	10.60	14.90	15.30	12.90	12.10	12.80	14.50	14.93	13.04	11.10	14.50	8.28
Fe2O3	6.43	2.20	5.82	5.96	3.94	7.03	1.92	8.49	4.70	6.25	1.96	3.93	7.20
MnO	0.05	0.05	0.06	0.05	0.04	0.04	0.06	0.13	0.04	0.06	0.06	0.05	0.06
MgO	2.15	0.68	1.68	2.14	1.14	1.11	0.67	4.46	1.67	0.63	0.59	1.28	2.34
CaO	3.53	3.06	4.04	3.42	3.32	1.29	2.72	6.44	3.15	5.27	3.55	2.23	1.61
Na2O3	2.43	2.09	2.59	2.58	2.98	2.32	0.27	4.63	1.20	1.58	2.58	6.50	0.71
K2O	2.12	1.91	2.41	2.17	1.76	1.61	3.68		3.16	2.85	1.89	0.55	1.23
P2O5	0.11	0.03	0.11	0.12	0.09	0.04	0.05	0.24	0.07	0.05	0.05	0.13	0.02
PAF	4.88	3.72	5.90	5.12	4.36	3.17	4.72	6.00	5.74	7.30	4.85	2.79	3.89
Total	99.16	98.75	98.65	98.60	98.99	99.94	99.28	100.51	98.50	100.25	99.56	98.81	99.25
Ga (ppm)	17	13	22	25	19	14	16	19	25	20	10	22	14
Nb	8	9	6	8	8	9	4	8	8	7	11	7	10
Rb	79	66	86	79	63	51	110	4	98	85	59	23	48
Sr	110	110	170	150	120	64	50	360	87	110	79	80	33
Y	23	35	14	16	24	22	7	18	14	12	29	9	27
Zr	230	230	130	240	220	170	120	170	140	130	210	160	200
La (ppm)	18	19	14	17	30			21	14			17	26
Lu	0.3	0.54	0.14	0.23	0.36			0.24	0.16			0.076	0.42
Sm	4.1	4.3	2.5	3.3	5.8			4.7	2.4			2.6	4.8
Yb	1.8	3.4	1	1.2	2.2			1.9	0.8			0.4	2.4
Ce	37	40	27	33	58			46	27			35	55
Cs	1.2	1.2	1.5	1.4	1				1.8			0.4	1
Eu	1	0.5	0.7	1	0.9			1.3	0.5			0.8	0.8
Hf	5.6	5.8	2.9	5.7	5.3			3.2	2.9			3.6	5.4
Nd	17	18	13	15	25			23	12			15	24
Sc	9.4	3.5	12	9.9	5.9			19	7			5.7	6.3
Ta	0.6	0.9	0.5	0.5	0.8			0.5	0.7			0.9	0.9
Tb	0.5	0.6	0.3	0.4	0.6			0.5	0.2			0.2	0.6
Th	1.9	3.8	2	1.4	3.5			1.3	1.8			2	3.5

Annexe 2. Données géochimiques brutes

#	563	567	597	612	622	623	701	71	109	114	115	116	130
Roche	DAC	DAC	DAC	DAC	DAC	DAC	DAC	FP	FP	FP	FP	FP	FP
SiO2 (%)	74.90	73.20	63.60	62.70	62.10	60.30	67.40	65.68	65.04	60.76	61.18	57.12	70.17
TiO2	0.17	0.19	0.55	0.55	0.54	0.53	0.37	0.48	0.52	0.77	0.77	0.77	0.32
Al2O3	11.80	12.10	15.60	15.80	15.70	15.20	12.60	14.36	14.55	15.49	15.49	15.68	13.98
Fe2O3	2.48	2.53	4.89	5.19	5.81	5.03	6.13	4.40	3.95	5.98	6.33	7.23	3.02
MnO	0.02	0.06	0.04	0.06	0.06	0.10	0.07	0.05	0.05	0.05	0.05	0.08	0.04
MgO	0.76	0.80	1.68	1.33	1.91	1.63	3.11	1.13	1.24	1.87	2.45	2.21	0.70
CaO	1.49	1.81	2.61	4.67	3.74	4.81	1.82	4.00	3.97	2.88	2.94	4.23	2.22
Na2O3	2.07	0.22	3.71	4.57	4.38	1.87	3.59	2.51	3.53	1.82	0.88	0.94	4.08
K2O	2.30	3.64	2.23	1.00	0.94	3.14	1.03	2.32	2.00	3.02	3.48	3.42	1.53
P2O5	0.02	0.03	0.11	0.12	0.11	0.10	0.08	0.11	0.07	0.16	0.18	0.18	0.02
PAF	2.95	4.71	4.39	3.78	5.45	6.62	3.29	5.52	5.11	6.21	6.65	7.39	3.21
Total	98.96	99.29	99.41	99.77	100.74	99.33	99.49	100.56	100.03	99.01	100.40	99.25	99.29
Ga (ppm)	14	15	19	19	16	17	16	26	24	21	28	24	22
Nb	15	15	6	7	6	6	5	8	6	9	11	8	8
Rb	72	120	67	45	37	83	42	71	60	98	110	91	38
Sr	75	45	96	240	260	50	100	110	70	68	56	51	120
Y	40	41	12	12	11	11	13	11	12	19	21	18	15
Zr	270	300	140	170	160	140	150	170	160	160	160	150	160
La (ppm)			13		15		14		16				
Lu			0.14		0.16		0.18		0.11				
Sm			2.4		2.7		2.7		2.7				
Yb			0.9		1		1		1				
Ce			26		30		29		31				
Cs			1.3		1		1.7		1.5				
Eu			0.7		0.8		0.8		0.6				
Hf			3		3.6		3.6		3.5				
Nd			10		11		12		14				
Sc			8		8.9		6.5		8				
Ta			0.4		0.4		0.4		1.1				
Tb			0.3		0.3		0.3		0.2				
Th			1.9		2.1		1.9		2				

Annexe 2. Données géochimiques brutes

#	134	135	163	164	165	416	430	492	493	494	495	497	499
Roche	FP	FP	FP	FP	FP	FP	FP	FP	FP	FP	FP	FP	FP
SiO2 (%)	64.39	60.97	60.11	60.11	60.33	70.70	70.10	67.40	62.10	62.70	54.60	75.60	70.90
TiO2	0.47	0.75	0.77	0.75	0.77	0.34	0.34	0.31	0.63	0.69	0.95	0.15	0.22
Al2O3	14.36	15.87	15.49	15.49	15.68	13.70	14.10	13.60	14.60	14.90	14.80	10.80	11.50
Fe2O3	5.09	6.61	6.81	5.85	5.90	2.76	2.96	3.92	5.59	5.22	8.44	2.21	3.29
MnO	0.06	0.08	0.06	0.06	0.06	0.04	0.03	0.04	0.06	0.07	0.12	0.05	0.04
MgO	1.29	2.22	2.45	2.07	1.67	1.15	0.93	0.95	1.73	1.77	4.27	0.98	0.81
CaO	3.97	3.67	4.48	4.30	3.89	3.00	3.08	3.00	3.39	2.99	5.44	2.11	3.35
Na2O3	1.47	2.93	1.79	2.62	1.43	4.87	4.19	2.33	0.24	3.50	2.90	0.94	1.15
K2O	3.04	2.17	2.35	2.13	3.26	0.86	0.97	2.27	3.86	1.99	1.22	2.64	2.89
P2O5	0.07	0.16	0.16	0.18	0.18	0.05	0.08	0.05	0.17	0.21	0.26	0.01	0.03
PAF	6.42	5.14	6.49	6.05	7.44	2.65	2.31	4.74	6.19	4.50	6.73	3.49	4.59
Total	100.63	100.57	100.96	99.61	100.61	100.12	99.09	98.61	98.56	98.54	99.73	98.98	98.77
Ga (ppm)	21	27	25	22	23	16	18	15	19	16	18	11	17
Nb	5	7	6	9	9	6	7	7	8	8	9	13	6
Rb	87	72	76	67	96	28	37	68	130	76	53	82	100
Sr	54	130	150	170	88	110	230	91	47	110	190	50	48
Y	10	19	20	19	19	16	10	15	14	15	17	24	14
Zr	150	150	160	160	160	160	160	170	170	180	150	230	130
La (ppm)		16				20							
Lu		0.21				0.2							
Sm		3.7				3.2							
Yb		1.3				1.2							
Ce		35				39							
Cs		1.6				0.6							
Eu		1				0.8							
Hf		3.4				3.9							
Nd		16				16							
Sc		10				6.3							
Ta		1				0.5							
Tb		0.4				0.4							
Th		1.9				2.3							

Annexe 2. Données géochimiques brutes

#	526	555	572	579	32	73	107	131	132	138	146	155	418
Roche	FP	FP	FP	FP	QFP	QFP	QFP	QFP	QFP	QFP	QFP	QFP	QFP
SiO2 (%)	55.00	65.40	69.80	69.90	68.46	58.19	69.96	66.75	65.04	70.17	66.75	67.17	69.20
TiO2	0.98	0.50	0.34	0.36	0.43	0.63	0.23	0.37	0.47	0.22	0.35	0.52	0.27
Al2O3	15.00	14.80	14.10	13.70	13.42	12.47	13.98	14.17	14.36	13.42	13.98	15.30	13.40
Fe2O3	9.40	5.14	3.61	3.49	2.67	7.51	2.29	4.95	4.48	2.77	2.62	4.02	2.61
MnO	0.11	0.05	0.03	0.03	0.04	0.13	0.03	0.06	0.06	0.05	0.06	0.05	0.04
MgO	3.91	1.48	0.96	0.95	0.83	2.06	0.45	0.78	1.11	0.45	0.71	1.44	0.77
CaO	5.16	4.43	2.19	2.27	3.81	6.44	3.53	3.18	3.36	3.71	4.94	2.48	3.39
Na2O3	3.36	4.20	3.09	5.12	0.15	0.24	2.93	0.28	3.14	0.61	0.24	3.46	3.40
K2O	1.01	0.67	2.37	0.86	4.00	2.70	2.45	3.73	1.83	3.48	3.99	2.22	2.18
P2O5	0.26	0.11	0.06	0.07	0.07	0.16	0.02	0.07	0.09	0.02	0.07	0.07	0.06
PAF	4.84	2.54	3.55	2.51	6.06	8.56	4.53	6.10	4.77	5.83	6.73	3.88	4.06
Total	99.03	99.32	100.10	99.26	99.94	99.09	100.40	100.44	98.71	100.73	100.44	100.61	99.38
Ga (ppm)	21	21	18	17	18	21	26	27	26	17	19	25	14
Nb	10	5	6	6	7	7	6	7	7	6	5	6	4
Rb	36	24	83	30	120	79	63	91	56	96	110	72	66
Sr	450	270	94	160	36	62	120	47	120	120	49	81	87
Y	19	12	16	15	11	16	8	12	9	9	7	12	9
Zr	160	160	160	160	150	140	120	140	180	110	140	160	140
La (ppm)	20	16	16										17
Lu	0.24	0.16	0.18										0.099
Sm	4.4	2.7	2.7										2.2
Yb	1.5	0.9	1.3										0.7
Ce	44	33	32										32
Cs	0.9	0.6	1.9										1.6
Eu	1.3	0.8	0.8										0.6
Hf	3.1	3.6	4.1										3.5
Nd	20	15	11										9
Sc	15	8.1	6.3										3.9
Ta	0.6	0.5	0.5										0.4
Tb	0.4	0.3	0.3										0.3
Th	1.3	2.1	2.3										2.4

Annexe 2. Données géochimiques brutes

# Roche	496 QFP	498 QFP	500 QFP	815 QFP	460 DM2	461 DM2	465 DM2	502 DM2	582 DM2	610 DM2	611 DM2	613 DM2	627 DM2
SiO2 (%)	70.90	70.70	70.20	69.20	40.10	42.00	38.60	44.10	43.80	49.90	39.90	43.80	39.90
TiO2	0.24	0.23	0.20	0.33	0.59	0.63	0.46	0.69	0.65	1.18	0.67	0.66	0.58
Al2O3	13.10	12.90	13.40	14.40	9.58	10.20	7.59	10.20	9.61	11.50	9.43	10.60	9.02
Fe2O3	2.79	2.60	1.77	3.17	8.41	8.78	9.48	11.40	8.86	10.00	9.35	10.50	7.77
MnO	0.03	0.05	0.07	0.07	0.18	0.16	0.21	0.23	0.18	0.17	0.18	0.19	0.15
MgO	0.80	0.81	0.80	1.10	11.90	13.40	5.95	13.10	15.20	8.76	10.70	14.10	14.20
CaO	2.35	2.21	3.42	2.95	12.90	12.80	18.90	12.80	15.10	1.03	13.40	12.00	13.00
Na2O3	1.91	2.22	0.22	0.10				1.62	0.54	2.68	1.21	1.33	0.18
K2O	2.95	2.85	4.17	4.12				0.24	0.78			0.65	
P2O5	0.04	0.06	0.05	0.08	0.49	0.55	0.38	0.59	0.56	0.44	0.73	0.51	0.42
PAF	4.28	4.58	4.93	4.50	14.70	11.50	17.80	5.38	4.43	4.32	14.10	6.46	14.40
Total	99.39	99.21	99.23	100.02	98.85	100.02	99.37	100.35	99.71	89.98	99.67	100.80	99.62
Ga (ppm)	15	19	16	12	10	8	3	13	13	18	14	14	9
Nb	7	7	5	16	6	4	4	8	3	4	6	3	3
Rb	87	86	110	100				5	30			28	
Sr	72	83	60	16	250	470	250	970	740	720	1000	450	370
Y	15	17	8	8	19	19	13	26	20	20	22	20	16
Zr	140	140	130	150	140	150	110	180	140	190	210	180	150
La (ppm)				24			38	68	40	33			42
Lu				0.18			0.15	0.21	0.16	0.21			0.13
Sm				3.2			9	18	14	11			13
Yb				1.1			0.9	1.1	0.9	1.8			1.1
Ce				50			86	170	110	82			100
Cs				2.1			0.2	0.7	1.9	0.4			0.2
Eu				0.7			1.6	4	3.3	2.7			3.2
Hf				4			2	3.5	2.7	4			2.6
Nd				19			47	95	66	52			65
Sc				2.1			20	27	35	27			36
Ta				0.4			0.5	0.5	0.1	0.4			0.2
Tb				0.3			0.7	1.1	0.9	0.9			0.9
Th				2.4			2.4	6.3	2.2	2.9			3.4

ANNEXE 3: Analyses à la microsonde

Les analyses chimiques de certains minéraux ont été réalisées avec une microsonde électronique SEMQ-II à l'Université du Québec à Chicoutimi. Les paramètres suivants ont été utilisés pour l'analyse quantitative des silicates, à l'exception des carbonates: un voltage d'accélération de 15kV avec un courant de 10nA, un faisceau de 5 μm de diamètre et un temps de comptage de 100 s. Les carbonates ont été analysés pendant 50 s. Les résultats analytiques ont été corrigés par la matrice de Bence-Albee. La précision analytique est de ± 0,5 % pour des concentrations > 20%; ± 0,2 % pour des concentrations entre 10-20% et ± 0,1 % pour des concentrations < 10%. Les sulfures ont été analysés d'une manière semi-quantitative en utilisant les paramètres précédents mais sans échantillon de référence pour la calibration et avec un temps de comptage de 50 s.

Les sulfures ont été analysés essentiellement pour fins d'identification. D'autre part, le contenu en éléments traces (Au, Au, Ni, As et Co) est cohérent avec les données analytiques de l'activation neutronique sur les sulfures (Chap. 4). L'analyse quantitative des chlorites a permis de déterminer leur formule chimique et d'estimer leur température de formation selon la formule suivante (Kranidiotis et MacLean, 1987: Chap. 5): T °C = 106 Al^{iv} + 18. La valeur Al^{iv} est corrigée pour les changements du rapport Fe/Fe + Mg comme suit: Al^{iv} corrigée = Al^{iv} + 0,7 (Fe/Fe+Mg).

L'analyse des carbonates dans les veines démontre que ceux-ci correspondent essentiellement à de la calcite. Enfin, l'analyse des amphiboles métamorphiques indique une composition typique de l'actinote.

Tableau 3a. Analyses semi-quantitatives des sulfures (% poids)

LM	Sulfure	No	S	Fe	Cu	Zn	As	Au	Ag	Ni	Co	Te	Total
006F	Py	1	53.19	42.15				3.80				0.86	100.00
006F	Py	2	52.91	43.53	1.15					0.25	1.16	1.00	100.00
006F	Py	5	54.08	44.63					0.37		0.72	0.20	100.00
006F	Py	6	54.38	45.04					0.24		0.34		100.00
006F	Py	9	55.01	44.99									100.00
409	Py	23	54.98	42.93	0.56						1.16	0.37	100.00
021E	Py	25	51.87	40.60	0.30	0.42	0.58	4.97			1.26		100.00
021E	Py	26	53.21	44.29						0.31	0.84	1.36	100.01
021E	Py	27	53.13	42.89				3.71			0.26		99.99
002F	Py	35	54.36	45.01						0.31	0.32		100.00
590	Py	39	53.88	43.95			0.67		0.68			0.82	100.00
590	Py	40	47.11	39.46			0.64		0.22	0.31		12.27	100.01
590	Py	41	54.70	44.17		1.13							100.00
086F	Py	45	54.55	43.34	0.69					0.27	1.15		100.00
086F	Py	49	53.89	44.33			0.36				0.84	0.57	99.99
464	Py	54	55.01	44.99									100.00
464	Py	57	51.31	40.64			0.29	7.00			0.76		100.00
086F	Py	60	54.54	44.59						0.25	0.35	0.27	100.00
086F	Py	61	54.59	44.56					0.39	0.26		0.20	100.00
601	Py	67	54.59	44.35		1.06							100.00
601	Py	72	54.96	44.41						0.28	0.35		100.00
601	Py	73	55.33	44.67									100.00
432A	Py	74	54.93	44.51			0.56						100.00
441	Py	78	54.05	45.58			0.37						100.00
441	Py	81	54.48	44.68	0.84								100.00

Tableau 3a. Analyses semi-quantitatives des sulfures (% poids)

LM	Sulfure	No	S	Fe	Cu	Zn	As	Au	Ag	Ni	Co	Te	Total
077E	Py	95	52.56	41.81			0.46	3.81	1.08			0.28	100.00
454	Py	103	54.49	43.21	0.76				0.33		1.21		100.00
450A	Py	113	54.61	45.39									100.00
427B	Py	119	54.68	44.48							0.84		100.00
427B	Py	121	53.01	41.88	0.52			3.70	0.33		0.56		100.00
427A	Py	123	53.79	43.70					0.27		0.33	1.90	99.99
427A	Py	125	54.82	43.58			0.43		0.88	0.28			99.99
006G	Py	128	53.88	44.47			0.17				0.84	0.65	100.01
467C	Py	129	55.35	43.88	0.31					0.46			100.00
467C	Py	131	54.60	43.04			0.27			0.27	1.83		100.01
002F	Apy	34	19.22	32.20	0.67		46.13			0.40	0.42	0.26	99.30
601	Apy (?)	71	21.67	16.76			40.93			20.64			100.00
077E	Apy	92	17.09	18.56			64.35						100.00
006F	Po	7	52.06	40.82				6.46			0.66		100.00
006F	Po	8	54.21	44.39	0.37					0.38	0.65		100.00
027F	Po	12	38.73	56.15				4.58				0.53	100.00
027F	Po	13	40.21	58.24		1.22					0.34		100.01
027F	Po	14	41.27	58.53			0.21						100.01
027F	Po	15	40.41	58.17						0.47	0.96		100.01
409	Po	20	40.72	58.47							0.81		100.00
002F	Po	29	40.4	57.76	1.20							0.65	100.01
002F	Po	36	40.69	58.32					0.26		0.74		100.01
086F	Po	58	40.43	58.56	0.75					0.27			100.01
601	Po	66	40.47	56.30		0.91					0.31	2.00	99.99
81	Po	84	38.41	54.86				5.37	0.23		0.33	0.80	100.00

Tableau 3a. Analyses semi-quantitatives des sulfures (% poids)

LM	Sulfure	No	S	Fe	Cu	Zn	As	Au	Ag	Ni	Co	Te	Total
602	Po	97	38.26	53.98				6.62	0.28			0.85	99.99
602	Po	99	37.61	56.00						0.33	0.99	5.06	99.99
602	Po	100	41.12	57.25	0.35						0.47	0.81	100.00
602	Po	101	40.53	59.03						0.44			100.00
13	Po	109	41.05	57.29			0.47				1.19		100.00
13	Po	112	40.89	57.46					0.46	0.35	0.84		100.00
450A	Po	114	39.75	60.25									100.00
450A	Po	115	40.42	59.58									100.00
450A	Po	118	35.65	51.83				4.25		0.32	0.97	6.99	100.01
427B	Po	120	39.69	58.71			0.27			0.60	0.40	0.32	99.99
427B	Po	122	40.72	58.37							0.41	0.50	100.00
006G	Po	127	39.13	58.21					0.62	0.27	1.44	0.33	100.00
467C	Po	130	41.25	58.75									100.00
467C	Po	132	40.07	58.13			0.32			0.31	0.37	0.80	100.00
027E	Po	134	38.28	52.77		0.44		8.51					100.00
002F	Po	135	39.92	57.15	0.34				0.58		2.01		100.00
006F	Cpy	3	34.16	28.17	33.95	1.03	2.01				0.43	0.25	100.00
006F	Cpy	4	35.26	28.63	33.60		2.51						100.00
409	Cpy	21	34.65	28.39	34.17		2.46		0.34				100.01
002F	Cpy	28	33.68	27.29	33.97	1.40	2.17				0.42	1.07	100.00
086F	Cpy	46	33.22	27.69	35.19	0.59	1.99		0.50	0.47		0.34	99.99
464	Cpy	43	34.07	28.31	33.95	0.56	2.27				0.84		100.00
086F	Cpy	63	34.31	28.43	33.96		2.13			0.24	0.94		100.01
601	Cpy	65	33.71	24.27	23.24		9.85			3.95		4.97	99.99
601	Cpy	68	33.25	26.42	31.25	0.85	1.92	5.00	0.20	0.61		0.51	100.01

Tableau 3a. Analyses semi-quantitatives des sulfures (% poids)

LM	Sulfure	No	S	Fe	Cu	Zn	As	Au	Ag	Ni	Co	Te	Total
441	Cpy	80	35.21	28.29	34.16		1.37			0.25		0.71	99.99
81	Cpy	86	34.64	28.97	33.88		2.51						100.00
077E	Cpy	93	34.70	27.83	34.90		2.56						99.99
602	Cpy	102	33.60	28.65	34.37		2.77		0.33			0.27	99.99
454	Cpy	104	33.11	26.56	31.97		1.98	6.37					99.99
450A	Cpy	116	34.28	27.88	34.01		1.95			0.30	0.50	1.08	100.00
006G	Cpy	126	34.51	28.35	33.87	0.48	2.57		0.22				100.00
590	Cpy	136	34.71	28.12	34.68		1.20			0.35	0.65	0.29	100.00
590	Cpy	137	35.77	29.37	34.66		0.20						100.00
81	Sph	85	31.91	6.04		61.44				0.22		0.40	100.01
81	Sph	87	29.35	4.98		50.08	0.22	15.36					99.99
409	Sph	17	32.76	6.09		60.91					0.24		100.00
409	Sph	18	32.41	6.12		60.44				1.03			100.00
409	Sph	19	30.71	4.99		54.40		9.58		0.32			100.00
409	Sph	22	29.91	4.66		55.00	0.27	9.15		0.74	0.26		99.99
409	Sph	24	31.39	5.95		56.69		5.38		0.59			100.00
409	Sph	139	25.22	6.89		66.35	0.51			0.39		0.63	99.99
441	Sph	79	31.69	3.80		63.20				0.60		0.70	99.99
441	Sph	82	32.91	3.41	0.96	62.71							99.99
441	Sph	83	30.89	3.43	1.05	54.98	0.20	8.70		0.35	0.40		100.00
464	Sph	52	30.91	2.57		58.54	0.32	7.37		0.29			100.00
464	Sph	56	32.19	2.36	0.48	64.57	0.41						100.01
601	Sph	69	31.85	5.91		61.33	0.40			0.27		0.25	100.01
002F	Sph	37	30.29	5.38		56.68		7.06		0.31	0.27		99.99
002F	Sph	38	48.93	6.39		42.46	2.23						100.01

Tableau 3a. Analyses semi-quantitatives des sulfures (% poids)

LM	Sulfure	No	S	Fe	Cu	Zn	As	Au	Ag	Ni	Co	Te	Total
027E	Sph	132b	30.40	5.28		55.33		8.07			0.29	0.62	99.99
027E	Sph	133	32.60	6.47		60.64	0.29						100.00
027F	Sph	10	30.11	5.86		53.37	0.18	10.47					99.99
027F	Sph	11	31.06	6.74		56.53	0.37	4.75		0.55			100.00
027F	Sph	16	32.31	6.36		60.43	0.57			0.33			100.00
077E	Sph	94	32.55	5.89	0.37	60.63	0.56						100.00
077E	Sph	96	32.66	6.20		60.84				0.29			99.99
077E	Sph	96b	31.00	5.42		55.23		7.83		0.26	0.26		100.00
086F	Sph	43	31.29	4.22	0.36	54.96		8.65		0.27	0.25		100.00
086F	Sph	44	29.73	5.20		50.60	0.42	13.30		0.49	0.25		99.99
086F	Sph	47	30.33	4.84	0.53	52.14		11.15		0.78	0.23		100.00
086F	Sph	48	29.93	5.07	0.73	57.34		6.04		0.63	0.27		100.01
086F	Sph	50	32.90	5.16		61.45				0.31		0.19	100.01
086F	Sph	51	32.06	7.16		52.82		7.42		0.54			100.00
086F	Sph	59	31.60	5.48		57.76		4.69		0.46			99.99
086F	Sph	62	30.53	5.74		54.13		9.13		0.46			100.00
086F	Sph	64	31.03	5.82		55.51		7.14		0.19	0.31		100.00
432A	Sph	75	31.88	6.26		54.98	0.46	6.43					100.01
432A	Sph	76	33.05	7.49	0.70	58.01				0.38		0.37	100.00
432A	Sph	77	30.03	6.08		53.12		10.34		0.21	0.22		100.00

Tableau 3b. Analyses des chlorites dans les veines

LM #	006F	006F	006F	021E	021E	021E		409	409	409	409	002F
Minéral	Chl	Chl	Chl	Chl	Chl	Chl	Chl	Chl	Chl	Chl	Chl	Chl
No	1	2	4	8	14	16	17	18	19	20	22	
SiO2 (%)	25.57	24.59	26.14	27.55	27.33	27.49	25.12	22.47	26.54	26.82	26.38	
Tio2				0.15					0.09			
Al2O3	20.25	20.48	20.51	23.77	22.37	23.22	23.77	20.55	24.45	24.25	22.82	
FeO	29.46	29.35	30.12	23.99	22.81	21.93	25.22	29.83	22.25	22.29	24.98	
MgO	12.34	12.18	13.15	18.15	18.36	19.21	14.48	14.95	18.31	18.82	16.21	
MnO				0.45		0.44		0.73	0.63	0.67		
CaO												
Na2O							2.17					
K2O												
Cr2O3												
Cl												
SO3							1.80	10.26				
Total	87.62	86.60	89.92	94.06	90.87	92.29	92.56	98.79	92.27	92.85	90.39	
	Nombre d'ions sur une base de 28 atomes d'oxygène											
Si	5.508	5.375	5.489	5.325	5.440	5.368	4.985	4.133	5.201	5.223	5.346	
AlIV	2.492	2.625	2.511	2.675	2.560	2.632	3.015	3.867	2.799	2.777	2.654	
AlVI	2.651	2.653	2.567	2.742	2.690	2.714	2.546	0.589	2.850	2.790	2.798	
Mg	3.962	3.968	4.115	5.229	5.447	5.591	4.282	4.098	5.347	5.462	4.896	
Fe	5.308	5.365	5.290	3.878	3.797	3.582	4.185	4.589	3.647	3.630	4.234	
Mn				0.074		0.073		0.114	0.105	0.111		
Ti				0.022					0.013			
Ca												
K												
T cation	19.920	19.986	19.972	19.944	19.935	19.959	19.013	17.390	19.961	19.993	19.928	
Fe/Fe+Mg	0.573	0.575	0.562	0.426	0.411	0.390	0.494	0.528	0.405	0.399	0.464	
T°C	240	254	242	270	259	268	301	389	285	283	265	

Tableau 3b. Analyses des chlorites dans les veines

LM #	002F	002F	002F	590	590	464	464	464	086F	086F	058F
Minéral	Chl	Chl	Chl	Chl	Chl	Chl	Chl	Chl	Chl	Chl	Chl
No	24	25	29	31	32	34	35	36	39	40	43
SiO2 (%)	25.33	25.43	20.63	26.24	26.21	25.56	24.64	24.64	26.02	25.03	26.89
Tio2		0.16			0.14						
Al2O3	20.27	23.12	16.91	23.65	24.04	23.53	23.86	23.74	24.52	22.38	21.81
FeO	19.34	22.85	12.22	24.89	25.00	31.77	31.91	31.69	25.07	27.74	23.51
MgO	16.87	16.46	14.09	16.46	16.15	11.24	11.03	11.31	15.46	12.97	16.97
MnO				0.47	0.65	0.90	0.50	0.61	0.61	0.55	
CaO											
Na2O											
K2O											
Cr2O3											
Cl											
SO3	0.24		0.30								0.39
Total	82.05	88.02	64.15	91.71	92.19	93.00	91.94	91.99	91.68	88.67	89.57
	Nombre d'ions sur une base de 28 atomes d'oxygène										
Si	5.525	5.250	5.605	5.246	5.217	5.231	5.110	5.105	5.207	5.284	5.449
AlIV	2.475	2.750	2.395	2.754	2.783	2.769	2.890	2.895	2.793	2.716	2.551
AlVI	2.738	2.877	3.021	2.821	2.858	2.908	2.943	2.904	2.991	2.854	2.659
Mg	5.484	5.064	5.705	4.904	4.791	3.428	3.409	3.492	4.611	4.081	5.125
Fe	3.528	3.945	2.777	4.162	4.162	5.438	5.534	5.491	4.196	4.898	3.984
Mn				0.080	0.110	0.156	0.088	0.107	0.103	0.098	
Ti		0.025			0.021						
Ca											
K											
T cation	19.750	19.912	19.503	19.967	19.941	19.930	19.974	19.995	19.901	19.931	19.768
Fe/Fe+Mg	0.391	0.438	0.327	0.459	0.465	0.613	0.619	0.611	0.476	0.545	0.437
T°C	251	277	248	276	279	266	278	279	279	265	256

Tableau 3b. Analyses des chlorites dans les veines

LM #	058F		601		601	432A	432A	432A		441		441	077E	077E		81
Minéral	Chl	Chl		Chl		Chl	Chl	Chl	Chl		Chl		Chl	Chl	Chl	
No	44		46		47	49	50	51		52		53	54	56		58
SiO2 (%)	24.90		25.59		26.85	24.49	24.34	24.01		23.88		23.95	23.60	23.72		25.91
Tio2																
Al2O3	24.40		23.09		23.57	24.48	24.40	24.45		25.61		25.71	25.48	25.95		18.17
FeO	26.34		26.88		23.98	36.68	35.95	35.76		32.78		32.69	31.45	31.09		21.84
MgO	14.08		13.63		17.11	8.17	7.96	7.67		9.11		9.44	10.51	10.54		13.30
MnO			0.74		0.59											
CaO			0.65													1.18
Na2O																
K2O																
Cr2O3			0.16													
Cl																
SO3																1.10
Total	89.72		90.74		92.10	93.82	92.65	91.89		91.38		91.79	91.04	91.30		81.50
	Nombre d'ions sur une base de 28 atomes d'oxygène															
Si	5.128		5.256		5.316	5.075	5.095	5.070		4.988		4.976	4.923	4.918		5.768
AlIV	2.872		2.744		2.684	2.925	2.905	2.930		3.012		3.024	3.077	3.082		2.232
AlVI	3.052		2.848		2.817	3.055	3.117	3.157		3.295		3.273	3.189	3.262		2.536
Mg	4.321		4.172		5.048	2.523	2.483	2.414		2.836		2.923	3.267	3.257		4.412
Fe	4.537		4.617		3.970	6.357	6.294	6.315		5.727		5.680	5.487	5.391		4.066
Mn			0.129		0.099											
Ti																
Ca			0.143													0.281
K																
T cation	19.910		19.909		19.934	19.935	19.894	19.886		19.858		19.876	19.944	19.910		19.296
Fe/Fe+Mg	0.512		0.525		0.440	0.716	0.717	0.723		0.669		0.660	0.627	0.623		0.480
T°C	284		270		270	275	273	275		288		290	298	298		219

Tableau 3b. Analyses des chlorites dans les veines

LM #	81	454B	454B	450A	450A	13	13	467C	467C	006G	006G
Minéral	Chl	Chl	Chl	Chl	Chl	Chl	Chl	Chl	Chl	Chl	Chl
No	59	60	61	66	67	70	71	72	73	76	77
SiO2 (%)	28.78	25.73	24.86	25.65	24.89	25.93	25.22	26.33	26.80	26.27	26.22
Tio2				0.10			0.09				
Al2O3	18.58	20.46	21.51	22.30	23.37	21.86	22.76	19.61	19.86	20.20	20.05
FeO	19.12	32.08	30.55	27.35	27.90	26.74	27.46	31.82	25.12	30.32	29.51
MgO	21.88	12.13	12.70	14.23	13.97	15.19	14.12	12.46	17.27	12.94	13.34
MnO						0.44	0.54				
CaO				0.44							
Na2O											
K2O											
Cr2O3											
Cl											
SO3											
Total	88.36	90.40	89.62	90.07	90.13	90.16	90.19	90.22	89.05	89.73	89.12
	Nombre d'ions sur une base de 28 atomes d'oxygène										
Si	5.797	5.435	5.264	5.303	5.152	5.343	5.220	5.563	5.539	5.535	5.543
AlIV	2.203	2.565	2.736	2.697	2.848	2.657	2.780	2.437	2.461	2.465	2.457
AlVI	2.209	2.531	2.634	2.738	2.856	2.653	2.773	2.448	2.379	2.552	2.539
Mg	6.568	3.819	4.008	4.384	4.310	4.665	4.355	3.924	5.320	4.063	4.203
Fe	3.221	5.668	5.410	4.729	4.830	4.608	4.753	5.623	4.342	5.342	5.217
Mn						0.077	0.095				
Ti				0.016			0.014				
Ca				0.097							
K											
T cation	19.997	20.017	20.051	19.964	19.996	20.002	19.990	19.994	20.041	19.957	19.959
Fe/Fe+Mg	0.329	0.597	0.574	0.519	0.528	0.497	0.522	0.589	0.449	0.568	0.554
T°C	227	246	265	265	281	263	274	233	245	237	237

Tableau 3b. Analyses des chlorites dans les veines

LM #	427B	427B	427A	427A	077E	077E	077E
Minéral	Chl	Chl	Chl	Chl	Chl (?)	Chl	Chl
No	79	80	81	82	84	85	87
SiO2 (%)	24.10	24.37	23.49	23.22	28.50	22.67	23.13
Tio2		0.11		0.24	0.15		
Al2O3	22.36	21.54	23.10	24.44	31.65	26.52	26.07
FeO	36.91	35.77	37.50	37.55	26.71	34.50	34.22
MgO	7.86	7.96	6.50	6.22	4.78	6.84	7.24
MnO		0.44				0.58	0.53
CaO							
Na2O							
K2O					2.55		
Cr2O3					0.20		
Cl							
SO3							
Total	91.23	90.19	90.59	91.67	94.54	91.11	91.19
	Nombre d'ions sur une base de 28 atomes d'oxygène						
Si	5.178	5.284	5.103	4.975	5.522	4.817	4.898
AlIV	2.822	2.716	2.897	3.025	2.478	3.183	3.102
AlVI	2.841	2.789	3.020	3.148	4.751	3.460	3.407
Mg	2.517	2.572	2.105	1.986	1.380	2.166	2.285
Fe	6.632	6.486	6.814	6.728	4.328	6.131	6.061
Mn		0.081				0.104	0.095
Ti		0.018		0.039	0.022		
Ca							
K					0.630		
T cation	19.990	19.946	19.938	19.900	19.111	19.861	19.847
Fe/Fe+Mg	0.725	0.716	0.764	0.772	0.758	0.739	0.726
T°C	263	253	268	281	224	301	293

Tableau 3c. Analyses des carbonates dans les veines (% poids)

LM	Minéral	No	CaO	MnO	FeO	MgO	CO2
006F	Car	3	51.93	0.51	0.38		47.17
006F	Car	5	55.79	0.81		0.23	43.17
027E	Car	6	56.32	0.63			43.05
027E	Car	7	58.51				41.49
021E	Car	10	52.78				47.22
409	Car	21	54.65				45.35
002F	Car	23	57.27	0.65			42.08
590	Car	30	53.74				46.26
590	Car	33	53.42	0.39			46.19
464	Car	37	51.79		0.42		47.79
086F	Car	38	54.38	0.56			45.06
058F	Car	41	56.5	0.67			42.83
058F	Car	42	54.47	0.52			45.01
601	Car	45	55.04				44.96
077E	Car	55	60.6	1.01	0.88	0.47	37.04
81	Car	81	50.32				49.68
454B	Car	62	29.11	0.46	10.37	13.63	46.43
464B	Car	63	56.61	0.6	0.58	0.43	41.78
602	Car	64	55.34				44.66
450A	Car	68	52.7	0.76	0.68	0.48	45.38
13	Car	69	54.41				45.59
467C	Car	75	46.59				53.41
006G	Car	78	46.97	0.4		0.27	52.36

Tableau 3d. Analyses des amphiboles

LM #	021E	021E	467C
Minéral	Act	Act	Act
No	12	13	74
SiO2 (%)	59.32	57.95	53.83
Tio2			
Al2O3			
FeO	11.32	10.74	19.91
MgO	18.51	18.11	13.04
MnO			
CaO	12.76	12.44	11.37
Na2O			
K2O			
Cr2O3			
Cl			
S03			
Total	101.91	99.24	98.15
	Nombre d'ions sur une base de 24 atomes d'oxygène		
Si	8.406	8.419	8.285
AlIV			
AlVI			
Mg	3.909	3.921	2.991
Fe	1.342	1.305	2.563
Mn			
Ti			
Na			
Ca	1.937	1.936	1.875
K	0.000	0.000	0.000
T cation	15.594	15.581	15.715
Fe/Fe+Mg	0.256	0.250	0.461
Note	Actinote Si 8.41 Fe-Mg 5.25 Ca 1.94	Actinote Si 8.42 Fe-Mg 5.22 Ca 1.94	Actinote Si 8.29 Fe-Mg 5.55 Ca 1.88

ANNEXE 4: Caractéristiques des veines

Les échantillons mésoscopiques de veines ont été systématiquement décrits en utilisant une feuille canevas adaptée aux caractéristiques des veines. La proportion de minéraux et les différentes textures ont été recueillis. Ces données empiriques ont permis d'établir la séquence paragénétique présentée au chapitre 5. La compilation des données texturales démontre qu'il n'y a pas de zonalité dans le système de veines, tant à l'échelle de la veine que de la mine. Cette absence de zonalité s'accorde également avec l'homogénéité des données isotopiques et des éléments traces dans les sulfures.

Tableau 4a. Composition minéralogique (%) des échantillons de veines

Échan.	Veine	X(E)	Y(N)	Z	Qz	Py	Po	Cp	Sp	Chl	Ser	Act	Cal	Tm	Host
96-008	1	3074	3711	235	70	18	0	2	0	1	0	0	2	0	7
93-086	3	3100	3600	235	47	40	0	0	10	0	0	2	Tr	0	1
93-168	3	3130	3500	295	60	26	0	5	4	1	0	0	0	0	4
93-169	3	3130	3500	295	75	12	0	4	4	0	0	0	0	0	5
94-432	3	3115	3635	240	19	72	0	3	5	0	0	0	0	0	1
94-537	3	3050	3630	190	63	34	0	1	0	0	0	0	0	0	2
94-590	3	3120	3450	270	85	7	0	3	0	5	0	0	0	0	0
95-601	3	3100	3470	225	24	60	0	8	8	0	0	0	1	0	0
96-001	3	3100	3480	255	60	21	0	7	7	0	0	0	2	0	4
96-003	3	3075	3475	235	50	15	0	2	14	0	0	0	16	0	4
96-004	3	3095	3445	255	70	7	0	6	7	7	0	0	1	0	2
96-005	3	3100	3448	255	98	1	0	0	0	1	0	0	0	0	0
96-006	3	3115	3607	255	70	13	0	2	0	0	8	0	8	0	0
96-007	3	3045	3500	230	18	54	12	12	2	1	0	0	1	Tr	0
96-009	3	3017	3572	190	75	10	1	1	10	Tr	0	0	2	0	0
96-010	3	3027	3583	190	78	12	0	4	4	1	0	0	1	0	0
96-011	3	3048	3603	190	50	12	12	16	0	0	0	2	6	0	2
96-014	3	3068	3527	235	60	15	11	2	3	0	0	0	3	0	7
96-020	3	3147	3607	295	70	18	Tr	5	3	Tr	0	3	2	0	0
96-021	3	3148	3588	295	89	3	0	7	0	0	0	0	1	0	0
94-599	10	2800	3630	145	97	2	0	Tr	0	0	0	0	1	0	0
94-428	15	3080	4080	350	90	0	3	3	0	5	0	0	0	0	0
93-002	20	2980	4172	415	55	20	2	10	8	0	0	0	3	0	3
93-021	20	3000	4207	355	55	8	0	1	1	0	0	35	0	0	0
93-023	20	2998	4202	355	75	5	0	0	0	0	4	0	16	0	0
93-049	20	2930	4163	355	94	2	0	Tr	3	1	0	0	0	0	0

Tableau 4a. Composition minéralogique (%) des échantillons de veines

Échan.	Veine	X(E)	Y(N)	Z	Qz	Py	Po	Cp	Sp	Chl	Ser	Act	Cal	Tm	Host
93-055	20	3002	4210	338	70	10	0	1	9	2	0	3	1	0	5
93-056	20	2985	4190	340	55	25	0	6	11	0	0	0	3	0	0
93-079	20	2864	4192	245	80	10	0	0	0	10	0	0	0	0	0
93-080	20	2878	4196	245	75	15	0	6	4	0	0	0	0	0	0
93-081	20	2932	4225	245	30	63	0	4	4	0	0	0	0	0	0
93-082	20	2907	4209	245	75	15	Tr	7	0	1	0	0	1	0	0
93-083	20	2899	4205	245	85	5	0	0	0	0	0	1	1	0	9
93-085	20	2965	4225	245	65	16	1	3	5	5	0	0	1	0	0
93-087	20	2909	4126	415	55	4	14	22	0	1	0	0	5	0	0
93-088	20	2910	4122	415	50	16	8	16	0	5	0	0	3	2	0
93-089	20	2907	4121	415	65	9	3	9	5	6	Tr	Tr	1	0	3
93-094	20	2908	4123	415	45	8	5	20	18	0	0	0	2	1	3
96-016	20	2945	4124	485	83	9	1	5	0	2	0	0	0	0	0
96-017	20	3005	4155	470	75	9	0	5	2	5	0	0	2	0	3
96-018	20	3039	4147	605	75	4	2	4	0	0	8	1	4	0	3
96-019	20	2930	4092	605	50	3	0	7	0	2	0	0	0	0	38
93-076	30	2830	4334	228	50	18	11	7	9	0	0	0	1	0	5
93-077	30	2824	4334	228	55	16	0	18	6	0	0	0	2	0	4
94-450	30	2980	4240	355	78	15	0	0	5	2	0	0	0	0	0
94-453	30	2910	4318	355	20	51	0	2	7	0	0	0	Tr	0	20
94-544	30	2860	4320	215	49	8	25	18	0	0	0	0	1	0	0
96-015	40	2980	3347	365	30	28	18	3	3	0	0	0	4	0	16
93-070	20-30	2850	4290	235	80	10	0	0	0	2	0	0	0	0	8
94-541	20S	2730	3612	190	65	11	0	8	0	0	0	0	1	0	14
94-409	A	2988	3591	235	30	14	11	7	14	0	0	8	18	0	0
94-425	A	2870	3600	190	55	32	0	4	4	5	0	0	0	0	0

Tableau 4a. Composition minéralogique (%) des échantillons de veines

Échan.	Veine	X(E)	Y(N)	Z	Qz	Py	Po	Cp	Sp	Chl	Ser	Act	Cal	Tm	Host
94-442	H	3128	3786	235	35	12	30	12	6	3	0	0	3	0	0
94-443	H	3115	3785	235	65	10	0	Tr	5	11	0	0	1	0	8
94-435	I	3110	3714	235	65	15	0	Tr	0	6	0	0	2	0	12
94-523	I	3114	3720	190	35	5	0	0	Tr	24	0	0	12	0	24
94-561	I	3065	3727	190	50	1	0	Tr	Tr	19	0	0	19	0	10
94-441	NW	3102	3757	235	80	9	0	2	4	4	1	0	Tr	0	0
94-509	NW	3090	3793	190	50	28	0	4	8	9	0	0	1	0	0
94-512	NW	3097	3785	190	80	17	0	2	Tr	1	0	0	0	0	0
94-513	NW	3097	3785	190	67	1	0	2	0	0	0	0	3	0	23
94-566	NW	3095	3844	100	50	23	0	4	9	9	0	0	2	0	5
95-609	veinule	2860	4254	190	40	10	1	Tr	9	0	0	24	8	0	8

Tableau 4b. Caractéristiques texturales des veines

Échantillon	93-002	93-021	93-023	93-049	93-055	93-056	93-070	93-076
Veine #	20	20	20	20	20	20	20-30	30
Niveau	415	355	355	355	338	340	235	228
Encaissant	FCM	FCM	FCM?			BC		
Alteration		Chl	Ser			Chl-Ser		Ser
Py cataclasé		x	x	x	x	x		x
Py idiomorphe		x	x	x	x	x	x	x
Py ruban				x	x		x	x
Py amas						x		
Py fine en ciment Qz		x						
Py fine en plage	x				x			
Py fine en ruban			x					
Py tardive								
Py diss					Qz			
Po ciment Qz								x
Po remplacement								
Po amas	Py							
Cp ciment Qz	x	x				x		
Cp amas								
Cp ciment Py cata						x		
Cp diss				Qz	Qz			
Sp en amas avec Py	x			x	x	x		x
Sp en ruban								x
Sp en ciment Qz	x			x	x	x		x
Sp en ciment Py cata						x		
Sp idiomorphe								
Veinule Qz-B massif								
Qz-B massif								
Qz-G massif								
Qz-B ruban					x			
Qz-G-Bx	x						x	
Qz-G-L ruban	x							x
Qz-G-L marbré		x	x	x	x	x		x
Ciment Chl-Ser-Qz			x					
Fragment rx chl								
Fragment rx ser							x	
Fragment rx	x				x			x
Calcite en ciment	x		x		x	x		x
Chlorite				x	x		x	
Séricite			x					
Actinote		x			x			
Tourmaline								

Tableau 4b. Caractéristiques texturales des veines

Échantillon	93-077	93-079	93-080	93-081	93-082	93-083	93-085	93-086
Veine #	30	20	20	20	20	20	20	3
Niveau	228	245	245	245	245	245	245	235
Encaissant		Sédi	Sédi					FCM
Alteration		Chl	Chl					Nil
Py cataclasé				x	x	x	x	x
Py idiomorphe		2		x	x	x	x	x
Py ruban						x	x	x
Py amas				x				x
Py fine en ciment Qz			x		x		x	
Py fine en plage							x	
Py fine en ruban	x	1			x		x	
Py tardive		2						
Py diss		2						
Po ciment Qz					x		x	
Po remplacement								
Po amas							Py F	
Cp ciment Qz	x		x	x	x		x	
Cp amas								
Cp ciment Py cata	x			x				
Cp diss								
Sp en amas avec Py	x							x
Sp en ruban	x							x
Sp en ciment Qz	x		x					x
Sp en ciment Py cata								x
Sp idiomorphe								
Veinule Qz-B massif								
Qz-B massif								
Qz-G massif								
Qz-B ruban							Chl	
Qz-G-Bx				x	x			
Qz-G-L ruban	x	x			x			x
Qz-G-L marbré	x		x			x	x	x
Ciment Chl-Ser-Qz					x		x	
Fragment rx chl								
Fragment rx ser	x					x		
Fragment rx								x
Calcite en ciment	x				x	x	x	x
Chlorite		x			x		x	
Séricite								
Actinote						x		x
Tourmaline								

Tableau 4b. Caractéristiques texturales des veines

Échantillon	93-087	93-088	93-089	93-094	93-168	93-169	94-409	94-425
Veine #	20	20	20	20	3	3	A	A
Niveau	415	415	415	415	295	295	235	190
Encaissant				FCM	FCM?	QFP	FCM	
Alteration				Chl	Chl-Ser-S	Ser	Chl-Leu	
Py cataclasé	x			x	x	x		x
Py idiomorphe	x	2		x	x	x	x	x
Py ruban				x	x	x		x
Py amas								
Py fine en ciment Qz		1	x		x			x
Py fine en plage		1			x			
Py fine en ruban			x				x	
Py tardive		2					PyF-Sp	
Py diss								
Po ciment Qz	x	x	x	x			x	
Po remplacement				Py-Sp				
Po amas	x	x	Cp					
Cp ciment Qz	x	x	x	x	x	x	x	x
Cp amas	x	x	Py		Py F			
Cp ciment Py cata								x
Cp diss						Qz		
Sp en amas avec Py			x	x	x	x		x
Sp en ruban			x	x		x		
Sp en ciment Qz							x	x
Sp en ciment Py cata				x	x			x
Sp idiomorphe								x
Veinule Qz-B massif							x	
Qz-B massif							x	
Qz-G massif								
Qz-B ruban		Chl	Chl	x	Chl			
Qz-G-Bx	x		x			x		x
Qz-G-L ruban								x
Qz-G-L marbré		x		x	x		x	
Ciment Chl-Ser-Qz								
Fragment rx chl			x		x			
Fragment rx ser					x			
Fragment rx				x		x		
Calcite en ciment	x	x	x	x			x	
Chlorite	x	x	x		x			x
Séricite								
Actinote			x				x	
Tourmaline		x		x				

Tableau 4b. Caractéristiques texturales des veines

Échantillon	94-428	94-432	94-435	94-441	94-442	94-443	94-450	94-453
Veine #	15	3	I	NW	H	H	30	30
Niveau	350	240	235	235	235	235	355	355
Encaissant	Sédi		Sédi	Sédi			Sédi	
Alteration	Chl-Ser			Chl-Ser			Chl	
Py cataclasé		x	x	x	2	2	2	x
Py idiomorphe		x	x	x	2	2	2	x
Py ruban			x		2			
Py amas		x		x		2		x
Py fine en ciment Qz						1		
Py fine en plage					1			
Py fine en ruban							1	
Py tardive					2	2	2	
Py diss							2	
Po ciment Qz	x			x				
Po remplacement								
Po amas								
Cp ciment Qz	x	x		x	x	x	x	
Cp amas					Chl			
Cp ciment Py cata		x						
Cp diss				Qz				
Sp en amas avec Py		x		x	x	2	x	x
Sp en ruban		x		x				
Sp en ciment Qz		x				x		
Sp en ciment Py cata		x				x		x
Sp idiomorphe								
Veinule Qz-B massif					x			
Qz-B massif		x						
Qz-G massif								
Qz-B ruban					Chl			
Qz-G-Bx		x			x		x	
Qz-G-L ruban			x			x	x	x
Qz-G-L marbré	x		x	x		x		x
Ciment Chl-Ser-Qz								
Fragment rx chl			x			x		x
Fragment rx ser								
Fragment rx		x						
Calcite en ciment			x		x	x	x	x
Chlorite	x		x	x	x	x	x	
Séricite								
Actinote								
Tourmaline								

Tableau 4b. Caractéristiques texturales des veines

Échantillon	94-454	94-464	94-509	94-512	94-513	94-523	94-537	94-541
Veine #	H	H	NW	NW	NW	I	3	20S
Niveau	235	235	190	190	190	190	190	190
Encaissant		FCM			DAC		FCM	
Alteration		Chl			Ser		Ser-Chl	
Py cataclasé	x	x	x		x		x	x
Py idiomorphe	x	x	x		x	x	x	x
Py ruban								x
Py amas	x					Qz-T	x	
Py fine en ciment Qz				x				
Py fine en plage			x					x
Py fine en ruban				x				
Py tardive			x					
Py diss		x		x				
Po ciment Qz								
Po remplacement								
Po amas								
Cp ciment Qz			x	x	x		x	x
Cp amas								
Cp ciment Py cata								
Cp diss	Qz							
Sp en amas avec Py	x		x	x				
Sp en ruban								
Sp en ciment Qz			x			x		
Sp en ciment Py cata								
Sp idiomorphe								
Veinule Qz-B massif								
Qz-B massif		x						
Qz-G massif								
Qz-B ruban	Chl	Chl				x		
Qz-G-Bx							x	
Qz-G-L ruban					x			x
Qz-G-L marbré	x		x	x	x			x
Ciment Chl-Ser-Qz					x			
Fragment rx chl	x	x	x					x
Fragment rx ser					x	x	x	
Fragment rx								
Calcite en ciment		x				x		x
Chlorite	x	x	x	x		x		
Séricite								
Actinote								
Tourmaline								

Tableau 4b. Caractéristiques texturales des veines

Échantillon	94-543	94-544	94-561	94-566	94-590	94-599	95-601	95-609
Veine #	A	30	I	NW	3	10	3	veinule
Niveau	190	215	190	100	270	145	225	190
Encaissant		BC		FCM	FCM	QFP	FCM	FCM
Alteration		Chl-Ser		Nil	Chl-Ser	Ser	Chl-Ser	Chl
Py cataclasé	x			x		x	x	x
Py idiomorphe	x	x	x	x	2	x	x	
Py ruban			x				x	
Py amas	x					x	x	x
Py fine en ciment Qz				x	1			
Py fine en plage					1			
Py fine en ruban								
Py tardive		Po			2			
Py diss								
Po ciment Qz		x						x
Po remplacement								
Po amas								
Cp ciment Qz		x		x	x	x	x	x
Cp amas								
Cp ciment Py cata	x						x	
Cp diss			Qz-Chl					
Sp en amas avec Py	x			x				
Sp en ruban	x							
Sp en ciment Qz				x		x	x	x
Sp en ciment Py cata	x							
Sp idiomorphe								
Veinule Qz-B massif								
Qz-B massif								
Qz-G massif		x				x		
Qz-B ruban			x	Chl	Chl			
Qz-G-Bx		x			x			
Qz-G-L ruban	x				x			
Qz-G-L marbré	x			x			x	x
Ciment Chl-Ser-Qz								
Fragment rx chl	x			x				
Fragment rx ser			x					
Fragment rx								x
Calcite en ciment	x	x	x	x		x	x	x
Chlorite			x	x	x			
Séricite								
Actinote								x
Tourmaline								

Tableau 4b. Caractéristiques texturales des veines

Échantillon	96-001	96-003	96-004	96-005	96-006	96-007	96-008	96-009
Veine #	3	3	3	3	3	3	1	3
Niveau	255	235	255	255	255	230	235	190
Encaissant				FCM			FCM	
Alteration							Chl-Leu	
Py cataclasé	x	x	x		x	x	x	x
Py idiomorphe	x	x	x	x	x		x	x
Py ruban		x	x		x			
Py amas	x						x	x
Py fine en ciment Qz					x			
Py fine en plage						x		
Py fine en ruban								
Py tardive								
Py diss		Qz		Qz			Qz	
Po ciment Qz								x
Po remplacement								
Po amas						x		Sp
Cp ciment Qz	x		x		x	x		x
Cp amas		x				Po	Py	
Cp ciment Py cata	x				x	x		
Cp diss		Qz					Qz	
Sp en amas avec Py			x			x		
Sp en ruban		x						
Sp en ciment Qz	1		x					x
Sp en ciment Py cata								
Sp idiomorphe	2	x						
Veinule Qz-B massif	x					x		x
Qz-B massif								
Qz-G massif								
Qz-B ruban		x	Chl	Chl			Chl	x
Qz-G-Bx								x
Qz-G-L ruban		x						
Qz-G-L marbré	x		x	x	x	x	x	
Ciment Chl-Ser-Qz								
Fragment rx chl	x							
Fragment rx ser			x					
Fragment rx		x				x	x	
Calcite en ciment			x		x	x	x	
Chlorite			x	x		x	x	x
Séricite					x			
Actinote								
Tourmaline								

Tableau 4b. Caractéristiques texturales des veines

Échantillon	96-010	96-011	96-014	96-015	96-016	96-017	96-018	96-019
Veine #	3	3	3	40	20	20	20	20
Niveau	190	190	235	365	485	470	605	605
Encaissant	FCM		FCM				FCM ?	FCM
Alteration	Ser-Leu		Ser-Leu				Chl	Leu
Py cataclasé	x		x	x	x		x	
Py idiomorphe	x	2	x	x	x	2	x	
Py ruban	x		x	x			x	
Py amas		2						
Py fine en ciment Qz						1		
Py fine en plage		1			x			
Py fine en ruban								
Py tardive		2 Po				2 Sp		
Py diss			Qz-N			2		Qz-Frag
Po ciment Qz		x	x	x	x		x	
Po remplacement								
Po amas								
Cp ciment Qz	x	x	x	x	x	x	x	x
Cp amas								
Cp ciment Py cata	x							
Cp diss								
Sp en amas avec Py	x		x					
Sp en ruban								
Sp en ciment Qz						x		
Sp en ciment Py cata				x				
Sp idiomorphe								
Veinule Qz-B massif			x					
Qz-B massif								
Qz-G massif								
Qz-B ruban	x	x				Chl		
Qz-G-Bx	x		x		x		x	
Qz-G-L ruban								
Qz-G-L marbré		x		x		x		x
Ciment Chl-Ser-Qz								
Fragment rx chl								x
Fragment rx ser			x				x	
Fragment rx		x		x		x		
Calcite en ciment	x	x		x		x	x	
Chlorite	x				x	x		x
Séricite							x	
Actinote		x					x	
Tourmaline								

Tableau 4b. Caractéristiques texturales des veines

Échantillon	96-020	96-021
Veine #	3	3
Niveau	295	295
Encaissant		FCM
Alteration		Ser
Py cataclasé		
Py idiomorphe	x	
Py ruban		
Py amas	x	
Py fine en ciment Qz		x
Py fine en plage		
Py fine en ruban		
Py tardive		
Py diss		
Po ciment Qz	x	
Po remplacement		
Po amas		
Cp ciment Qz	x	x
Cp amas		
Cp ciment Py cata		
Cp diss		
Sp en amas avec Py		
Sp en ruban		
Sp en ciment Qz	x	
Sp en ciment Py cata		
Sp idiomorphe		
Veinule Qz-B massif		x
Qz-B massif		
Qz-G massif		
Qz-B ruban		
Qz-G-Bx	x	
Qz-G-L ruban		
Qz-G-L marbré		x
Ciment Chl-Ser-Qz		
Fragment rx chl		
Fragment rx ser		
Fragment rx		
Calcite en ciment		x
Chlorite	x	
Séricite		
Actinote	x	
Tourmaline		

Tableau 4c. Comparaison des caractéristiques texturales entre les veines 20 et 3.

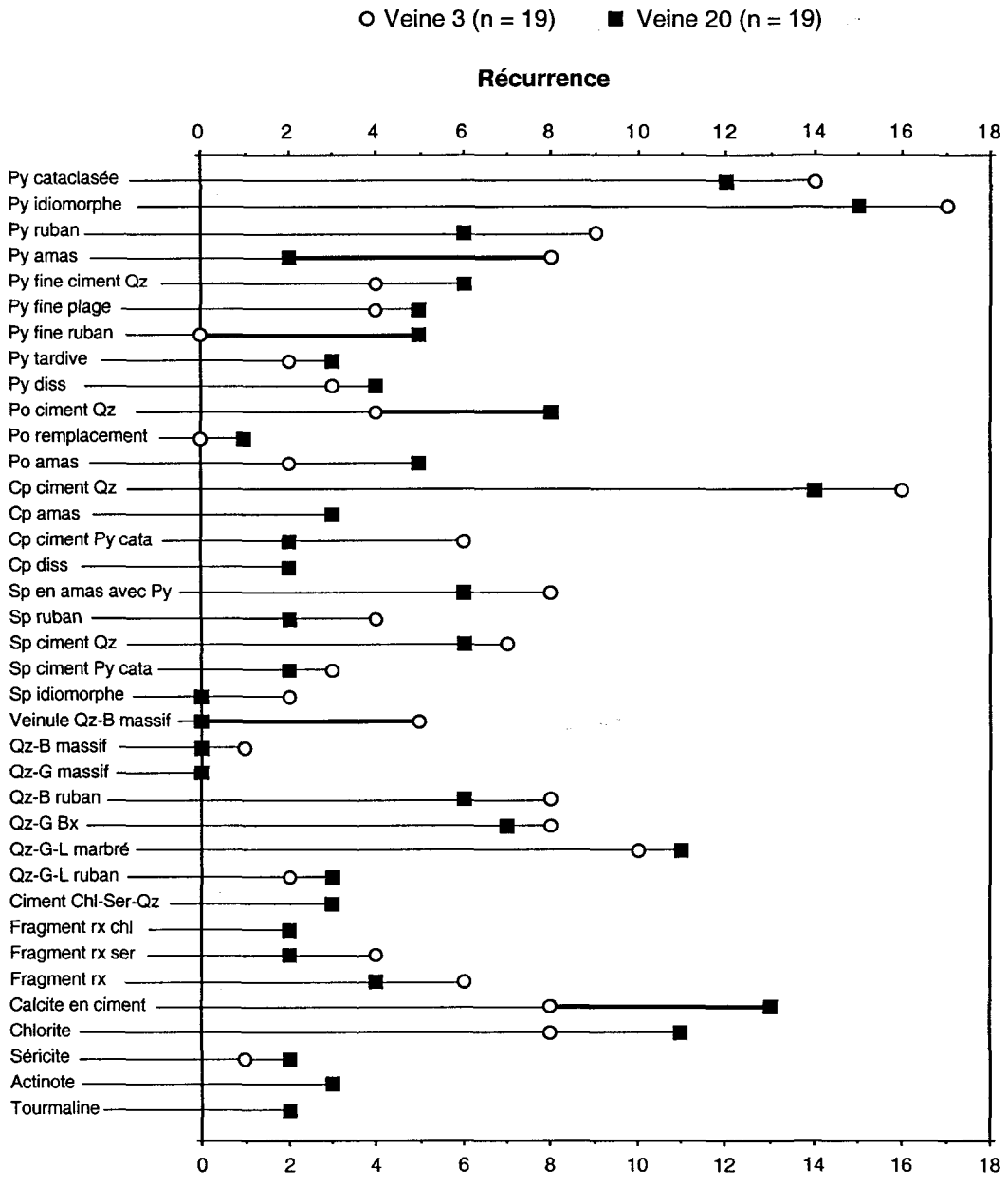

Tableau 4d. Comparaison des caractéristiques texturales entre les veines 30 et NW.

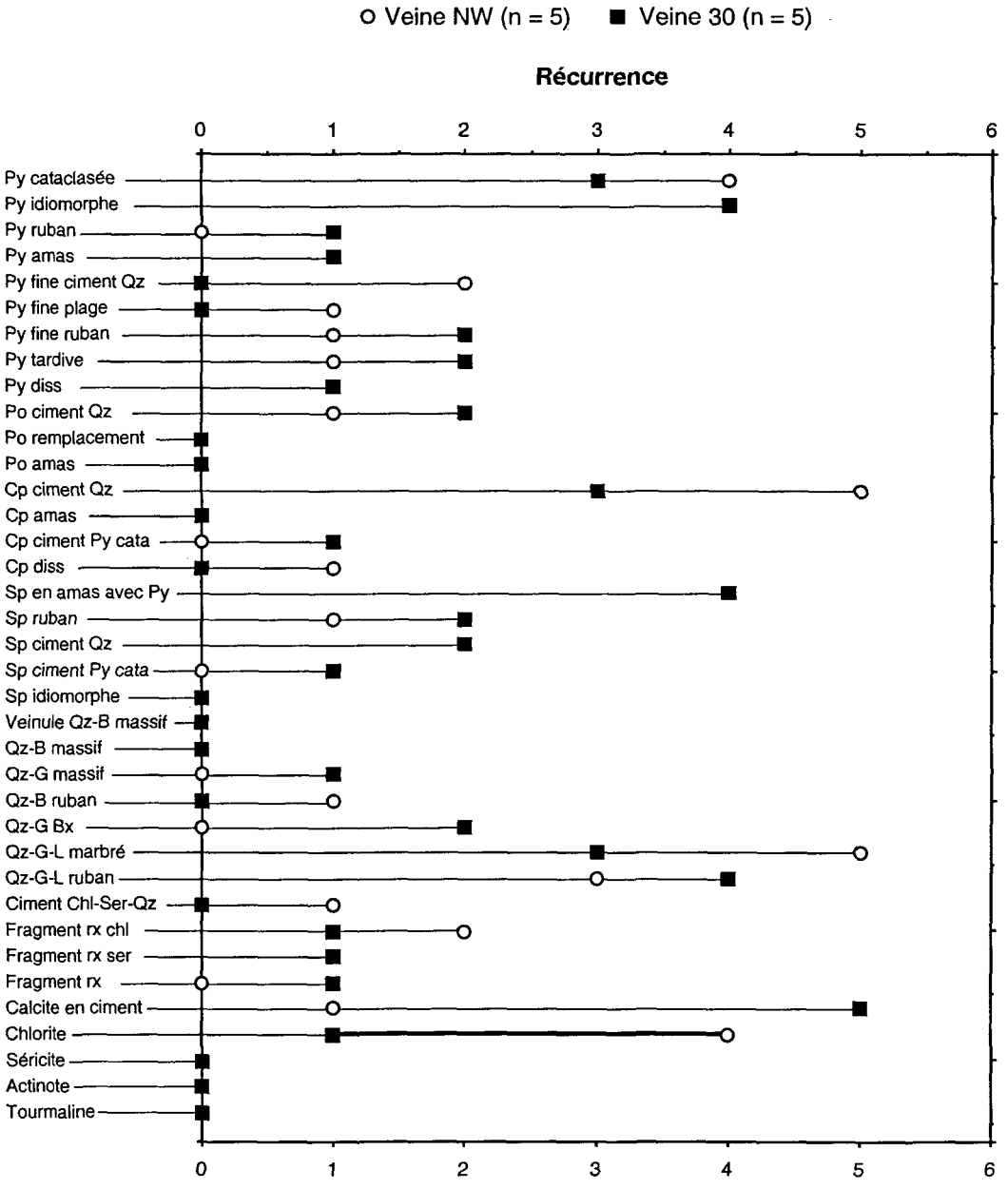

Tableau 4e. Comparaison des caractéristiques texturales entre les veines du nord (20-30) et du sud (3-NW)

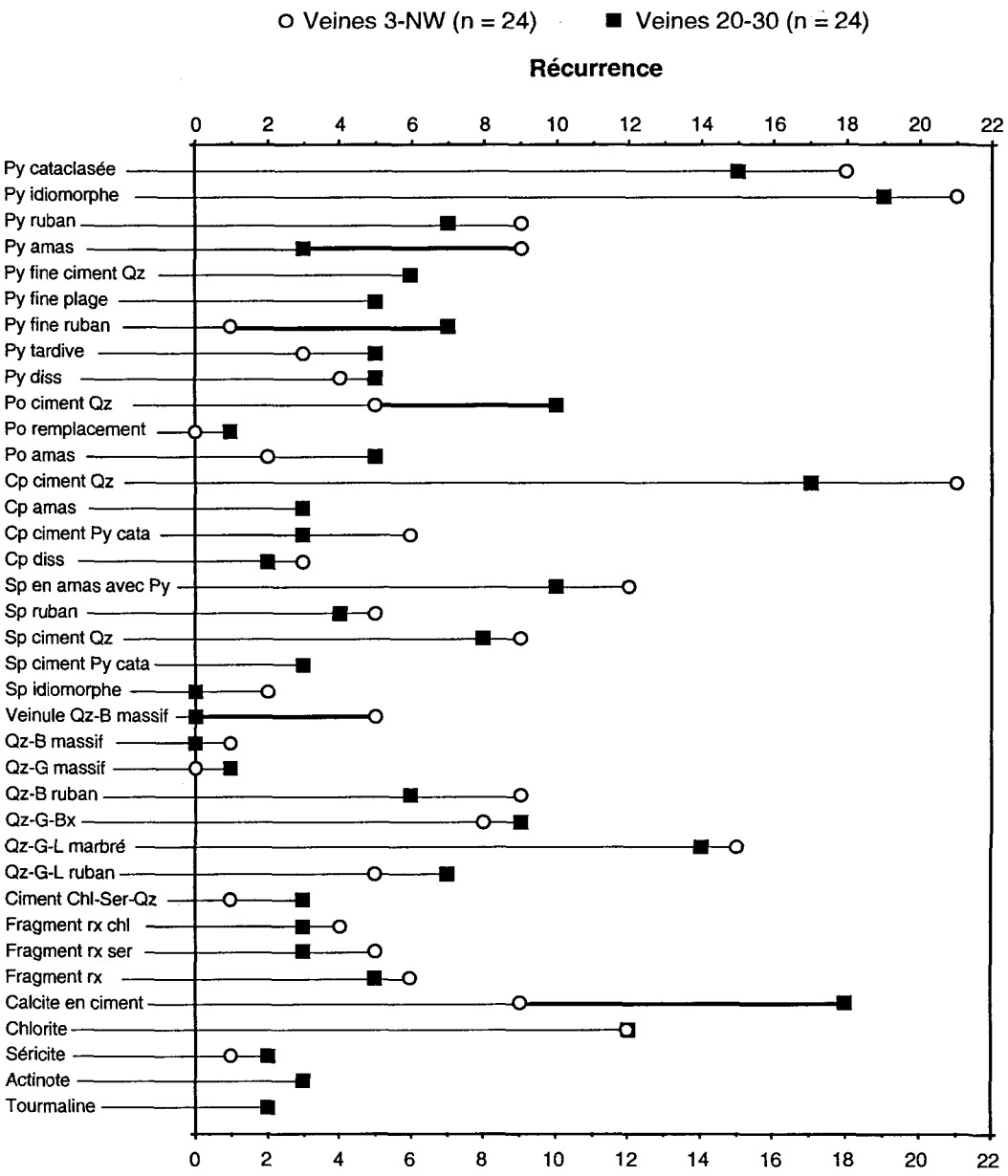

Tableau 4f. Comparaison des caractéristiques texturales des veines 20 et 30 en fonction de la profondeur.

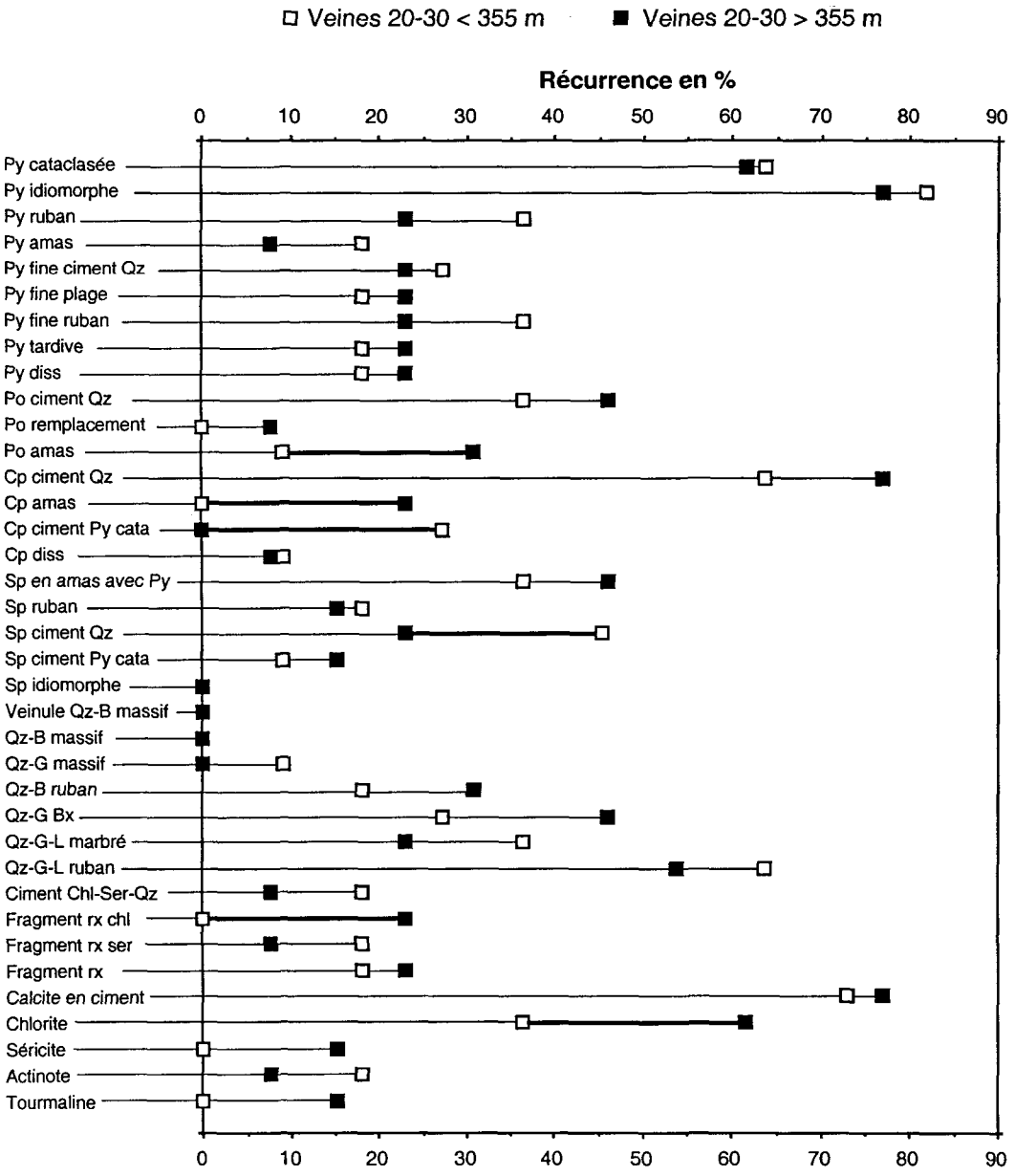

ANNEXE 5: Datation U-Pb d'un dyke de QFP

La datation U-Pb a été réalisée au Royal Ontario Museum (Toronto) sous un contact octroyé par le Ministère des Ressources naturelles du Québec. Les procédures techniques se résument comme suit. Après une séparation au Frantz, les zircons sont choisis manuellement sous le microscope. Leur surface extérieure est épurée par une abrasion à l'air. Ensuite, les zircons sont lavés avec du HNO_3 et sont subséquemment dissous en utilisant du HF chauffé à 200 °C. Les solutions sont converties en HCl puis asséchées et montées directement sur les filaments du spectromètre de masse. Le Pb et l'U sont montés ensemble sur des filaments de Re en utilisant un gel de silice et sont analysés avec un spectromètre de masse VG354. La correction pour la masse du détecteur est constante à 0,40% / AMU. Les corrections thermiques sont de 0,10% / AMU. Le tableau suivant présente les résultats d'analyse à 1σ d'incertitude. Le contenu en Pb commun est corrigé avec la composition isotopique de l'échantillon témoin du laboratoire. Le rapport Th/U est estimé sur la base de la mesure du $^{208}Pb/^{206}Pb$ et des âges $^{207}Pb/^{206}Pb$.

L'échantillon de dyke de QFP soumis pour analyse possède de nombreux zircons frais, prismatiques et clairs. Les trois zircons analysés ont produit des âges consistants. Une moyenne $^{207}Pb/^{206}Pb$ de 2721,7 ± 1,6 Ma représente le meilleur estimé de l'âge de la cristallisation du dyke.

Tableau 5. Données isotopiques U-Pb pour les zircons

No	Poids (mg)	U (ppm)	Th/U	Pb Com (pg)	207/204	206/238	1σ	207/235	1σ	207/206 Âge (Ma)	1σ	% Disc.
1	0,001	56	0,4	1,3	288,7	0,52568	0,00094	13,6111	0,0323	2722,9	2,0	0
2	0,002	41	0,5	0,6	289,4	0,52435	0,00086	13,5640	0,0244	2721,4	1,0	0,2
3	0,001	48	0,5	0,6	284,6	0,52520	0,00153	13,5885	0,0466	2721,7	2,4	0

% Disc. = % de discordance par rapport à l'âge 207Pb/206 Pb